Università degli studi di Genova

Facoltà di Scienze Matematiche Fisiche e Naturali

Dottorato in Scienze e Tecnologie della Chimica e dei Materiali

Scienze e Tecnologie Chimiche XXX ciclo

INVESTIGATION OF SOLID-LIQUID INTERACTIONS IN HIGH TEMPERATURE METAL-CERAMIC SYSTEMS

Sofia Gambaro

Internal supervisor: Prof. Paola Riani

External supervisor: Dr.ssa Maria Luigia Muolo

Genoa, December 2017

Acknowledgments

I would like to really thank and express my gratitude to the people who allowed me to work on this interesting and challenging research field.

First, I would like to sincerely thank the ICMATE-CNR Research Group who has guided and sustained the work during all my PhD course: my supervisor Maria Luigia Muolo, Fabrizio Valenza and Alberto Passerone. Thank you all for your invaluable support in the scientific discussion, for your essential help during the writing of this Thesis and also for making me feel totally part of the Group on every occasion.

I would like to express my gratitude to Prof. Paola Riani and to Prof. Gabriele Cacciamani, for having shown me how to walk through the forest of Thermodynamics.

Moreover I want to express my sincere thanks to Prof. Oliver Dezellus for his hospitality in Lyon, for always giving me clear explanations and suggestions which have been fundamental during my last PhD year. Thank you also to Francois and to Rodica for their great support inside and outside the lab.

A special thanks goes to the two Referees of this Thesis, Prof. Mike Reece and Prof. Milena Salvo, for their positive comments and important suggestions.

I am sincerely thankful to my colleagues for the time we spent together during these years. In particular, I would like to thank all the ICMATE's friends: Giovanna, Donatella, Fabrizio, Francesco, Eva, Italo e Circide (La Maestra).

Many thanks to the new friends I had the chance to meet during my stay in Lyon and to the historical ones: Fany, Sonia, Marta, Alex, Ado, Laus, Michigan, Fly, Ans, Ife, Priele, Abs, Fre and to Alice.

Thanks to my parents, my brother Francesco, Conni, Zimma, Zia Bel and Manu, for their unconditional help.

I would like to dedicate this Thesis to my Granma, Ottavia, who, while doing the crosswords, used to call me to ask the chemical symbols of the elements.

Table of Contents

Abstract

In this PhD Thesis the solid-liquid interactions occurring in metal-ceramic systems at high temperatures have been experimentally determined, both in terms of wettability, by the use of the sessile drop technique, and in terms of reactivity, by the EDS and DSC analyses. All interactions have also been interpreted by thermodynamics (CALPHAD).

Two Projects (RITMARE flagship Italian project and ADMACOM European project) made it possible to conduct a wettability and reactivity evaluation on two metal-ceramic systems involving an oxidic and a non-oxidic substrate, respectively.

With reference to the oxidic systems, the reactivity and the wettability of the transparent $Y_3Al_5O_{12}$ (YAG) by Ag-based alloys has been studied, for the first time, with the aim to understand the metal-ceramic interactions under different experimental conditions (such as the temperature or the alloy composition) and to investigate the possibility to validate the use of these materials in metal-ceramic joints (such as YAG-alloys-Ti6Al4V) to be used as optical windows in marine applications.

The role of the Ti activity as well as the evolution of the Ag-Cu-Ti system with the temperature has been determined by the support of the thermodynamic approach. A significant reactivity occurred at the solid–liquid interfaces, with the formation of continuous and defect-free metal-ceramic layers as, for instance, TiY_2O_5 at Ag–Ti/YAG interfaces, while a second layer, identified as “M4X”, associated to a significant wettability improvement, has been specifically found only in the AgCuTi/YAG samples tested at 950°C. All these phases have been identified by the re-calculated Ag–Cu–Ti phase diagram and confirmed by SEM and EDS analyses. The measured good wettability, due to the Ti migration to the interface, as well asthe maintained transparency of the YAG, promising for the production of brazed optical windows, allowed this study to proceed towards the joining evaluation of YAG to Ti6Al4V.

Different fillers (Ag, AgCu, AgCuTi) and temperatures (1050 and 970, 950, 850°C) have been taken into account. No intermetallic compound formation has been observed using the pure Ag at 970 and at 1050°C, a very promising result from the mechanical point of view. In this case the Ti migration from the metallic support (Ti6Al4V) made it possible to avoid the use of an active element filler generating a continuous metal-ceramic layer on the YAG surface.

The phase formation has been interpreted using the CALPHAD method by means of recalculated Ag-Cu-Ti and Ag-Al-Ti isothermal sections.

As an example of non-oxidic systems, the reactivity and the wettability of two Al-Ti alloys (84 and 75 Al at%, respectively) on SiC have been evaluated to determine the interfacial interactions as well as the evolution of the system as a function of time and temperature. The first interaction, identified in terms of temperature and phase composition by the use of DSC and EDS analyses, has been defined for each system, revealing the formation of a TiC layer as the main interfacial layer, in the first case, and a compact and defect-free $Ti_3Si(Al)C_2$layer, in the second case.

As in the previous system, Ti plays again the role of active element migrating to the interface and promoting the formation of metal-ceramic compounds ensuring adhesion between the two different materials.

The first interaction and the subsequent evolution of the liquid phase were also interpreted by the thermodynamic evaluation of Al-C-Si-Ti quaternary and Al-Si-Ti ternary systems, respectively.

A home-made thermodynamic database has been built merging the literature parameters and adapting them in order to obtain a self-consistent set of phase models and interaction parameters. By the use of different kinds of representations the evolution of the system as well as the equilibria occurring at high temperature have been determined and used to define the best process parameters, such as temperature and alloy composition, to be used in the joining of SiC-based materials.

Aim of the work

The aim of this PhD research work is to evaluate the solid-liquid interactions occurring in metal-ceramic systems when high temperatures are reached.

In order to analyse the different interfacial phenomena that can take place when liquid metals and ceramic materials are in contact, the wetting behaviour and the reactivity of two kinds of metal-ceramic couples are analysed:

- a "*reactive system*"involving an oxidic ceramic substrate, Yttrium Aluminium garnet-$Y_3Al_5O_{12}$, and Ag-based brazing alloys;
- a "*reactive and dissolutive system*" involving a non-oxidic ceramic substrate, SiC, and Al-Ti brazing alloys.

As *reactive* system, the until now unexplored wettability of YAG ($Y_3Al_5O_{12}$) by Ag-based alloys is investigated. The study of this system is aimed at determining the possible use of these alloys in the production of a metal-ceramic joint (Ti6Al4V-YAG) where the transparent YAG is coupled to the metallic support to form a vacuum tight optical window. The term "*reactive system*" identifies a situation in which chemical interactions between the metal and the ceramic part occur without a consistent dissolution and/or bulk structural modifications of the substrate by the liquid metal. In fact, in this kind of systems, the elements of the ceramic substrate are not significantly dissolved and then hardly detected inside the surrounding liquid metal.

As *reactive and dissolutive* system, SiC in contact to Al-Ti brazing alloys is selected.
This non-oxidic ceramic material represents a typical substrate of very high interest for advanced applications such as the aerospace ones.
SiC, when in contact with an Al-Ti alloy, is significantly dissolved by the liquid metal: a relevant amount of Si is found in the whole bulk while the formation of a metal-ceramic layer, containing both Si and C, is promoted at the contact zone, protruding into the bulk liquid phase.

These solid-liquid interactions studies have the aim to set up a consistent knowledge to be used in the design and realisation of metal-ceramic joints.
Moreover, the microstructural characterization of the metal-like phases formed at or through the metal-ceramic interface have a central role in determining the final joint performances. Indeed, the

joints have to be strong, thanks to the good adhesion and to a thermal expansion coefficient value close to that of the ceramic part.

Table 0.1. Metal-ceramic systems investigated during the PhD research.

Systems	Wetting test	Joining test	CALPHAD approach
Reactive	YAG/Ag-based alloys	YAG-Ti6Al4V	Recalculation of Ag-Cu-Ti
Reactive + dissolutive	SiC/Al-Ti alloys	SiC-SiC	Construction of Al-C-Si-Ti database

The characterization, common to both the systems, is based on a combination of two different but complementary approaches:

- An experimental approach that includes: a) the choice of the materials and of the process conditions; b)the execution of high temperature liquid metal-ceramic interaction tests and the production of the metal-ceramic samples; c) the determination of their interfacial microstructure. Before performing the joining process, it is necessary to conduct wettability tests in order to primarily explore the kinetics and the reactivity of the system.

  The composition of the different phases at the interfacial zone as well as the final microstructure of the whole system have been defined by Scanning Electron Microscopy analysis (EDS) and Differential Scanning Calorimetry (DSC).

- A theoretical approach, strictly related to the first one, that uses the CALPHAD method. Thermodynamic calculations have been performed by the Thermo-Calc software in order to guide the choice of the materials to be tested and to better interpret the experimental results. To this end, the metallic Ag-Cu-Ti and the metal-ceramic Al-Ti/SiC systems have been considered. In the first case, different sections of the Ag-Cu-Ti phase diagram have been computed, based on an existing thermodynamic databases; in the second case, literature data from different sources have been combined and adapted into a home-made database. This database has been used to predict the different phases formed during wetting and joining processes, as a function of the process conditions as well as to evaluate, for example, the diffusion path, the activity of the elements in the system and other relevant thermodynamic properties.

From the comparison between experimental results and calculations, different pathways are hypothesized and discussed for the systems under investigation.

Thanks to these combined evaluations it is possible to determine the best process conditions needed to obtain brazed materials to be used in very demanding environments.

Introduction

The design of materials and devices for applications in extreme conditions requests the solution of problems related to basic science (physical chemistry, thermodynamics, physical metallurgy etc.) as well as an appropriate choice of the materials depending on the application (e.g. ceramic systems, superalloys, intermetallic systems and metal-ceramic and ceramic-ceramic structures) and of the material production process (composites, joints, surface coatings etc.). In particular, this complex process should also go through their microstructural, thermomechanical and functional characterization. In general, these materials must have a high melting point, high oxidation resistance, good thermal shock resistance, low thermal expansion coefficient, low vapour tension and good resistance to creep and fatigue. In particular cases, optical transparency is an additional critical property to be preserved. No material combining all these properties is known up to now. For this reason, the most common approach consists in selecting different materials which, synergically, provide the functions of mechanical resistance, thermal barrier, protection against oxidation and so on. Refractory oxides, carbides and borides, most of them members of the family of the Ultra High Temperature Ceramics (UHTCs) [1], are considered as excellent candidates.

The main problem of the joining process is that it is necessary to consider and take into account several kinds of interactions that occur at the interfacial zone of the system (as explained in the next paragraph).

Many techniques can be used to join two solid parts such as, for example, the brazing process (that uses a molten filler alloy to “glue” the two parts), the welding process (that consists in melting the surfaces to be joined) as well as the diffusion bonding process (the two parts, pressed together, remain in the solid state) [2].

Brazing, adopted to realize the joining samples of this work, involves a pure metal or an alloy as filler material. The choice of this material, inserted as a layer between the two parts to be joined, represents one crucial point of the brazing process and it has to take into account different critical points:

- the melting temperature has to be as lower as possible (to obtain a promising brazing process in terms of cost and applications avoiding to damage the substrate);
- the liquid has to wet both the faying surfaces;
- the newly formed phases have to ensure adhesion, to show good mechanical properties and have a melting point compatible with the working temperature of the final devices;

- the new interface has to present a thermal expansion coefficient value close to that of the substrates.

Most of metal-ceramic systems are not wet by liquid metals, so that this point represents one of the main issues of the technique. To overcome this problem it is possible to modify the factors that influence the wettability: in particular atmosphere, temperature, thermodynamic stability of the liquid and solid phases, alloy composition and surface roughness condition of the solid.
This PhD work, develops along the following logical lines:

(a) Understanding the basic concepts of surface thermodynamics and kinetics involving the presence of liquid metallic phases in contact with ceramic substrates;

(b) Selection of the active-elements to be used as wetting "promoters" on the basis of thermochemical principles and verified experience;

(c) Design and execution of specific wettability tests by means of ad-hoc developed experimental set-up;

(d) Analysis, by image processing, of the wettability tests leading to the evaluation of the wetting kinetics and of the final "equilibrium" contact angles;

(e) Definition of the morphology, composition and structure of the interfaces as well as of the reactions occurring at the metal-ceramic contact zone, by different methods of characterization (SEM, EDS, DSC described in *4.3* and *4.4*);

(f) Interpretation of the experimental data supported by the CALPHAD thermodynamic approach (*5.1*). It will be shown that, through the use of thermodynamic models based on the CALPHAD formalism, it is possible to perform thermodynamic calculations that allow the prediction of diffusion paths across ceramic/active-metal interfaces; equilibrium calculations of activity diagrams will be applied to understand the complex interfacial reactions occurring during active metal brazing of ceramic-ceramic and metal-ceramic joints.

(g) Production and characterization of metal-ceramic joints (YAG-Ti6Al4V) and a first exploratory work on the realization of brazed SiC-SiC joints.

In particular, the wettability and joining experimental procedures as well as the thermodynamic evaluations have been conducted at CNR-ICMATE laboratory in Genoa.

In addition, an important part of the thermodynamic and reactivity evaluations of the non-oxidic system (SiC/Al-Ti alloys) has been conducted at Claude Bernard University of Lyon.

1. Basics of High Temperature Wetting (HTW)

1.1 The surface tension

Before defining the rules of a wetting process some basic definitions of the main interfacial parameters are needed.

When two immiscible fluids are in contact and maintained at a temperature below the critical one, result separated by a thin layer known as **interface** whose properties are different from those of both the adjoining bulk phases.

The surface tension σ_{LV} is defined by Gibbs (1875-1987)[3]as the work needed for a reversible creation of an additional surface of a liquid L in contact with vapour V:

$$\sigma_{LV} = \left(\frac{\delta F}{\delta \Omega}\right)_{T,V,n_i} \qquad (1)$$

where F represents the total free energy of the system, Ω the surface area, T the temperature, V the volume and n_i the number of moles of component i.

It is possible to visualize the surface tension acting between the phases A and B: an AB line may be imagined to divide the interface into two regions (*Figure 1.1*).

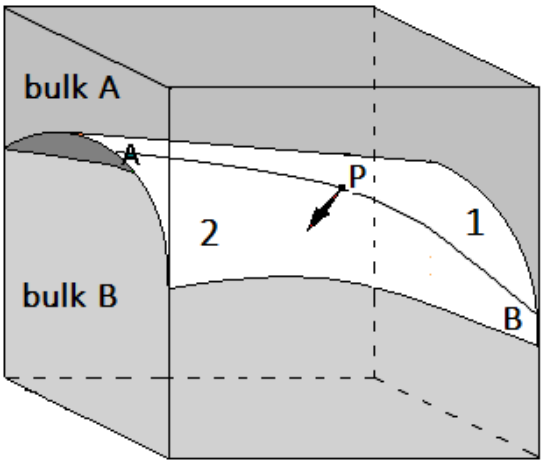

Figure 1.1. Schematic visualization of AB interface

If region 2 is "ideally" eliminated, in order to maintain the system at equilibrium, it is necessary to apply a tangential force at the AB line: the surface tension (or interfacial tension)σ_{12}represents this force per unit length at any point P of this line.

The dimension of σ_{LV} is force per length; it is then measured in N/m (or, more often, in mN/m).

Let's take a non-planar interface between a vapour V and a liquid L phase (*Figure 1.2*): each point of this surface is subject to this surface tension σ_{LV} and to the external (p') and internal (p'') pressures at each surface point.

The balance of all the forces acting in z direction, leads to the Laplace equation:

$$p'' - p' = \Delta\rho g h - \sigma_{LV}\left(\frac{1}{r_1} + \frac{1}{r_2}\right) \qquad (2)$$

where r_1 and r_2 are the principal radii of curvature of the surface at the point considered, $\Delta\rho$ the density difference of the two phases, h distance from the point 0.

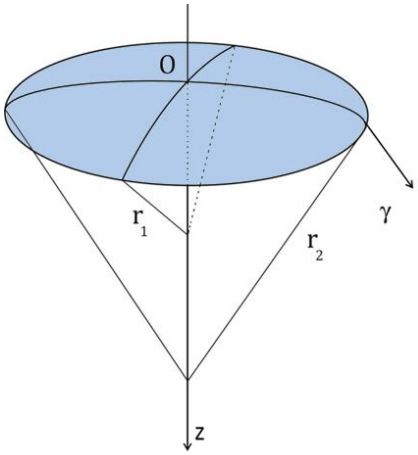

Figure 1.2Schematic representation of Laplace equation parameters.

It is important to remember that the Laplace equation cannot suppose how p' and p'' vary, but just puts these quantities in relation to the surface tension and the curvature radii at each interface point.

If there gravitational effects can be neglected, as in microgravity conditions or when dealing with iso-dense fluids ($\Delta\rho \cdot g = 0$), p'' and p' in the two phases are uniform, the two main radius of curvature are the same at each surface point and equation 2 reduces to equation 3:

$$p'' - p' = \frac{2\sigma_{LV}}{r} \qquad (3)$$

Then in this case the surface has a spherical symmetry.

When dealing with solids, the definition of surface tension becomes a more complex topic as, in this case, in particular mechanical stresses, anisotropy of the crystalline structure and surface defects have to be taken into account [4]–[6].

1.2 The contact angle

In this work, the wettability evaluation of a ceramic substrate by a liquid metal and the reactivity evaluation of this system represent the first and necessary steps that guide the choice of the materials and the process parameters of the brazing procedures.

The contact angle θ is the most used parameter defining the wettability of a substrate by a liquid, in our case a pure metal or an alloy.

The contact angle value is related to the nature of the different interfaces (liquid-gas, solid-liquid and solid-gas) and represents a clear and suggestive measure of the liquid ability to wet a solid surface.

A schematic representation of a wetting (θ<90°) and non-wetting system (θ>90°) is given in *Figure 1.3(a)*. Moreover, the phenomena occurring at the solid-liquid interfacial zone of a three phase system (solid, liquid, gas) at equilibrium condition along the Triple Line (TL) is shown in *Figure 1.3(b)*.

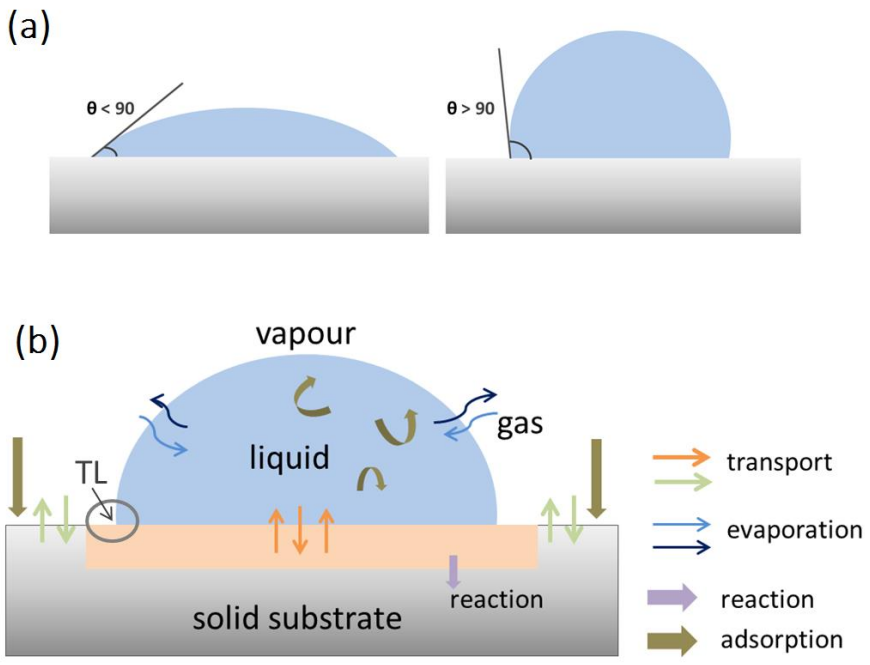

Figure 1.3Schematic representation of wetting and non-wetting systems and of phenomena at solid/liquid interphase (b)

To connect the contact angle to the surface tensions of the system the Young equation [7] is introduced:

$$\cos\theta = \frac{\sigma_{SV} - \sigma_{SL}}{\sigma_{LV}} \qquad (4)$$

where σ_{SV}, σ_{SL}, σ_{LV} represent, as usual, the solid-vapour, solid-liquid, liquid-vapour surface tensions and θ the contact angle at the triple line (TL).

As suggested by Dupré [8], the surface tensions can be related to the "Work of adhesion", a quantity describing the reversible work to separate a solid-liquid interface into solid-vapour and liquid-vapour interfaces.

In the Dupré equation (6) "σ" represents the work to create a new interface of unit area:

$$W_a = \sigma_{LV} + \sigma_{SV} - \sigma_{SL} \qquad (5)$$

Combining equation (4) and (5) the Young-Dupré equation is obtained allowing to express the Work of Adhesion in quantities accessible and measurable from sessile drop tests:

$$W_a = \sigma_{LV}(1 + \cos\theta) \qquad (6)$$

From this equation it is possible to deduce that the equilibrium contact angle, resulting from liquid metal-solid phase contact, emerges from the competition among two different kinds of forces: the adhesion and the cohesion ones.

Formally, when θ< 90°, the surface is considered wettable by the liquid; not wettable when θ> 90°.

Usually, to define easily the wettability of a system, the "wettability coefficient" K is utilised:

$$K = \frac{\sigma_{SV} - \sigma_{SL}}{\sigma_{LV}} \qquad (7)$$

If $K \geq +1$ the solid is completely wet by the liquid while if $K \leq -1$ the solid is not wet. When $-1 \leq K \leq 1$ the solid it is partially wet, and $K \equiv \cos\theta$.

If we consider then the equation (4), we can see that the wettability of a liquid depends on the difference $\sigma_{SV} - \sigma_{SL}$. It is clear that if we want to increase the system wettability, first of all this difference should be negative (e.g. by decreasing σ_{SV}) and then, decreasing also σ_{LV}, cosθ can be made to approach -1 (i.e. θ=0°) defining the ideal situation of "perfect wetting".

Contact angle θ= 0° means that the liquid covers completely the solid surface $\sigma_{SV} \geq \sigma_{SL} + \sigma_{LV}$.

If the contact angle is 180° the liquid does not wet at all the solid ($\sigma_{SL} = \sigma_{SV} + \sigma_{LV}$).

1.3 The interfacial phenomena

To be able to design new joining processes through brazing it is fundamental to define and characterize the different kinds of interactions that occur when the molten metal and the solid substrate are in contact, known as “wetting phenomena”.

Their characterization allows us to understand how well the liquid wets the ceramic substrate, how to control the interfacial reaction, the interplay between liquid and solid chemistry as well as the interfacial energetics.

Interaction phenomena involving wetting, reaction and dissolution become extremely relevant at high temperatures, as this aggressive environment [3], [9] is characterized by high atomic mobility, very active diffusion processes and strong chemical reactivity between the different phases, due to the large amount of chemical energy that comes into play.

In order to understand the interfacial interactions in such conditions, the following processes must be taken into consideration (*Figure 1.3*)*:*

a) dissolution of the solid into the liquid;

b) penetration/diffusion of the liquid components into the solid;

c) adsorption of components of the liquid or the vapour phase at the solid-liquid or liquid-vapour interfaces;

d) reaction of some components of the liquid with the solid and formation of new phases;

e) dynamic restructuring of the solid surface.

The exchange of chemical species can modify the surface tensions of the liquid-vapour, solid- liquid and solid-vapour interfaces, and, as a consequence, of the contact angle θ as described by the Young equation (4).

A system reaches the (mechanical) equilibrium condition when the resulting action of the solid/gas and solid/liquid interfacial tensions, is able to balance the force $\sigma_{LV}\cos\theta$.

Equation 4 in [10], [11] is justified on the basis of a thermodynamic approach.

However this approach does not consider the vertical components of the surface tension but only the one that is parallel to solid surface[11]. Thus equation 4 is strictly correct for undeformable solid surfaces, whose rigid reaction compensate the vertical component $\sigma_{LV}\sin\theta$.

Indeed, it was proven that, in general, the deformation of the solid surface at the triple line TL region is also influenced by the vertical component of the surface tension.

When working with non-rigid substrates, it is possible to identify two main possibilities: a) the solid is easily deformable, b) the solid can be partially dissolved.

In general, in the presence of three immiscible phases (e.g. liquid 1, liquid 2, vapour), the equilibrium condition at the TL should be evaluated by considering the horizontal and vertical components of the three vectors , e.g. it can be shown that the equilibrium condition is described by the equation:

$$\frac{\sin\theta_3}{\sigma_{LV}} = \frac{\sin\theta_2}{\sigma_{SV}} = \frac{\sin\theta_1}{\sigma_{SL}} \qquad (8)$$

where θ_3, θ_2, θ_1 are the dihedral angles in the solid, liquid and vapour phases respectively (*Figure 1.4*).

In the case of important solid dissolution, local irregular curvatures (known as “non-Laplacian”) and ridges of micrometric size are found at the TL line of the solid-liquid contact zone [12]–[16].

When the contact angle value is constant, the system is considered to be at equilibrium.

However, some factors as roughness, chemical reactions or structural inhomogeneity do not allow to use the equation of Young to obtain the “true” equilibrium contact angle value of the system. In fact, in this case an “advancing” or “receding” behaviour of the triple line is observed due to complex hysteresis phenomena.

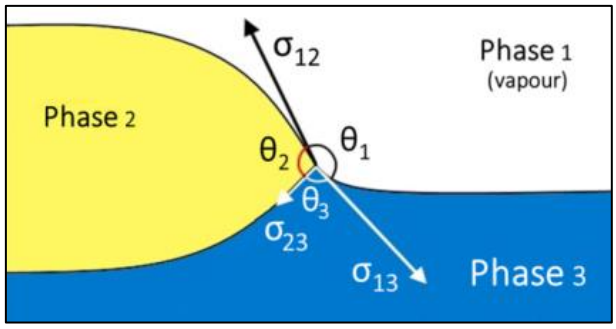

Figure 1.4. Equilibrium configuration in the presence of dissolution of the solid.

2. Kinds of wetting process

It is possible to identify two main categories of wetting processes: non-reactive wetting (*2.1*) and reactive wetting (*2.2*).

2.1 Non reactive wetting

Non-reactive wetting is reached when the interplay of the three interfacial tensions allows a low contact angle to be established and, at the same time, the following conditions occur:

a) no chemical reactions take place between the liquid and solid phases;

b) the solid and the liquid phases are mutually immiscible;

c) the liquid phase is in chemical equilibrium with the solid one (i.e. it is saturated of the solid elements).

It is important to underline that it is possible to have these conditions in particular when the temperature is not high enough to allow a fast exchange of atoms through diffusion between the solid and the liquid phase.

The intrinsic contact angle in a non-reactive solid-liquid system, according to the Young-Dupré equation (6), results from the competitions of two forces:

- the adhesion forces between the liquid and the solid phases, expressed by the quantity of adhesion energy;
- the cohesion forces of the liquid related to the surface energy of the liquid σ_{LV} acting in the opposite direction (the cohesion energy of the liquid is roughly equal to $2\sigma_{LV}$). Usually liquid metals, due to their metallic bonding, are high surface energy liquids.

According to the Young-Dupré equation (6) then, good wetting of a liquid metal on a solid substrate can be reached only if the interfacial bond is strong as can be a metallic one.

This condition is fulfilled in case of liquid metals on solid metals as well as with liquid metals on semi-conductor substrates as Si, Ge or SiC [17].

It is important to remind that, even with wettable solids, the contact angle value can be influenced by the presence of wetting barriers on the substrate surface such as the formation of oxide films[18]. Examples of non-reactive wetting systems are reported in *Table 2.1*.

It is important to underline that the spreading rate of a non-reactive system is controlled by viscous flow and described by a power function of triple line velocity U versus the instantaneous contact angle θ ($U \approx \theta_n$).

Table 2.1. Wetting of different types of solids by non-reactive liquid metals at temperatures close to the metal melting point. The contact angle values are from the Eustathopoulos et al [10].

Substrate	Type of interaction	θ (degrees)	Examples
Solid metals Semiconductors Ceramics with a partially metallic character	Strong (chemical)	θ << 90°	Cu/Mo: 10°–30° Sn/Ge: 40°; Si/SiC: 35°-45° Cu/WC: 20°; Au/ZrB_2: 25°
Carbon materials Ionocovalent ceramics	Weak (physical)	θ >> 90°	Au/C: 120°–135° Ag/Al_2O_3, Cu/SiO_2: 120°-140°; Au/BN: 135°-150°
Ionocovalent oxides	Moderate (chemical)	θ ≈ 90°	(Ag+O)/Al_2O_3; Al/Al_2O_3

The Ni-Si/SiC system offers an interesting example of the possible transition from a dissolutive-reactive wetting regime to the non-reactive one. Liquid Ni in contact with SiC dissolves the substrate and forms Ni silicides. However, if the Si content in the Ni matrix reaches values above 40%, i.e. Ni is saturated in Si, the equilibrium is established between the Ni-Si alloy and SiC; indeed, one can see (*Figure 2.1*) that the resulting solid-liquid interface in Ni-56Si/SiC system is smooth and clean without any precipitates also in the region close to the triple line [18].

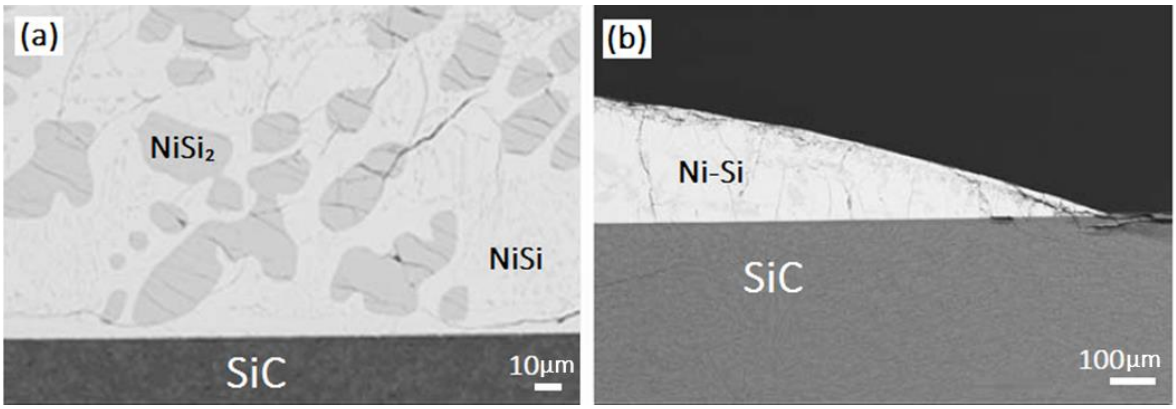

Figure 2.1. Cross-section SEM micrographs of Ni-Si/SiC system [18].

2.2 Reactive wetting

The interactions in metal/ceramic or metal/metal systems, due to the high temperatures reached, are usually considered as "reactive wetting": the interactions occurring at the solid-liquid interface can produce the dissolution of the substrate into the liquid phase and/or the formation of new compounds typically in the form of a more or less compact layer at the solid-liquid interface. Considering these two different phenomena, the reactive wetting can be classified as: dissolutive wetting (par. *2.2.1*) and wetting with formation of a new compound at the interface (par. *2.2.2*).

The final equilibrium configuration, in the presence of reactions, is determined by the formation of continuous layers of specific reaction products, such as the M_6X metal-like compounds in metal-oxide systems [19], [20], [21], or in case of wetting of carbides [22].

The nature of the new compounds is related to the chemistry of the system and to the kinetics of the advancement of the triple line. In some cases, the presence of even a small amount of certain elements in the liquid is determinant to promote the interfacial reactions. Indeed, the activity of these elements in the liquid phase under the given experimental conditions determines the formation of new compounds through heterogeneous nucleation at the S/L interface. This can happen just when a certain amount of super-saturation in the liquid phase is reached. For this reason, some elements as Ti, Zr, Cr,V, Nb, Al are called "active elements" and are utilised as alloying elements at low concentration in the brazing process [23], [24].
Moreover, it is important to take into account that when a continuous layer of the new compound is formed at the S/L interface, the transport of the atoms necessary to sustain the reaction must occur through the layer by solid-state diffusion, with consequent substantial reduction of the growing rate of this same layer.

2.2.1 Dissolutive wetting

The dissolution of the solid into the liquid phase is caused bythe high atom mobility occurring at high temperature driven by the activity gradient of the diffusing species across the interface.
Dissolutive wetting is a common phenomenon in liquid metal/solid metal systems but it is also relevant in some metal/ceramic systems such as Ni/SiC [25], Ni/HfB_2 [26] and AuNi/ZrB_2 [27],

CoTa/graphite system [28]. In these cases wetting is accompanied by dissolution of the solid into the liquid with formation of a macroscopically non-planar solid/liquid interfacial zone [29].
Even if no reactions occur, the composition of the liquid phase changes with time so that the dissolution process can produce: a decrease of the surface tension of the liquid (in general, when the surface tension of the diffusing solid component is lower than the surface tension of the liquid); the formation of a crater under the droplet modifying the contact angle geometry; the formation of new solid phases/precipitates during the cooling process.

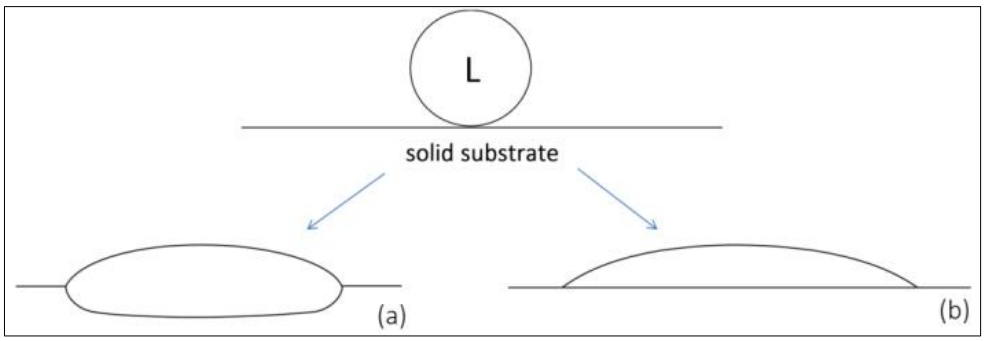

Figure 2.2. Schematic representation of two cases of dissolutive wetting . Dissolution of the solid modifies the geometry of the triple line (a); slight dissolution modifies the surface energies of the system but the solid substrate/L interface remains macroscopically planar (b).

In the first situation (*Figure 2.2(b)*), a negligible dissolution of the solid phase into the molten matrix may also occur until the chemical potential of the diffusing species is the same in both the phases [17], [30]–[34]. A modification of the surface energies of the system occurs even if the solid/liquid interface remains macroscopically planar (*Figure 2.2(b)*).

In the second case (*Figure 2.2(a)*), the dissolution of the solid into the liquid is assumed not only to change significantly the surface and the interfacial energies (σ_{LV}, σ_{SL}) but also the geometry at the triple line making the use of the Young law subject to cautions application.

According to the approach of Warren [29] when a droplet of pure B is placed on pure solid A, different steps can occur, having different time scales, in order to reach the equilibrium:

- a non-reactive spreading occurs in a short time t_1 (considering t_1 more or less equal to 10^{-2} sec) (*Figure 2.3 (b)*); during this step, the dissolution does not significantly modify the system geometry that can then be considered near to the Young contact angle configuration.

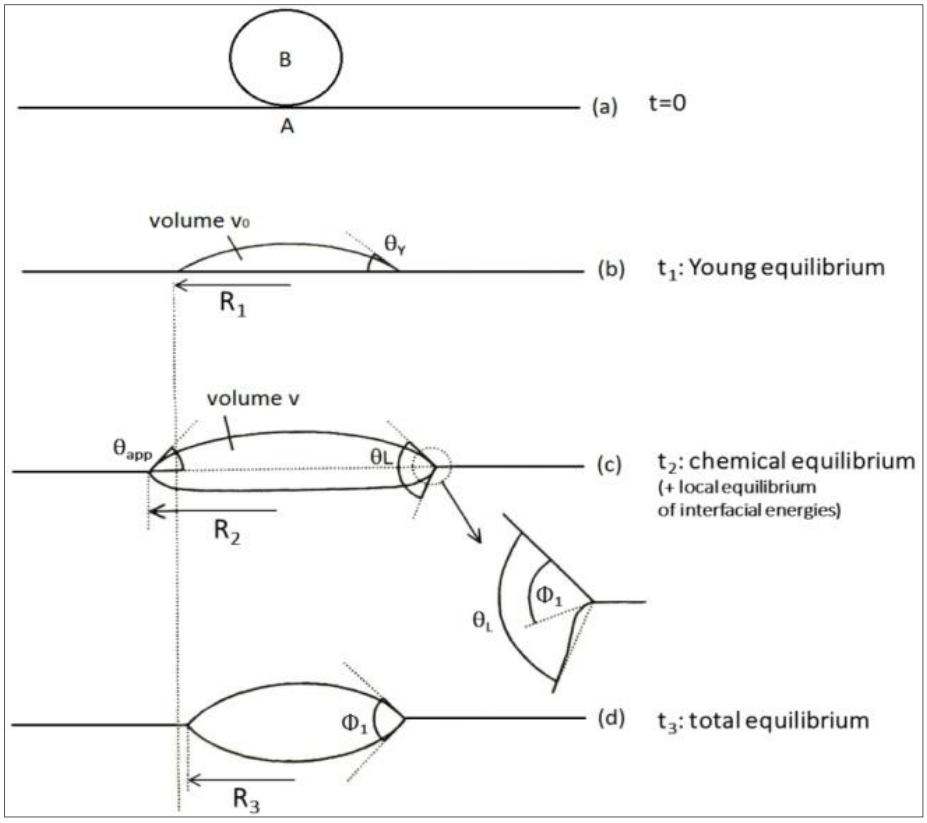

Figure 2.3. Schematic representation of dissolutive wetting steps.

- dissolution of the solid into the liquid phase takes place (t_2) and this fact produces the modification of the planar configuration (*Figure 2.3 (c)*): this is followed by diffusion, driven by differences of the activity of the diffusing element(s) in the adjacent solid and liquid phases. The changes of morphology with time were calculated by Warren (1998) by considering that the microscopic dihedral angle at the triple line is given by the Smith equation (8) (assuming that the triple line remains on the plane of the substrate).

The surface tension changes and a dynamic condition is set up, where both contact angle and drop dimensions (base diameter, height and also volume) are a function of time. The solid-liquid interface does not lie anymore on a plane, but a groove under the drop forms in general with a nearly spherical profile or a "sigmoidal" shape [26]:

- at much longer times (t_3), it is possible to observe that the shape of solid/liquid interface changes and assumes a uniform curvature.

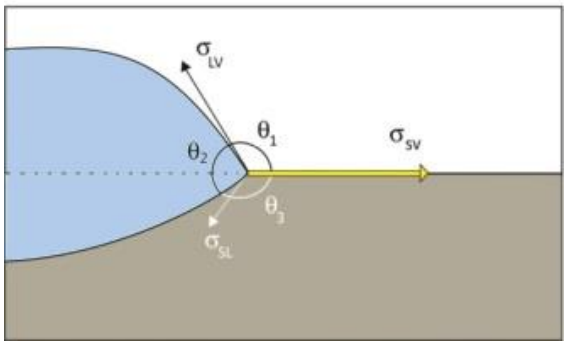

Figure 2.4. Equilibrium configuration in the presence of dissolution of the solid.

Thus, in this case, what is measured in a sessile drop test is the "apparent" contact angle, that is the one "above" the plane defined by the solid surface (i.e. π-θ_1 in *Figure 2.4*). This point is extremely important when interpreting sessile-drop results, as any quantitative utilization of contact angle data, especially to derive thermodynamic quantities such as the work of adhesion, should take this effect into serious consideration.

As an example also reported literature [35], it is possible to mention the Ni-Al_2O_3 system, where ridges and grooves of the nanometre size form at the solid-liquid interface close to the triple line (*Figure 2.5*).

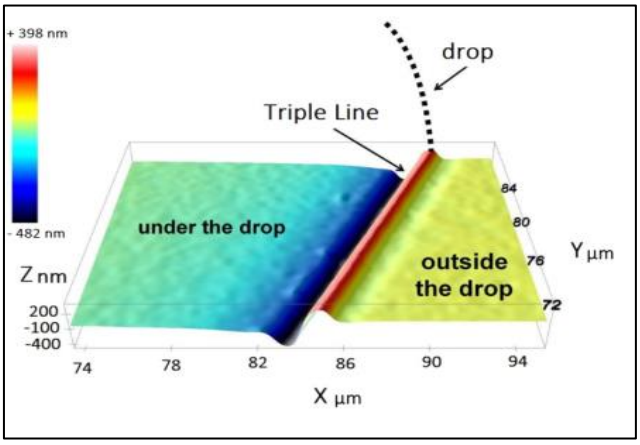

Figure 2.5. 3D confocal profile of the surface of sapphire after contact with molten Ni at 1500°C and removal of the drop. The scan reveals the presence of a ridge located at the triple line junction (h ≈ 250 nm) , and of deep groove (depth ≈ 400 nm) adjacent to it (Courtesy F. Valenza).

2.2.2 Formation of 3D compounds

As underlined before, reactive wetting occurs when the interfacial reactions produce the formation of 3D dense layers as solid reaction products.

The chemical interactions developed at the solid-liquid interface, producing new species, modify the wetting behaviour of the whole system because the new products have different interfacial energies and thus different wetting characteristics.

In fact, the nature and the distribution of these new phases, produce differences in terms of the spreading rate and final contact angles.

Different approaches aim at defining and interpreting how the reactive wetting with formation of 3D compounds take place.

A simplified explanation is reported here. It is important to underline that reaction products can be more wettable or less wettable than the substrate [36].

The first case is the more common and the one we observe in the systems investigated in this Thesis.

In particular, two configurations, one stable and the other metastable, can be produced at the triple line when the final contact angle θ_F is reached.

The stable configuration occurs when a layer of reaction product P forms extending on the free surface of the substrate S (*Figure 2.6*).

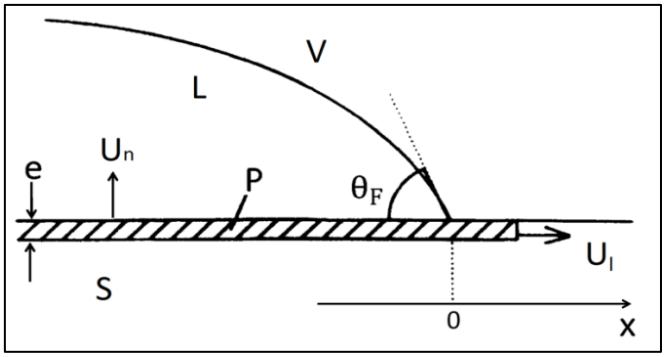

Figure 2.6. Schematic representation of the stable configuration of a reacting system at the solid/liquid/vapour triple (more wettable products case).

Neglecting any effect of roughness of the reaction layer, θ_F is simply given by the Young equation (4) applied to the P/L/V system:

$$\cos\theta_F = \cos\theta_P \cong \frac{\sigma_{PV} - \sigma_{PL}}{\sigma_{LV}} \qquad (9)$$

in which θ_P represents the equilibrium contact angle on the reaction product P.

In the metastable configuration the reaction product layer does not extend beyond the edge of the drop (*Figure 2.7*).

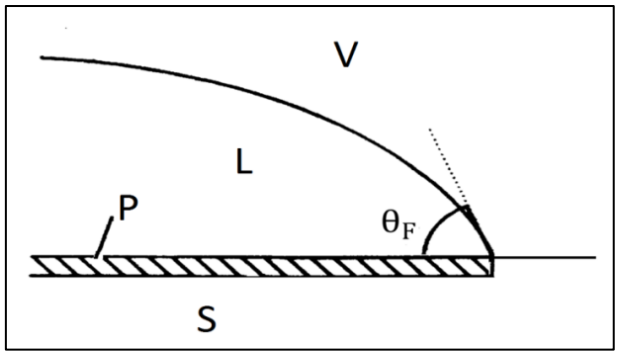

Figure 2.7. Metastable configuration of the reaction product layer.

The final contact angle, calculated considering the effect of a small displacement of the triple line around the equilibrium position, is:

$$\cos\theta_F \cong \frac{\sigma_{SV}-(\sigma_{SP}+\sigma_{PL})}{\sigma_{LV}} \qquad (10)$$

Reaching the configuration of *Figure 2.7* is possible if the extension of the reaction layer outside the P/L interface is blocked by thermodynamic barriers.

The size of the barriers can be calculated by considering the change of the Gibbs energy G per unit length of the triple line produced by a lateral extension δx of the reaction product layer outside the drop , thus:

$$\delta G = \Delta G_V e\delta x + (\sigma_{PV} + \sigma_{PS} - \sigma_{SV})\delta x = \Delta G_V e\delta x + \Delta\sigma\delta x \qquad (11)$$

Where ΔG_V is the Gibbs energy of the reaction per unit volume of P. Setting $d(\delta G)/d(\delta x)=0$, a critical layer thickness (e*) is obtained such that: $e^* = \Delta\sigma/\Delta G_V$.

For e>e*, no thermodynamic barrier to the extension of reaction product outside the drop exists, while if e<e*, the configuration of *Figure 2.7* showing a metastable equilibrium, is possible. Considering typical values $\Delta\sigma$ = 1 $Jm^{-2}$and $|\Delta G_V|=10^9$ to 10^{10} Jm^{-3}, the value of e* is of the order of 1nm.

The common values of $e^*$are too low to create a true barrier to the formation of product P outside the drop.

So, except for very high Δσ values or very low $|\Delta G_V|$ values, thermodynamic barriers to the lateral growth of P on the substrate free surface are unlikely. When the stable configuration (*Figure 2.6*) of reactive wetting is obtained, the P layer growth goes on, both inside the liquid, by diffusion through

the P layer, and over the substrate free surface, for example by evaporation/condensation or by surface diffusion.

Moreover, so far as this growth does not produce any significant change of liquid composition, the final contact angle (θ_F) reported in the equation (10), remains nearly constant with time.

Among the several metal/ceramic systems that produce formation of more wettable or less wettable interfacial layers, we can mention the ones reported respectively in [37] and [38].

In the first case the Au-Ti alloy was tested in contact with Al_2O_3: while pure Au does not wet Al_2O_3 (at 1150°C), the addition of 6 at% of Ti decreases the contact angle to 69°, forming an interfacial layer of Ti_2O_3, more wettable than Al_2O_3.

In the second case, the work of Landry et al demonstrates that the addition of 1 at% of active element (Cr here) promotes wetting of Cu on graphite. In fact a continuous, metal-like and wettable layer of Cr_7C_3 extends at the liquid-solid interface (*Figure 2.8*).

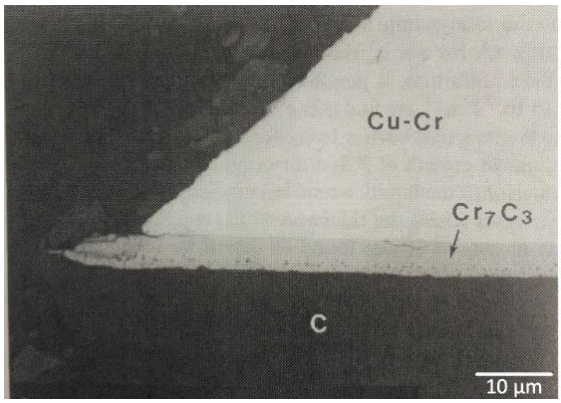

Figure 2.8. SEM micrograph of cross-section of the interface of a Cu-Cr alloy on vitreous carbon cooled from 1100°C [38].

2.3 The Brazing process: its relation to capillarity

Brazing is a kind of liquid based process where two solid materials are joined using a liquid alloy as connecting material.

In the presence of good wetting, the liquid can easily infiltrate the interface zone (capillary gap) avoiding the use of high pressure and allowing to limit the surface preparation as well as to join also not flat materials.

The alloy, the "filler", should have a melting point conventionally higher than 450°C and lower than that of the two components of the joint. Below 450°C we speak of "soldering".

Brazing can be used to join metal to metal, metal to ceramic and ceramic to ceramic and in all cases the two pieces can be assembled using different configurations (*Figure 2.9*).

The choice is related to the specific application but in all cases it is necessary to include a narrow capillary space placed between the two parts; this space will be filled by the brazing alloy [39]–[41].

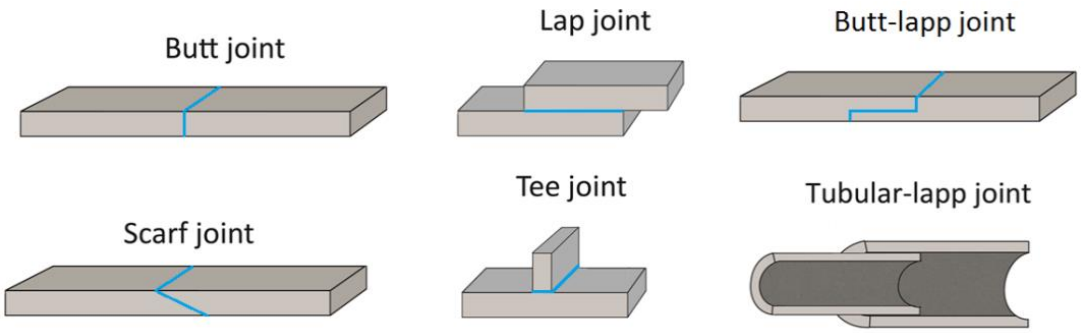

Figure 2.9. Six different kinds of joint configurations.

The filler material, applied outside the joint rim to exploit the capillary gap penetration or inserted between the two pieces as a thin foil or as a paste, melts during the joining process allowing the formation of different configurations in terms of contact angle and assembly (*Figure 2.10*(d)).

It is possible to consider configurations in which the angles formed between the liquid and the solid are above or below the limit of 90° (*Figure 2.10*(a-c)).

This first case (*Figure 2.10* (a)) shows a situation of non-wettability in which the liquid phase remains mainly located in the capillary gap.

Then applying an external pressure, bigger than the "Laplace pressure" due to the curvature (equation 3),it is possible to obtain the formation of the contact angles θ_1 and θ_2 between the liquid and the solid parts:

$$p_{ex} > \sigma_{LV} \frac{(\sin\theta_1 - \cos\theta_2)}{\Delta} \qquad (12)$$

where Δ and σ_{LV} are respectively the width of the gap and the liquid-vapour surface tension.

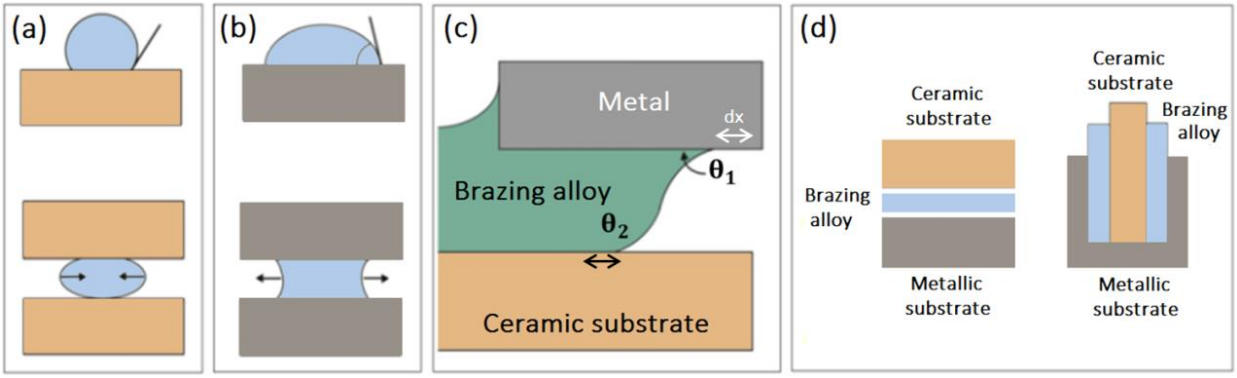

Figure 2.10. Effect of contact angles on the wetting and capillary penetration.

Considering the Laplace equation, we can conclude that under the condition of equation (12), the external pressure applied p_{ex} can squeeze the liquid out of the gap allowing the formation of a continuous layer that represents the joint interface after the solidification process.

It is possible to consider a second configuration in which the liquid wets the two surfaces. In this case the Laplace pressure acts inside the liquid phase pushing the liquid to fill the space between the two components to be joined (*Figure 2.10*(b)). This is the ideal case of capillary penetration.

In the third configuration, the general case of capillary penetration is represented: the filler material is located outside the gap and when it melts it penetrates inside the capillary gap thanks to the surface tension forces. This is straight forward when the contact angles between the liquid and the two solid surfaces are both less than 90°. If the contact angles reach different values, some different considerations are needed. For example, considering a metal-ceramic system, it is known that there is a significant difference between the way the liquid wets the ceramic part and the metallic part; in fact, very often, the wettability of the ceramic part is poor.

Let's consider the capillarity gap, avoiding to take into account the influence of gravity.

Generally, when a liquid enters into the capillary gap, the free energy variation for an elementary displacement *dx* of the solid-liquid interfaces has to be negative (or 0 at equilibrium (*Figure 2.10*(c)):

$$dF = dx(\sigma_{SL} - \sigma_{SV})_m + dx(\sigma_{SL} - \sigma_{SV})_c \leq 0 \qquad (13)$$

where σ_{SL} and σ_{SV} represent the solid-liquid and solid-vapour energies per unit area of the liquid-metal at the metal and ceramic interfaces respectively.

Combining equation (13) with the Young equation (4), applied to both the liquid-metal and liquid-ceramic interfaces, we get:

$$\frac{dF}{dx} = \sigma_{LV} (\cos\theta_1 + \cos\theta_2) \leq 0 \qquad (14)$$

which, recalling that $(\cos\theta_1 + \cos\theta_2) = 2\cos[(\theta_1 + \theta_2)/2]\cos[(\theta_1 - \theta_2)/2]$, being $\cos[(\theta_1 - \theta_2)/2]$, we are left with the condition: $\cos[(\theta_1 + \theta_2)/2] \leq 0$ i.e. $[(\theta_1 + \theta_2)/2] \leq \pi/2$, that is $(\theta_1 + \theta_2) \leq 180°$.

This simple condition is valid when ideal surfaces are taken into account.

Considering a metal-ceramic couple, the metallic part is well wet by the liquid filler (this means that generally $\theta_1 < 50°$). Thus the liquid may enter and spread into the gap even if the ceramic substrate is not well wettable ($\theta_2 > 90°$).

However, it is important to add that the non-ideal conditions of the surfaces forming the capillary gap(such as the roughness, for example) can lead to situations where hysteresis phenomena with advancing contact angles well larger than the equilibrium ones, obstruct the capillary penetration, or, on the contrary, the presence of longitudinal grooves increase the liquid metal penetration.

3. Materials

3.1 $Y_3Al_5O_{12}$-alloys-Ti6Al4V system

In this thesis, transparent ceramic windows made of sintered YAG ($Y_3Al_5O_{12}$) brazed to Ti6Al4V supports have been studied as potential candidates in the marine applications mentioned before. This is due to their transparency, good mechanical properties and to the outstanding corrosion resistance of the individual components. Indeed, Ti6Al4V exhibits an exceptional erosion-corrosion resistance [42], [43], a high fatigue strength in air [44]–[46], as well as in chloride environments [47]and a low coefficient of thermal expansion. This improves the interface compatibility with the ceramic counterpart.

In this work, a comparison was performed between joints produced using filler alloys with or without an active element in order to capture the differences in terms of interface reactivity and to find some possible suggestions to be adopted in the potential industrial process.

Indeed, to avoid the use of an active filler material could allow a simplification of the process and test the spontaneous Ti migration from the Ti6Al4V bulk to the interfacial zone promoting wettability and adhesion.

Very dense, polycrystalline YAG materials are characterized by a good grade of transparency that makes them suitable for different applications that can involve the necessity of a brazed window. In this case, the capability of the ceramic part to maintain its transparency after the joining process and when employed in the working environment (e.g. in marine water) represents a necessary requirement.

Many other fields need these particular materials; atomic physics and frequency metrology applications, for instance, require nonmagnetic optical windows for ultra-high vacuum chambers; in this context sapphire and titanium joints were obtained by Ag-Cu-Ti brazes [48].

Jacobs et al. have analysed the silica/PbAg/304 stainless steel interfaces, a material potentially required for various plasma diagnostic systems in the ITER vacuum vessel [49].

Gustarov has investigated how an ITER simulated environment can influence the mechanical stability and the optical characteristics of prototype windows assemblies in which Si_3N_4, silica and sapphire are the transmission elements bonded or brazed to a stainless steel or Ti ferrule. They found that the bonds at ceramic-metal interfaces remained leak-tight after irradiation and thermal cycling [50].

A thorough investigation on transparent and gas-tight optical windows in low-temperature co-fired ceramics (LTCC) was conducted recently [51]. Thin glasses (borosilicate glasses and fused silica) were bonded by thermo-compression in an LTCC substrate in order to obtain materials used as optical analysis systems, for innovative applications such as observing chemiluminescent reactions. Laser welding techniques for glass–glass and glass-metal joining have recently been considered, including hermetic sealing applications [52].

Reactivity and wettability data regarding the YAG/AgCuTi system are not available from literature, even if the wetting behaviour of other ceramic substrates by AgCuTi has been already widely investigated. Generally, the filler alloys used for joining dissimilar materials contain an active element such as Ta, Nb, Zr, V or especially Ti [23], [24], [53], [54], [55] that promotes wetting of the ceramic surface and chemical bonding with the metallic member of the joint by adsorbing at/or reacting with the ceramic oxide.

For the brazing of Al_2O_3, SiC, and Si_3N_4 with AgCuTi active fillers, many research efforts have shown that Ti additions to fillers can react with Al_2O_3, SiC, and Si_3N_4 to form titanium oxides [56], titanium silicides [57], titanium carbides [57][58][59] and titanium nitrides [60], respectively.

For example, materials such alumina [61], [62] or zirconia stabilized with yttria [53] have been studied and discussed. Voytovytch et al. [63] found that droplets of AgCu alloys without Ti do not wet alumina substrates. At 900°C they form contact angles much higher than 90°, a typical value for noble metal/oxide systems; while additions of 3 to 8 at% of Ti allow a drastic decrease in the equilibrium contact angle down to about 10°, a value typical of metal/metal systems. In this specific case the improved adhesion and the wettability of the alumina substrates have been attributed to the formation of a TiO_x and Cu-Ti-O layer at the interface [20], [64].

The work of adhesion of liquid metals on oxides increases with increasing of the metal affinity for oxygen, i.e. with decreasing of the oxide standard free energy of formation; in the case of molten binary alloys, for example, a strong adsorption of the more electropositive metal takes place at the solid-liquid interface (ex. titanium in Ni-Ti alloys).

Wettability and work of adhesion then increase with decreasing the metal-oxygen bond strength in the oxide phase; this increased interaction is often correlated to a partial dissolution of the oxide into the molten metallic phase. The Work of Adhesion is a function not only of the liquid metal interaction with the oxygen in the oxide, but also of the interaction and dissolution of the oxide forming metal into the metal matrix.

The metallic materials (as AgCuTi, AgCu, AgTi, Ag, Cu) tested in contact to YAG and also to both YAG and Ti6Al4V (as AgCuTi, AgCu, Ag) are evaluated in terms of wettability [65] and reactivity do define the capability of the system to form an adherent interface layer [66].

Titanium is the active element mostly chosen among the several active elements known [67]–[71].

The eutectic composition of the system Ag–Cu (T_m= 780°C) is widely used as a basis for brazing alloys because it is relatively ductile and therefore able to limit the stresses arising between two materials with different thermal expansion coefficients.

The wettability and the role of Ti in Ag-Cu liquid braze have been discussed by many researchers [67], [70], [72]–[74].

Paulasto et al. [75] found and confirmed the existence of a miscibility gap which divides the liquid phase into solutions of low and high Ti content in the Ag–Cu–Ti system above a certain temperature; they also found that the Ti activity varies by changing the metal ratio Ag/(Cu + Ag).

Nicholas et al. [76] concluded that the wettability of a ceramic surface (Al_2O_3 or SiC) by Ag–Cu–Ti brazing alloys would be improved by increasing the Ag content, because of the low solubility of Ti in the Ag.

The thermodynamics of Ti in Ag-Cu-Ti alloy using solid electrolyte sensors was evaluated by Pack et al. [77]; they found that the activity coefficient of Ti showed a positive deviation from an ideal solution behaviour at 1000°C in the Ag–Cu eutectic system. It was also found that the activity coefficient of Ti in Ag–Cu melts [78] decreases with the increment of Cu concentration and increases with a higher Ag concentration. Moreover at variance with the segregating interactions between Ag and Cu, both the Ag–Ti and the Cu–Ti systems exhibit high negative values of the heat of mixing leading to spontaneous heteroatomic coordination, which is reflected in intermetallic compounds formation. This fact allows these systems to be classified as compound-forming [79].

3.2 SiC-AlTi alloys system

Among carbides, SiC has a great technological significance due to its good thermal, chemical and mechanical properties. SiC is often used as matrix or reinforcing phase in ceramic matrix composite materials [80] (e.g. SiC_f/SiC, C_f/SiC, ZrB_2/SiC, etc.) to be used in many high-temperature applications such as in aerospace, nuclear plants, gas turbines, heat exchangers, automotive components [81]–[83]; in the specific case of aerospace field, the ceramic bodies should constitute the shield for the metal structure [84],[85].

Therefore, joining of SiC to itself or to special alloys by using high temperature liquid phase bonding techniques, can lead to optimized highly performing applications and to overcome existing mechanical fastening methods [80].

At present, there are still some problems in the SiC/special alloy joining, such as the large thermal residual stresses and excessive interfacial reactions, resulting in the formation of cracks and invalidation of joint. For these reasons, the design of reliable joints between ceramic is a complex task requiring commitment in several scientific and technological fields such as thermodynamics, surface science and mechanics.

Up to now, some conventional diffusion bonding methods are suitable for SiC-based materials.

However, even though effective, solid-state processes require high temperatures and high pressures to allow a good contact between the faying surfaces granting an effective mass transport. Thus, the surfaces to be joined must be accurately prepared in order to minimize voids and imperfections which can constitute strength-limiting defects after processing. These aspects make this technique unreliable in case of curved surfaces or when the adjoining surfaces are rough as in the case of SiC based composites.

For these reasons, a liquid based process such as brazing is preferable.

However, in conventional brazing methods the liquid medium is solidified by cooling leading to interfacial thermal stresses in case of expansion and elastic mismatch between the adjoining materials. Moreover, either degradation of the ceramic phase or interfacial reactions that form brittle interfacial layers are aspects to be considered when designing brazing processes.

The transient liquid phase bonding (TLPB) technique applied to ceramics may overcome these issues [86],[87].

The most peculiar feature of the TLPB process is that the interfacial products have a re-melting temperature higher than that of the process itself. This technique exploits interlayers that are

heated up to melting temperatures and wet the seam between the materials being joined, allowing their adhesion and the fabrication of well-bonded, hermetic seals. The interlayers solidify and homogenize at joining temperatures through chemical interactions and the isothermal formation of phases in the solid state through diffusion processes involving the adjoining solids. This enables their use at temperatures potentially well above the joining temperature, provided that the resulting phases may comply with the CTE and the elastic modulus of the joined materials.

An accurate research of the filler alloys and the wettability test in contact to SiC are, of course, specifically required to arrive at satisfactory brazing processes taking into account the reactivity with the substrate, with a special attention to the stability and performance of the new interface compounds.

Table 3.1. Reactivity of some transition metals in contact with SiC.

Reactivity for pure metals	Reaction products	Ex.
None		Pb, Au, Ag.
Me + SiC → Si + carbide	No stable carbide, stable silicides	Ni, Co, Fe, Cu
Me + SiC → Si + carbide	Stable carbides	V, Al, Nb
Me + SiC → silicide + carbide	Stable carbide, stable silicides	Zr, Hf, Cr, Ta, W, Ti, Mo

The reactivity of liquid metals with SiC must be controlled in order to select the nature of the reaction products (*Table 3.1*) and the thickness of the reaction zone [88],[89].

As an example, some elements such as Ni, Co, Fe, etc. react with SiC to form brittle silicides which are accompanied by carbon precipitation in the form of graphitic layers which weaken the joint [90].

To control this process Ta was added, as an example, to Co and Ni promoting the formation of a layer of TaC on the SiC surface that can act as a diffusion barrier preventing a high ceramic dissolution [28], [91].

Some investigation show that a series of binary Si alloys, such as Ni-Si [23] [84], Co-Si [93], Fe-Si [94], Au-Si [87] [88], Ag-Si [96], Cu-Si [97]–[99] present a good non-reactive wettability in contact to SiC.

While Zr, Ti, Hf, Mn, etc., that react with both silicon and carbon, can lead to a high reactivity with SiC. Other elements (Si, Ag, Al, etc.) may be added in order to control the strength of the interactions and the final products.

As an example, Al, reacting with SiC, promotes the formation of stable carbides while Ti forms both carbides and silicides [100]–[103].

Al-Ti alloys [104] as well as Al-Ti-X-Y (X=Cu, Ti; Y=Si) multielement alloys [105] are materials already tested as fillers in different kinds of joints in which SiC is involved. This because they show a good wettability on the ceramic and promote the formation of a new interfacial phases.

Al and Ti are also selected as alloying elements in filler alloys for joining processes including composite materials.

For example a method to produce structural materials in packaging applications is the in situ joining of Ti to SiC/Al composite by low pressure infiltration [106]. In this way, the production of joints allows to prevent the formation of Al_4C_3 brittle phase which was confirmed harmful for the joint strength.

Therefore, the interface produced by the in situ joining is more promising than that by laser beam welding [107] and is supposed to improve the bending strength of the interface.

In this work, an Al-Ti alloy with a specific stoichiometry, Al_3Ti, and an Al-richer alloy, are selected.

The reactivity of the Al-Ti alloys in contact to the SiC is evaluated and a study aiming to determine how the ceramic dissolution can influence the first interaction temperature is conducted.

The aim of the study is then to define both experimentally and theoretically the reactivity and the thermodynamics of the Al-C-Si-Ti system in order to be able to understand the interfacial phenomena occurring at the metal/ceramic interface under the defined conditions.

The Al-Ti alloys are chosen because they contain:

- a low melting temperature element (Al) thatserves as a melting point depressant so that the process involving the melting of the filler alloy occur at not a too high temperature(this is useful in terms of the cost of the process);

- an active element (Ti) that, diffusing towards SiC and reacting with it, forms new metal-ceramic phases better wettable than the SiC.

In addition, this system has the capability to form interfacial high melting compounds, offers the possibility to apply a Transient Liquid Phase Bonding (TLPB) process [91], [108]–[110] .

In particular, very promising stable metal-ceramic phases, known as MAX-phases,(Al-C-Ti and Si-C-Ti) can form for both the systems.

The “MAX” terminology denotes the compounds$M_{n+1}AX_n$ (n=1-3), where M represents an early transition metal, A is an A-group element, and X is C or N [111]. Because the structural units of these materials contain a NaCl-type non-stoichiometric MX slab and a close-packed A-group atomic plane, they demonstrate unusual properties such as low density [112], high thermal and electrical conductivity, exceptional oxidation resistance, high elastic modulus, damage tolerance, and good machinability [113].

Indeed, Ti_3SiC_2 MAX-phase has been recently adopted as a joining medium in solid state processes with successful outcome [114]–[116] using, in particular, the Spark-Plasma-Sintering technique [117][118][119].

Other works reported the possibility to join the MAX phase to itself using Al interlayers in a TLPB process [87]; the existence of a $Ti_3Si(Al)C_2$ solid solution made up by substitution of Si by Al made this process appealing [120]. However, the formation is also possible of the $Ti_3Si(Al)C_2$ MAX-phase, in which we can find the presence of both Al and Si located as substitutional elements on the same site [121]. These elements, in fact, having similar electronegativity and dimension, can occupy the same atomic site.

This phase was found to be an interesting material because it displays, as mentioned before, a unique combination of metallic and ceramic properties. It shows, as a metal, a huge number of promising properties: good thermal and electrical conductivity, significant thermal shock resistance, low hardness (Vickers: 4GPa), low density (4.53 g/cm^3), good machinability and ductility; as a ceramic material, it shows: high melting point (above 3000°C), high elastic modulus (about 32 GPa), high strength (bending strength 475 MPa), relatively low thermal expansion coefficient and high oxidation and corrosion resistance. The thermal expansion coefficient of the MAX-phase is very close to that of the SiC and this constitutes a good asset for the final interface.

4. Experimental part

The wetting and the joining processes concerning the two metal-ceramic systems have been investigated following both an experimental and a theoretical approach.

Experiments involve the use of:

1) an ad-hoc designed furnace to produce the metal/ceramic couples and to define the wetting kinetics of the systems at high temperature;
2) the SEM-EDS to identify the different phases found in the samples section microstructure;
3) the DSC to determine the first temperature of the metal/ceramic interaction.

The theoretical approach involves the use of the Thermo-Calc software (belonging to CALPHAD method) in order to obtain different kinds of graphs (i.e. the isothermal sections of the systems, the activity of the active element and the cooling path of the liquid considering the experimental conditions) and compare them with the experimental results in order to be able to define and to predict the interfacial interactions. In particular, this approach allows to modify the test procedures taking into account the results of the thermodynamic calculations.

4.1 Samples preparation

Before the wetting tests, the alloys are prepared mixing stoichiometric metal quantities and melting them by an arc-melting furnace working under purified Ar atmosphere. To remove any oxygen contamination from the melting chamber, a zirconium getter is previously melted. The alloys are re-melted at least five times to ensure homogeneity in their composition. The ceramic materials (YAG and SiC) as well as the Ti6Al4V metallic substrate are carefully polished, before wetting and joining tests, in order to minimize the surface roughness that could pin the metal liquid during the spreading process avoiding an “ideal” wetting evaluation. The wetting configuration is schematically shown in *Figure 4.1.*

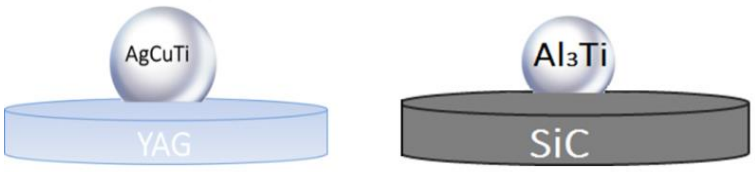

Figure 4.1. The configuration adopted, common to both the systems, before the wetting test.

Before the joining tests, Ag-based alloys foils (in the first system) and Al_3Ti paste (in the second system) are prepared and interposed between the two substrate materials (*Figure 4.2*).

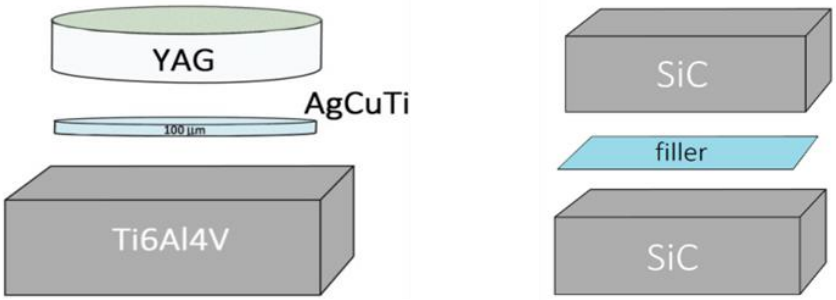

Figure 4.2. Sandwich configuration adopted for the brazing process of both the systems under investigation.

After all these steps and prior to all the experiments (wetting and brazing tests), pre-melted alloys, ceramic substrates and alloy foils are ultrasonically cleaned in ethanol using an ultrasonic bath.

4.1.1 YAG-Ti6Al4V system

4.1.1.1 YAG ceramic and Ti6Al4V substrates

The same types of ceramic materials are used for the wetting and the joining tests.

The YAG polycrystalline ceramics are prepared by CNR-ISTEC following the experimental procedure of Esposito et al. [122] that I have personally performed during a week stage in Faenza.

The materials are synthesized starting from extremely pure (≥ 99.99%) and sub-micrometric ceramic oxide powders of Al_2O_3 and of Y_2O_3 accurately mixed and heated at 1735°C for 16 h under high vacuum conditions (10^{-4} Pa) to obtain discs of 10 mm diameter.

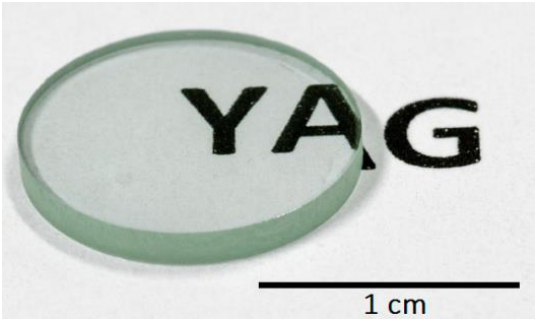

Figure 4.3. The YAG sample optically polished.

Before the wetting and the brazing processes, the substrates, characterized by a transparency of about 80% [123], (*Figure 4.3*), are polished on diamond grinding discs to reach a final surface roughness (S_a) below the value of 10 nm. This value has been measured by an optical confocal-interferometric profilometer (Sensofar S-neox) (*Figure 4.4*).

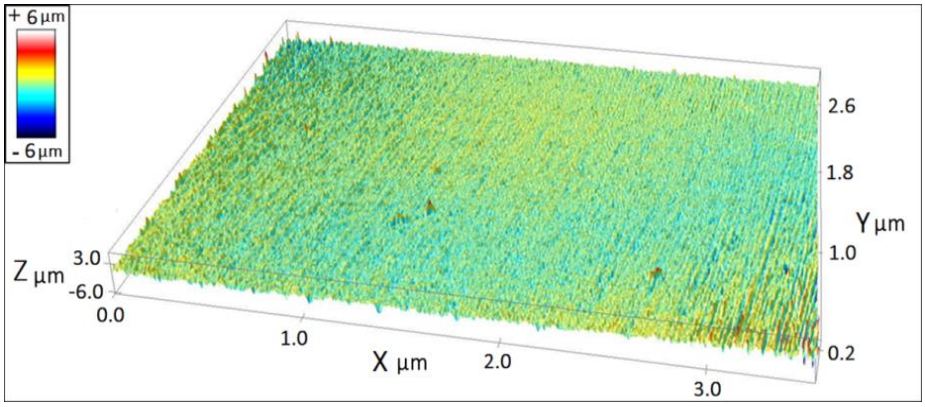

Figure 4.4. YAG roughness surface acquired using the optical confocal-interferometric profilometer.

The metallic support Ti6Al4V, utilized in the joining tests (grade 5 Ti, Titalia, Milano, I) and characterized by a composition of 6 wt% Al and 4 wt% V (10 at% Al, 3.5 at% V), is cut in order to obtain parallelepipeds of 1 cm length and polished on diamond grinding discs to reach a final surface roughness S_a of 10 nm.

4.1.1.2 Ag-based alloy

In order to perform the wetting tests, different metallic drops (diameter = 4.0–5.0 mm; average weight = 0.3 g) are prepared by arc-melting. Ag, Cu, Ti rods (purity > 99.9%) or wires of CB4 (Degussa-Germany) alloys are used. The alloys composition is reported in *Table 4.1:*

Table 4.1. Composition of the different filler alloys used.

	Ag		Cu		Ti	
	wt%	at%	wt%	at%	at%	at%
AgCuTi (CB4)	70.5	57.7	26.5	36.8	3.0	5.5
AgCu	72.0	60.2	28.0	39.8	-	-
AgTi	96.0	91.4	-	-	4.0	8.6

The CB4-AgCuTi alloy has a density of 9.9 gcm^{-3}, a thermal expansion coefficient equal to 18 × 10^{-6}/K, a melting range of 780–805°C [124] and is considered a member of a family defined as medium-melting-point active fillers (melting point between 700°C and 1000°C[56], [125]).
Before the joining tests, foils of CB4-AgCuTi alloy (Degussa-Germany), AgCu eutectic (99.9% purity, Metalli Preziosi-Milano, Italy) and Ag (99.997%, Goodfellow, Cambridge, UK) are laminated until a thickness of 100 µm and cut to the desired dimensions.

4.1.2 SiC/Al-Ti system

4.1.2.1 SiC substrate

Fully dense and pure (purity> 98 at%; open pore < 3%) SiC discs (Frialit SiC 198D, Mannheim, Germany), characterized by a diameter of 15 mm and a height of 2 mm, are used as ceramic substrates (density of 3.1 g/cm^3, a Vickers hardness of 26 GPa). These SiC discs were polished down to 1 µm diamond paste to reach a surface roughness (S_a) of about 20 nm.
The same SiC material was utilized during the wetting and joining tests but in a different shape:

- pieces (Goodfellow, Hungtingdon, UK) already cut as disc (diameter= 15 mm and height= 2 mm) have been used for the wetting evaluation;
- pieces (Goodfellow, Hungtingdon, UK) already cut as parallelepipeds (5 x 10 x 3 mm^3) have been used for the joining process.

The substrates were polished down to 1 µm diamond paste to reach a surface roughness of S_a= 4nm, measured using an optical confocal profilometer (Sensofar S-neox) over a 1.75 x 1.32 mm^2 surface area (*Figure 4.5 (a)*).

4.1.2.2 Al-Ti alloys

Two compositions of Al-Ti alloys have been chosen: the first is the stoichiometric Al_3Ti compound with 75 at% Al (alloy A of *Figure 4.5 (b)*); the second alloy corresponds to an Al-rich alloy with 84 at% of Al (alloy B of *Figure 4.5 (b)*).
In order to get reference data without any possible contamination, wetting tests were performed starting from commercially available very high purity materials:

- the purity of Al was 99.9999 at% where the main impurities (in ppm) in Al were Fe:180, Ni:800, C: 30, S:150;
- the minimum purity of Ti (Goodfellow, Hungtingdon, UK) was 99.99 at% where the main impurities (in ppm) were Fe:10, Si: 5, Nb: 5.

Both the alloys are tested in terms of wettability in contact to SiC while an Al_3Ti powder (produced by Goodfellow) with a defined granulometry of 45 µm is used to obtain the filler-paste to cover the SiC substrates before the joining test.

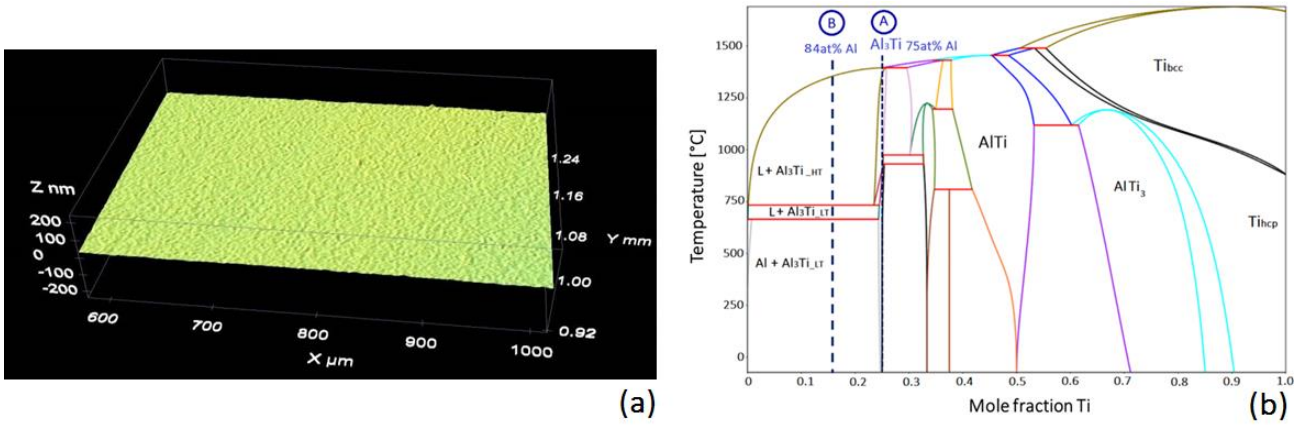

Figure 4.5. Profilometer acquisition of the roughness of SiC surface (a); binary Al-Ti systems recalculated taking into account the data of [126] *(b).*

The stoichiometric compound (Al_3Ti) has a density of 3.3 g/cm^3, a Vickers hardness of 3.9-4.2 GPa and Young's modulus of 160 GPa; this alloy is chosen to be tested as filler material in the SiC-SiC brazed samples.

In particular, as it will be explained in *6.2*, two different joining procedures are taken into account:

- the first one is the infiltration technique that involves the use of Al_3Ti pieces or drop, produced by the use of the arc-melting (as for the alloy used for the wetting evaluation);
- the second one is based on a sandwich configuration involving both the use of an Al_3Ti paste (formed mixing the intermetallic compound powder with the α-Terpineol organic solvent) and of an Al_3Ti paste or a Ti foil (50 µm of thickness).

After deposition on the surface of the paste-layer (about 100 or 50 µm of thickness measured by optical interferometry (*Figure 4.6*(b),(c)), the coated SiC is maintained at 70°C for 3 days in order to make possible the solvent evaporation.

Then, the assembled system is inserted and fixed inside the graphite clamp reported in *Figure 4.9* and it is introduced in the central part of the furnace (*Figure 4.7*).

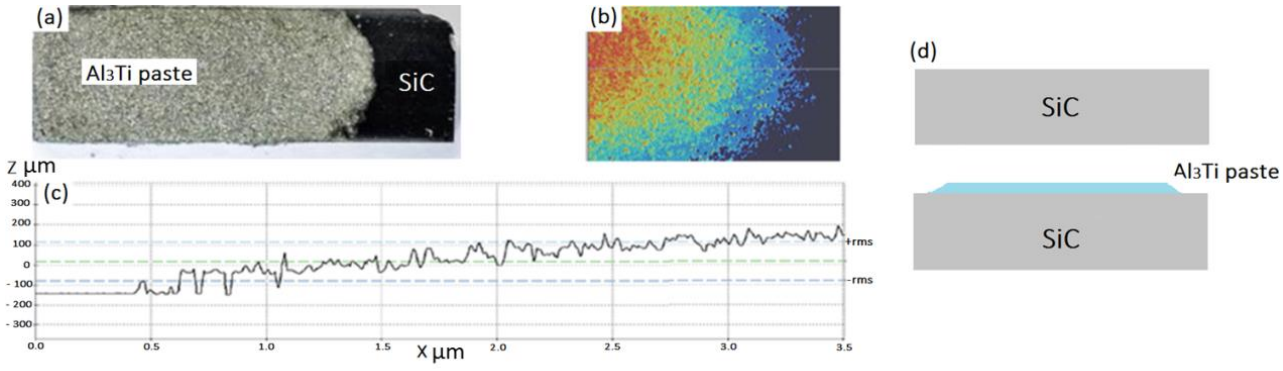

Figure 4.6. Al_3Ti paste on SiC (a, b); thickness of the paste deposition using the interferometric profilometer (c); schematic representation of the sandwich configuration (d).

4.2 Wetting apparatus

The experiments are carried out by the sessile drop method [3], [127] using a dedicated apparatus that can be schematized in two main parts: the furnace and the software connected to the optical system, as depicted in *Figure 4.7*.

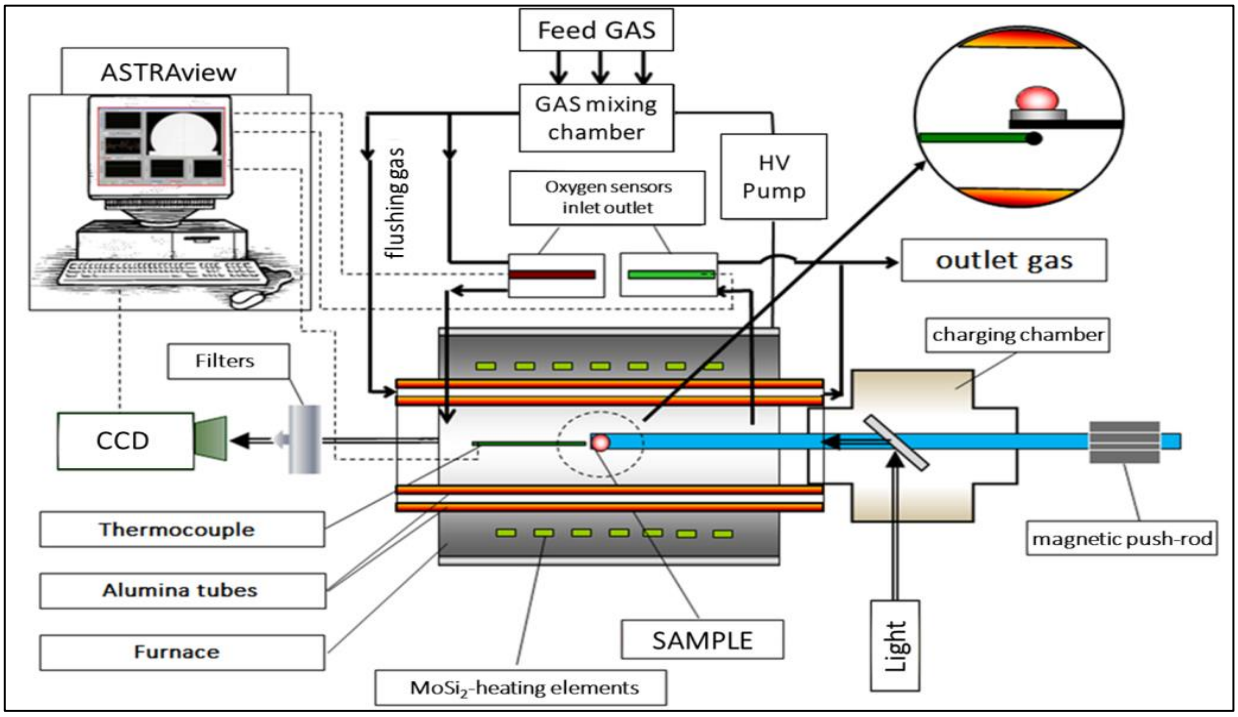

Figure 4.7. Schematic representation of the furnace using for wetting and joining experiments.

The furnace reaches a maximum temperature of 1600°C and is made of two concentric, horizontal, alumina tubes. A constant flux of argon flowing between these two tubes prevents any oxygen diffusion inside the experimental chamber even in the temperature range up to 1600°C [72].

The temperature is read by a type S thermocouple, placed just below the test specimen, which was calibrated against the melting point of small pieces of Au, Cu, Ni and Fe placed in the same part of the furnace where the specimens are tested.

The precision of the temperature readings can be estimated better than ± 5°C.

Tests are performed after making an ultra-high vacuum ($10E^{-6}$ mbar at 1000°C) thanks to a turbo-molecular pump or under atmospheres with an oxygen partial pressure that can be set from 10^{-12} mbar (with argon + hydrogen mixture atmosphere) to pure oxygen at 1 bar.

In our experiments, the oxygen partial pressure of the working atmosphere (pO_2), continuously monitored by solid-state oxygen sensors at the chamber inlet and outlet (Figure 4.8), is of the order of $pO_2 = 10^{-18}$ Pa at 700 °C.

However at 1500 °C, the water equilibrium reaction would raise the pO_2 value to about 1 Pa or 10^{-5} Pa for pure Ar or Ar–5%H_2 respectively due to the presence of impurities (1 ppm of O_2 and H_2O) in these gases.

A first attempt was made to conduct experiments under a vacuum in the case of the non-oxidic system; however, these tests were unsuccessful because of the excessive evaporation of Al.

Therefore, all the results hereby reported were obtained under a protective atmosphere (Ar/H_2) gettered by Zr foils wrapped around samples.

This configuration avoided both evaporation and strong oxidation of the liquid alloys, allowing the formation of clean droplets because the surrounding Zr foil captures, locally, any oxygen trace.

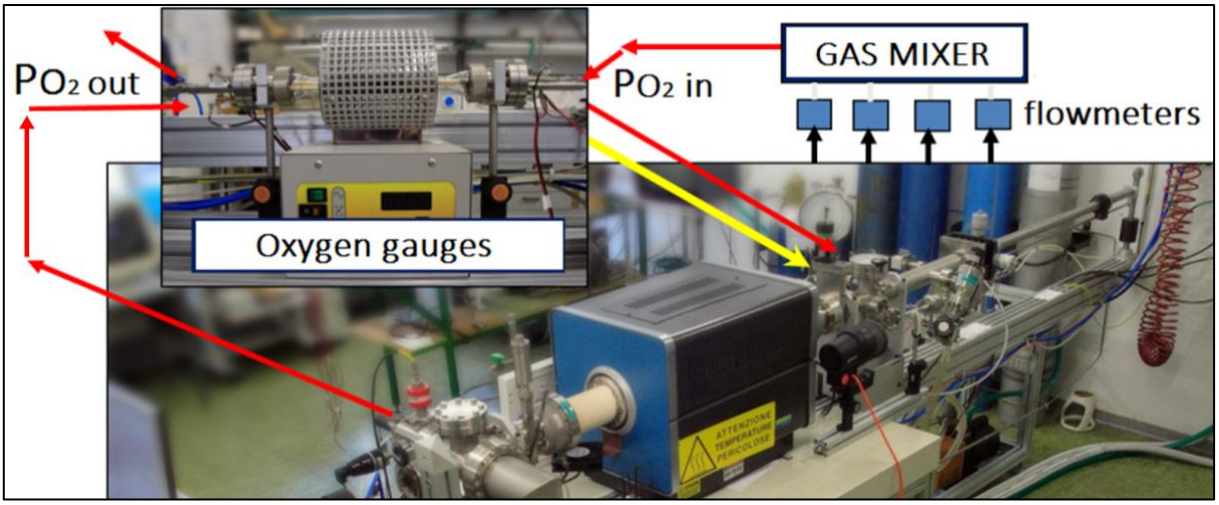

Figure 4.8. Solid-state oxygen sensors located at the chamber inlet and outlet.

A magnetic manipulator allows the introduction of the samples inside the furnace to be made as soon as temperature and environmental conditions reach constant and selected values.

Experiments are controlled and recorded using an optical system made of a CCD camera equipped with a 300mm objective. The software ASTRAView 2, entirely developed by CNR-ICMATE, acquires images of droplets at high resolution and calculates surface tension and contact angles as well as the drop dimensions (height, base diameter, surface and interfacial areas [128]–[130]).

Measuring these quantities is very sensitive to the quality of images (high contrast, high resolution and absence of any reflections) and to the precise determination of the magnification factor i.e. the

determination of the drop real dimensions which should have the precision of microns. Thus, extreme care must be taken in the optical line: set up is carefully aligned, samples are backlit by a photographic lamp and images are filtered so that the drop/substrate couples are recorded as sharp b/w images.

The drops profiles are acquired, stored, and then elaborated off-line.

The drop and substrate profile can be measured with a precision of ±1 μm through a careful determination of the magnification factor while the intrinsic precision of the calculated contact angle data is of the order of ± 0.5°; however, possible optical distortions mainly due to the high temperature involved lead to uncertainties in the measured profiles with a final contact angle accuracy of the order of ±2°.

This apparatus is also used to perform the joining experiments.

A graphite clamp, shown in *Figure 4.9*, is used to assembly the sample in a sandwich configuration before the test.

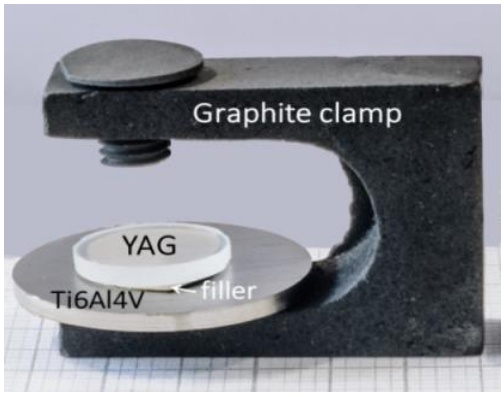

Figure 4.9. The YAG/filler/Ti6Al4V sandwich configuration obtained using a graphite clamp.

After the tests, the samples are extracted from the hot chamber to the cold side of the furnace using the same push rod utilized for their introduction reaching room temperature in ∼30 s, so that the specimens are allowed to cool quite rapidly still in controlled atmosphere.

The interfacial zones and the cross sections of the drops were observed and analyzed by optical and scanning electron microscopy (SEM) coupled with energy-dispersive spectroscopy (EDS) analysis.

4.3 Microstructural characterization

The interfacial and the bulk structure of all the systems have been characterized by the use of:

- optical microscopy (LOM), in order to check continuity of the interface, the phases to be analyzed as well as the morphology of the section after the high temperature processes;
- scanning electron microscopy (SEM-EDS), in order to define the microstructure and the composition of the phases formed after the process and to observe the element diffusion along the vertical profile of the samples allowing to evaluate the diffusion and the dissolution occurred in the system.

In particular, for the oxidic system, (YAG/Ag-based alloys and YAG/Ag-based alloys/Ti6Al4V), quantitative analyses are carried out with a SEM-EDS instrument (LE= 1450 UP-Zeiss; INCA ENERGY 300) with a W emitter, an acceleration voltage of 20 kV, an aperture of 50 µm, a working distance of 15 mm and a live time of 40 sec.

Quantitative optimization has been performed before each analysis session with a Co standard; ZAF (atomic number-absorption-fluorescence), a correction procedure, is embedded in the analysis software.For the non-oxidic system (SiC/Al-Ti alloys and SiC/Al-Ti alloys/SiC), quantitative analyses are carried out with an acceleration voltage of 14 kV, an aperture of 50 µm, a working distance of 15 mm and a live time of 40 sec.

4.4Differential Scanning Calorimetry

DSC-TGA (*Figure 4.10*) is used to define specifically the Al-Ti alloy/SiC interactions at the interface.

The aim is to define the temperature of the first interaction that occurred when the alloy is in contact to the ceramic substrate.

The TGA instrument (TGA/DSC2 from Mettler Toledo), used at the Claude Bernard University of Lyon 1, presents a horizontal configuration that helps to minimize possible turbulence caused by thermal buoyancy and the purge gas. Its temperature limits vary from 20 to 1600°C and the heating program for our analyses from 30 to 1400 (1450°C) at 10°C/min (then 20°C).

The DSC sensor consists of six thermocouples (visible in *Figure 4.11* (b)) located directly below a protective support which measure the sample and the reference temperatures.

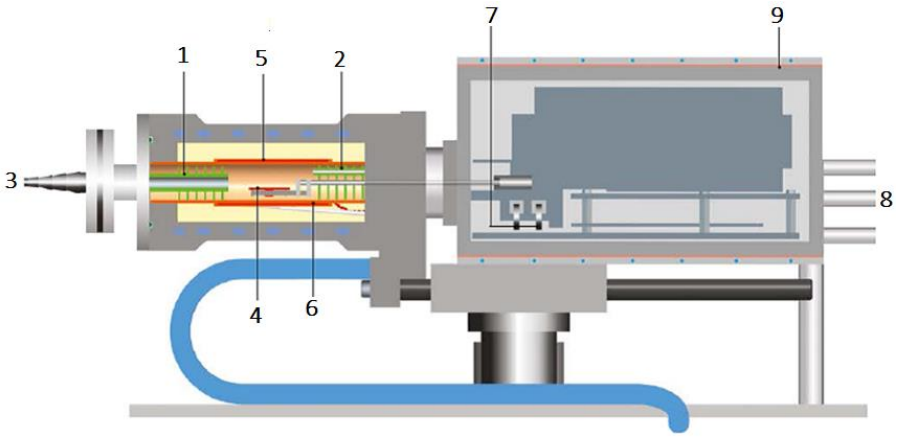

Figure 4.10. TGA-DSC apparatus used to determine the first forming liquid temperature of the samples and where 1: baffles, 2: reactive gas capillary, 3: gas outlet, 4: temperature sensors, 5: furnace heater, 6: furnace temperature sensor, 7: adjustment ring weights, 8: protective/purge gas connector, 9: thermostatic micro-balance chamber.

The six thermocouples generate a large measurement signal which improves the signal-to-noise ratio. The heat flow is determined from the measured temperature difference.

DSC signal allows us to measure the thermal phenomena occurring when the sample is heated.

The samples have been tested inside alumina crucibles of 150 µL volume with a pierced lid.

The sample temperature sensor is directly attached to the crucible holder (*Figure 4.11*(a)) and detects temperature deviations of $\pm$ 0.25 K.

The micro-balance cell is thermostated to minimize the environmental influences.

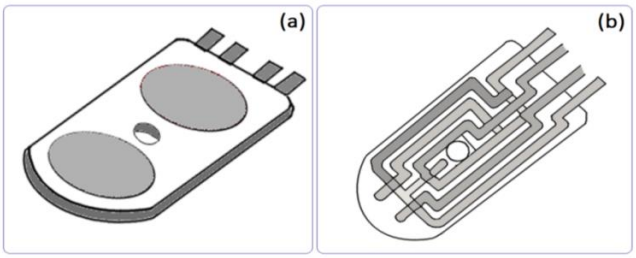

*Figure 4.11.Alumina crucible holder (a) and the six thermocouples**that constitute the DSC sensor (b).***

A cryostat is used to rapidly cool the furnace and to control the regulation of the heating rate.

Argon of high purity (O_2< 100 ppb) has been used as inert gas.

In order to remove air from the TGA oven, a screening under argon at a rate of 100 mL.min^{-1} has been done during 30 minutes just before the beginning of analysis.

In some cases a heating rate of 20°C/min is used to accelerate the phenomena and to identify the temperature of the first liquid formed. However, the use of a heating rate of 10°C/min is preferred to better distinguish the different phenomena that can occur.

5. CALPHAD approach

5.1 The CALPHAD method

Design, preparation and use of different kinds of industrial materials, require a deep knowledge of their constitutional properties such as phase stability and equilibria under the defined operating conditions [131].

The thermochemistry and the microstructure of new interfacial products represent crucial points that have to be carefully controlled in order to obtain the desired mechanical performances when different materials are in contact.

The CALPHAD (CALculation of PHAse Diagrams) method represents a phase based approach to the modeling the thermodynamics and phase equilibria of a system through a self-consistent framework that allows extrapolation to multicomponent systems. For this reason it gives a significant support to the experimental work providing the thermodynamic basis to predict the system behavior and then to reduce the number of experiments needed to investigate and characterize the interactions and the properties of the selected materials.

The CALPHAD approach, introduced by Kaufman and Bernstein (1970) and then developed by others [132], [133], has maintained the same operating steps that are schematized in *Figure 5.1*.

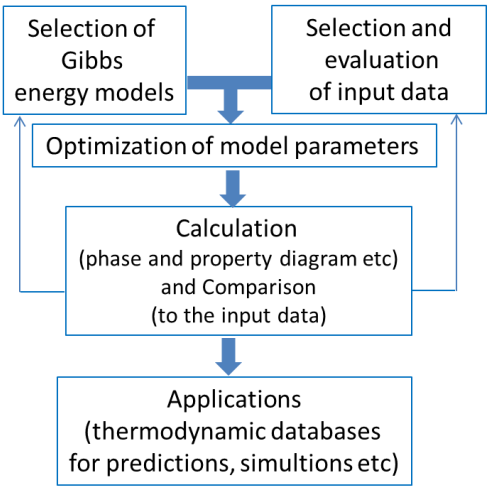

Figure 5.1. Schematic representation of the CALPHAD approach [131].

The first requirement of this approach is to define a thermodynamic database that includes a description of Gibbs free energy function for each phase (G^{Φ}) that takes part in the considered

system. The parameterized thermodynamic functions depend on state variables (such as pressure, temperature and composition) and on some empirical parameters to be assessed from experimental data.

Each G^{ϕ} (P, T, x) function, inserted in the thermodynamic database, is necessary to make calculations (phase equilibria, phase diagrams, thermodynamic properties) with the final aim to support the experimental work.

In particular, CALPHAD calculations, performed using the Thermo-Calc software, produce thermochemical data (as enthalpy, entropy, heat capacity, activity) that are fundamental for drawing phase equilibria (liquidus, solidus, phase boundary) through the minimization of the total Gibbs free energy of the system under given conditions ($\delta G/\delta x_i^{\phi} = 0$).

Specifically, the process includes four steps:

1) Selection of models for the Gibbs Energy functions:

   All the phases competing for equilibrium in the system under investigation are described by a Gibbs free energy function in terms of state variables (x_i) and empirical parameters (a_k):

$$G^{\Phi} = G^{\Phi}(x_1, \dots, x_i, a_1, \dots, a_i) \qquad (15)$$

   The G^{ϕ} function can assume different forms depending on the nature of the phase ϕ that can be a disordered solid solution, a stoichiometric compound, an ordered metallic solution, an ionic liquid, etc.

   Generally, the composition dependence of G can be expressed using a formalism known as Compound Energy Formalism (CEF) and described in*5.2.*

2) Selection and evaluation of input data:

   An accurate selection of all the available and reliable literature data about the possible phases occurring in the system under study is needed. In this way an evaluation of the empirical parameters (a_K) can be done.

   The selected input data that have been considered during this step include:

   a) experimental results coming from DTA, DSC, calorimetry, SEM, X-ray diffraction etc;
   b) results from ab-initio and first principles calculations etc;
   c) estimated data by extrapolation/interpolation procedures etc.

3) Optimization of models parameters:

An error minimization procedure, as the non-linear least-square method, is used to evaluate the empirical parameters a_k and an appropriate weight factor has to be related to each input datum. It is then necessary to verify the correlation between input data and model parameters.

4) Calculations and comparison:

   Phases and properties diagrams are then calculated using the Gibbs energy functions with the optimized parameters a_k. These calculations are compared to the equilibria and data already defined and known. It is also necessary to check the metastable equilibria and to make an extrapolation to higher order systems. If the comparison is not satisfactory a modification of thermodynamic models for the phases or of the selection of the input data is required.

5) Applications:

   The optimized interaction parameters are used to implement a new database or to improve the existing ones. Thanks to these databases it is possible to predict phase equilibria, thermodynamic properties, materials properties (e.g. microstructures) and to simulate a material behavior in the process conditions.

One of the advantages of the CALPHAD method is its ability to make predictions. It consists, in fact, in an optimization method for 2-3 component systems, which could not be calculated without the support of experiments. However, for multicomponent systems, it works as a prediction method: as the number of system components increases, the number of new empirical parameters, needed to have a good description of Gibbs energy of the phases, tends to decrease. In most cases for more than four component systems, ideal interactions approximate well the real behavior of the system. For this reason the method is very promising in multicomponent materials processes.

5.2 Compound energy formalism

While the Gibbs energy dependence on temperature and pressure can be estimated by a general expression used for all kinds of phases, its dependence on composition is significantly related to the nature and strength of the atomic interactions. For this reason a single model is not sufficient for all phases. To overcome this problem the “Compound Energy Formalism” (CFE) [134] is used which

allows to select the most appropriate model for each phase in the framework of the same formalism. According to CFE, the Gibbs energy of the phases depends on the site fractions. Phase constituents, such as neutral atoms, ions, vacancies, etc. are located inside one or more thermodynamic sub-lattices in which they mix according to the classical solution theory, with different interaction parameters in different sub-lattices.
Thermodynamic sub-lattices are used to divide anions and cations in the case of ionic compounds while they represent crystallographic sub-lattices in case of alloys.

The Gibbs energy of a phase can be defined as the sum of four contributions:

$$G^{\phi} = {}^{ref}G^{\phi} + {}^{id}G^{\phi} + {}^{ex}G^{\phi} + {}^{mag}G^{\phi} \qquad (16)$$

Where ${}^{ref}G^{\phi}$ is the reference term, ${}^{id}G^{\phi}$ is the ideal mixing term, ${}^{ex}G^{\phi}$ is the excess term and ${}^{mag}G^{\phi}$ takes into account further interactions as the magnetic ones.
In the case of a pure element the dependence on composition is neglected and equation (16) becomes simpler:

$$G^{\phi} = {}^{ref}G^{\phi} + {}^{mag}G^{\phi} \qquad (17)$$

The two addenda of equation (17) are extendedly expressed in the following equations:

$${}^{ref}G^{\phi} = A^{\phi} + B^{\phi}T + C^{\phi}T\ln T + D^{\phi}T^{2} + \ldots \qquad (18)$$

$${}^{mag}G^{\phi} = RT \cdot f(\tau) \cdot \ln(\beta(x) + 1) \qquad (19)$$

where A, B, C, D,.. are the empirical parameters evaluated thanks to the experimental data, β is the average magnetic moment per mol of atoms in Bohr magnetons, τ is the ratio T/T_C (T_C=critical temperature for magnetic order), f(τ) is a polynomial expression.
The SGTE (Scientific Group Thermodata Europe) database [135] is used to obtain temperature and magnetic parameters for pure elements.

Depending on the system components and then on the mixing or not mixing mechanism, different cases have to be considered: substitutional random solutions, stoichiometric phases (or compounds), ordered solutions and ordered phases related to random solutions.
In the following table (*Table 5.1*) some examples for the different cases are given and in the next paragraphs all these situations will be separately explained.

Table 5.1. Examples of CFE modelling.

Phase type	Sub-lattice model	Example phase	Example sub-lattice model
Substitutional disordered solutions	(A,B)	liquid-(Cu,Ni)	(Cu,Ni)
Stoichiometric compounds	$(A)_u(B)_v$	Al_3Ni	$(Al)_3(Ni)_1$
Sub. solutions with vacancies	$(A)_u(B,VA)_v$	bcc-(Fe-N)	$(Fe)_1(N,VA)_3$
Substitutional ordered solutions	$(A,B)_u(A,B)_v$	C15- Cu_2Mg	$(Cu,Mg)_2(Cu,Mg)_1$
Ionic solids	$(Cations)_u(Anions)_v$	NaCl+ $CaCl_2$	$(Ca^{2+},Na^{+})_1(Cl^{-},VA)_2$
Ordered/disordered relations	(A,B) $(A,B)_u(A,B)_v$	fcc-(Au,Cu) ($AuCu_3$)	$(Au,Cu)(Au,Cu)_{1/4}(Au,Cu)_{3/4}$

5.2.1 Substitutional random solutions

The random mixing case, valid for liquid and terminal solid solutions, takes into account a unique sub-lattice. The Gibbs energy terms are expressed here:

$$^{ref}G^{\phi} = \sum_i x_i G_i^{\phi}(T) \qquad (20)$$

$$^{id}G^{\phi} = RT\sum_i x_i \ln x_i \qquad (21)$$

$$^{ex}G^{\phi} = {}^{ex2}G^{\phi} + {}^{ex3}G^{\phi} + \cdots (22)$$

Where x_i represents the mole fraction of component i, $^{ex2}G^{\phi}$ and $^{ex3}G^{\phi}$ the binary and the ternary excess terms.

5.2.2 Stoichiometric phases (or compounds)

In this case, an n-sub-lattice model is used and in each sub-lattice just one element is located. The mixing term of course is not present:

$$^{ref}G^{\phi} = \sum_i x_i G_i^{SER}(T) + {}^{form}G^{\phi}(T) \qquad (23)$$

where G_i^{SER} is the Gibbs energy of the pure component i in the standard reference state SER and $^{form}G^{\phi}(T)$ is the Gibbs energy of formation of the compound.

5.2.3 Ordered solutions

In this case intermetallics with a solubility range are taken into account and the components can occupy, by reciprocal substitution, all the crystallographic sites; each sub-lattice is mainly occupied by one component in particular. In this situation the Gibbs energy is written as a function of the site fraction $y_i^{(s)}$ (mole fractions of each component i in the sub-lattice s) and the site fraction is regulated by the following equation:

$$\sum_i y_i^{(s)} = 1 \qquad (24)$$

$$\frac{\sum_s n^{(s)} y_i^{(s)}}{\sum_s n^{(s)}(1-y_{VA})} = x_i \qquad (25)$$

Where $n^{(s)}$ are the stoichiometric coefficients of the sub-lattices and VA the vacancies that can occupy one or more sub-lattices.

5.3 CALPHAD approach used to interpret the experimental results

The CALPHAD based software is helpful for the design and the optimization of the process as well as of the alloy compositions tested in contact to the ceramic substrates examined in this Thesis.
In fact it is used to calculate phase equilibria, amount and composition of phases, driving forces for phase transformations, phase diagrams (binary, ternary, quaternary, isothermal, isoplethal..), thermochemical data (enthalpies, heat capacities, activities).

The theoretical prediction of the different phases formed during the high temperature process is done, mainly, on the basis of the isothermal sections including the elements of the system under investigation at different temperatures.
Comparing this thermodynamic prediction to the experimental determination of the interface products defined by the EDS analysis, it is possible to better define the process parameters (time and temperature)as well as the filler alloy composition in order to define the best conditions to obtain the more promising interface for the desired applications.

Even if the systems have been studied under dynamic conditions, a comparison with phase equilibrium calculations is a useful way to understand both high temperature isothermal interactions and the phase transformations occurring during the subsequent cooling process.
Indeed, the high temperature environment should promote atom mobility and, as a consequence, should make easier to reach conditions not far from the equilibrium ones.

5.3.1 CALPHAD approach in YAG/filler alloy and YAG/filler alloy/Ti6Al4V systems

Thanks to CALPHAD method, it is possible to make some hypotheses about the evaluation of the experimental results regarding the high temperature filler/YAG and metal/filler/YAG reactivity.
However it is important to underline that to clearly and deeply discuss the experimental results, a quaternary (Ag-Cu-Ti-Al), a quinary (Ag-Cu-Ti-Al-V) or even higher order system (Ag-Cu-Ti-Al-V-O) should be considered.
However, at present, no thermodynamic database is available for such complex systems.
Then, in order to interpret the wetting (AgCuTi/YAG) and the joining (YAG/filler alloy/Ti6Al4V)) experimental results, the attention is focalized on the metallic part of the samples, using the existing database available from the literature for the Ag-Cu-Ti ternary system [135]–[137].

Indeed, as it will be explained in the results section, Y does not migrate from the substrate towards the bulk liquid metal.

Moreover, observing the metal-ceramic interface, it is possible to see the metal-ceramic interface layer formed without an important dissolution of the substrate. For these reasons, in order to simplify the interpretation, the thermodynamic evaluation is focused on the metallic part of the system.

The phase formation as well as the role of the activity of Ti in determining the interface interactions is, in fact, interpreted using the CALPHAD method by means of recalculated Ag-Cu-Ti and Ag-Al-Ti isothermal sections.

5.3.2 CALPHAD approach in SiC/Al-Ti and SiC/Al-Ti/SiC systems

The experimental results regarding the high temperature reactivity between the filler alloy Al_3Ti and the silicon carbide, interpreted by CALPHAD modeling, show that, both the elements of the ceramic substrate enter inside the liquid metal promoting a significant dissolution.

For this reason it is not possible to avoid taking Si and C into consideration when discussing the final equilibrium configurations.

In order to foresee the different phase equilibria occurring during the wetting experiments and the cooling process, a specific thermodynamic database has been developed, including the elements C, Si, Al and Ti.

Binary and ternary interaction parameters have preliminarily been taken from literature assessments (Al-Si from [138], Al-Ti [126], Al-C from [139], C-Si from [138], C-Ti from [140], Ti-Si [141], Al-C-Si [138], Al-C-Ti [140], C-Si-Ti [142] and subsequently adapted in order to obtain a self-consistent set of phase models and interaction parameters.

6. Results and discussion

The results obtained during the investigation of solid-liquid interactions occurring in these two different metal-ceramic systems (oxidic and non-oxidic), representative of a reactive system in the first case ($Y_3Al_5O_{12}$/Ag-based alloys and $Y_3Al_5O_{12}$/alloy/Ti6Al4V) and of a reactive and dissolutive system (Al-Ti alloy/SiC and SiC/Al-Ti/SiC) in the second one, are shown respectively in *ch.6.1* and in *ch.6.2.*

To reach this goal the wettability evaluation of the systems in inert atmosphere is conducted. For both the systems the wetting tests are performed using the sessile drop technique and the reactivity is evaluated using EDS analysis: the sample sections are observed (LOM) and analysed (SEM-EDS). The interactions between the brazing alloys and the substrates have been also analysed by the CALPHAD method: the experimental results are interpreted on the basis of thermodynamic calculations conducted using specific thermodynamic databases.

In the first case (oxidic system) an existing thermodynamic database was used to follow the evolution of the metallic part of the system at the selected conditions (*ch.5.3.1*) while in the second case (non-oxidic system; *ch.5.3.2*) a home-made (Al-C-Si-Ti) database was used, as already discussed.

6.1 Oxidic system: $Y_3Al_5O_{12}$/metals and $Y_3Al_5O_{12}$/metals/Ti6Al4V

Pure metals as well as ternary and binary Ag-based alloys are tested in contact to the YAG substrate (*Table 6.1*) and evaluated in terms of wettability and interfacial reactivity.

1) First of all the wettability of AgCuTi on this ceramic is evaluated starting from the higher selected temperature (950°C) and defining:

- the contact angle value in function of the time as well as the kinetics of the spreading and the changing drop profiles;
- the nature of the liquid phase after the high temperature test analyzing and comparing the microstructure of the bulk and the thermodynamic prediction of the Ag-Cu-Ti metallic system at the test conditions.

These results, as well as the wetting evaluation, are compared to the ones related to the lower temperature (850°C) tests for the same system (AgCuTi/YAG).

2) Then, the reactivity of the metal-ceramic couple is investigated, on the basis of:

- the different metal-ceramic layers as well as the intermetallic compounds formed at the interface are defined in terms of composition and thickness;
- the element mobility, analyzed observing the map distributions of each component from the YAG to the bulk.

Table 6.1- Different metals and alloys tested in contact to the YAG substrate at the selected process parameters.

Wettability of YAG by metals/alloys		
Ag (1050°C), Cu (1150°C)	AgTi (1050°C), AgCu (850°C)	AgCuTi (820, 850, 950°C)
Brazing of YAG to Ti6Al4V		
Ag (1050°C)	AgCu (850°C)	AgCuTi (850, 950°C)

The wettability and the reactivity are reported also for the systems involving the pure metals (Ag and Cu) and the Ag-Cu and AgTi binary alloys.
The kinetics is briefly explained taking into account the interfacial microstructure. The absence of a substantial metal-ceramic interaction is clearly shown by a careful analysis of the contact zone.
The temperatures are selected considering the melting temperatures of each alloy.
In the specific case of the AgCuTi system three different temperatures are chosen to compare specific experimental conditions.

6.1.1 Wettability evaluation

As underlined before, the wettability evaluation of metal-ceramic couples, allowing to understand the interfacial interactions between the two different materials, represents the preliminary step to define brazing process parameters as filler alloy composition, temperature and time.
In *ch.6.1.1.1* the wettability and the kinetics of AgCuTi on YAG are evaluated and a thermodynamic interpretation of the system is given using the CALPHAD approach explained in *ch.5.1*.
In order to define the role the different elements have in the system, the wettability and the reactivity of pure metals (Ag and Cu) and binary alloys (AgCu and AgTi) is also evaluated and

reported in *ch.6.1.1.2*. Then the interfaces of the different systems are characterized in terms of morphology and composition of the phases formed starting from the metal-ceramic contact zone. The aid of the isothermal sections (Ag-Cu-Ti) is essential to predict the alloy behavior (*ch.6.1.2*).

Table 6.2 reports the different metallic materials tested on the YAG substrate with the corresponding testing temperature, the contact angle after 1h test and the Ti activity value.

Table 6.2. The different metals tested on the YAG substrate with the corresponding testing temperature, the contact angle after 1h test and the Ti activity values and activity coefficient γ.

Alloy/metal	T [°C]	θ_{eq} [°]	a_{Ti}	γ_{Ti}
AgCuTi	820	71	0.199	11.06
	850	73	0.234	9.36
	950	10	0.318	5.70
AgCu	850	107	-	-
AgTi	1050	64	0.74	9.25
Ag	1050	116	-	-
Cu	1150	127	-	-

6.1.1.1 $Y_3Al_5O_{12}$/AgCuTi

The wettability tests of the AgCuTi on YAG substrate have been conducted at temperatures between 800°C and 950°C to cover the whole range of suggested conditions for brazing processes as well as to define the modification occurring in the liquid composition.

The results of the AgCuTi tests on YAG at 950°C for 1h,reveal that the wetting process is characteristic of a reactive regime: the contact angle varies quite slowly with time and the equilibrium configuration should be reached after one hour of contact at 950°C (*Figure 6.1*).

However, given the small slope of the θ vs. time curve at the end of the tests, a final "equilibrium" contact angle $\theta \approx 10°$ can be safely assumed.

As observed in *Figure 6.1* (b), the sessile drop profile after a contact time of about 25 min, evolves from a symmetrical "Laplacian" profile to a perturbed shape characterized by a dome on the drop apex.

The section microstructure of *Figure 6.2* demonstrates that this phenomenon is due to the presence of a miscibility gap in the liquid phase involving two different liquids L_1 and L_2.

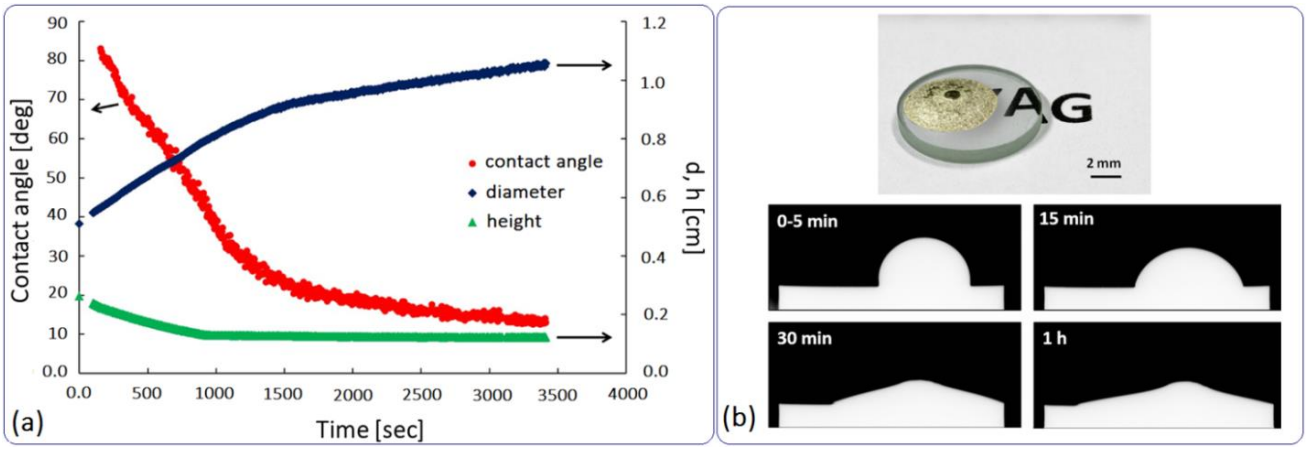

Figure 6.1. Contact angle, base diameter and height of drop plotted as function of time (a); YAG/AgCuTi sample after 1h test(b, up) and profile images of the system at 950°C (b, down).

The currently available ternary phase diagrams are mainly based on the Eremenko work [143] and the thermodynamic modelling of Dezellus [137].

Thus, starting from these data, the Ag-Cu-Ti ternary equilibria have been recalculated by CALPHAD.

The resulting isothermal section at 950°C (*Figure 6.3*) clearly shows that the point representing the Ag-Cu-Ti alloy used in this work should fall very close to the border of the L_1+L_2 two-phase field.

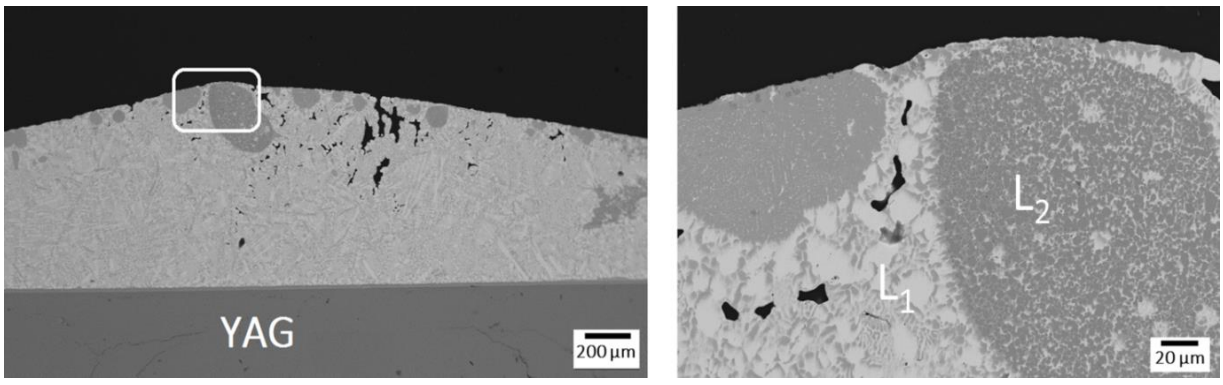

Figure 6.2. Image of the drop section for AgCuTi/YAG system after testing at 950°C (on the left) and the zoomed area indicated by the white rectangle (on the right).

This result does not seem to be completely confirmed by experimental results showing the clear presence of a 2nd lighter phase in the molten drop (zoomed rectangle of *Figure 6.2*).

However, calculations made at 940°C demonstrated that the two immiscible liquids should exist for this specific AgCuTi composition, with a relative volume fraction of L_2 of the order of 10%.

Nevertheless, the discussions below will be referred to the temperature of 950°C and to the phase diagram in *Figure 6.3*, given the overall uncertainty due to: the inherent approximation of the CALPHAD calculations, the measurement uncertainty of the liquid drop temperature and the small amount of the second liquid phase.

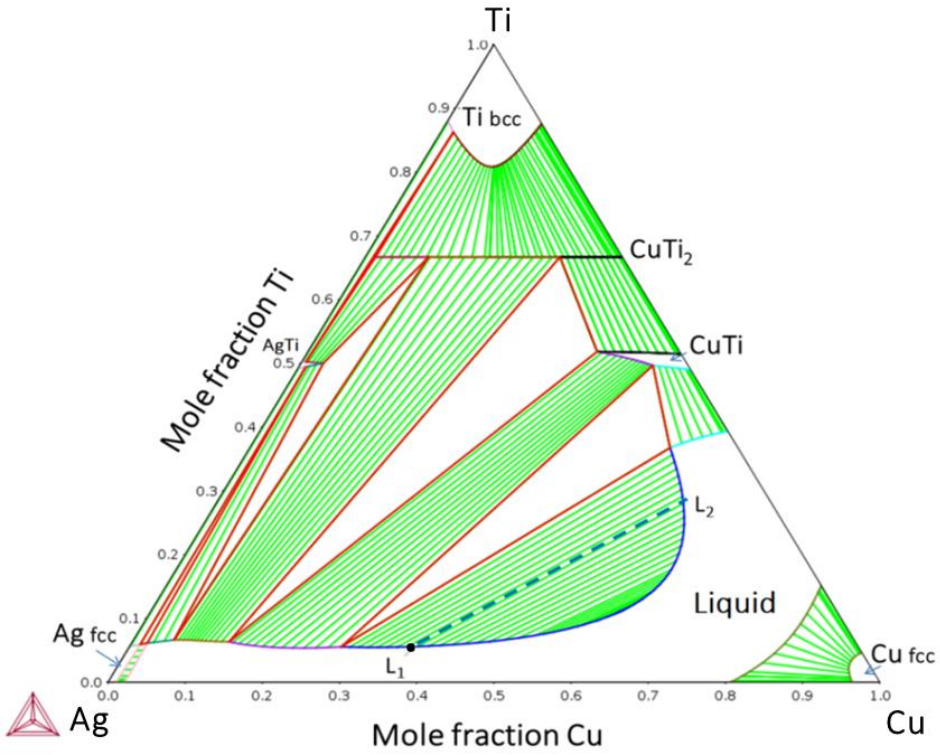

Figure 6.3. Recalculated ternary phase diagram for the Ag-Cu-Ti system; section at 950°C; the black circle represents the alloy composition used. The line connecting points L_1 and L_2* represents the trace of the vertical section in Figure 6.5(b).*

Indeed, the equilibrium phase amounts during the solidification path of AgCuTi as a function of temperature of *Figure 6.4* shows that L_1 and L_2 co-exist only in the range of 910-950°C, where L_2 is always present in a quantity less than 10 vol%.

The formation of the two liquids, already known, and its effect on the wetting process, has been discussed by other authors.

In particular, Hinryj and Indacochea [124] have addressed this specific item from a thermodynamic point of view.

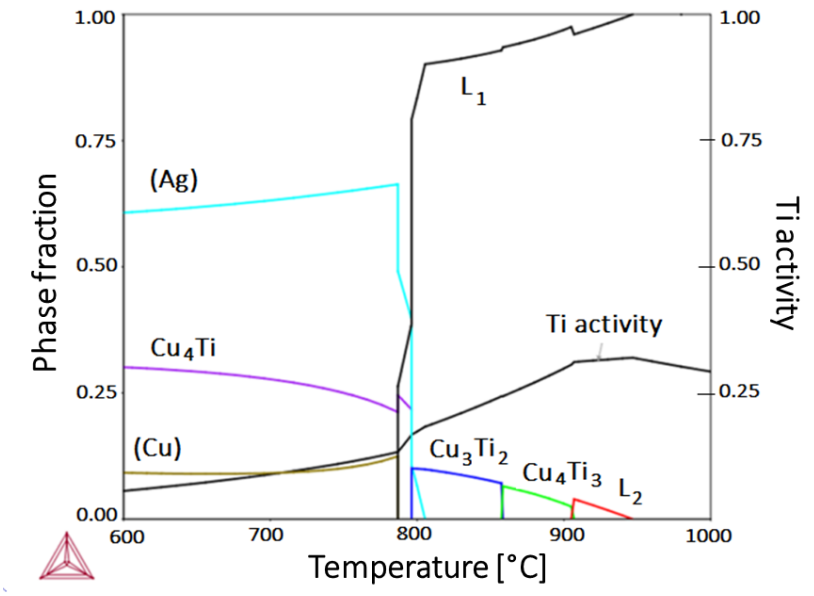

Figure 6.4. Solidification sequence of the starting alloy and Ti activity values as a function of T (ref. state: solid Ti, hcp).

Extending their analysis, on the basis of our CALPHAD calculations, it can be seen (*Figure 6.5*) that, above 900°C, the starting alloy demixes into two liquids (*Figure 6.5*), whose compositions, recalculated by CALPHAD, are reported in *Table 6.3* (T= 950°C).

The data reported in *Table 6.3* show the estimated densities of the two alloys: even if this is an estimation on the basis of published data for the binary systems, it is clear that L_1* is much denser than L_2* (L_1*≈ 1.30 L_2*), so that L_2* should float on top of L_1*.

Table 6.3. Compositions of the L_1 and L_2*liquids at 950°C, their estimated densities ρ (values for Ag-Cu and Cu-Ti alloys interpolated from data reported in* [144] *and*[145]*), the Ag fraction u =$x_{Ag}/(x_{Ag}+x_{Cu})$, and the Ti activity (a_{Ti}) and activity coefficients (γ_{Ti}) in the two liquids (Ref. state: solid Ti, hcp structure).*

Composition	Ag	Cu	Ti	ρ	u	a_{Ti}	γ_{Ti}
at%				[g/cm^3]			
Starting alloy	57.70	36.80	5.50	9.9	0.612		
L^*_1	57.24	36.72	5.58	8.6	0.606	0.318	5.70
L^*_2	11.36	60.45	28.18	6.6	0.158	0.318	1.13

Then the wetting between 910°C and 950°C should be governed by the L_1 liquid, which represents the major phase of the system. As underlined in [124] it has often been argued that the L_2 liquid should wet the underlying oxide much better than L_1, because of its much higher Ti content. However, as the L_1 and L_2 liquids are in equilibrium, the Ti chemical potential and its activity in the

two phases must be the same and sufficient to make the phase L_1 a good wetting liquid even if at a much lower Ti concentration. Therefore the compositions of the corresponding L_1* and L_2* liquids with the same Ti activity can be evaluated (*Table 6.3*) confirming a much higher activity coefficient γ_{Ti} in L_1* than in L_2*.

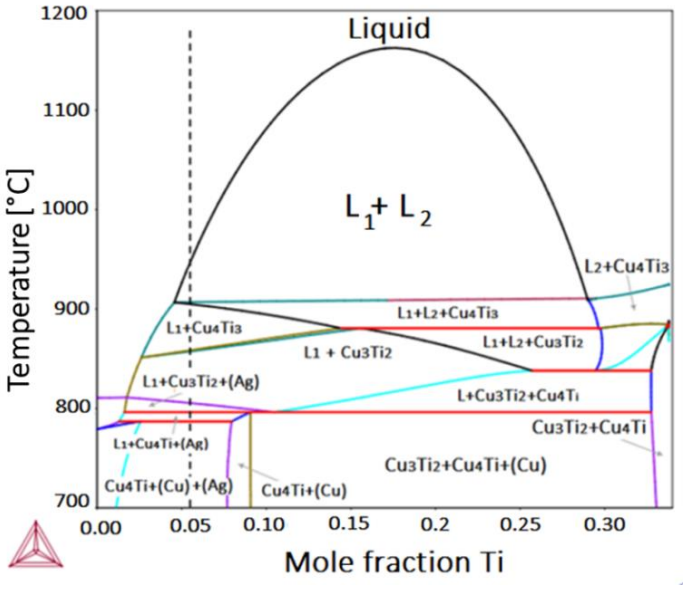

Figure 6.5.Ccalculated vertical section passing through the L_1 and L_2* tie line at 950°C. The dotted line represents the alloy initial composition.*

In *Figure 6.6*the horizontal line at a_{Ti}=0.318 corresponds to the composition of the Ti-containing starting alloy and to the tie-line through this point at 950°C connecting the L_1* and L_2* liquids, in the phase diagram shown in *Figure 6.3.*

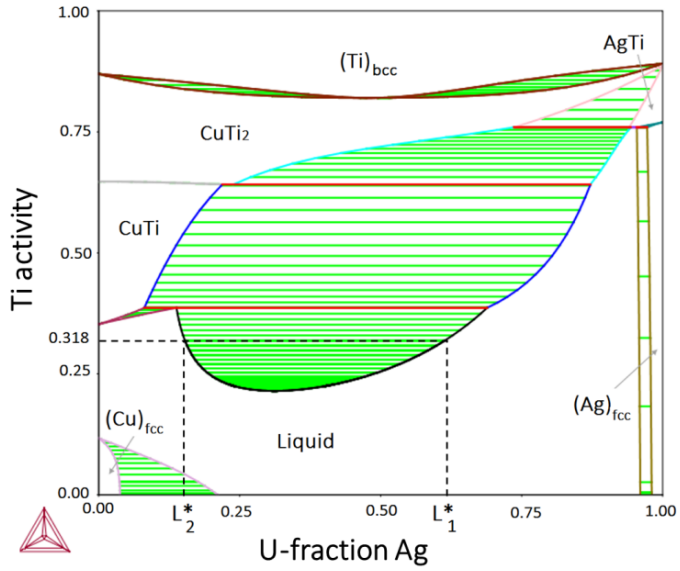

Figure 6.6. Ti activity aTi plotted as the Ag function $u=x_{Ag}/(x_{Ag}+x_{Cu})$ at 950°C. L_1 and L_2* are the liquids in equilibrium at 950°C.*

Other wetting tests have been conducted at lower temperatures in order to explore the feasibility of brazing at 820°C and 850°C. The corresponding sessile drop profiles, shown in *Figure 6.7*(b) and *Figure 6.8*, are quite regular and the spreading kinetics tends to reach an equilibrium value before the end of the tests giving final contact angles less than 90° at both temperatures. However it should be noted that at 820°C the spreading is much slower than that at 850°C reaching a "final" contact angle close to the one at 850°C only after 1 h contact *Figure 6.7*(a).

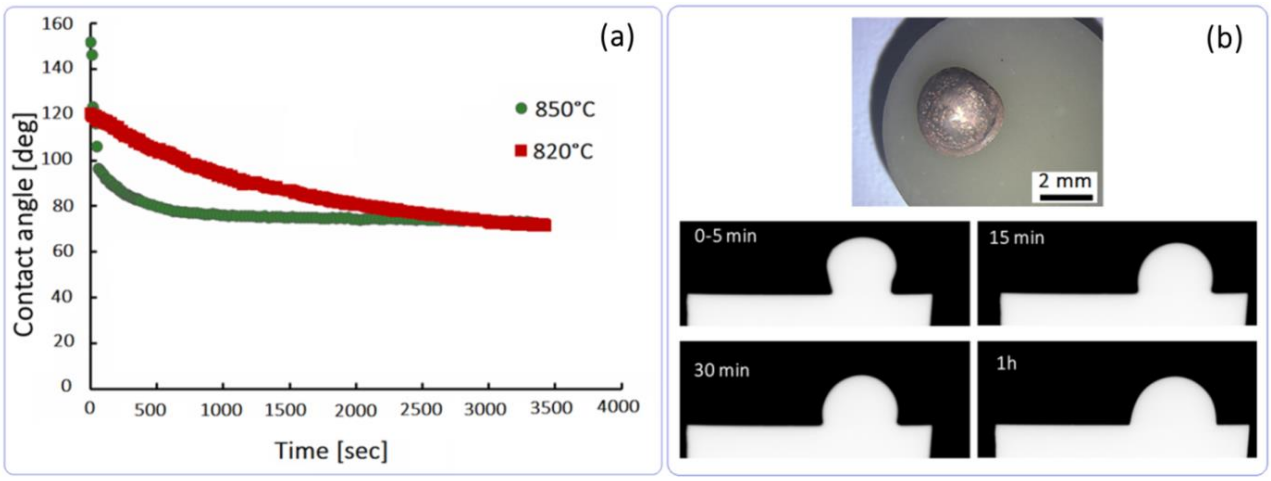

Figure 6.7. Contact angle as a function of time for AgCuTi system at 820, 850°C (a); the YAG/AgCuTi sample after 1h test (b, up) and profile images of AgCuTi system at 850°C (b, down).

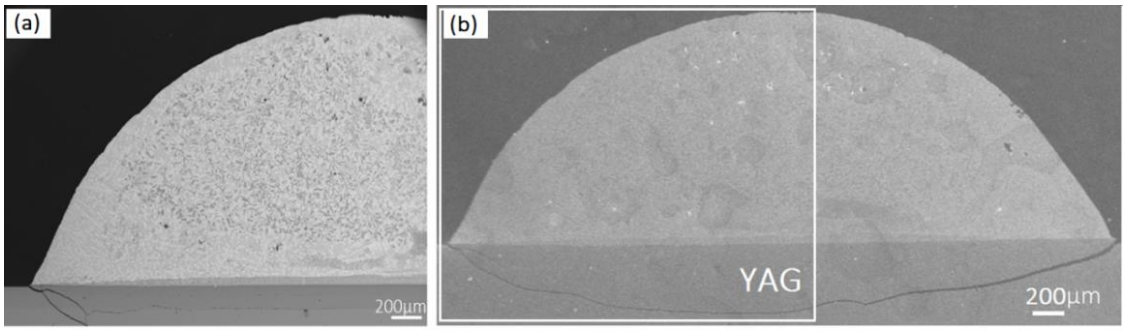

Figure 6.8. Image of the drop profile section for AgCuTi/YAG system after testing at 850°C (b) and the zoomed area indicated by the white rectangle (a).

At these temperatures most of the drop volume consists of the liquid L_1 co-existing with the intermetallic compound Cu_3Ti_2 to a max of 10 vol% (*Figure 6.9*). These differences confirm that the extent of interfacial reactions between Ti (and Cu to a minor extent) with the underlying YAG substrate depends certainly on the temperature (slower diffusion kinetics at lower T) but, to a large extent, on the Ti activity in the liquid phase. Indeed, as shown in *Figure 6.4*, when going from 820°C to 950°C, the Ti activity in the liquid drop increases sharply, maintaining, at the same time, a high

value of the activity coefficient. From the drop profile of *Figure 6.8,* it is possible to observe a homogenous microstructure coming from the solidification of a liquid composition at variance with what happened testing the same sample at higher temperature (*Figure 6.2*).

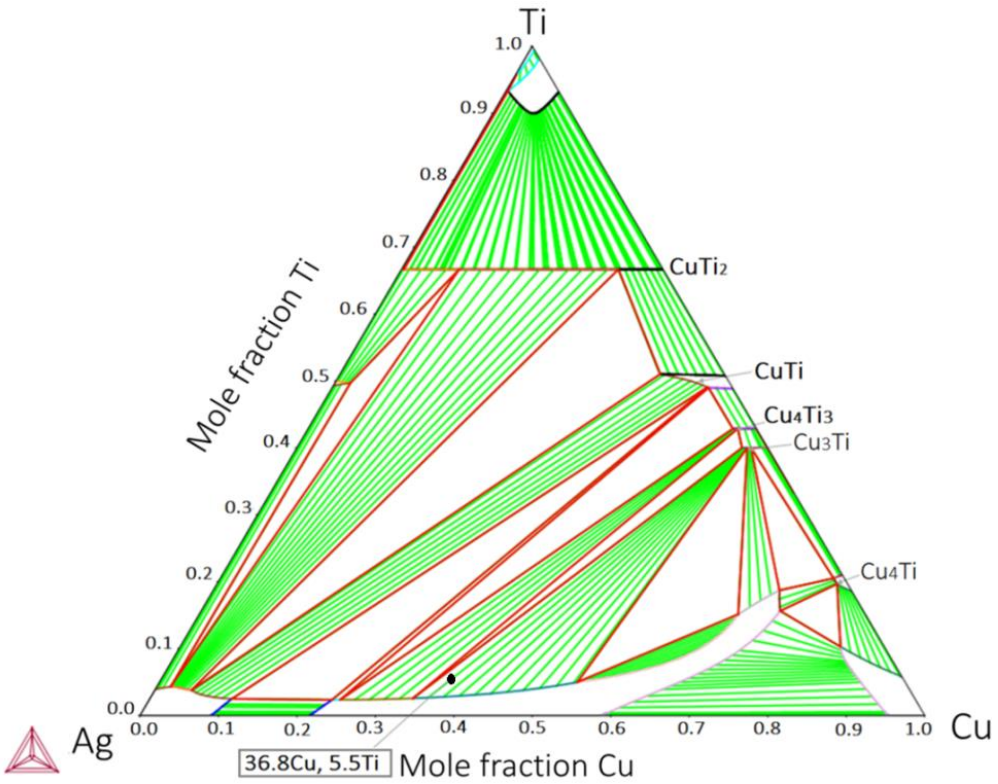

Figure 6.9. Recalculated ternary phase diagram for the Ag-Cu-Ti system; isothermal section at 850°C.

6.1.1.2 $Y_3Al_5O_{12}$/(pure metals, binary alloys): wettability and reactivity

Reference tests using Ag, Cu and AgCu, AgTi alloys have been conducted at various temperatures (close to T=1.05 T_m[K]) to clarify the role the different elements have on the wetting when in contact with the YAG substrate. From the wetting and kinetics study of pure metals/YAG and binary alloys/YAG samples (*Table 6.4*) it is observed that only the AgTi/YAG system does reach a contact angle value (θ_{eq}=64°) which is characteristic of a fair wetting condition (*Figure 6.10*).

$Y_3Al_5O_{12}$/pure metals

The analyses of the Ag/YAG and Cu/YAG interfaces show that no layers containing new phases or compounds grew between the substrate and the alloy, demonstrating that no significant interactions took place between the ceramic and the metallic material.

For this reason no wettability was obtained for the Ag/YAG and Cu/YAG systems; the strong decrease of contact angle values observed after the first 5 min for both systems isa consequence of the alloy change of shape due to the melting of the drop.

In particular, the equilibrium contact angle measured after 1 h for the Ag/YAG systemis 116° (*Figure 6.10*).

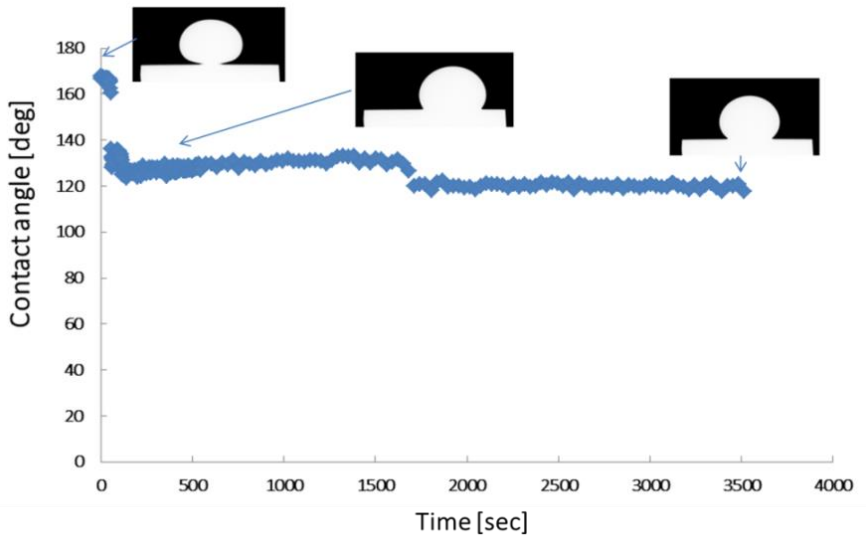

Figure 6.10. Contact angle as a function of time for Ag/YAG system at 1050°C.

As it is clearly visible in the SE image of the section reported in *Figure 6.11*, no intermediate phases formed in contact to the YAG substrate.

The EDS analysis of the bulk confirmed the presence of an Ag matrix without any traces of other elements dissolved in it.

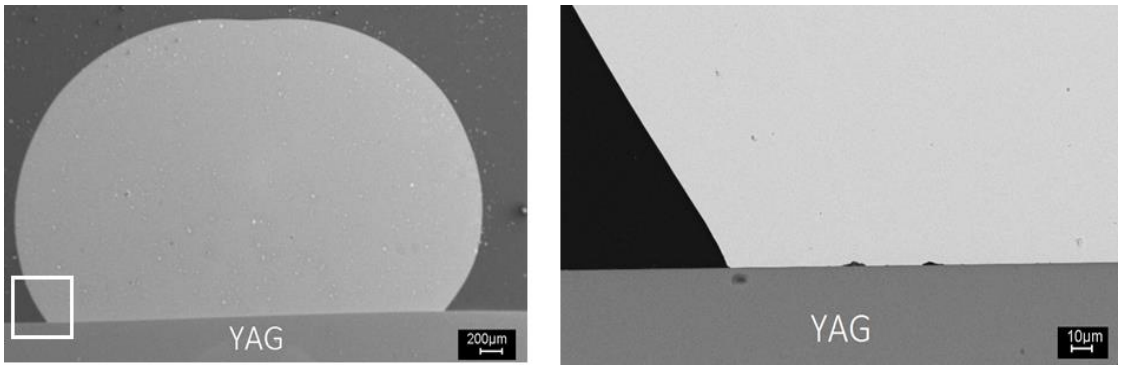

Figure 6.11. Interfacial microstructure of Ag/YAG system maintained at 1050°C for 1 h..

The equilibrium contact angle measured after 1 h for Cu/YAG systemis 127° (*Figure 6.12*).

From the analysis reported in *Figure 6.13*, it is possible to deduce that also in the Cu/YAG interfacial section no intermediate phases are detected in contact to the YAG.

The EDS analysis confirmed the presence of a Cu matrix without any traces of other elements.

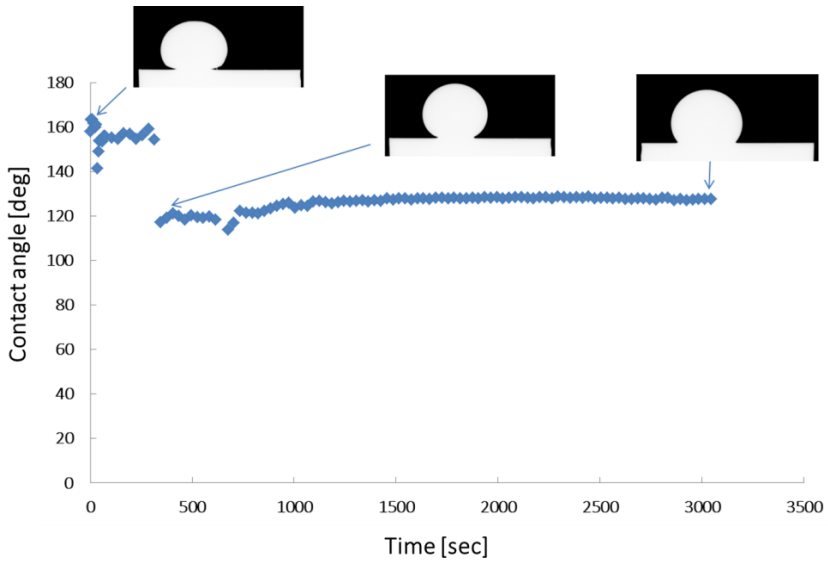

Figure 6.12. Contact angle as a function of time for Cu/YAG system at 1150°C.

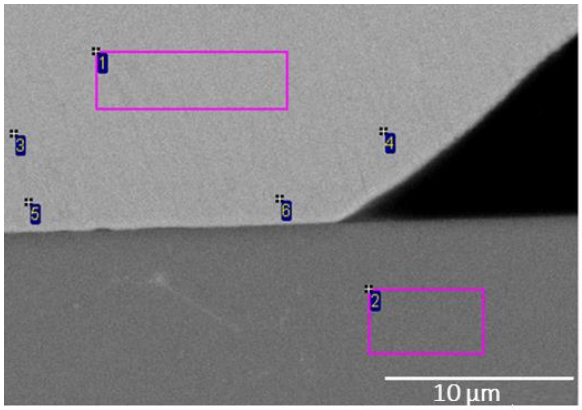

Spectrum	O	Al	Cu	Y
1			100.0	
2	60.2	24.11		15.7
3			100.0	
4			100.0	
5			100.0	
6			100.0	

Figure 6.13. Interfacial microstructure of Cu/YAG system maintained at 1150°C for 1 h.

The wetting behaviour of the different alloys and pure metals can also be interpreted in terms of the Work of Adhesion, defined, after Young-Dupré [3] (equation 6).

For alloys pertaining to the AgCuTi system, the liquid surface tension has been evaluated both theoretically[146]and experimentally [79] at various temperatures.

Taking into account that small Ti additions (of the order of 5 at%)to the Ag-Cu eutectic alloy cause an increase of the liquid surface tension lower than about 1% [146], an extrapolation of the values reported in [79] can be safely applied. The results are shown in*Table 6.4.*

Table 6.4. Work of adhesion (W_a) calculated from experimental contact angles (ϑ) and surface tension (σ^*) values extrapolated from [79], [146]. *The σ^* is the surface tension of the pure metal or of the Ag-Cu alloy and the σ_c the corrected ones (5 at% ofTi addition).*

	T [°C]	Θ[°]	σ^* [mN/m]	σ_c[mN/m]	W_a [mJ/m^2]
AgCuTi	820	71	969	979	1298
	850	73	967	977	1262
	950	10	955	965	1914
Ag	1150	116	898	-	504
Cu	1150	127	1274	-	506
AgCu	850	129	-	-	-
AgTi	1050	64	907	952	1904

These data underline that in this specific case the liquid surface tension does not play a central role in the adhesion; rather, that the interfacial structure, originated by the interactions of Ti with the solid substrate through an important decrease of the interfacial tension, causes a drop in contact angle and thus the large increase of the Work of Adhesion found at 950°C.

The reasons for this decrease in the interfacial tension value are linked to important changes in the chemical nature of the solid-liquid interface, that will be discussed in the next paragraphs.

From *Table 6.4* it is possible to notice that low Work of Adhesion values are typical of pure non-wetting metals while AgTi shows a significant high value, comparable to the one of the ternary alloy at 950°C.

$Y_3Al_5O_{12}$/AgTi

As mentioned before, from the wetting study of pure metals/YAG and binary alloys/YAG samples (*Table 6.4*) it is observed that just the AgTi/YAG system does reach a contact angle value (θ_{eq}=64°) which is characteristic of the wetting region (*Figure 6.14*). Indeed, at the AgTi/YAG interface, two layers are found at the solid-liquid interface (*Figure 6.15*).

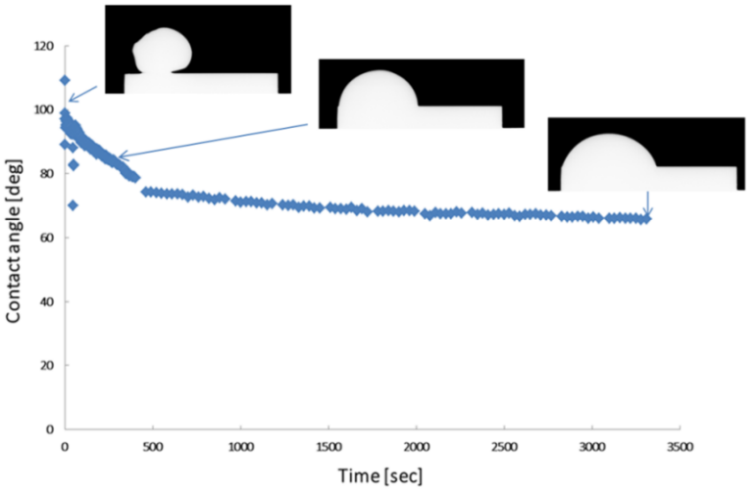

Figure 6.14. Contact angle as a function of time for AgTi/YAG system at 1050°C.

On top of the YAG bulk substrate, whose composition corresponds to the theoretical one: 60 at% O, 25 at% Al, 15 at% Y, a 1st layer is found, with an average thickness of about 7 µm, extending along the whole interface profile. Its composition analysed by SEM-EDS analysis (54.5 at% O, 16.5 at% Ti, 27 at% Y, 2.0 at% Ag) is very close to the stoichiometry TiY_2O_5.

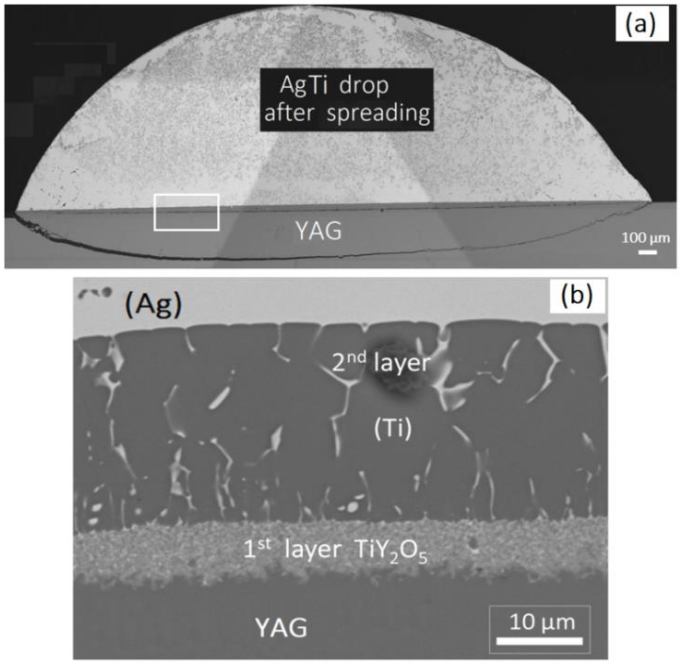

Figure 6.15. AgTi/YAG cross section of samples tested at 1050°C; drop profile composite image which shows the lens crack characteristic of the quick cooling (a); zoomed BSE image of the metal-ceramic contact zone (b).

This compound should come from the reaction:

$$3\ Ti + 2\ Y_3Al_5O_{12} \rightarrow 3\ TiY_2O_5 + 3\ Al_2O_3 + 4\ (Al) \qquad 1)$$

This reaction is meant to formalize that Ti, migrating to the solid-liquid interface, partially reacts with the Al contained in the YAG, entering into the solid structure to substitute a certain number of Al places, while causing the separation of small quantities of Al_2O_3 and of metallic Al which enters into the liquid metallic phase, as proved by the Al traces found in the bulk drop after solidification. In other words, this process could be formally depicted through the following reaction cycle:

$$2\ Y_3Al_5O_{12} \leftrightarrow 5\ Al_2O_3 + 3\ Y_2O_3 \qquad 2)$$

$$2\ Al_2O_3 + 3\ Ti \rightarrow 3\ TiO_2 + 4\ (Al) \qquad 3)$$

$$3\ Y_2O_3 + 3\ TiO_2 \rightarrow 3\ TiY_2O_5 \qquad 4)$$

The sum of these reactions gives reaction 1), allowing the formation of a ceramic phase with fixed stoichiometry, stable at low temperature and with a hexagonal or orthorhombic structure [147], the first found in the Y_2O_3-TiO_2 phase diagram for increasing Ti contents [148]. The 2nd layer, about 30 µm thick (Figure 6.15), extends also over the whole interfacial area. While the bulk drop is essentially constituted of (Ag), the Ti active element is concentrated at the interface, in particular in the 2nd layer, formed by columnar grains of (Ti) separated by several white silver rich phases.
The reduced dimension of this last phase does not allow to carefully define its composition by EDS.
The growth of columnar grains at the solid-liquid interface should take place in two steps:

1) at the temperature of the experiment, the Ti migrated to the YAG surface gives rise to the TiY_2O_5 compound, followed by the nucleation of metallic nuclei on top of it;

2) during cooling, due to Ti decreased solubility in Ag, columnar grains develop producing a metallic layer of the Ti solid solution, very diluted in Ag, with its maximum thickness at the center of the solid-liquid interface. It is clear that step 1) is the relevant process promoting the observed good wettability: the TiY_2O_5results better wettable then the original ceramic substrate.

$Y_3Al_5O_{12}$/AgCu

The AgCu/YAG system, that includes the use of a binary alloy without the addition of active elements, does not reach a contact angle value characteristic of the wetting region, as the value of the equilibrium contact angle (θ_{eq}=129°) is significantly higher than 90° (*Figure 6.16*).

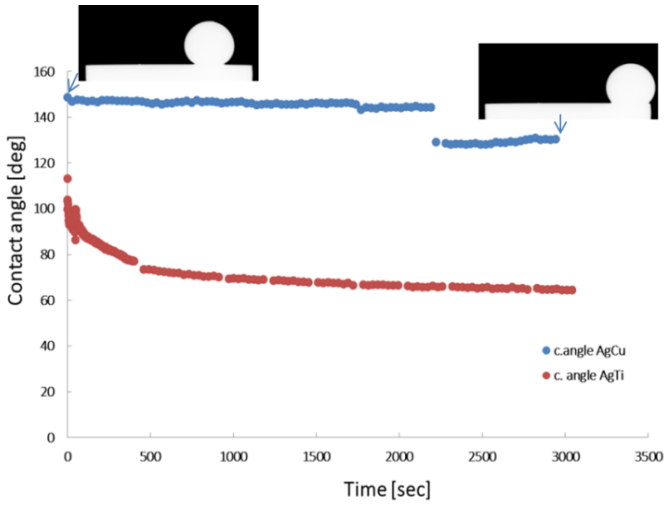

Figure 6.16. Contact angle as a function of time for AgCu/YAG system at 1150°C.

In the AgCu/YAG system the eutectic structure extends in the whole drop, from the top to the metal-ceramic interface. This phase distribution has been proven by removing the alloy from the ceramic substrate after the wetting test.

The AgCu drop, mechanically detached from the YAG surface, is observed by EDS analysis on the base (*Figure 6.17*) that was in contact to the ceramic.

The eutectic structure and composition is found on the whole base drop surface as well as some small holes.

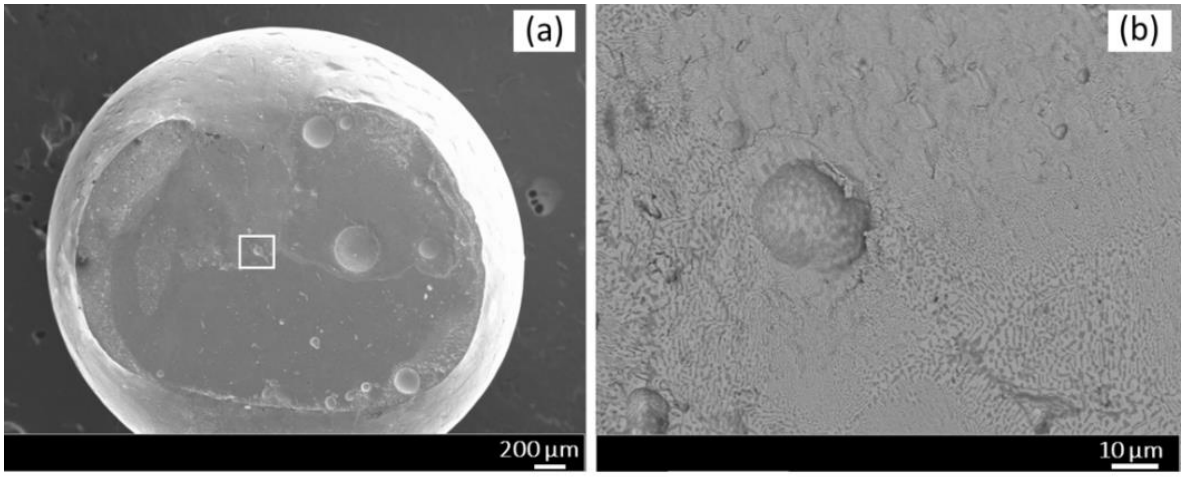

Figure 6.17.Topview of AgCu drop base after the wetting test (a); zoomed area of the base (b).

The drop has also been observed on its meridian section (*Figure 6.18*) and the EDS analysis has confirmed the presence of the Ag-Cu eutectic up to the YAG surface.

The same structure and composition is also found in the bulk of the drop and at the metal-YAG contact zone where there a total absence of visible interactions between the ceramic and the metal is found (*Figure 6.17*).

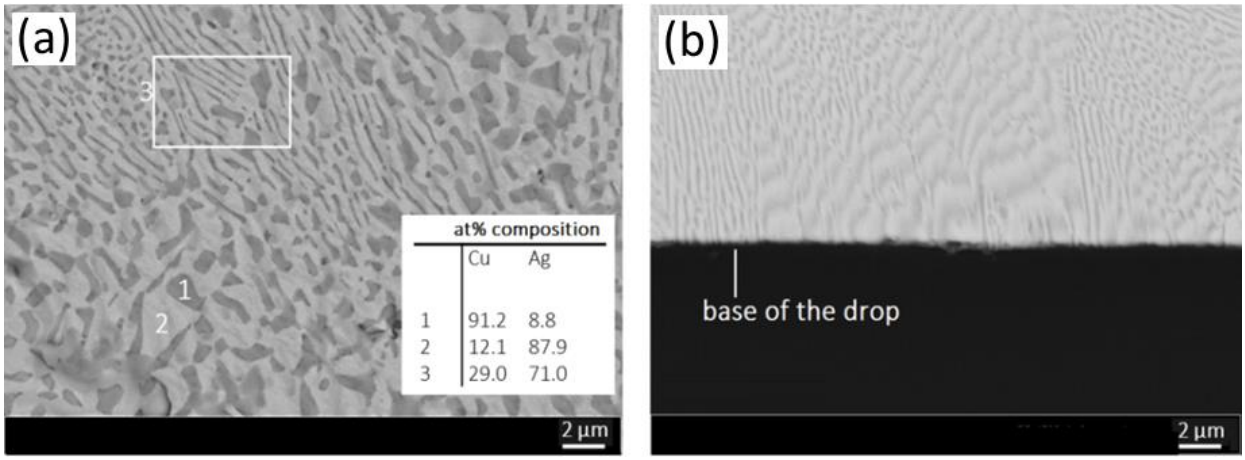

Figure 6.18. Matrix microstructure of AgCu section after the wetting test at 850°C including the EDS analysis composition (a); contact zone of the detached drop section (b).

6.1.2 Reactivity results

6.1.2.1 Discussion: AgCuTi/YAG (950,850, 820°C)

To evaluate the reactivity of the system the attention is focused on the evaluation of the interfacial zone where most of the phenomena related to the wetting process take place.

The section of the AgCuTi/YAG sample, tested at 950°C for 1 h, confirms the system reactivity showing four different layers grown at the metal-ceramic interface (*Figure 6.19*).

The composition of the continuous 1st layer (light grey in *Figure 6.19*) demonstrates that both Cu and Ti migrated at the interface. On the other hand, a small amount of Al diffused from YAG into the molten drop, entering as traces in various phases.

The Al diffusion in the liquid phase is compensated by Cu and Ti migration to the interfacial zone while traces of Ag (0.6 at%; *Table 6.5*) can be found also in the 1st ceramic-metal layer.

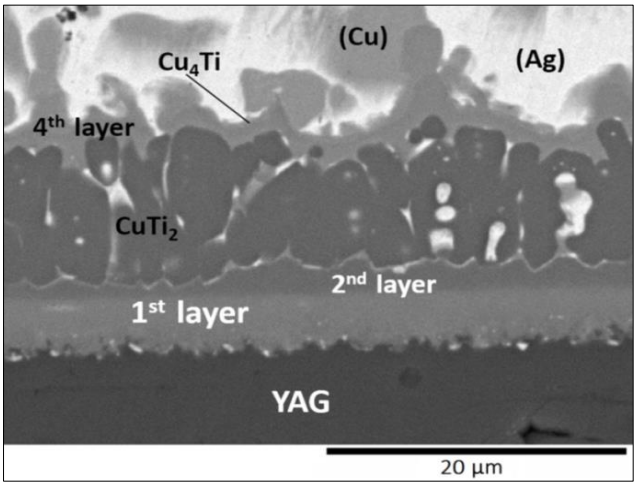

Figure 6.19. Interfacial layers of AgCuTi/YAG tested at 950°C for 1 h.

The 2nd layer, continuous and thinner than the 1st one, is characterized by a decreased O amount (from 41 at% to 18.6 at%;*Table 6.5*) while the concentration of Ti and Cu increases.

The presence of Y in this layer is drastically less than in the 1st one, while Al composition does not change significantly.

As confirmed in the map of *Figure 6.20*, Y is not dissolved into the liquid.

It means that the liquid reacts with the ceramic to form the first metal-ceramic layer without any significant substrate dissolution.

Table 6.5. Composition of the layers of AgCuTi/YAG tested at 950°C for 1h.

Layer	Composition (at%)						
	Ag	Al	Cu	O	Ti	Y	
YAG	-	26	-	64	-	15	
1st	0.6	3.5	16.5	41	15.2	19.8	
2nd	1.5	2.40	35.6	18.6	41.1	0.8	M_4X
3rd	2.5	0.8	33	-	63.7	-	$Cu\ Ti_2$
4th	2.3	0.8	72.5	-	24.4	-	Cu_4Ti

It is possible to suppose, referring to *Table 6.5*, that this 2nd layer is mainly formed of an intermetallic compound with stoichiometry $M_{23}X_6$ (shortly: M_4X) known as τ phase [149], [150].

This phase is one of a class of dilute ceramic compounds that are metal-rich compared to the conventional ceramics and which have properties in-between those typical of ceramics and those typical of metals. This 2nd layer seems to be perfectly adherent to the 1st layer: in fact no defects or pores are formed along the contact line. Its increased metallic character improves the wetting behaviour significantly. The 3rd layer, about 10 µm thick, is constituted of columnar grains in which it is possible to identify the intermetallic compound $CuTi_2$ dissolving small quantities of Ag (2.5 at%) and Al traces (0.8 at%). The existence and the stability of $CuTi_2$ under our experimental conditions are confirmed by literature data [151]. This phase, stable at room temperature, is often used in chemical industry [151] because of its outstanding corrosion resistance which is considerably higher than that of pure Cu or Ti. Its presence can be beneficial for a sector in which transparent windows should withstand highly corrosive environments, such as in case of deep sea applications. No ternary compounds have been found in the Ag-Cu-Ti system but it is known that in the Cu_xTi_y compounds the Ag solubility decreases continuously as Cu content increases [137].

The white regions of the 3rd layer, placed inside the Ti-rich dark grey columnar grains, are too small to be quantitatively defined by SEM-EDS but they are Ag-rich as demonstrated by element maps of *Figure 6.20*. The reaction allowing the formation of Cu_4Ti intermetallic compound of the 4th layer (*Figure 6.19*) occurs at 808°C (at equilibrium condition; *Figure 6.5*) and it is the most important reaction with respect to the amount of liquid transformed into solid [124]:

$$L + Cu_3Ti \leftrightarrow Cu_4Ti + Ag(Cu) \qquad 5)$$

During this transformation, both at equilibrium or not, most of the alloy is liquid; for this reason this is a crucial point for the wetting behavior.

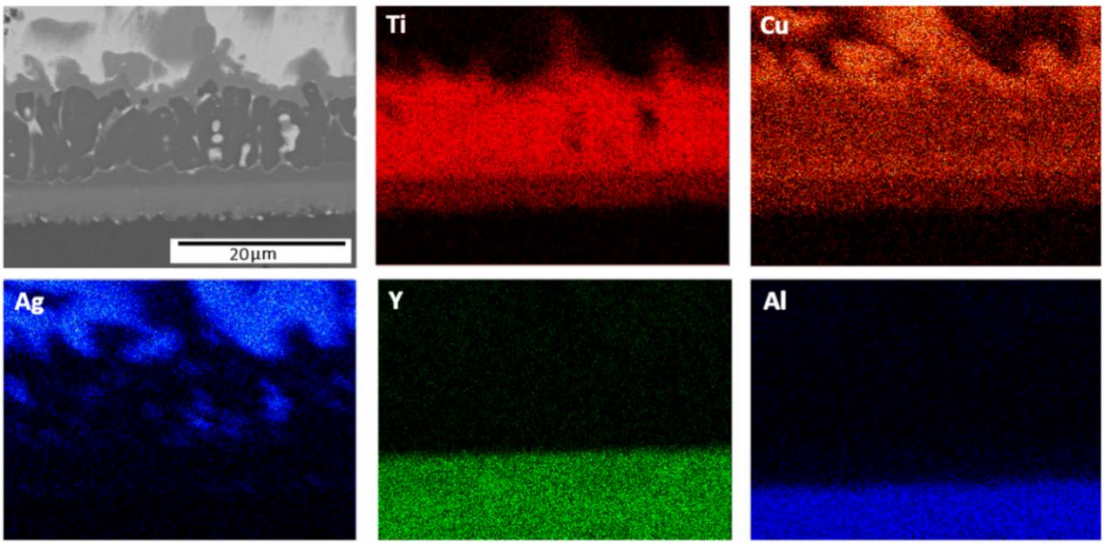

Figure 6.20. Elements map of AgCuTi/YAG interface layers of the samples tested at 950°C.

It is known from literature that there are three equilibrium phases at low temperature: Ag- and Cu-based solid solutions and Cu_4Ti. In the present work the system tested at high temperature is cooled quickly following non-equilibrium paths, especially at lower temperatures. The presence of Cu_3Ti_2, for example, was reported in previous works and proves that the alloy was not at equilibrium [152], while structures similar to the ones found here, even if in different conditions, have also been reported [153]. In the alloys tested during our experimental work, part of the $CuTi_2$ intermetallic formed the interface zone at 950° and the rest was involved in the reactions leading to the formation of Cu_4Ti as predicted from the equilibrium path. It is important to underline that the adhesion is obtained also in the sample tested for only 10 min at 950°C (*Figure 6.21*); the liquid metal infiltrated few micrometric YAG pores allowing the formation of a continuous and homogeneous interface.

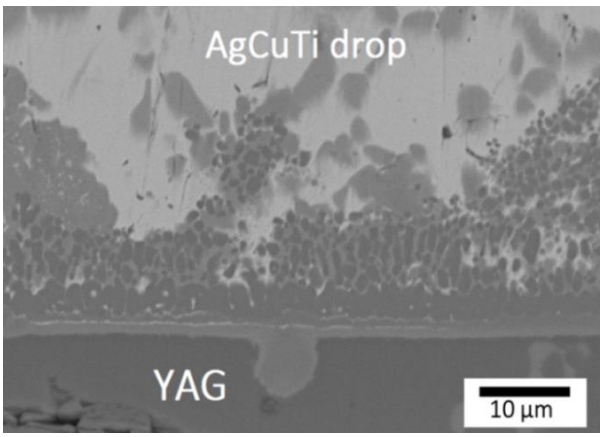

Figure 6.21. Interfacial morphology of AgCuTi/YAG tested at 850°C for 1 h.

The AgCuTi/YAG systems tested at 850°C and 820°C for 1 h show a worse wettability than that found at 950°C, even if the values obtained (*Table 6.4*) are still useful for brazing processes (see *2.3*).

The reactivity at the interface zones is similar for both the temperatures (850, 820°C).

At 850°C the 1st layer of the interface zone is thinner (4 µm) than the corresponding layer found in samples tested at 950°C (*Figure 6.22*), with similar compositions (*Table 6.6*).

Table 6.6. Composition of the layers of AgCuTi/YAG tested at 850°C.

Layer	Compositions (at%)						
	Ag	Al	Cu	O	Ti	Y	
YAG		25.3	0.3	58		16.4	
1st	0.4	3.1	15.7	44	17.2	19.6	
2nd	83.6		12.9	-	3.5	-	(Ag)
2nd	3	2.3	50.5	-	44.2	-	CuTi
3rd	2.5	2.7	45.0	-	49.8	-	CuTi
4th	60.0	-	39.1	-	0.9	-	Ag-Cu

A 20 µm thick 2nd layer, with a bright (Ag) phase and a dark CuTi phase, can be observed on top of the first metal-ceramic layer (*Figure 6.22*).

Moreover a 2 µm layer of CuTi extends between the 2nd layer and the eutectic structure that characterizes the whole drop.

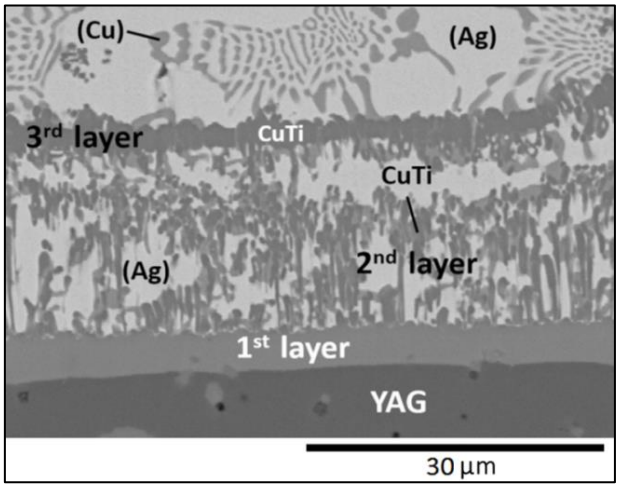

Figure 6.22. Interfacial morphology of AgCuTi/YAG tested at 850°C for 1 h.

The small quantity of Ti in the 4th layer (eutectic structure) is justified by the Ti migration to the interface zone. A map of the different distribution of elements is presented in *Figure 6.23.*

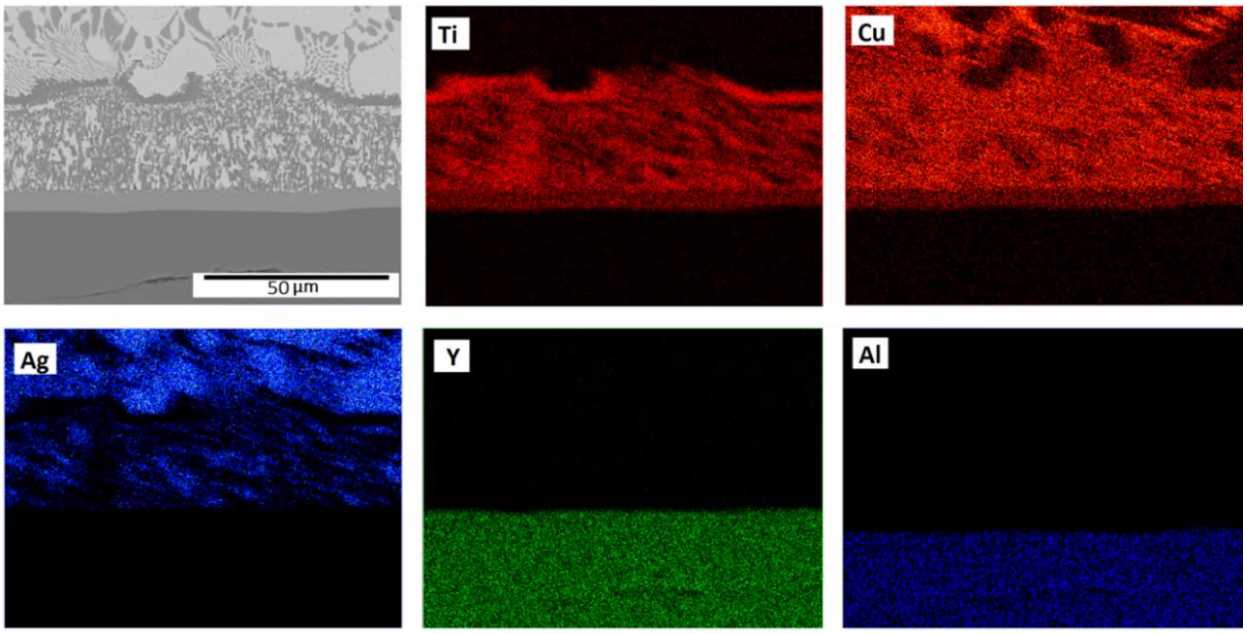

Figure 6.23. Elements map of AgCuTi/YAG interface layers of samples tested at 850C.

The AgCuTi/YAG samples tested at 820°C (*Figure 6.24*) show the same layers of the ones tested at 850°C, regarding both thickness and composition.

From *Figure 6.24*(a) the dendritic Ag grains dispersed inside the Ag-Cu eutectic matrix are clearly visible.

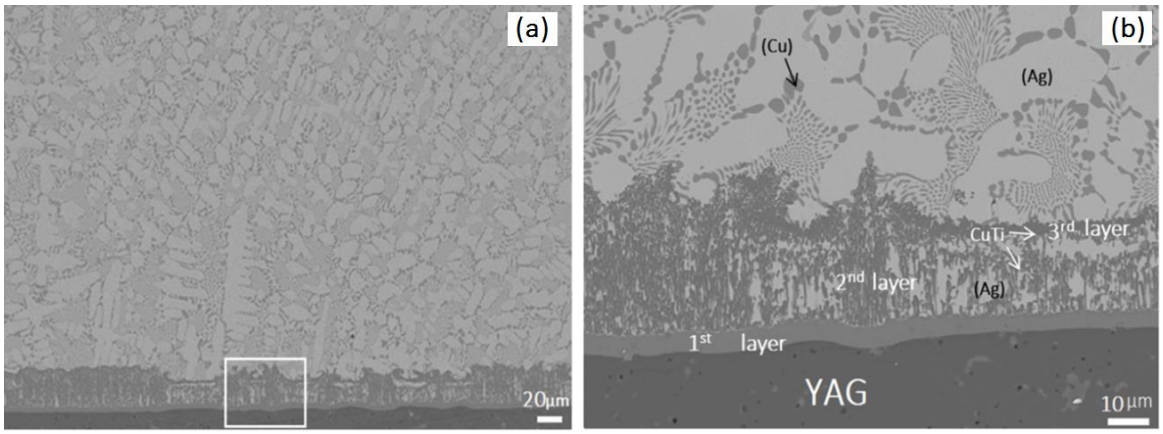

Figure 6.24. Interfacial morphology of AgCuTi/YAG tested at 820°C for 1 h (a); zoomed of the contact zone (b).

Comparing the samples tested at 850 and 950°C, we can observe that the general overview offered by the elemental maps (*Figure 6.20; Figure 6.23*), together with the quantitative analyses already discussed, allow us to state that:

1) at all temperatures Ti migrates from the bulk AgCuTi molten alloy towards the YAG/alloy interface, modifying a thin layer (≈ 5–8 μm) of the YAG substrate into a new compound which is more complex than the TiY_2O_5 found in the AgTi system due to the presence of Cu atoms at a concentration close to that of Ti;

2) a striking difference between the structure of the 950°C samples and the ones treated at lower temperature is that, on top of the complex first layer, the specimens treated at a higher temperature show the presence of the so-called M_4X layer, a promoter of wettability which is absent in the specimens treated at 850°C and 820°C.In addition at 820<T<850°C, the Ti concentration x_{Ti} in the liquid phase is much lower than x_{Ti} in L_1 at 950°C. These differences are directly reflected into the values of the work of adhesion and thus in the wetting behaviour of the AgCuTi alloy which is very good at 950°C, lower but still acceptable for brazing applications, at 850°C and at 820°C;

3) the elemental maps show that Ti segregates close to the solid-liquid interface, leaving the core of the molten drop formed by the “nearly pure” Ag-Cu eutectic.

In all the samples examined, no Cu-Ti intermetallic compounds inside the drop, outside the interfacial region of 30 μm thick, are found. However, as reported in the above mentioned tables, traces of Ti (max 1 at%) can be found in the Cu-rich phase of the eutectic Ag-Cu structures.
Al diffuses into the 1st layer and, as traces, into molten drop, while Y does not leave the original YAG substrate, except for taking part in the formation of the 1st interfacial layer.

6.1.3 Wetting and Reactivity: conclusions

The wetting of transparent YAG ($Y_3Al_5O_{12}$) by Ag-based alloys has been investigated, as far as we know, for the first time. The main results produced by this study are:

- the role of Ti activity in determining the interactions between the brazing alloys and the YAG substrate has been analysed by CALPHAD method. Thermodynamic calculations allowed to highlight the relevant role of the Ti activity in the liquid alloy to determine the final contact angles, as well as to clarify the role in the wetting process of the L_1 and L_2 liquids, coexisting in the miscibility gap between 910 and 950°C;
- the low contact angle values ensure very good (θ_{eq}=10° at 950°C) and fair (θ_{eq}=73°and 71°at 850°C and 820°C) wettability;
- a significant reactivity occurred at the solid-liquid interfaces, with the formation of new phases. The intermediate phase TiY_2O_5 was found at Ag-Ti/YAG contact zone constituting a continuous and defect-free layer. The same metal-ceramic phase was found in the 1st layer in contact with the substrate for the all AgCuTi/YAG samples while a 2nd layer, identified as a "M_4X" metal-ceramic compound, was found only at the interface of the samples tested at 950°C. Its presence was associated to the significant improvement in the wettability because of its more pronounced metallic behaviour. This layer presented the same amount of Y (19 at%) in all the samples and a decrease of the Al amount compared to YAG stoichiometry (from 25 at% to 3 at%). Moreover it was observed that Cu and Ti have migrated in about the same quantities to this 1st layer;
- from the analyses of the pure elements and binary alloys/YAG interfaces, it was possible to evaluate the different role the elements have in the wetting phenomena.
  Although the amount of Ag in the layer in contact with the ceramic substrate was not significant (<1 at%), its presence in the rest of the drop is absolutely determinant for the final wettability, as it increases the activity of Ti to a large extent.

The excellent reactivity, wettability and the maintained transparency of the YAG obtained allow these systems to be considered as good candidates for the production of brazed optical windows to be used in extreme conditions, such as the ones found in marine environments or aerospace applications.

6.1.4 Brazing evaluation

The following paragraphs deal with the interfacial microstructure of the different types of the metal-ceramic joints (*Table 6.7*) characterized by the EDS analysis and interpreted using the CALPHAD approach, as indicated in *paragraph 5.3.1.*

First of all, it should be underlined that all the brazed samples show the same crucial and required characteristics of an excellent grade of transparency, confirming the results obtained during the wettability evaluation (*6.1.1*).

Table 6.7. Fillers used in the brazing samples tested during the work.

Filler	Temperature [°C]	Time [min]
AgCuTi	950, 850	10
AgCu	850	10
Ag	970, 1050	10

The all samples reported in *Table 6.7* were maintained 10 min at the selected temperature and then control cooled with a rate at 5°C/min. After the cooling, the samples (example given in *Figure 6.25*) are embedded inside the epoxy resin, then sectioned and cut in order to obtain the vertical sections, analysed by the EDS analysis after the polishing process.

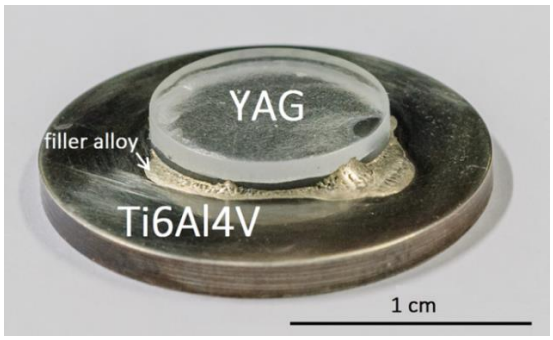

Figure 6.25. Brazing sample tested at 850°C for 10 min and extracted from the furnace after the cooling process.

6.1.4.1 YAG/AgCuTi/Ti6Al4V (950, 850°C)

The performances of the joints are closely related to the chemical, chemical-physical and mechanical characteristics of the new phases formed by the reactive interactions between the filler alloy and the adjoining ceramic parts.

As far as we know, YAG/AgCuTi/Ti6Al4V joints have not been studied before, but some similarities can be found with other metal-ceramic brazed joints in the literature, in particular in the temperature range 840-870°C [23]. Analyzing the YAG/AgCuTi/Ti6Al4V samples tested for 10 min at 950°C, the highest temperature suggested for these filler alloys [124], a few fracture paths are observed along the contact line, due to the dissimilar thermal expansion coefficients, as well as the formation of some different layers characterized by specific morphology and composition.

Four different interfacial layers can be singled out starting from the Ti6Al4V alloy (*Figure 6.26*):

- a 1st layer constituted by several grains (light color) dispersed inside a matrix (dark color);
- a 2nd layer consisting of Ti solid solution polygonal grains dispersed in a Ag solid solution (white);
- a 3rd layer composed of CuTi intermetallic grains and of Cu and Ag solid solutions;
- a 4th thin layer grown in contact with the YAG ceramic substrate.

The composition of the metallic substrate (*Table 6.8; Figure 6.26*(a) left part) is well confirmed by the SEM-EDS analysis.

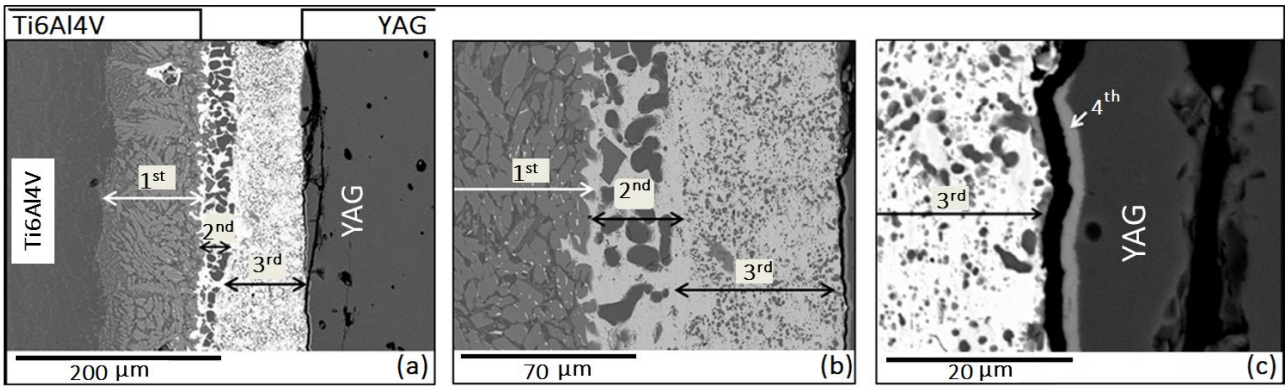

Figure 6.26. Interface microstructure (Back-scattered electrons images) of YAG/AgCuTi/Ti6Al4V samples after 10 min test at 950°C and cooled at 5°C/min (a); (b),(c) zoomed areas of the intermediate layers.

The composition of the 1st layer, 100 µm thick, does not appear significantly different from that of the Ti6Al4V substrate; in fact, the Al content of the dark phase of the 1st layer remains about 10.0 at% while V increases from 3.5 at% to 12.0 at%

Because of this modified distribution, a lower concentration of Ti is found: from 86.0 at% in the Ti6Al4V to 70.0 at% in the 1st layer matrix. A small amount of Cu (6.0 at%) and Ag traces (2.0 at%) are also detected. The Cu concentration in the light grey grains of the 1st layer is found to be higher than the Cu amount in the dark matrix, reaching 25.0 at% while both the Al and V content decrease from 10.0 at% to 4.0 at% and from 12.0 at% to 1.0 at% respectively.

Table 6.8. Composition (at%) of the different layers (Figure 6.26) formed at the metal-ceramic interface of the YAG/AgCuTi/Ti6Al4V samples tested at 950°C under $Ar_{(g)}$.

Layer		Thickness	Ag	Al	Cu	O	Ti	V	Y
Ti6Al4V substrate			-	10.5	-	-	86.0	3.5	-
1st	light phase	100 µm	5.0	4.0	25.0	-	64.0	1.0	-
	dark phase		2.0	10.0	6.0	-	70.0	12.0	-
2nd	(Ag)	20 µm	95.0	-	3.6	-	1.4	-	-
	(Ti)		1.2	3.0	0.8	-	94.0	1.0	-
3rd	(Ag)	80 µm	98.2	-	0.6	-	0.2	-	-
	(Cu)		1.5	-	97.5	-	1.0	-	-
	CuTi		0.6	0.4	48.0	-	51.0	-	-
4th		2 µm	-	7.0	2.0	58.0	3.5	-	29.5
YAG			-	25.0	-	60.0	-	-	15.0

The 2nd layer, about 20 µm thick, is composed of an (Ag) matrix including (Ti) grains. Several (Ti) polygonal grains are, indeed, detected in contact with the 1st layer, showing small traces of the other elements (Ag, Cu, V, Y < 1.0 each). In the 3rd layer, about 80 µm thick, several small CuTi grains (grey phase) surrounded by (Cu) areas (*Figure 6.27*) are dispersed inside the (Ag) matrix that extends up to the 4th layer in contact with the ceramic substrate.

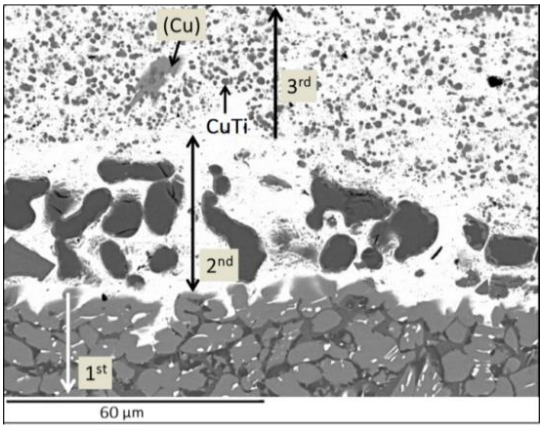

Figure 6.27. Zoomed interfacial zone of Figure 6.26 (b) close to Ti6Al4V. Samples tested at 950°C for 10 min and cooled at 5°C/min.

The 4th layer visible in *Figure 6.26*(c) is about 2 µm thick and extends as a light grey reaction sub layer on the oxidic surface. Because of its small dimensions, it is difficult to obtain accurate EDS quantitative analysis. This layer seems to contain about the same amount of O (58.0 at%) as the YAG (60.0 at%), a lower Al amount (7.0 at% instead of 25.0 at%) because of its high mobility in the molten metal [65] and an enrichment in Y compared to the theoretical stoichiometry of the ceramic (29.5 at% instead of 15.0 at%).

The Cu and the Ti amounts of the layer in contact with the YAG are larger in the wetting test samples [65].

Observing the data of *Table 6.8*it is possible to observe that:

- the Al amount (7 at%) in the 4th layer is mainly related to diffusion from Ti6Al4V;
- the concentration of Ti close to the ceramic substrate (in the 4th layer) is about 3.5 at%.

Considering the thickness of the AgCuTi layer (100 μm) and the absence of Y diffusion from the ceramic part, it is possible to locate the original contact surfaces of the starting materials (black lines of *Figure 6.26*(a)):

- on the alloy side, Ti6Al4V extends up to the (Ti) grains of the 2nd layer in the samples tested at 950°C. According to this consideration, the (Ti) grains are assumed to derive from the modification of the metallic part due to the intergranular penetration and diffusion of the filler alloys: they do not look like solid grains grown from the liquid filler;
- Cu is the element that migrated most deeply inside the metallic counterpart (*Figure 6.26;Table 6.8*): up to about 100 μm from the original Ti6Al4V surface.

On the opposite side, we have considered the original surface of YAG corresponding to the limit of the Y presence. The element maps (Figure 6.28) suggest that Y does not diffuse from the ceramic to the filler as in our previous wettability study of the same systems (YAG/AgCuTi) maintained at 950°C for 1 h. As underlined before, a miscibility gap is present in the Ag-Cu-Ti liquid (*Figure 6.3*).

At 950°C the starting brazing alloy composition falls on the border of the L_1+L_2 field, then it is mainly formed by liquid L_1. During the isothermal joining process, the amount of Cu contained in L_1 (36.8 at%) partly migrates inside the Ti6Al4V, promoting the formation of $CuTi_2$ (dark phase) and partly, as traces, diffuses in the Ti solid solution. This situation is confirmed by the SEM-EDS analysis.

The (Ag) contained in the 2nd layer as matrix and in the 3rd layer together with (Cu) and CuTi traces can be considered as cooling products of a Cu-depleted liquid.

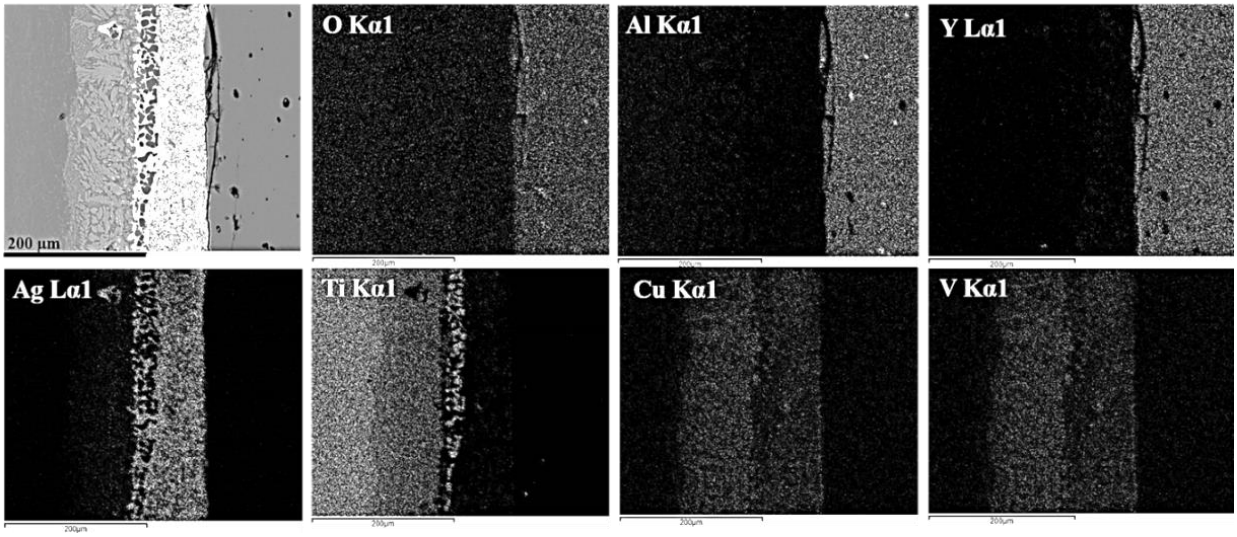

Figure 6.28. Elements map of the interface for YAG/AgCuTi/Ti6Al4V samples (950°C; 10 min).

However the sequence of solid phases which appears to be formed during the joining process ($CuTi_2$ in the 1st layer; (Ag) and (Ti) in the 2nd; (Ag), (Cu) and CuTi in the 3rd) cannot be explained on the basis of the ternary Ag-Cu-Ti isothermal section at 950°C.

It is, indeed, possible that in this case the Al and V presence in the (Ti) is determinant for its stabilization in the 2nd layer.

In *Figure 6.26(a)* fracture is clearly visible, probably due to the different thermal expansion coefficients of Ti6Al4V and YAG.

In order to overcome this problem, the same system (YAG/AgCuTi/Ti6Al4V) was tested at a lower temperature (850°C) but maintaining the same contact time (10 min).

The YAG/AgCuTi/Ti6Al4V interfacial zone of the samples tested at 850°C (*Figure 6.29*) shows:

- a 1st layer in contact with the Ti6Al4V characterized by several grains dispersed inside a dark matrix;
- a 2nd layer formed of a CuTi intermetallic compound (10 µm thick);
- a 3rd layer that includes some dark areas of CuTi and (Cu) dispersed inside a light (Ag) matrix;
- a 4th layer grown in contact with the YAG ceramic surface (more or less 2 µm thick).

The quantitative analysis of these 4 layers is reported in*Table 6.9.*

Table 6.9. Composition (at%) of the layers formed (Figure 6.29) at the metal-ceramic interface of the YAG/AgCuTi/Ti6Al4V samples tested at 850°C under $Ar_{(g)}$.

Layer		Thickness	Ag	Al	Cu	O	Ti	V	Y
Ti6Al4V substrate			-	10.5	-	-	86.0	3.5	-
1st	light phase	10 µm	2.0	10.0	20.0	-	66.0	2.0	-
	dark phase		-	20.0	3.0	-	73.0	4.0	-
2nd	CuTi	10 µm	1.5	1.5	49.0	-	47.0	1.0	-
3rd	(Ag)	80 µm	90.0	-	10.0	-	-	-	-
	(Cu)		3.0	2.0	87.0	-	8.0	-	-
	CuTi		5.3	7.2	42.0	-	45.5	-	-
4th		2 µm	1.0	-	24.0	44.0	5.0	-	26.0
YAG			-	25.0	-	65.0	-	-	15.0

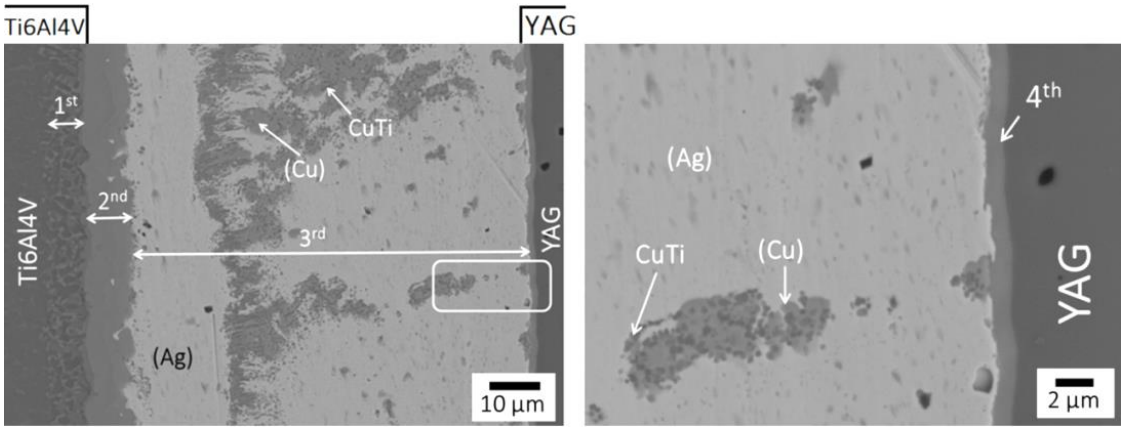

Figure 6.29. The YAG/AgCuTi/Ti6Al4V interface after being tested at 850°C; the image is obtained from the SEM-EDS analysis (on the right the zoomed area of the sample part indicated by the white box in the left image).

The 1st layer, 10 µm thick, appears significantly enriched in Cu present, mainly, as$CuTi_2$(light phase) (*Table 6.9*). Comparing the 1st layers of the samples, tested at higher and lower temperature (950°C and 850°C respectively), the main differences consist of:

- a decreased V amount inside the matrix at 850°C (V=4.0 at%; *Table 6.9*) compared to the V amount found in the interfacial zone maintained at 950°C (V=12.0 at%; *Table 6.8*);
- an increased Al amount at 850°C in the dark phase (Al=20.0 at%; *Table 6.9*) compared to the Al amount found in the same areas of the interfacial zone maintained at 950°C (Al=10.0 at%; *Table 6.8*);

- a decreased thickness of this 1st layer (*Figure 6.29*-850°C; *Figure 6.26*-950°C).

The 1st layer of the samples tested at 850°C is, in fact, about 10 µm thick while the thickness of the same layer of the 950°C samples is estimated to be more or less 100 µm.

The 2nd layer, 10 µm thick too, is formed of the intermetallic CuTi with Ag and Al traces and represents a sort of barrier for a deeper penetration and/or diffusion of the filler inside the metallic counterpart. This layer appears very similar to the layer found by Smorygo et al. [18], as will be shown in the following part, in terms of composition and morphology. These observations indicate that the interdiffusion, occurring during the brazing process, between the filler and the base metal led to a depletion of Cu from the molten filler alloy.

The 3rd layer, about 80 µm thick, is formed of both (Cu) and CuTi, the light and the dark grey areas respectively, dispersed in a (Ag) matrix extending more or less to the YAG substrate.

The 4th layer, about 2 µm thick and formed in direct contact with the ceramic substrate, is difficult to analyze by SEM-EDS. Nevertheless, this layer seems to contain about 5.0 at% of Ti (*Table 6.9*). Therefore, the ceramic sub layer is more enriched in the active element than the ceramic sub layer of the 950°C samples (Ti= 3.5at%; *Table 6.8*).

The point representing the starting alloy at 850°C, shown in the isothermal section reported in *Figure 6.9*, falls inside the two-phase field L+Cu_3Ti_2 of the Ag-Cu-Ti phase equilibria.

During the interactions between the filler and the Ti6Al4V at 850°C, Ti Al and V diffused into the liquid modifying its composition, which results significantly enriched in Ti.

By neglecting Al and V (composition < 1.5 at%) it is possible to approximate the liquid phase as a ternary Ag-Cu-Ti.

The CuTi intermetallic compound, already present in the liquid alloy at 850°C, promotes the formation of an intermetallic layer (2nd) along all the interface. This layer, grown in contact to the metallic counterpart, is considered as a Ti source. During the cooling of the system, the liquid alloy resulting poor in Ti (involved in the formation of the intermetallic and the sublayer) generates, first of all, an Ag solid solution and, after approaching the Ag-Cu eutectic stoichiometry, the Ag and Cu solid solutions of the 3rd layer. These phases extend to the interfacial zone with some CuTi traces.

At 850°C Cu represents the element that interacts most deeply with the two parts of the joint.

The formation of CuTi intermetallic phase in the 2nd and 3rd layers follows the Cu–Ti equilibrium phase diagram. Ag is the least active element of the filler while Cu has a strong tendency to rapidly form intermetallics with Ti [154]. Indeed, Ag has a low diffusivity through the CuTi layer. For this

reason, it remains in the central part of the sandwich configuration despite its solubility in Ti and its ability to form intermetallic compounds. It is also important to underline that CuTi and (Cu) formation do not significantly modify the Ti migration at the interface compared to the samples tested at 950°C.

In fact, the 4th layer in contact to the YAG contains up to 5.0 at% of Ti.

Although YAG/AgCuTi/Ti6Al4V joints have not been investigated before, interesting similarities can be found in the work of Smorygo et al. [23], who analyzed the interface microstructure between zirconia (3Y-PSZ) and Ti joined by active brazing in vacuum in the range of 840-870°C using 63Ag-35.25Cu-1.75Ti (wt%) as a filler. Analyzing, in particular, the part of the joint closest to the metallic counterpart, they identified and enumerated different layers (*Figure 6.30*) that are related to our findings: a reaction layer (I) between the filler and the zirconia (3-4 µm) and, a bond layer (II) between the zirconia and titanium (45-50 µm), formed of (Ag) with 10-15 at% Cu. Dark intermetallic inclusions of Ti (~40 at.%), Cu (~35 at%) and Ag (~25 at%) were also detected; a reaction layer between the filler and Ti (III) formed of CuTi with Ag traces; a diffusive layer (IV) containing traces of Ag and with a Cu concentration gradually decreasing inside Ti. Cu must be bound as $CuTi_2$ in this zone.

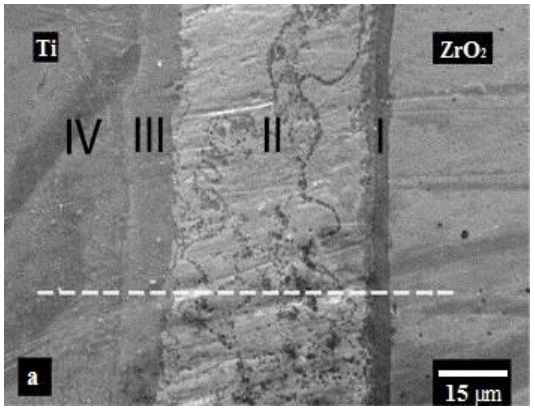

Figure 6.30. SEM image of Ti/AgCuTi/ZrO_2 joint section (870°C, 5 min) [from with [20] permission].

6.1.4.2 YAG/AgCu, Ag/Ti6Al4V

Samples brazed using alloys without an active metal addition were also tested, as was mentioned before, in order to define a production process as easy as possible and to evaluate how and in what quantity Ti can migrate from Ti6Al4V to the interface, thus playing its role of "active" element promoting the wettability [155].

Among the different elements (Cu, Ge, Si, Sn) capable of forming a homogeneous liquid with Ag, at temperatures lower than its melting point, Cu is widely used in commercial brazing alloys [156].

For this reason the AgCu alloy ($T_{eu\ Ag\text{-}Cu}$=780°C) was chosen as potential filler material in these joining tests conducted at 850°C.

The joining tests with pure Ag as filler (YAG/Ag/Ti6Al4V) were also investigated and they were carried out at a higher temperature (1050°C) compared to the other joining tests reported in the present work, but at the same temperature as the wetting tests previously reported for the Ag/YAG system. The T_{exp}/T_m (reduced temperature) in the two cases are very similar. Moreover, other ad hoc wetting tests on Ag/Ti6Al4V samples have been performed to get a full description of all the systems involved.

It should be noted that a pure Ag filler can reduce the formation of intermetallic compounds at the interface and promote the Ti diffusion toward the ceramic part.

In order to be able to compare the different specimens tested under the same operating conditions, the YAG/AgCu/Ti6Al4Vjoints were processed at 850°C, the lowest of the temperatures used previously for the YAG/AgCuTi/Ti6Al4V samples.

In this case too, the YAG/AgCu/Ti6Al4V samples tested for 10 min appear with a sound joint interface, visible in *Figure 6.31,* with a continuous and defect-free interfacial zone.

The different layers appearing at the YAG/AgCu/Ti6Al4V interface (*Figure 6.31; Table 6.10*) are very similar to the layers of the samples with AgCuTi as filler tested at the same temperature (850°C):

- a 1st layer in contact with the Ti6Al4V characterized by several grains dispersed inside a dark matrix;
- a 2nd layer formed of CuTi intermetallic compound (10 µm thick);
- a 3rd layer that includes some dark areas of CuTi and (Cu) dispersed inside a light (Ag) matrix;
- a 4th layer grown in contact with the YAG ceramic surface (more or less 2 µm of thickness).

The 1st layer, with the same morphology as the one observed in the other joining systems already shown, presents a lower amount of Al inside the matrix (12.0 at%) and a decreased Cu amount inside the grains (8.0 at%) compared to the 1st layer of the samples tested at the same temperature but with AgCuTi alloy as filler (*Table 6.9*; Al:20 at%; Cu:20 at%). A 2nd layer of CuTi is formed with the same thickness as in YAG/AgCuTi/Ti6Al4V samples tested at 850°C. We can conclude that the presence of this intermetallic compound is related to the testing temperature and it does not depend on the Ti coming from the filler. The CuTi is, in fact, formed inside the metallic counterpart

as explained below. The Cu has a stronger tendency to react with Ti compared to Ag as revealed by the Ti partial enthalpy of mixing in molten copper at infinite dilution (-10 kJ/mol) compared with that in the molten silver (39 kJ/mol) [157].

In the 3rd layer, the alternation of Ag and Cu solid solutions extends for more or less 65 µm and again traces of CuTi were detected. The continuous layer in contact with the YAG (4th layer, 2 µm thick) shows about the same O amount (60 at%) of the ceramic substrate (65 at%) and the same Ti amount (5 at%) of the YAG/AgCuTi/Ti6Al4V samples tested at the same temperature (850°C).

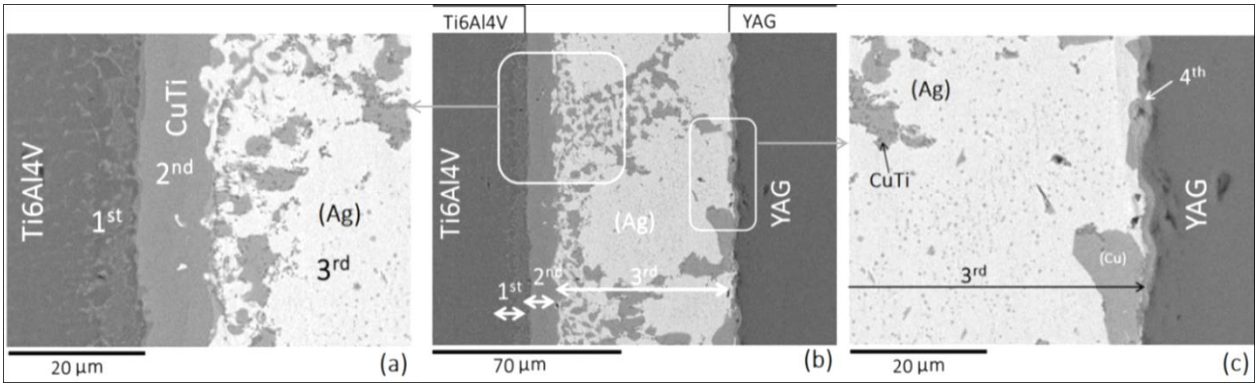

Figure 6.31. BSE images of the YAG/AgCu/Ti6Al4V interfacial zone tested at 850°C. In (a) and (c) the zoomed parts of (b) of the joint in contact to the Ti alloy support (a) and to the ceramic substrate (c) respectively.

Table 6.10. Composition (at%) of the different layers formed at the metal-ceramic interface of the YAG/AgCu/Ti6Al4V samples (Fig.6.19) tested at 850°C under Ar(g).

Layer		Thickness	Ag	Al	Cu	O	Ti	V	Y
Ti6Al4V substrate			-	10.5	-	-	86.0	3.5	-
1st	dark phase	50 µm	1.0	12.0	8.0	-	72.0	7.0	-
	light phase		-	12.0	-	-	85.0	3.0	-
2nd	CuTi	10 µm	1.4	1.6	47.0	-	50.0	-	-
3rd	(Ag)		96.0	1.0	1.0	-	2.0	-	-
	(Cu)	65 µm	3.0	4.5	87.0	-	5.5	-	-
	CuTi		1.2	1.5	45.8	-	51.5	-	-
4th		2 µm	2.0	6.5	3.5	60.0	5.0	-	23.0
YAG			-	25.0	-	65.0	-	-	15.0

We can deduce and conclude that the active element inside the filler alloy did not significantly improve the metal diffusion at the joint interface and the metal-ceramic phase formation.

Indeed, the Ti, dissolved and migrated from the metallic counterpart, played an important role in brazing the Ti6Al4V/YAG moving towards the metal-ceramic interface and forming both the intermetallic compounds and the sub layer on the ceramic substrate.

However, as underlined in previous works [154][158], the possible formation of intermetallic compounds pertaining to the Cu-Ti system is a good way to obtain a stable interface in the metal-ceramic joint.

In a work based on the Al_2O_3/Ti6Al4V [159], for example, diffusion bonded joints at 750°C with Ag-Cu interlayer present some similarities regarding the interface microstructure after 10 min testing (*Figure 6.32*):a 1st layer (A) in contact with the Ti6Al4V, composed of the α-Ti phase and η-Ti_2Cu phase; a 2nd layer (B), formed of the ζ-TiCu phase; a 3rd layer (E), silver rich, Ag(Cu, Ti), appeared close to the intermetallic compound containing Ag (white phase) and a Ti-Cu solid solution (dark phase).

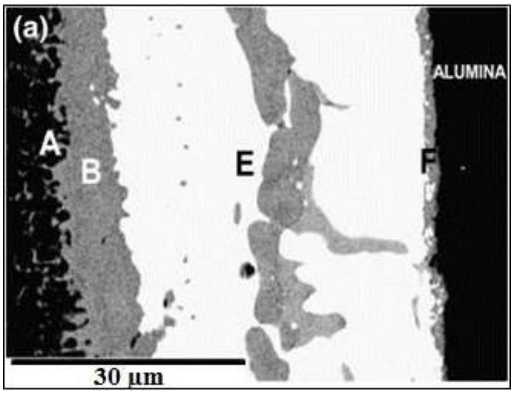

Figure 6.32. Ti6Al4V/Al_2O_3 interface at bonding temperature of 750°C for 10 min [From ref. [159]*, with permission].*

The different composition of the YAG/Ag/Ti6Al4V interfacial layers of the samples tested at the higher temperature of 1050°C for 10 min (*Table 6.11*) and their BSE analysis (*Figure 6.33*) are reported below.

Starting from the Ti6Al4V:

- a 1st layer showing traces of a white phase dispersed inside a dark matrix;
- a 2nd layer formed of light (Ag) and dark (Ti) areas;
- a 3rd thin layer in contact with the ceramic substrate.

Table 6.11. Composition (at%) of the different layers formed at the metal-ceramic interface of the YAG/Ag/Ti6Al4V samples (Figure 6.33) tested at 1050°C under Ar(g).

Layer		Thickness	Ag	Al	O	Ti	V	Y
Ti6Al4V substrate			-	10.5	-	86.0	3.5	-
1st		50 µm	2.6	12.4	-	81.0	4.0	-
2nd	(Ag)	75 µm	97.5	-	-	2.5	-	-
	(Ti)		2.0	10.0	-	87.0	1.0	-
3th		2 µm	12.5	3.5	60.5	2.0	-	21.5
YAG			-	25.0	60.0	-	-	15.0

The 1st layer shows the same composition of Ti6Al4V with Ag traces (on the left side of *Figure 6.33*). A continuous, homogeneous and pore-free alternation of silver and titanium solid solutions (respectively the white and the grey zones visible in *Figure 6.33*) extends up to the ceramic. Some small (grey) areas can be observed along the contact line with the YAG in which the same O amount as in the YAG was found as well as 2.0 at % of the active element (*Table 6.11*). The absence of intermetallic compounds is confirmed by the Ag-Al-Ti isothermal section at 1100°C (*Figure 6.34* (a)). At 1000°C we should expect to find the AgTi intermetallic (*Figure 6.34* (b)) but this phase was not detected by the SEM-EDS analysis. However, this compound shows a narrow stability range of about 60°C (*Figure 6.35*). We can, therefore, assume that it had not enough time to develop.

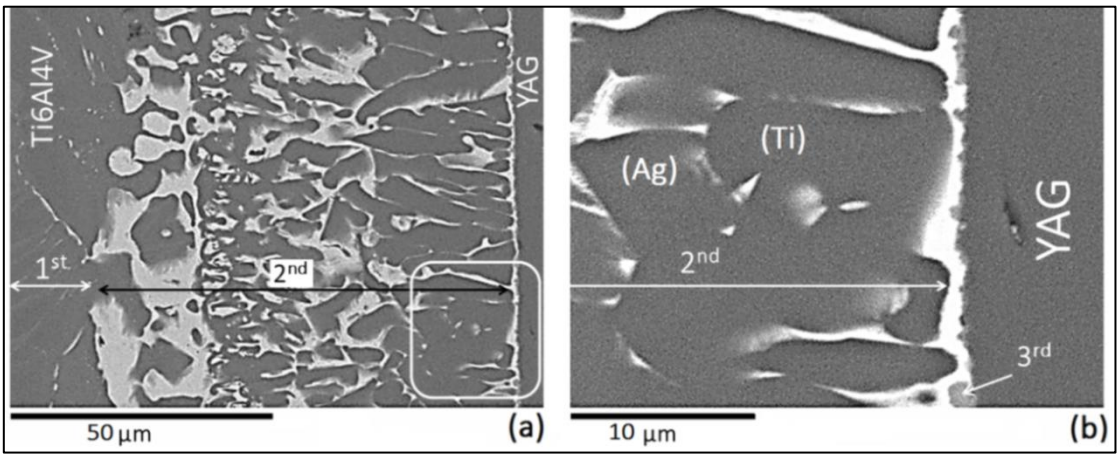

Figure 6.33. BSE image of the YAG/Ag/Ti6Al4V interface (a); the zoomed area of Fig.(a)(white box) (b); (T=1050°C; t=10 min).

The Ti counterpart remains in the solid state throughout the test, and below 962°C the Ag-rich liquid phase disappears, preventing the AgTi from forming anymore. In order to observe the inter-

diffusion phenomena which can occur at the Ag/Ti6Al4V interface, specific wetting tests have been carried out at a temperature (970°C) just above the Ag melting point.

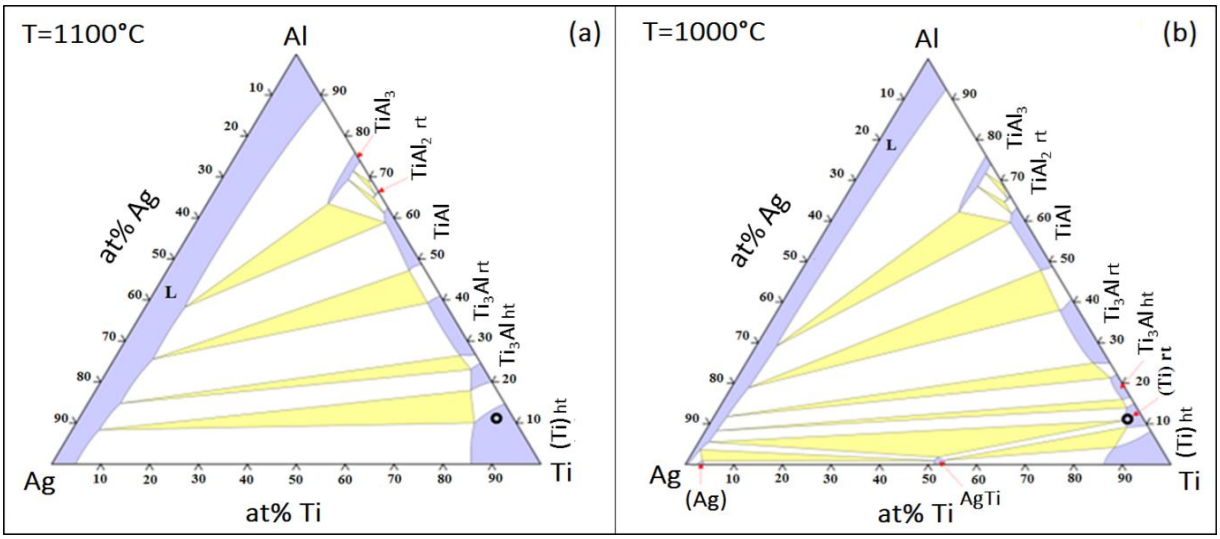

Figure 6.34. Isothermal section of the Ag-Al-Ti system at 1100°C (a) and at 1000°C (b)[66]*; the red arrows in the figures mark the Ag-Al, Ag-Ti and Al-Ti intermetallics.*

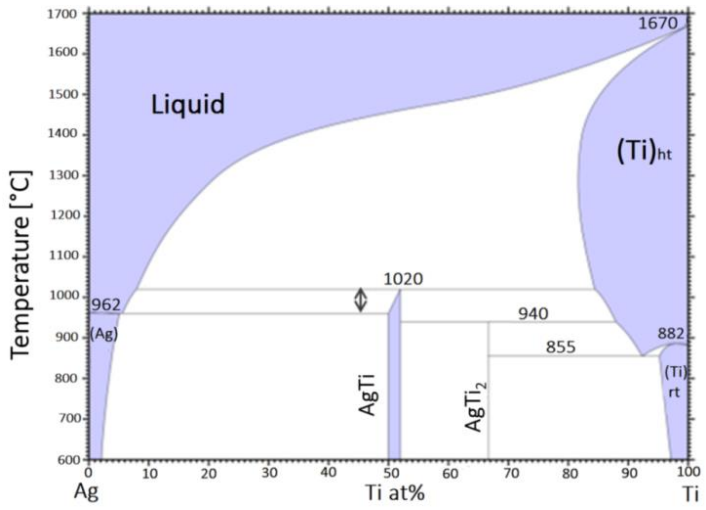

Figure 6.35. Ag-Ti binary phase diagram [36].

At this temperature a complete and ideal wetting of the Ag on the Ti6Al4V occurs (*Figure 6.36*(b),(c)).

The wetting behavior of this system was followed between 800-970°C, waiting for 20 min at each temperature (800, 850, 900, 950°C, 960°C, 970°C) in order to detect whether Al (max solubility in Ag= 18 at% (above 777°C; *Figure 6.37*), diffusing into (Ag), could give rise to contact melting.

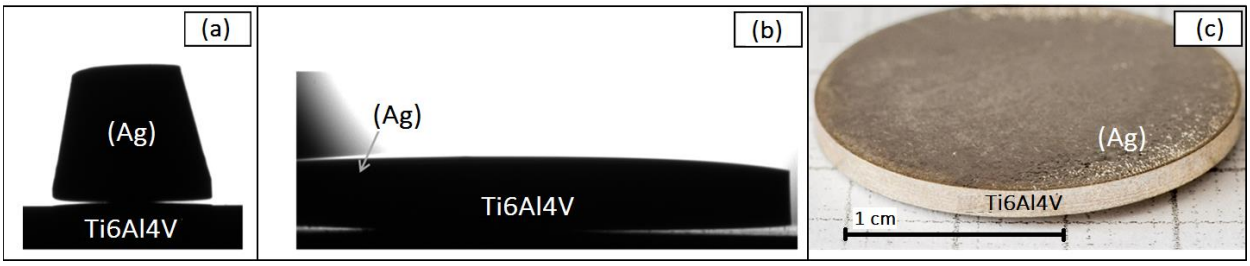

Figure 6.36. Ag/Ti6Al4V profiles of the sample step-heated: at 850°C (a) and at 970°C (b); image of a sample after the wetting test at 1050°C (c).

However, Ag spreading started just above its melting point and, after 5 min from the melting, the substrate was totally covered by the molten metal *Figure 6.36* ((b),(c)): observing the compositions of the Ag/Ti6Al4V interfaces, no Ag solid solution containing Al is found at all (*Figure 6.38*(a)*; Table 6.12*).

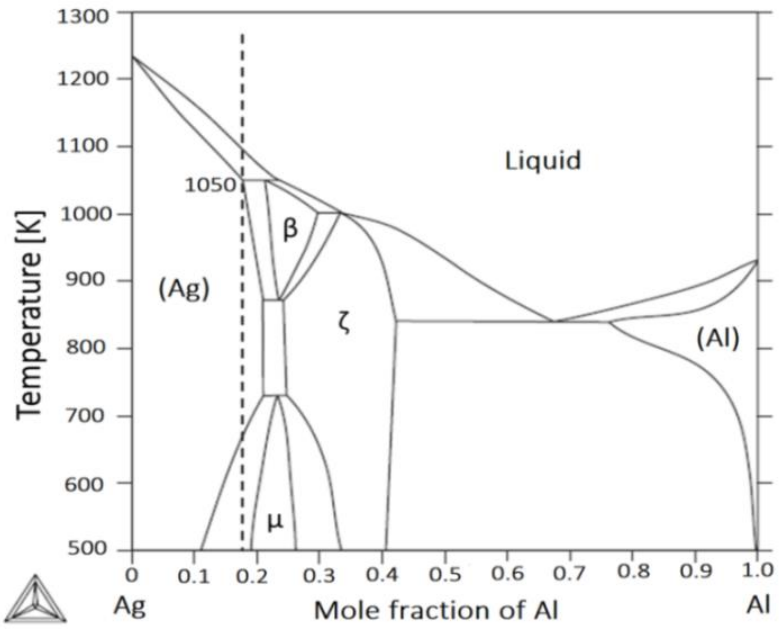

Figure 6.37. Binary phase diagram of Ag-Al system [37]; the dotted line indicates the maximum solubility the Al has in the silver solid solution in the presence of a liquid phase.

The Ag, indeed, first of all entered inside the Ti6Al4V bulk (point 3 in *Figure 6.38*(a)) and formed a solid solution with the Ti (dark areas detected in point 5 *Figure 6.38*(a)).

Al was found in the grey layer close to the metallic support in which the Ti6Al4V composition is maintained (point 3 in *Figure 6.38*(a)).

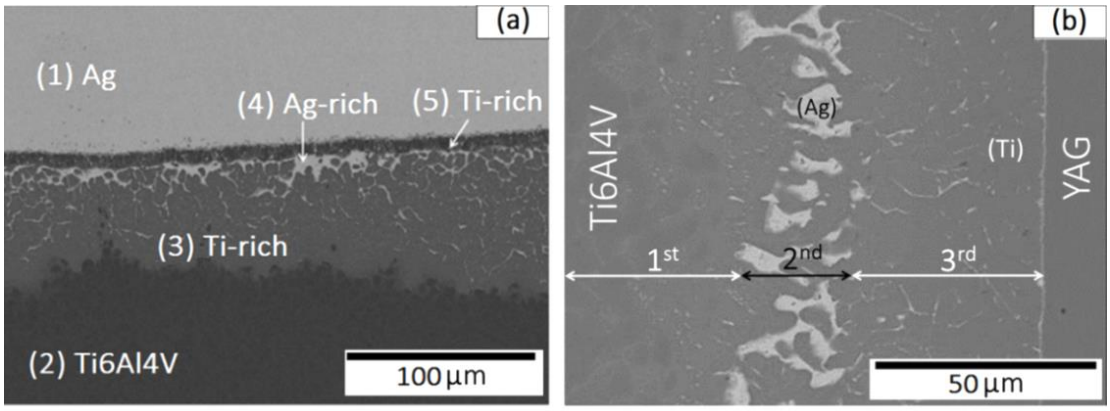

*Figure 6.38. Section microstructure of the Ag/Ti6Al4V samples after the **wetting tests** conducted at 970°C (a) and of the YAG/Ag/Ti6Al4V samples after the **joining tests** at 970°C for 1h.*

YAG/Ag/Ti6Al4V samples were also brazed at 970°C for 1h. Observing the phase composition at the interfacial zone (*Figure 6.38*(b)), we did not find significant differences in terms of microstructure and composition compared to the same samples tested at 1050°C (*Table 6.11* compared to *Table 6.13*). An increased amount of Ti in the solid solution closer to the YAG ((Ti) zone (b)) and a modified distribution of the (Ag) white areas were also found.

*Table 6.12. Composition (at%) of the different zones (Figure 6.38 (a))at the metal-ceramic interface of the **Ag/Ti6Al4V** samples tested at **970°C** and under Ar(g).*

Analysed zone	Ag	Al	Ti	V
(1)	100.0	-	-	-
(2)	-	10.0	86.1	3.9
(3)	9.5	7.1	79.5	3.8
(4)	95.0	-	5.0	-
(5)	4.1	8.3	85.2	2.4

*Table 6.13. Composition (at%) of the different layers formed at the metal-ceramic interface of the **YAG/Ag/Ti6Al4V** samples (*Figure 6.38 *(b)) tested at **970°C** and under Ar(g).*

Layer	Thickness	Ag	Al	O	Ti	V	Y
Ti6Al4V substrate		-	10.5	-	86.0	3.5	-
1st	100 µm	1.0	12.5	-	84.0	2.5	-
2nd (Ag)	25 µm	95.5	-	-	4.5	-	-
3th (Ti) zone (a)	50 µm	4.0	14.0	-	80.0	2.0	-
(Ti) zone (b)		2.0	8.0	-	90.0	-	-
YAG		-	25.0	65.0	-	-	15.0

Silver diffusion seems to be more pronounced at higher temperature (*Figure 6.33*); a significant amount of Ag was also found very close to the ceramic. The layer in contact with the ceramic maintained the same composition and thickness as that already found in the samples tested at 1050°C.

6.1.5 Conclusions about YAG/Ti6Al4V brazing and future work

Different types of metal-ceramic(YAG/filler/Ti6Al4V) joints were prepared to evaluate their reactivity and then to produce optical windows with possible applications in marine environment.
YAG/Ag/Ti6Al4V and YAG/AgCu/Ti6Al4V pairs were tested in addition to those using AgCuTi as filler. These tests have demonstrated that the use of filler alloys without the "active" component, works properly, producing reliable YAG/Ti6Al4V joints as the spontaneous Ti migration from bulk Ti6Al4V to the interfacial zone is sufficient to promote the wettability and the adhesion of the metal-ceramic components. Indeed, the Ti6Al4V counterpart could act as an active source of Ti for the brazing alloy.

Three systems have been investigated for the first time (YAG/AgCuTi or AgCu or Ag]/Ti6Al4V) at different temperatures.
The metal-ceramic interactions were also interpreted from a thermodynamic point of view: the high temperature isothermal sections obtained by CALPHAD methods allowed us to study and to predict the phases formed during each specific process and to compare the theoretical and experimental results. In particular, recalculated Ag-Cu-Ti and Ag-Al-Ti isothermal sections were used.
The interfacial zones, evaluated in terms of morphology and composition (SEM-EDS analysis), can be compared as follows:

- a thin and continuous metal-ceramic layer containing Ti (more than 2 at%) forms in contact with the YAG ensuring the adhesion between all the joined materials;
- only at 950°C the YAG/AgCuTi/Ti6Al4V samples show an important fracture at the contact line;
- at 850°C a homogenous CuTi layer formed when AgCuTi and AgCu have been used as filler material; this is considered to play the role of diffusion barrier for the filler's components;

- no intermetallic compound formation is observed when using the pure Ag at 970°C and 1050°C.

In particular, although the CuTi formation may not represent a negative point for the brazed samples performances, it is worth noting that no brittle and discontinuous intermetallic compounds were detected at the YAG/Ag/Ti6Al4V interface.

This point, as well as the homogenous and pore-free interfacial zone, makes this sound and promising joint a favorite candidate for the applications under investigation.

The ceramic oxide has been chosen because of its transparency and Ti6Al4V because of its corrosion resistance in seawater. For this reasons, the corrosion resistance of the joined materials in seawater, simulating a possible real operation on the joints produced and reported in *Figure 6.39*, is currently under way and will be reported in forthcoming papers.

Figure 6.39. Ti6Al4V pipe used for the optical window substrate prototype (a); top view (b) and lateral view (c) of the YAG/Ag/Ti6Al4V joining sample.

6.2 Non-oxidic system: SiC/Al-Ti alloys

Reactivity tests of two different Al-Ti alloys, containing 84 and 75 at% of Al respectively, in contact to SiC have been conducted, aimed at:

- defining temperature and microstructure of the first interaction occurring in the system;
- analyzing the composition of the intermediate phases formed in contact to the ceramic substrate as well as evaluating the microstructure of the bulk.

For each system, the first interaction between the ceramic and the alloy has been studied by Differential Scanning Calorimetry (the procedure is explained in *4.4*) in order to define the lower temperature at which the first liquid occurs, while the interfacial reactivity of the metal-ceramic couples has been evaluated by the EDS analysis on different samples:

- the samples tested at the first interaction temperature;
- the samples obtained increasing temperature and holding time.

The CALPHAD approach has been utilized to perform calculations that allow:

- to estimate the percentage of the liquid phase in each system at the defined conditions;
- to understand the nature of the phases formed;
- to simulate the cooling path of the liquid at the selected process parameters.

In addition, a thorough evaluation of the wettability of the $Al_{75}Ti_{25}$/SiC system has been conducted. The alloys composition as well as the corresponding temperatures and times are reported in *Table 6.14.*The stoichiometric$Al_{75}Ti_{25}$alloy is commonly indicated also as Al_3Ti.

Table 6.14. Al-Ti alloys with the testing temperatures and holding times used.

Filler	Temperature [°C]	Time [min]
$Al_{84}Ti_{16}$	1235	10
	1270	10
	1300	10; 60
$Al_{75}Ti_{25}$	1260	10
	1500	10; 30; 60

6.2.1 SiC/Al-Ti reactivity

In this part, the reactivity of the metal-ceramic couple is described: in particular, DSC and EDS analyses are reported for both the systems $Al_{75}Ti_{25}$/SiC and $Al_{84}Ti_{16}$/SiC, in *6.2.1.1* and *6.2.1.2* respectively. Then, in *6.2.2*, a thermodynamic discussion section is inserted providing an interpretation of the first interactions occurring at the interfacial zone as well as of the evolution of the liquid during and after the isothermal process considering different parameters (time and temperature).

A comparison section (*6.2.3*) is also proposed with the aim to observe the main differences occurring in the morphology and phases composition changing the process parameters.

6.2.1.1 $Al_{75}Ti_{25}$ on SiC

DSC test

SiC and $Al_{75}Ti_{25}$ alloy (prepared by arc-melting; *4.1.2.2*) were cut, using a wire saw, obtaining thin (2 mm of thickness) and flat pieces in order to make possible the introduction of the couple inside the alumina crucible (150 µL of volume) and to maximize the contact between their surfaces.

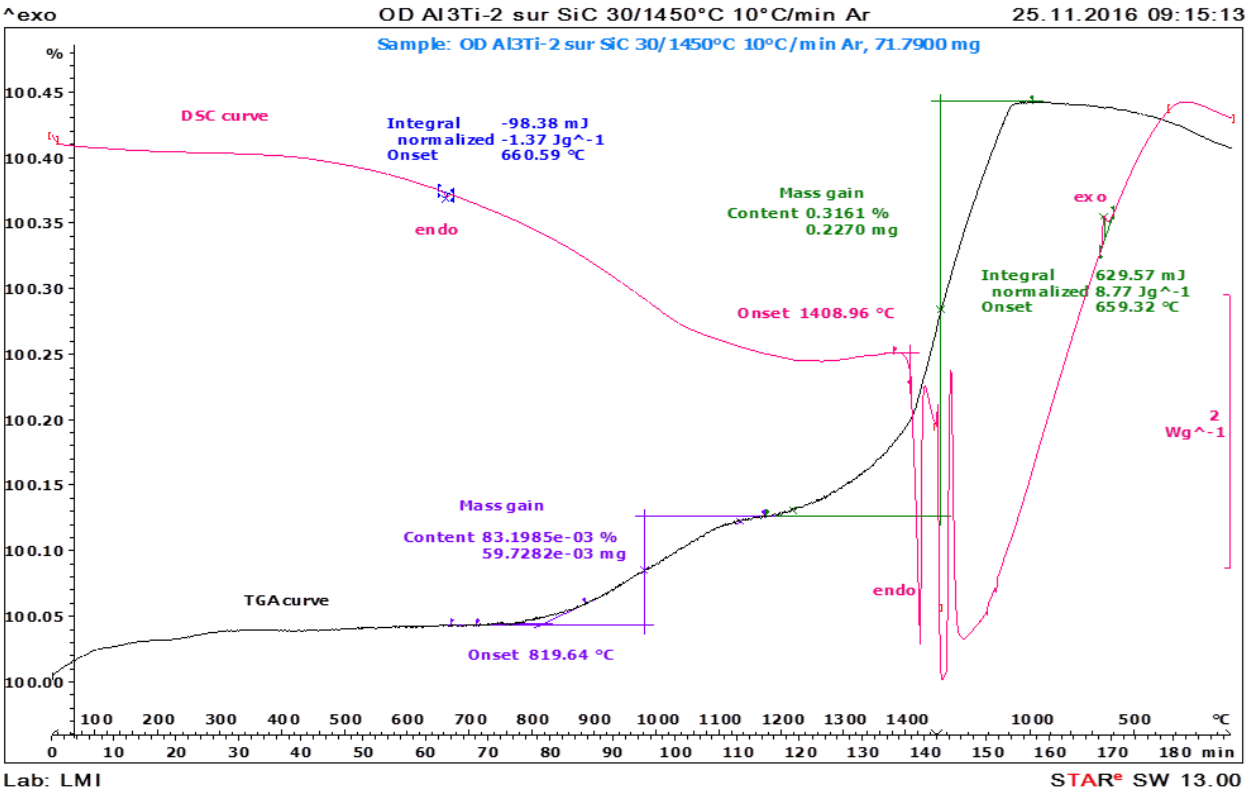

Figure 6.40. Differential Scanning Calorimetry analysis of the Al75Ti25/SiC sample (10°C/min).

The DSC test (details reported in *4.4*) was conducted using a heating program analysis set from 30 to 1450°C at 10°C/min and adopting an Ar (O_2< 100 ppb) working atmosphere.

As one can see from the graphs reported in *Figure 6.40* and *Figure 6.41* (red line) no significant signals appear until the deviation at 1260-1280°C.

To emphasize this small signal, the DSC analysis was repeated at a faster heating rate (20°C/min) (graph of *Figure 6.42*). From the graphs of *Figure 6.42* and *Figure 6.43* one can see:

- a small exothermic phenomenon occurring between 1260-1280°C;
- a clear endothermic peak which shows an onset temperature at 1409°C.

The exothermic phenomenon could be related to a chemical reaction taking place between $Al_{75}Ti_{25}$ and SiC just before the endothermic peak due to the melting of the alloy (even if its theoretical melting temperature is 1396°C).

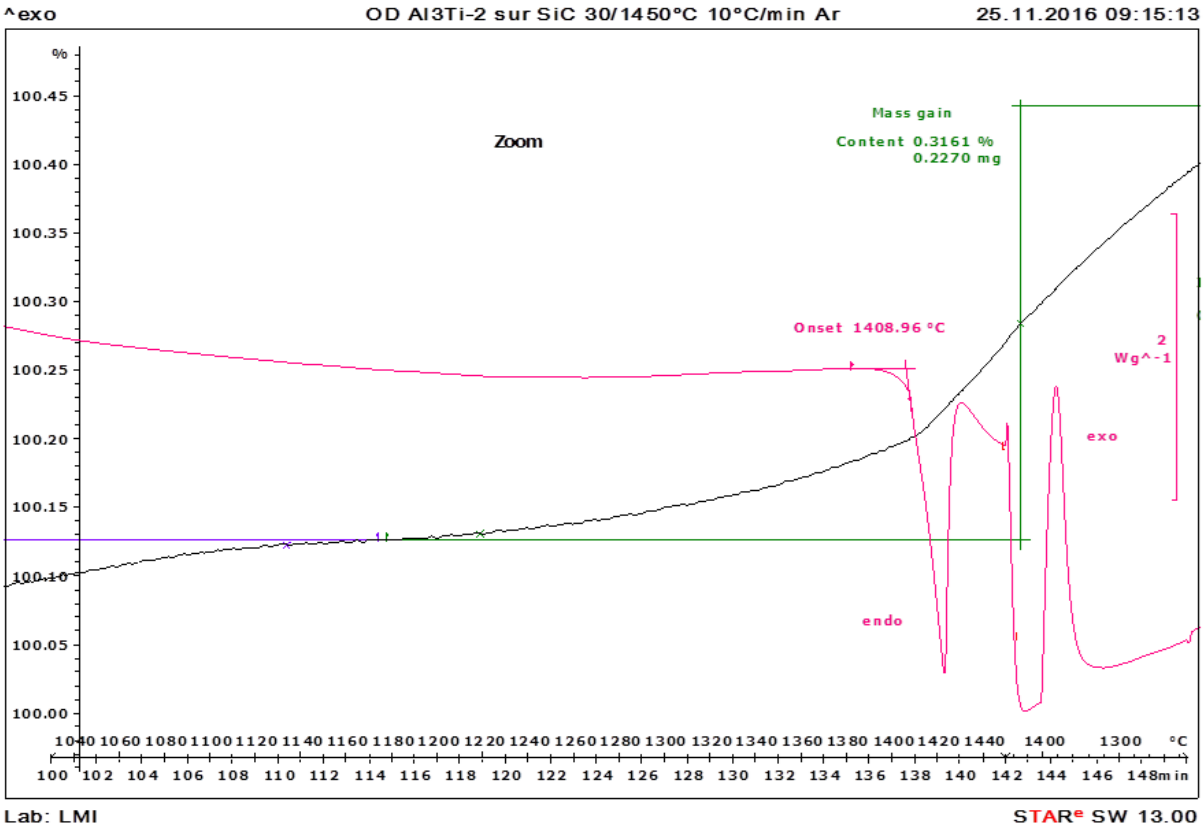

Figure 6.41. Zoom of the Differential Scanning Calorimetry analysis of the $Al_{75}Ti_{25}$/SiC sample(10°C/min).

The exothermic signal appears at the same temperature with both heating rates showing that the corresponding phenomenon is not dependent on kinetics.

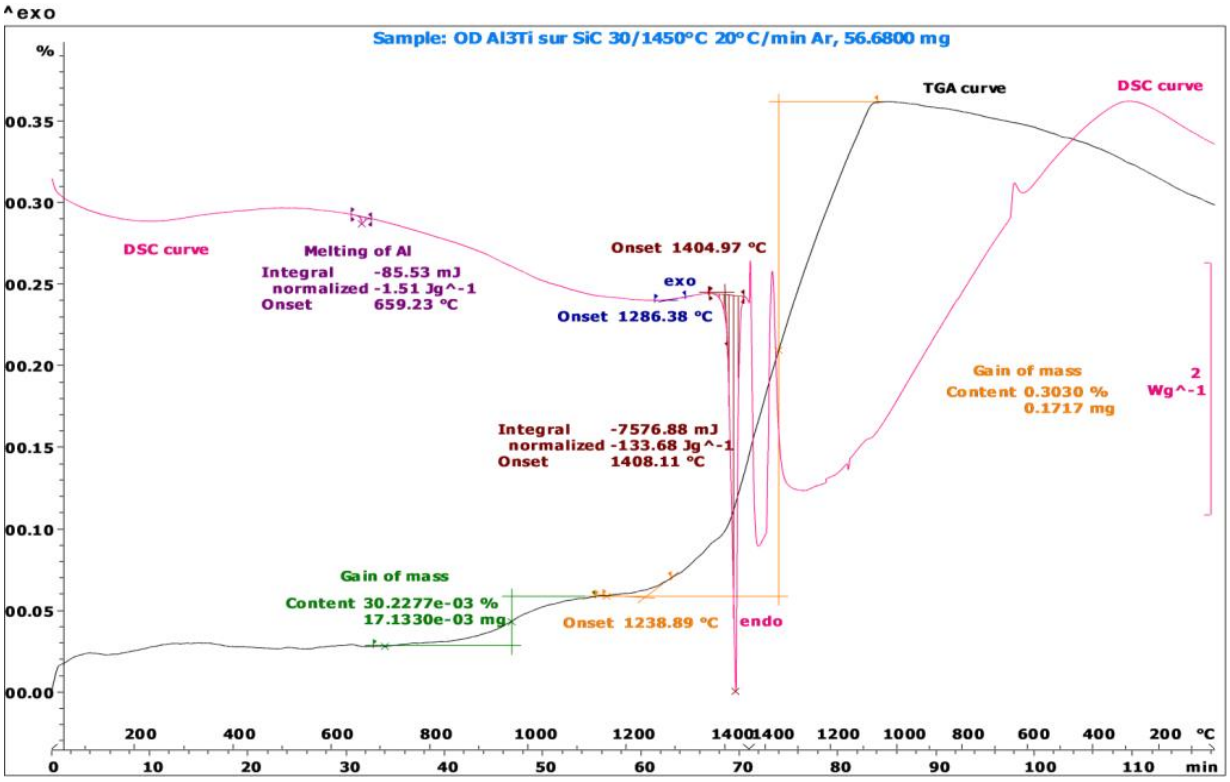

Figure 6.42. Differential Scanning Calorimetry analysis of the $Al_{75}Ti_{25}$/SiC sample (20°C/min).

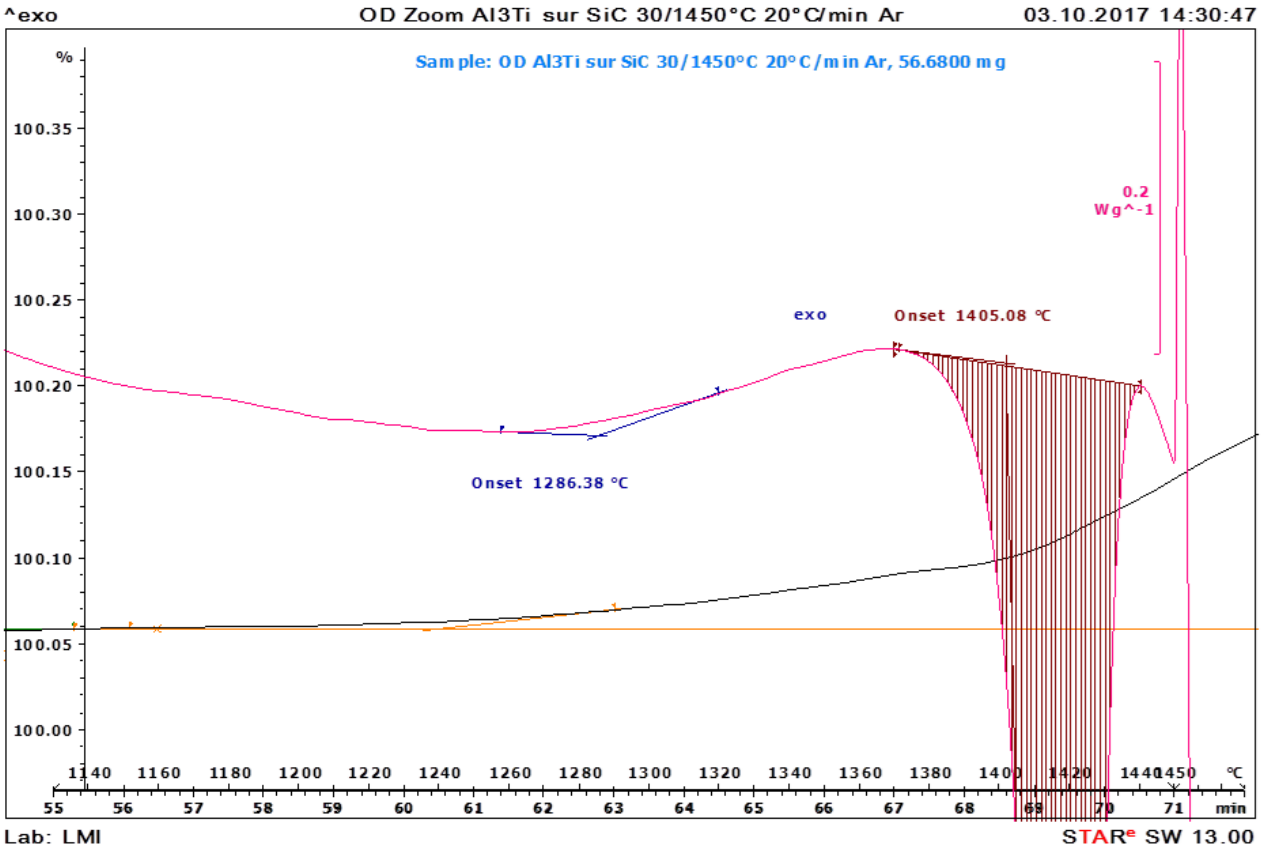

Figure 6.43- High zoom of Differential Scanning Calorimetry analysis of the $Al_{75}Ti_{25}$/SiC sample analysis (20°C/min).

Reactivity evaluation

$Al_{75}Ti_{25}$/SiC at 1260°C for 10 min

On the basis of the results already discussed, the reactivity of $Al_{75}Ti_{25}$/SiC system has been investigated at this specific temperature (T=1260°C) for 10 min.

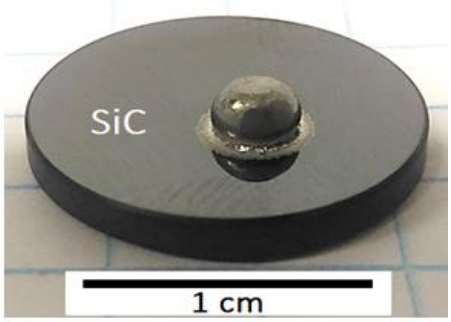

Figure 6.44. Al_3Ti/SiC sample tested at 1260°C for 10 min.

No evident wetting could be detected, but it is possible to see, from *Figure 6.44,* that indeed a first liquid formed in contact to the ceramic substrate.

The Al-Ti alloy is clearly not completely molten (*Figure 6.45* (a)) but several Al veins, coming from the solidification, are visible at the $Al_{75}Ti_{25}$ grain boundaries (*Figure 6.45*(b)); in fact the Al-rich liquid formed at the interface can migrate inside the drop following grain boundaries paths.

Analyzing the interfacial microstructures, reported in*Figure 6.46*, as well as the phases composition, reported in (*Table 6.15*), one can observe:

- a TiC layer (2 µm thick) grown on the SiC surface;
- a continuous $Ti_3Si(Al)C_2$MAX-phase layer (20 µm thick) composed of several elongated grains, extended in a direction orthogonal to the ceramic surface, and showing an average composition of 14.1 at% of Si, 2.1 at% of Al, 49.6 at% of Ti and 34.2 at% of C;
- an almost pure Al matrix containing less than 2 at% of Si;
- some elongated $Al_{75}Ti_{25}$ grains (25.4 at% Ti, 7.4 at% Si, 67.2 at% Al; *Table 6.15*), coming from the liquid solidification, dispersed inside the Al matrix;
- some $Ti_5Si_3C_x$ crystals, dispersed inside the $Al_{75}Ti_{25}$ grains, close to the MAX-phase; their presence will be explained in *6.2.2.1* by means of thermodynamic calculations.

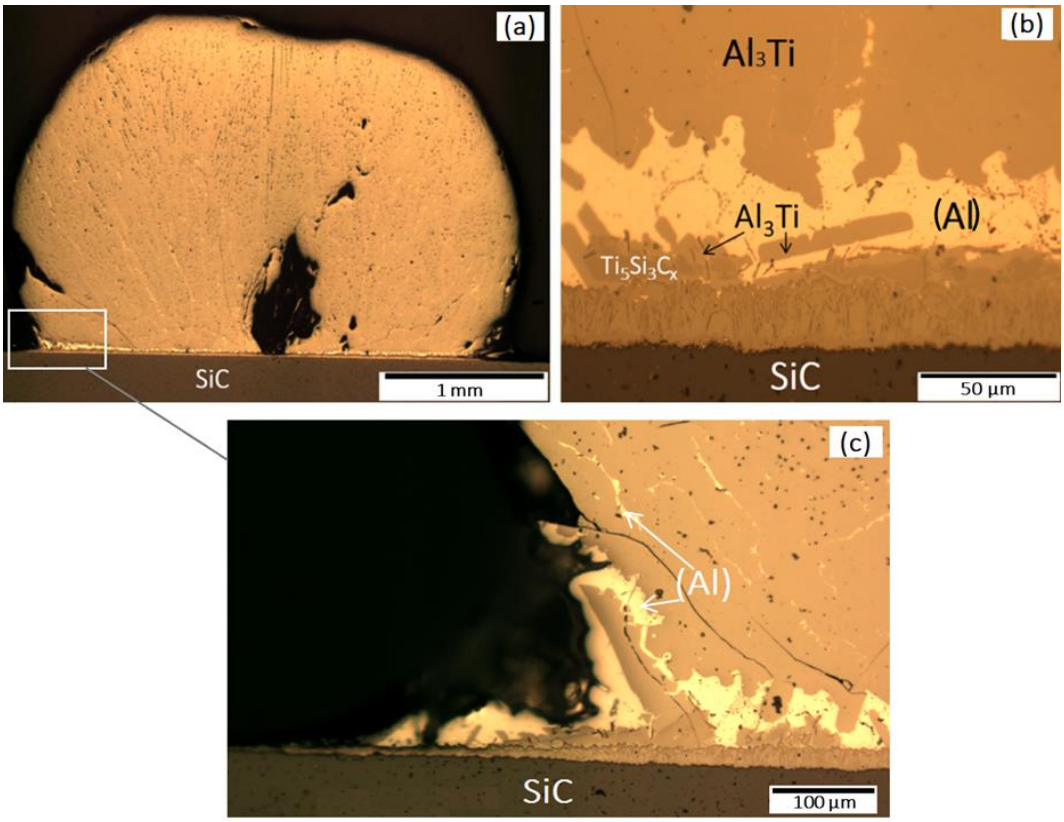

Figure 6.45. Drop profile section of the $Al_{75}Ti_{25}$/SiC after the test at 1260°C (10 min) (a) and the interfacial zone observed at the optical microscope (b).

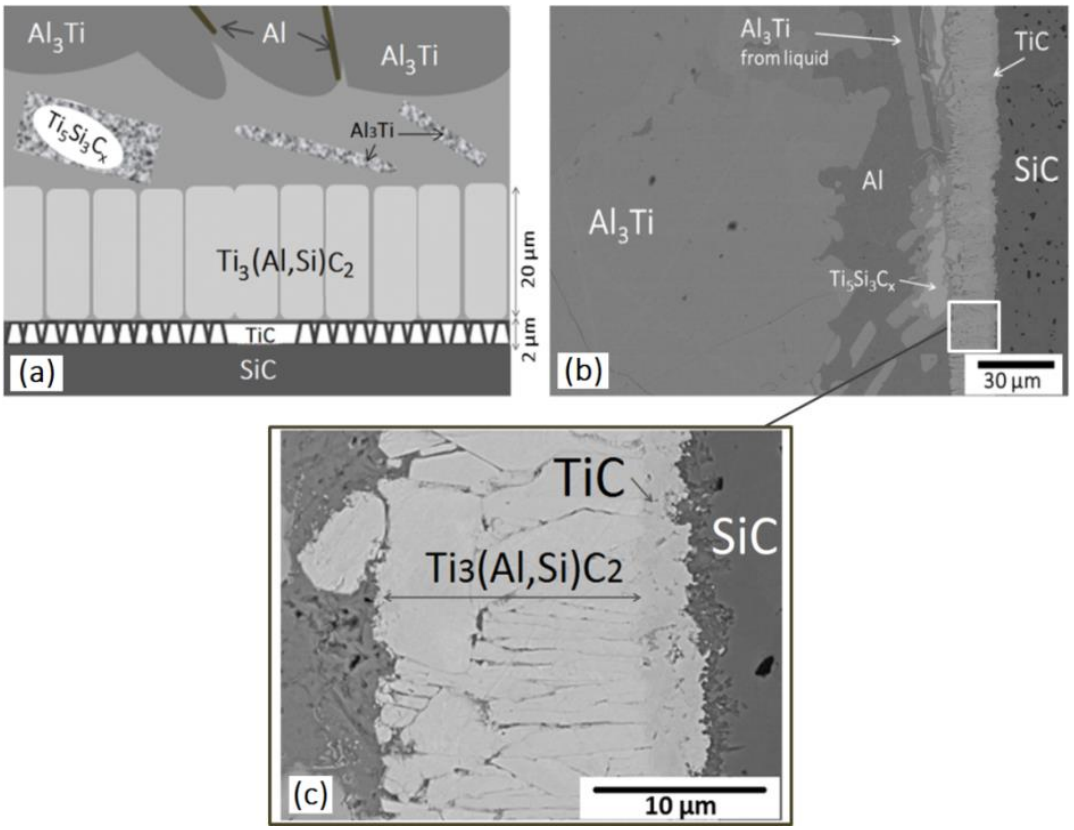

Figure 6.46. Interfacial zone of the $Al_{75}Ti_{25}$/SiC sample tested at 1260°C: schematic representation (a); BSE image (b); zoomed BSE image (c).

Table 6.15. Composition (at%) of the phases of $Al_{75}Ti_{25}$/SiC sample tested at 1260°C for10 min.

Phases	Composition at%			
	Al	C	Si	Ti
TiC	0.9	50.4	0.3	48.4
$Ti_3Si(Al)C_2$	2.1	34.2	14.1	49.6
$Ti_5Si_3C_x$	2.8	11.2	32.4	53.6
$Al_{75}Ti_{25interface}$	67.2	-	7.4	25.4
$(Al,Si)_{75}Ti_{25drop}$	71.5	-	3.2	25.3
$(Al)_{interface}$	97.8	-	1.5	0.7

In particular, the MAX-phase composition, analyzed along a vertical line inside the grains, does not vary significantly with their distance from SiC (*Figure 6.47*).

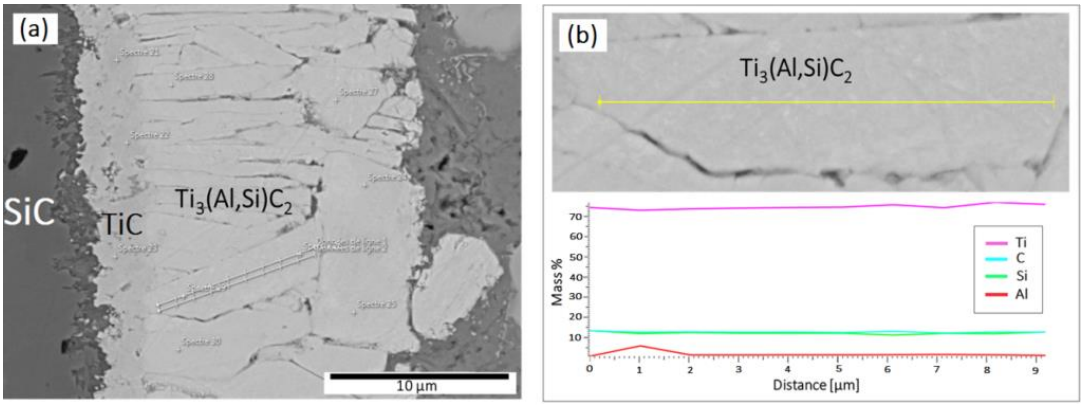

Figure 6.47. Interfacial section of the $Al_{75}Ti_{25}$/SiC after the wetting test at 1260°C (10 min) showing the line scan along the MAX-phase grain (a); the mass percentage of each element of the system plotted in function of the distance from the SiC (b).

$Al_{75}Ti_{25}$/SiC at 1500°C for 10 min

The same metal-ceramic system was investigated in terms of wettability (using the sessile drop technique described in *4.1*) and reactivity (using the EDS analysis) but increasing the testing temperature up to 1500°C.

At 1500°C a very good wetting is obtained and the interfacial microstructure of the system is clearly different from the one observed at 1260°C.

The alloy is, here, totally molten and the liquid spreads and covers all the ceramic surface (*Figure 6.48*(a)).

The system exhibits, indeed, very low contact angles (θ << 90°C) assuring an intimate contact between the materials. Moreover, fast kinetics is recorded and the final angle (about 22°; *Figure 6.48*(b)) is obtained in less than one minute.

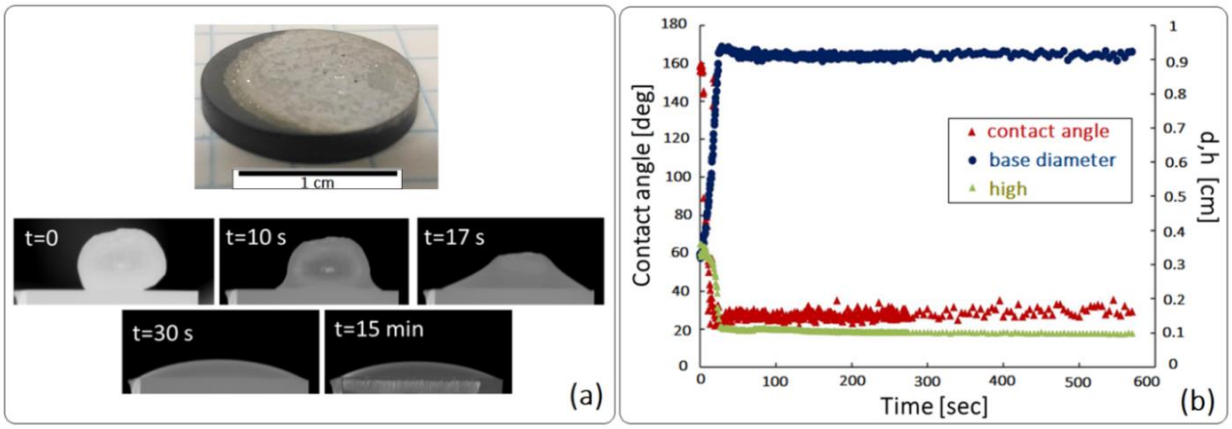

Figure 6.48. $Al_{75}Ti_{25}$/SiC sample tested at 1500°C for 10 min (a, top); drop profile images of the system (a, bottom); contact angle, base diameter and height of drop plotted as function of time (b).

The wettability and the interfacial reactivity have originated different interfacial phases (*Figure 6.49; Table 6.16*).

Starting from the ceramic substrate, one can find:

- a continuous layer of TiC (1 µm of thick)extending along the whole interface in contact to SiC;
- a continuous interlayer of the phase $Ti_3Si(Al)C_2$ (50 µm thick) grown on TiC and composed by several elongated and polygonal grains found also up to more than 100 µm far from the substrate. This MAX-phase exhibits a significant amount of Al (more than 6 at%; *Table 6.16*) that can replace Si in its lattice site;
- a matrix, formed of an Al solid solution (Al), with $Al_{75}Ti_{25}$ crystals inside it, constituting the whole bulk of the drop. $Al_{75}Ti_{25}$, the dark grey areas of *Figure 6.49,* dissolves some Si (between 2.5 and 5.4 at*%; Table 6.16*) that substitutes Al inside the intermetallic structure.
  The (Al), located at the grain boundaries, contains traces of Si and Ti (2.2 and 0.8 at%, respectively).

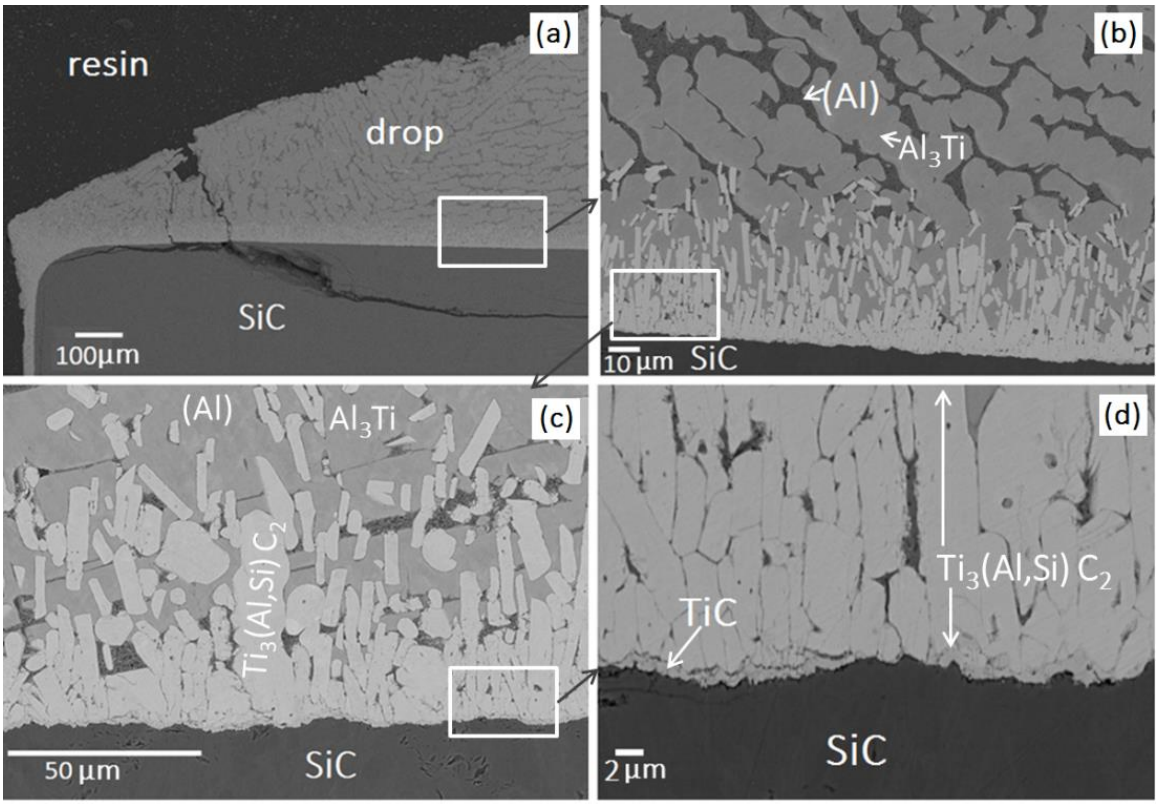

Figure 6.49- Interfacial section of the $Al_{75}Ti_{25}$/SiC after the wetting test at 1500°C (10 min) at the Triple Line (a); the central zone of the drop (b); the zoomed image of the central part of the drop (c) and of the first layers formed on the SiC (d).

Table 6.16. Composition (at%) of the phases detected in the $Al_{75}Ti_{25}$/SiC sample after the wetting test at 1500°C (10 min).

Phases	Composition at%			
	Al	C	Si	Ti
TiC	0.8	48.3	0.2	50.7
$Ti_3Si(Al)C_2$	6.7	35.2	9.5	48.6
$(Al,Si)_{75}Ti_{25}$	70.0	-	5.0	25.0
(Al)	97.0	-	2.2	0.8

A particular attention has been paid to evaluate the Si amount dissolved in the bulk of the sample in order to check the homogeneity of the system as well as to quantify the dissolution process.

The EDS analysis is conducted by selecting several points on the vertical section of the sample starting from the contact zone and moving toward the top of the drop (*Figure 6.50*).

The compositions obtained by these analyses, reported in *Table 6.17*, demonstrate that the Si concentration in a direction orthogonal to the SiC surface is practically constant after 10 min contact.

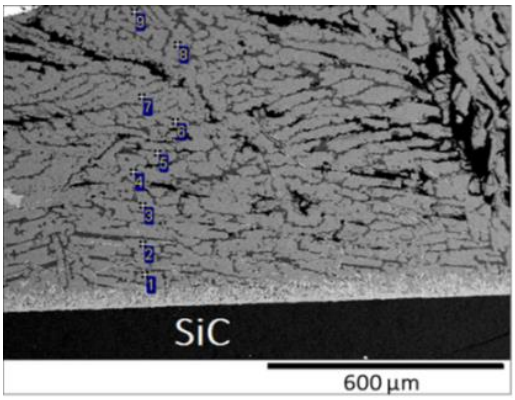

Figure 6.50. EDS analysis points (Table 6.17) along the cross section of the $Al_{75}Ti_{25}$/SiC sample after the wetting test at 1500°C (10 min).

Table 6.17. Compositions detected along the cross section of the $Al_{75}Ti_{25}$/SiC sample after the wetting test at 1500°C (10 min).

Composition (at%)			
Spectrum	Al	Si	Ti
1	70.7	3.0	26.3
2	70.9	2.8	26.3
3	71.2	2.6	26.1
4	70.8	3.0	21.6
5	68.5	2.5	29.0
6	70.7	3.0	26.3
7	69.5	4.8	25.7
8	68.5	5.4	26.1
9	83.7	4.0	12.3

Indeed, the amount of Si dissolved in the bulk is varying in a small composition range (from 2.5 to 5.4 at%). The almost constant composition of this element is confirmed by the map showing the distribution of the different elements along the vertical profile of the sample, shown in *Figure 6.51.*

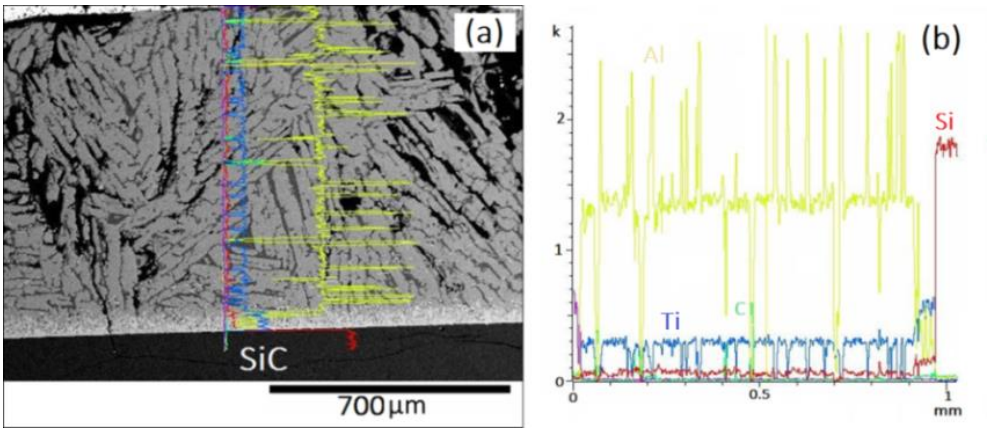

Figure 6.51.Cross section of the $Al_{75}Ti_{25}$/SiC sample after the wetting test at 1500°C (10min) (a) and distribution of the different elements along the vertical profile (b).

An estimation of the liquid composition at 1500°C after 10 min of contact will be performed (*6.2.2.1*) taking into account the approximated amounts (vol%) of the different bulk phases formed above the interfacial zone (*Figure 6.52*); the C amount is considered to be confined in the two interfacial layers (TiC, $Ti_3Si(Al)C_2$) only.

In order to have an appreciable reproducibility of the analyses, an average of the results obtained on more than ten different images, has been taken into account.

From this approximation, one can observe that the matrix of the $Al_{75}Ti_{25}$/SiC sample, after having been maintained 10 min at 1500°C, is composed of about 73% of Al_3Ti and 27% of Al.

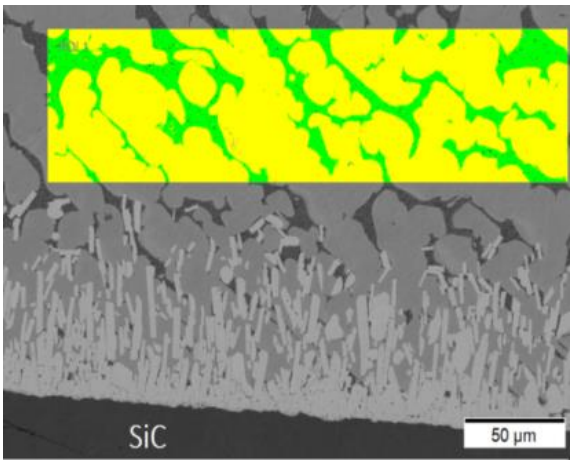

Figure 6.52. Cross section of the $Al_{75}Ti_{25}$/SiC sample tested at 1500°C for 10 min; the selected coloured areas show 27% of green areas representing theAl matrix and 73% of yellow areas representing $Al_{75}Ti_{25}$.

$Al_{75}Ti_{25}$/SiC at 1500°C for 30 min

The stoichiometric Al_3Ti ($Al_{75}Ti_{25}$) alloy is tested on SiC at the same temperature of 1500°C but increasing the time of contact (from 10 min up to 30 min).

The composition of the different phases, detected by the EDS-analysis, is reported in *Table 6.18.*

Their morphology and distribution, well visible in the microstructures of *Figure 6.53*, can be described as follow:

- a continuous TiC layer formed at the interface and characterized by a thickness smaller than 20 µm;
- a $Ti_3Si(Al)C_2$MAX-phase layer, extended up to about 40 µm far from the substrate, that contains more than 5 at% of Al;

- some Al(Si) grains appearing just above the MAX-phase and dispersed inside the Al-Si matrix;
- an Al-Si eutectic matrix containing several elongated τ-phase grains and dendritic Al_3Ti grains dissolving traces of Si (*Table 6.18*); *Figure 6.53* (a), *Figure 6.54*).

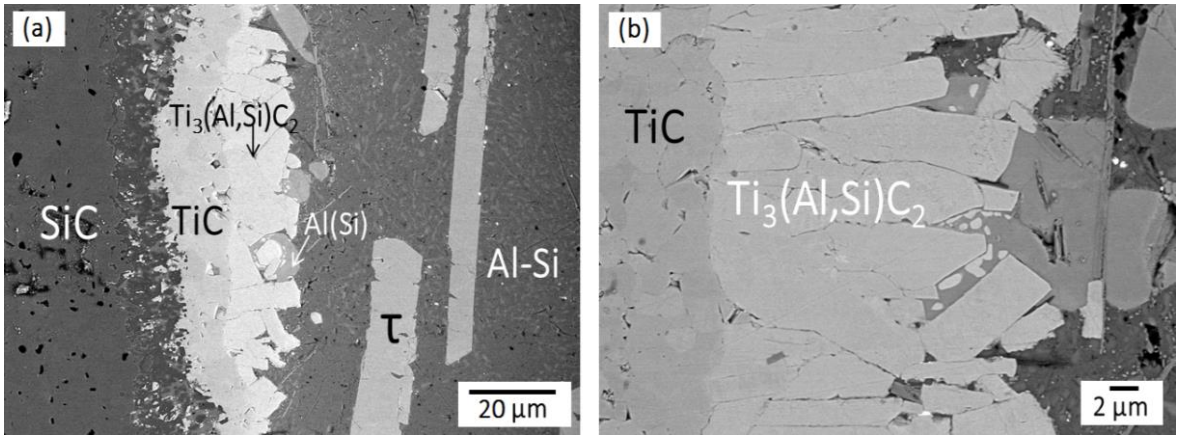

Figure 6.53. Interfacial section of the $Al_{75}Ti_{25}$/SiC sample tested at 1500°C for 30 min (a), zoomed area of the interface (b).

Table 6.18. Composition (at%) of the phases found in $Al_{75}Ti_{25}$/SiC sample tested at 1500°C for 30 min.

Phases	Composition at%			
	Al	C	Si	Ti
TiC	0.8	48.3	0.2	50.7
$Ti_3Si(Al)C_2$	6.7	35.2	9.5	48.6
τ-phase	13.7	-	53.2	33.1
$(Al,Si)_{75}Ti_{25}$	73.0	-	2.0	25.0
Al-Si	76.4	-	13.6	-
(Al)	97.0	-	2.2	0.8

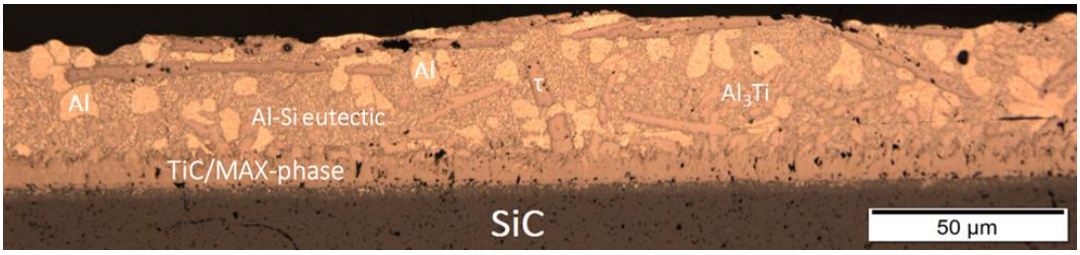

Figure 6.54. Profile drop of $Al_{75}Ti_{25}$/SiC sample after 30 min test at 1500°C.

As already done for the sample tested for 10 min, the estimation of the percentage of the different phases formed in the bulk of the sample after 30 min of contact has been conducted.

The selected coloured zones of *Figure 6.55* (vol%) show: 40% of yellow area (τ-phase), 20% of blue area ($Al_{75}Ti_{25}$), 25% of light blue area (Al) and 15% of purple area (Al-Si eutectic).

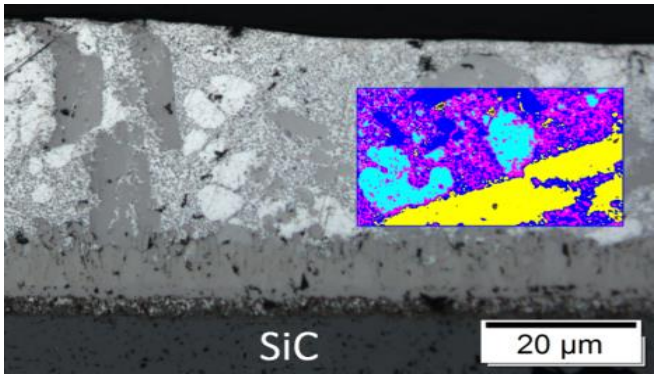

Figure 6.55. Cross section of $Al_{75}Ti_{25}$/SiC sample after 30 min test at 1500°C (a)the selected coloured area show 40% of yellow area (τ-phase), 20% of blue area ($Al_{75}Ti_{25}$), 25% of light blue (Al) and 15% of purple area (Al-Si eutectic).

$Al_{75}Ti_{25}$/SiC at 1500°C for 1 h

The $Al_{75}Ti_{25}$ alloy was also tested on SiC at the same temperature (1500°C) but maintaining the metal-ceramic couple at high temperature for 1h in order to reach a situation closer to the equilibrium one.

Observing the microstructure reported in *Figure 6.56,* one can notice a significant modification of the interfacial phase sequence:

- a TiC layer, formed of small polygonal grains, grown in contact to SiC and extended inside the interface up to more than 50 µm;
- traces of Ti_3SiC_2 just above TiC; in this case no significant amount of Al is detected inside the MAX-phase (about 0.5 at%; *Table 6.19*);
- a matrix composed of Al-Si eutectic showing the typical lamellar structure and a composition close to the theoretical one (12.2 at% of Si);
- two other phases dispersed inside this eutectic matrix and all along the section: the first one is an Al-Si-Ti ternary phase, known as τ-phase, in form of elongated grains; the second one is pure Si concentrated in the light grey crystals characterized by a polygonal shape.

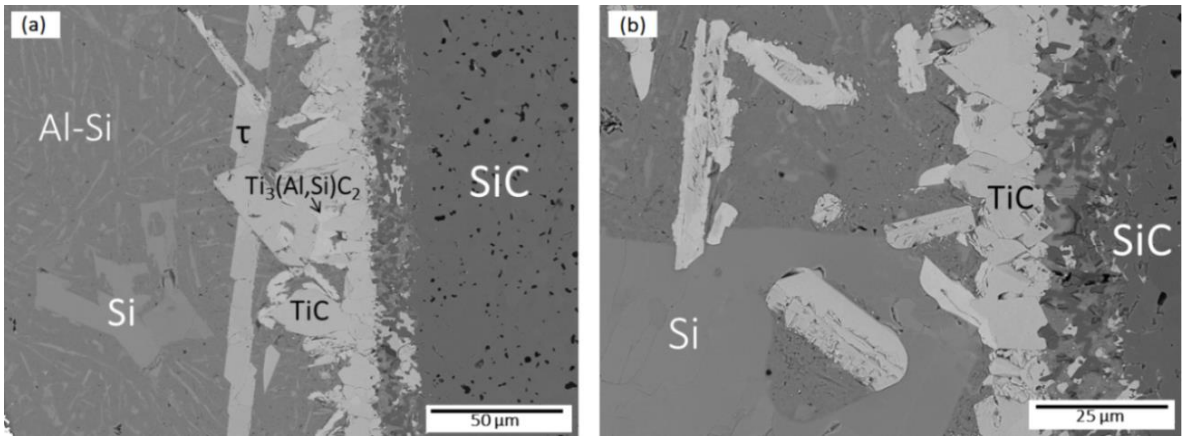

Figure 6.56. Interfacial section of the $Al_{75}Ti_{25}$/SiC sample tested at 1500°C for 1 h (a), zoomed area of the interface (b).

Table 6.19. Composition (at%) of phases found in the $Al_{75}Ti_{25}$/SiC sample tested at 1500°C for 1 h.

Phases	Composition at%			
	Al	C	Si	Ti
TiC	-	49.2	-	50.8
Ti_3SiC_2	0.5	33.8	15.5	50.2
τ-phase	13.7	-	53.2	33.1
Al-Si	77.6	-	12.4	-
Si	-	-	100	-

Observing the bulk microstructure of the sample (*Figure 6.57*), it is possible to identify a totally different situation in terms of morphology and composition compared to the one obtained after 10 min of contact at the same temperature of 1500°C.

This is due to the completely modified composition of the liquid phase that becomes significantly enriched in Si as it will be show (*6.2.2.1*).

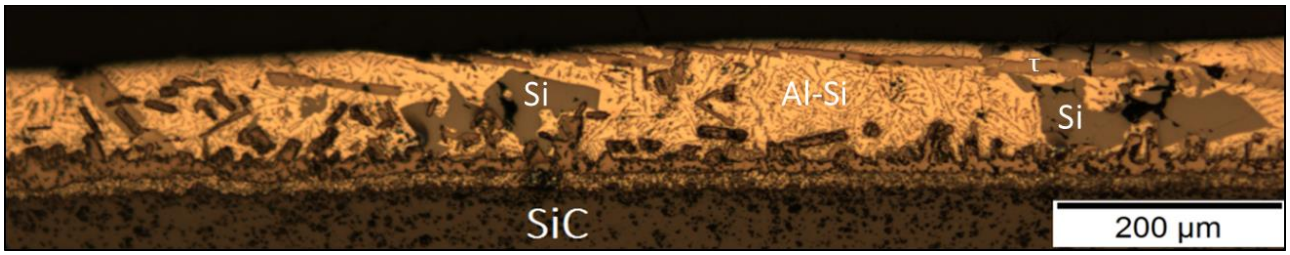

Figure 6.57. Profile section of the $Al_{75}Ti_{25}$/SiC sample tested at 1500°C for 1 h.

As already done for the previous samples (10 and 30 min), an estimation of the amounts (vol%) of the bulk phases has been performed by selecting several areas above the metal/ceramic interface. The selected coloured zones of *Figure 6.58* show: 40% of yellow area (Si crystals), 30% of bleu area (τ-phase) and 30% of purple area (Al-Si eutectic).

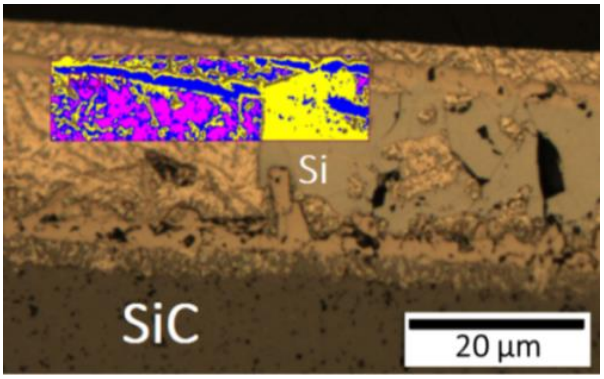

Figure 6.58. Cross section of the $Al_{75}Ti_{25}$/SiC sample tested at 1500°C for 1h; the selected coloured areas show 40% of yellow area (Si crystals), 30% of bleu area (τ-phase) 30% of purple area (Al-Si eutectic).

On the basis of the analytical and microstructural data (DSC and EDS analysis) of the different $Al_{75}Ti_{25}$/SiC samples analysed, one can summarize that:

1) the first liquid appears at a temperature lower then melting temperature of the aluminide and this first liquid formation is due to the metal/ceramic interaction at the interfacial zone;
2) the $Ti_3Si(Al)C_2$ MAX-phase is the main interfacial phase coming from the chemical reactions occurring at both the temperatures taken into account (1260, 1500°C);
3) the liquid composition changes drastically, in particular concerning its Si amount, increasing the contact time.

6.2.1.2 $Al_{84}Ti_{16}$/SiC

DSC tests

The DSC tests (*4.4*) were conducted selecting the same heating program from 30 to 1450°C at 10°C/min and using Ar (O_2< 100 ppb) working atmosphere, as performed for the previous system.

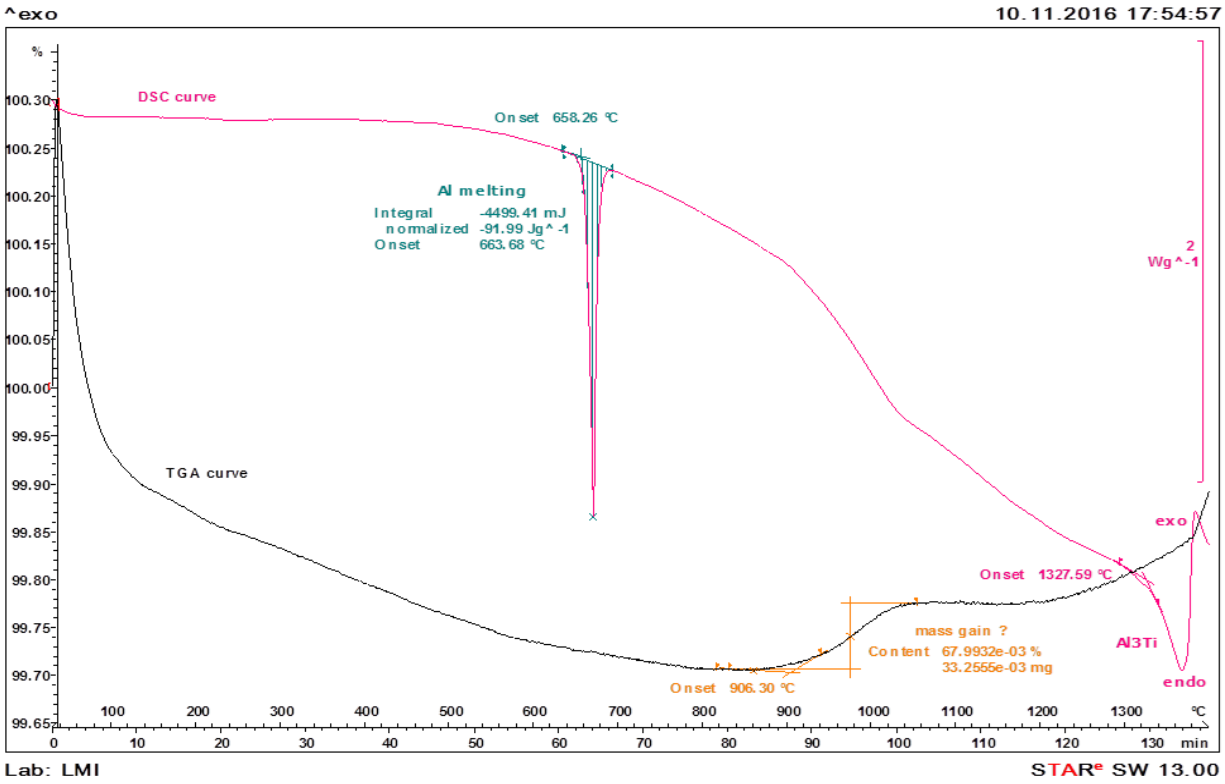

Figure 6.59. Differential Scanning Calorimetry graphof $Al_{84}Ti_{16}$/SiC sample obtained using a heating program set from 30 to 1450°C at 10°C/min.

Observing the DSC curve, reported in *Figure 6.59,* one can see an endothermic peak corresponding to the Al-rich liquid peritectic equilibrium (Liquid+Al_3Ti ↔Al), followed, at about 1330°C, by the liquidus (Liquid ↔Liquid + Al_3Ti).

Reactivity evaluation

$Al_{84}Ti_{16}$/SiC at 1235°C for 10 min

The $Al_{84}Ti_{16}$/SiC wetting test was performed at 1235°Cand the system was quickly extracted from the hot part of the furnace to the room temperature part after 10 min.

This temperature (1235°C) is the first interaction temperature identified by the high temperature test; in fact, even if a real complete wetting still did not occur in the system, it is possible to notice the formation of a first liquid phase in contact to the ceramic substrate (*Figure 6.60*).

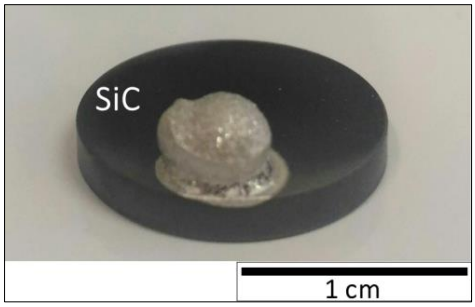

Figure 6.60. $Al_{84}Ti_{16}$/SiC sample after the wetting test at 1235°C (10 min).

Analysing the interfacial microstructures, reported in *Figure 6.61*,and the phases composition, reported in *Table 6.20,* one can detect:

- a very thin (~ 1 µm) Al_4C_3 layer in contact with SiC;
- the presence of a continuous layer of TiC (< 10 µm thick, white) that extends along all the interface;
- some grains of$Ti_3Si(Al)C_2$ MAX-phase detected mainly next to the triple line, just above the TiC (*Figure 6.61*(b)).

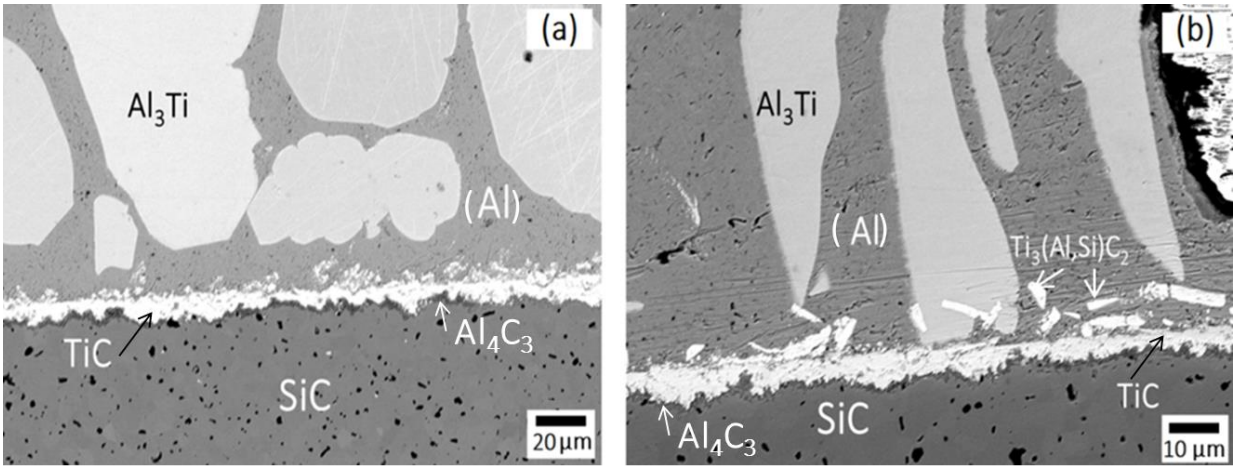

Figure 6.61. Interfacial zone microstructure of $Al_{84}Ti_{16}$/SiC sample (a); zoomed image of the sample at the interface(b).

The rest of the drop, above the interface, is still solid at 1235°C and composed by an (Al) matrix (the dark area of *Figure 6.61*) and Al_3Ti grains (light grey) dissolving just traces of Si and extending in all the bulk system.

Si is also dissolved inside the (Al) matrix solid solution (< 4.0 at%; *Table 6.20*).

Table 6.20Composition (at%) of the interfacial phases of $Al_{84}Ti_{16}$/SiC sample tested at 1235°C..

Phases	Composition at%			
	Al	C	Si	Ti
Al_4C_3	61.9	38.1	-	-
TiC	0.8	50.4	0.4	48.4
$Ti_3Si(Al)C_2$	5.3	38.8	10.5	45.5
$(Al,Si)_{75}Ti_{25}$	74.5	-	0.5	25.0
(Al)	99.1	-	0.8-4.0	0.6

The Si amount detected along the vertical drop profile varies from 0.8 to 4.0 at% (*Figure 6.62; Table 6.21*) depending on the distance from the SiC surface. Si is in fact mainly dissolved in the bulk areas closer to the ceramic substrate.

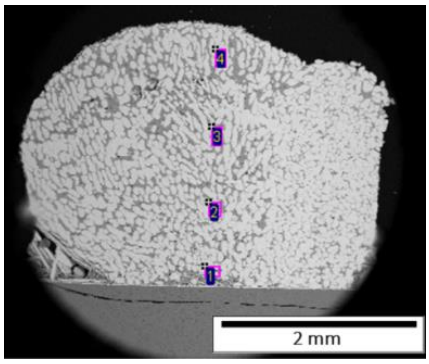

Figure 6.62. Vertical section of $Al_{84}Ti_{16}$/SiC sample after the test at 1235°C for 10 min; the numerated points refer to the EDS analyses reported in Table 6.21.

Table 6.21. Composition (at%) of small selected areas of the $Al_{84}Ti_{16}$/SiC vertical section moving from the metal-ceramic contact zone toward the top of the metallic drop.

Composition (at%)			
Spectrum	Al	Si	Ti
1	81.9	2.4	15.7
2	83.0	3.9	13.1
3	79.8	1.4	18.8
4	80.6	0.8	18.6

A schematic representation of the metal-ceramic system is proposed in *Figure 6.63*(b) while *Figure 6.63*(a) shows a typical lens shaped fracture inside the substrate, due to the quick extraction of the sample from the hot part of the furnace to the room temperature one. The black holes one can see

inside the bulk (left part of the drop of *Figure 6.63*(a)) have to be considered as artefacts coming from the polishing process of materials characterized by a significant brittleness. The two macroscopic zones visible in *Figure 6.63*(a), showing a similar grain texture but at a different scale, could be due to an asymmetric cooling rate, faster in the right-hand side, occurred during the extraction of the sample from the furnace test-zone.

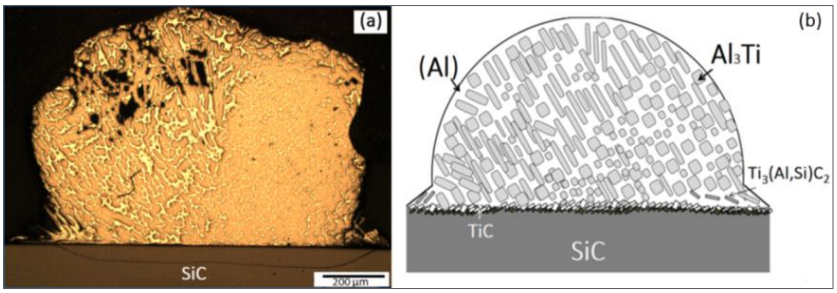

Figure 6.63. $Al_{84}Ti_{16}$/SiC drop profile observed at the optical microscope (a) and represented by a scheme (b).

$Al_{84}Ti_{16}$/SiC at 1270°C for 10 min

Increasing the temperature from 1235 up to 1270°Cand maintaining the same contact time (10 min), no significant differences are found for the $Al_{84}Ti_{16}$/SiC couple. It is in fact possible to observe the formation of a liquid phase, just in contact with the ceramic surface, wetting the SiC substrate, while the rest of the drop has maintained its original shape. Moreover, the morphology and the phases composition of the vertical section, reported in *Figure 6.64,* as well as the stoichiometry of the phases formed at 1270°C, reported in *Table 6.22*, are close to the ones detected for the same system tested at lower temperature (1235°C). The main difference is that the MAX-phase grains are located not only at the triple line but also close to the center of the horizontal profile.

It means that the formation of this intermediate phase is favored at higher temperatures.

Table 6.22. Composition (at%) of the phases found in the $Al_{84}Ti_{16}$/SiC section (1270°C; 10 min).

Phases	Composition at%			
	Al	C	Si	Ti
TiC	-	49.9	-	50.1
$Ti_3Si(Al)C_2$	5.5	34.2	10.5	49.8
$(Al,Si)_{75}Ti_{25}$	74.6	-	0.5	24.9
Al	98.9	-	0.7-4.1	0.8

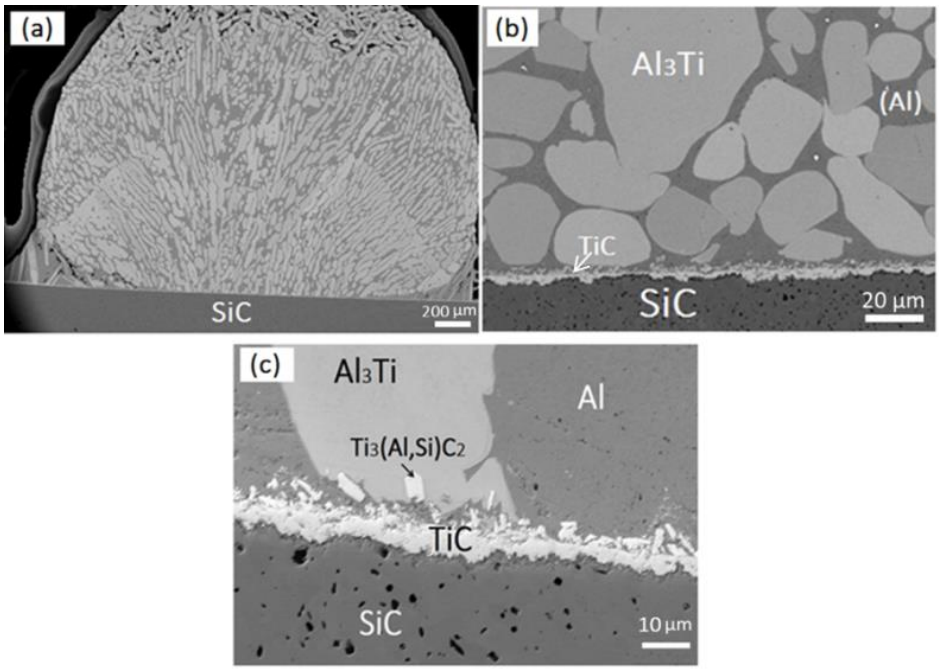

Figure 6.64. $Al_{84}Ti_{16}$/SiC drop profile after 10 min of wetting test at 1270°C (a); the zoomed interfacial area close to the center of the section (b) and at the contact zone (c).

Additionally the $Al_{84}Ti_{16}$/SiC couple was tested in the wetting furnace increasing the temperature step by step and waiting 8 min at each temperature step (*Figure 6.65*) in order to catch the temperature when the drop becomes totally liquid and spreads on SiC. Melting and nearly instantaneous spreading was observed at 1300°C (θ< 20°), with the liquid covering all the available ceramic surface (*Figure 6.66*). Then, the sample was maintained 10 min at this testing temperature and then rapidly extracted from the hot part to the room temperature part.

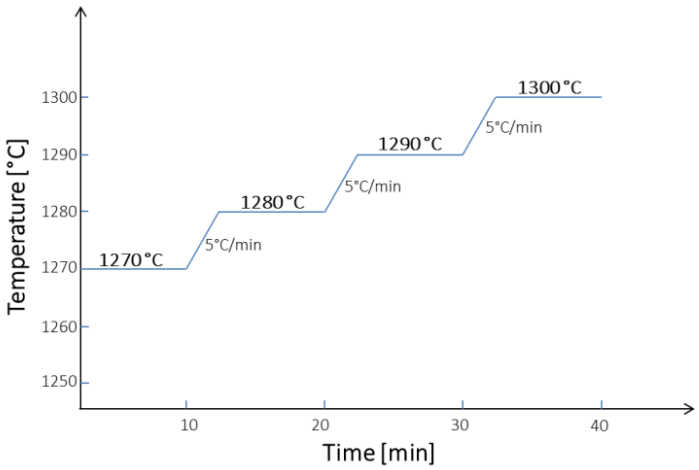

Figure 6.65. Graph Temperature-Time reporting the step-by-step test at high temperature.

$Al_{84}Ti_{16}$/SiC at 1300°C for 10 min

The interface of this sample after the final 10 min of contact is clearly different (*Figure 6.67*) from the ones previously observed (1235 and 1270°C; *Figure 6.61* and *Figure 6.64*).

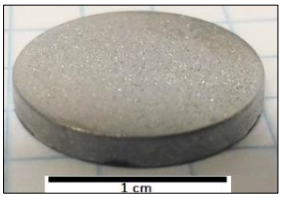

Figure 6.66. The $Al_{84}Ti_{16}$/SiC sample after the wetting test at 1300°C (10 min).

On the drop section it is possible to observe:

- an Al_4C_3 (dark) layer 3 µm thick (well visible in *Figure 6.67* (c));
- a compact TiC (white) layer 3 µm thick (well visible in *Figure 6.67* (b));
- a continuous mixed MAX-phase $Ti_3Si(Al)C_2$layer (composition given in *Table 6.23*) in the form of long grains, extending along the whole interface and characterized by an average thickness of 20 µm;
- a matrix, above the interface, coming from the solidification of the liquid, formed at 1300°C, composed of Al (the dark area of *Figure 6.67* (a),(b)) and Al_3Ti grains (white).

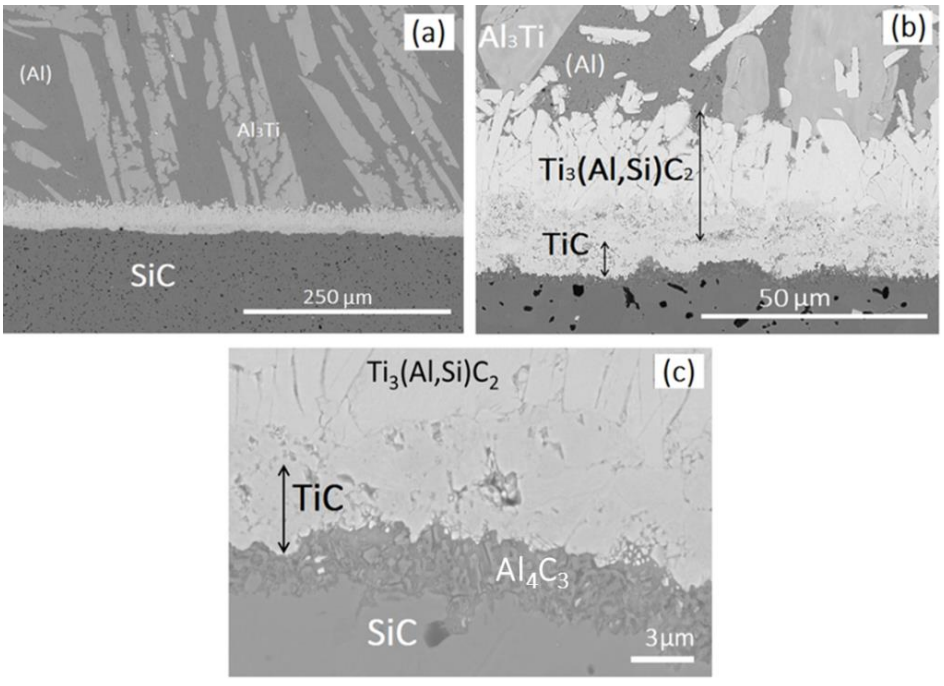

Figure 6.67. Interfacial section of the $Al_{84}Ti_{16}$/SiC sample after the wetting test at 1300°C (10min) (a); zoomed image of the contact zone (b) and of the first interaction layers (c).

Table 6.23. Composition (at%) of the phases of the $Al_{84}Ti_{16}$/SiC sample after the wetting test at 1300°C (10min).

Phases	Composition at%			
	Al	C	Si	Ti
Al_4C_3	62.2	37.8	-	-
TiC	-	50.9	-	49.1
$Ti_3Si(Al)C_2$	4.2	34.2	12.2	49.4
$(Al,Si)_{75}Ti_{25}$	70.0	-	5.1	24.9
(Al)	99.0	-	0.8	0.2

The (Al) matrix dissolves traces of Si and Ti (0.8 and 0.2 at%, respectively) and inside the Al_3Ti grains a presence of 5 at% of Si is also detected (*Table 6.23*). As it is possible to observe from *Figure 6.68,*the Al_3Ti grains are homogenously distributed along all the drop profile.

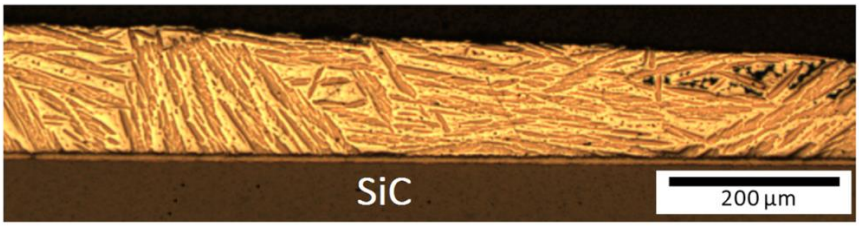

Figure 6.68. Drop profile section of the $Al_{84}Ti_{16}$/SiC after the wetting test at 1300°C (10min) obtained by optical microscopy.

$Al_{84}Ti_{16}$/SiC at 1300°C for 1 h

The $Al_{84}Ti_{16}$ alloy on SiC was also maintained at 1300°C for 1h in order to define the stable phases of the system. Observing the interfacial microstructure of *Figure 6.69* and starting from the metal-ceramic interface, one can observe:

- a continuous layer of TiC (about 8µm thick) extending along all the interface;
- a mixed MAX-phase ($Ti_3Si(Al)C_2$) layer without pores or defects and with an average thickness of about 40 µm (*Figure 6.69*(a));
- the rest of the spread drop composed of Al_3Ti grains dispersed in a matrix formed of Al-rich and Al-Si eutectic areas.

In this case the MAX-phase is mainly constituted of Si; just an amount of 1.5 at% of Al is detected in it (*Table 6.24*). In addition, the Al_3Ti grains coming from the solidification of the liquid dissolve a significant amount of Si (more than 10 at% as indicated in*Table 6.24*).

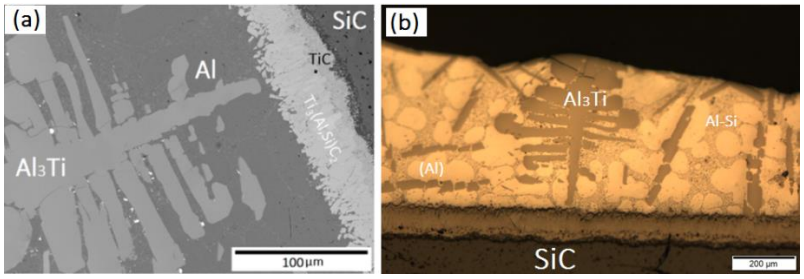

Figure 6.69. SEM image of the profile section of the $Al_{84}Ti_{16}$/SiC after the wetting test at 1300°C after 1 h of contact(a) and the same part of the sample observed at the optical microscope (b).

Si, having both dimension and electronegativity close to the Al ones, can partially substitute the Al inside the intermetallic structure.

Table 6.24. Composition (at%) of the phases formed when $Al_{84}Ti_{16}$/SiC is maintained at 1300°C for 1h.

Phases	Composition at%			
	Al	C	Si	Ti
TiC	-	49.5	-	50.5
$Ti_3Si(Al)C_2$	1.5	38.0	14.0	38.0
$(Al,Si)_{75}Ti_{25}$	64.4	-	10.6	25.0
Al-Si eutectic	77.6	-	12.4	-
(Al)	97.2	-	1.9	0.9

The (Al) matrix dissolves about 2.0 at% of Si and about 1.0 at% of Ti and it is represented by the dark grey area of *Figure 6.69*(a) and the lighter color areas of *Figure 6.70* (b), respectively. Around these (Al) grains the Al-Si eutectic appears with the characteristic lamellar structure and composition (*Table 6.24*).

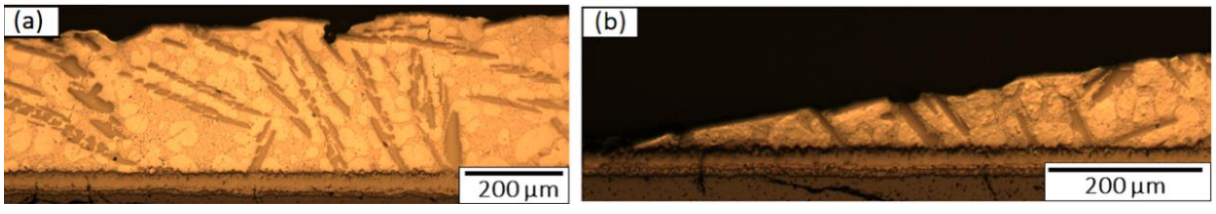

Figure 6.70. Microstructure of the bulk (a) and of triple line (b) of the $Al_{84}Ti_{16}$/SiC sample tested at 1300°C for 1h.

In order to be able to compare the experimental results concerning the interfacial reactivity to the thermodynamic predictions (*6.2.2.2*), an estimation of the volume percentage of the different

phases (*Figure 6.71*) is conducted, considering the C amount contained only in the two interfacial layers (TiC, $Ti_3Al(Si)C_2$). To have an appreciable reproducibility of the analyses, an average of the results obtained has been taken into account considering more than ten different images as, for instance, the one of *Figure 6.71.*

The selected coloured zones of *Figure 6.71* show: 39% of yellow area (Al-Si eutectic), 37% of bleu area (Al) and 24% of green area ($Al_{75}Ti_{25}$).

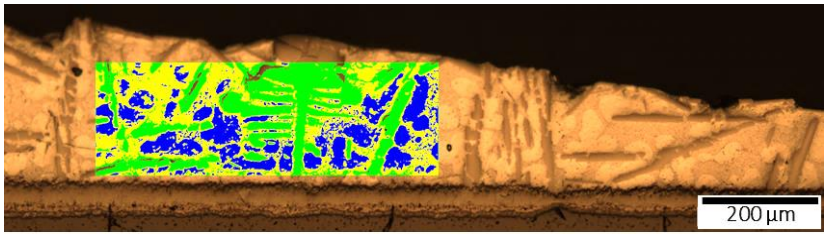

Figure 6.71. Estimation of the amount of the three main phases of the bulk system (average of about 10 estimations); 37% of bleu (Al), 39% of yellow (Al-Si eutectic),24%of green ($Al_{75}Ti_{25}$).

Thanks to the information obtained through the characterization results (EDS and DSC) of the different $Al_{84}Ti_{16}$/SiC microstructures, one can summarize that:

1) the first signal appearing on the DSC curve is here due to the liquid formation coming from the melting of the alloy and not, as for the Al_3Ti/SiC system, from the metal/ceramic interaction occurring at the interfacial zone;
2) at the first temperature (1235°C) the $Ti_3Si(Al)C_2$MAX-phase was found as traces, while TiC is the main interfacial layer;
3) the liquid composition changes depending on the contact time, gradually increasing its Si content.

6.2.2 Thermodynamic discussion

6.2.2.1 $Al_{75}Ti_{25}$/SiC

To understand and analyze the reactivity between Al_3Ti and SiC, different graphical representations, obtained as a result of the thermodynamic approach, are presented in the following. Because of the difficulties related to a clear reading of a 2D representation of a quaternary system, the ternary Al-

Si-Ti is initially proposed to identify the nature of the first liquid (*Figure 6.72*). In particular, the isothermal section calculated at the first interaction temperature (1260°C) is taken into account to show the wide extension of the liquid domain based on Al, where Si ranges from 0 to about 70 at%, and the Ti limit is about 8 at% (X_{Si}=0.7; X_{Ti}=0.08). The calculated C solubility limit in the Al-Si-Ti liquid at 1260°C is about 10 ppm ($X_i=10^{-5}$).

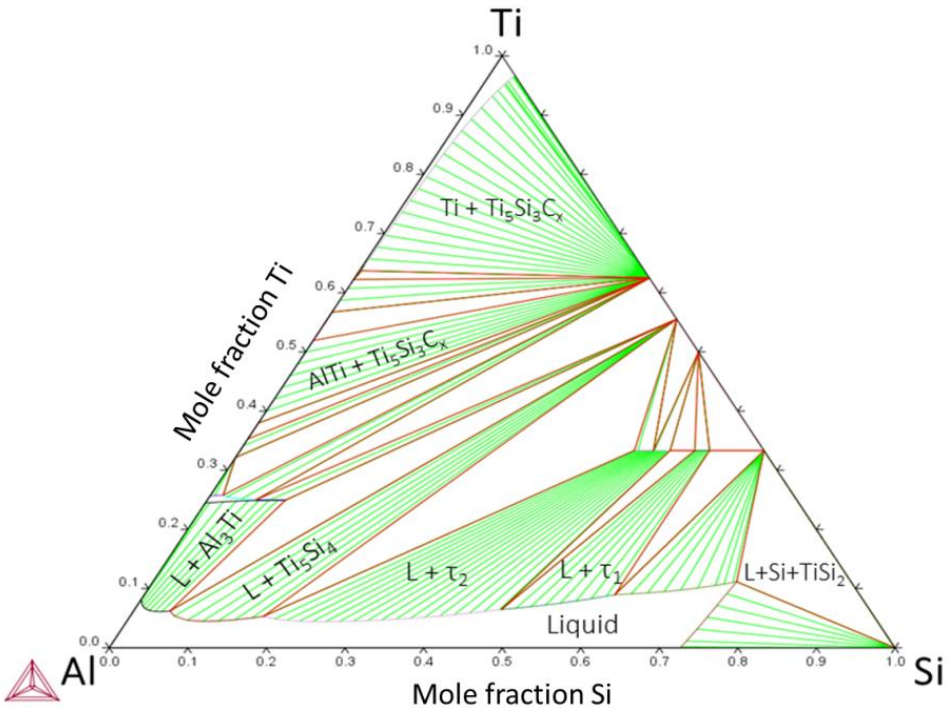

Figure 6.72. Al-Si-Ti isothermal section calculated at 1260°C.

It is then possible to calculate an isothermal section (1260°C) where one can visualize the two reacting materials connected by a dotted line (*Figure 6.73(a)).* As one can observe from this graph, the C-saturated liquid phase can lead to the formation of different C-based phases.

In fact, the end-members are not in equilibrium: the line connecting Al_3Ti and SiC crosses several domains underlining that different reactions take place. The first liquid formed, after the A_3Ti/SiC interaction, is in fact suddenly saturated in C, because of its low solubility, and enriched in Si (25 at%). It is then possible to visualize our system calculating the isothermal section of the Al-Si-Ti-C quaternary at 1260°C where the C amount is maintained constant (1%): in this case diagram surface is a section of the quaternary phase diagram just above the Al-Si-Ti plane(*Figure 6.73*(b)).

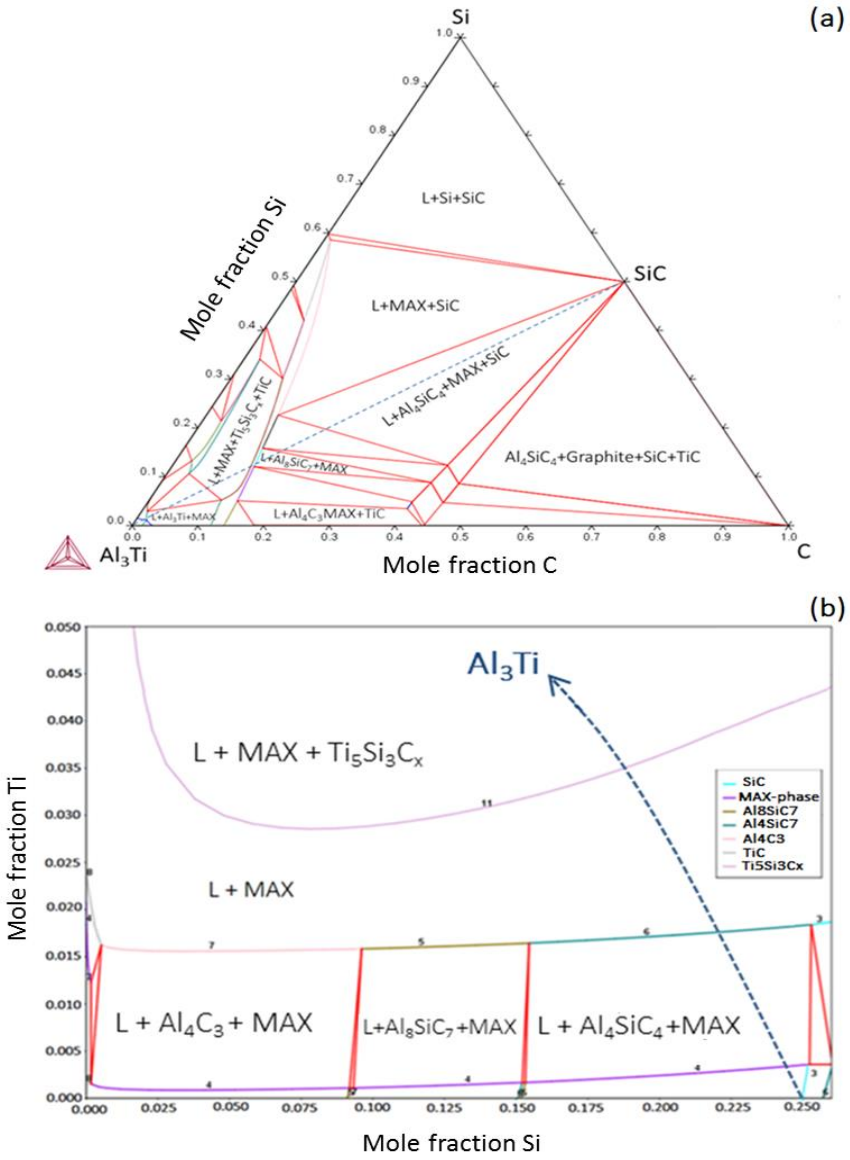

Figure 6.73. Al-C-Si-Ti isothermal section (C constant (1%); 1260°C) (a); zoomed on Al-Si corner (b).

From *Figure 6.73*(b), one can visualize the sequence of the interfacial phases precipitating from the C-saturated liquid at 1260°C. In our samples, the first reaction between Al_3Ti and SiC leads to the formation of the 2 µm TiC layer at the metal-ceramic interface (*Figure 6.46*) and of the already mentioned Si-rich liquid (25 at% of Si). Even if TiC does not appear as an equilibrium phase (*Figure 6.73*(b)), it remains anyway in the microstructure of the system (because of its stability due to the highly negative ΔG of formation) covering the ceramic surface. Thus, Al_3Ti and SiC are not directly in contact anymore as this new liquid phase extends between them. Even if the melting temperature of $Al_{75}Ti_{25}$ is 1396°C, thermodynamic calculations conducted at 1260°C (*Figure 6.74*) demonstrate and confirm that a first liquid forms when just a small amount of C is dissolved (X_c=0.05) supporting the experimental results.

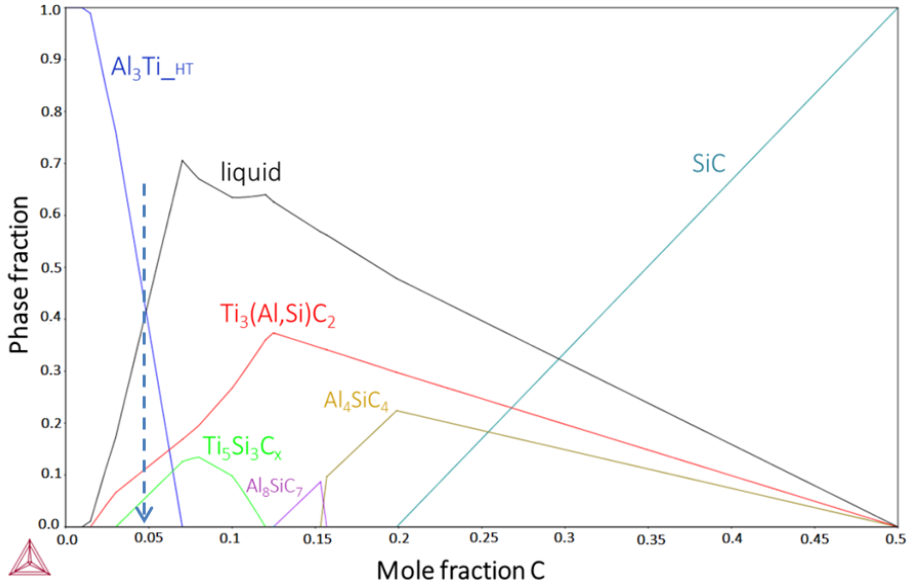

Figure 6.74. Phase formation as a function of mole fraction of C occurring at 1260°C during the $Al_{75}Ti_{25}$/SiC interaction.

The Si-enriched liquid, formed at the interface, interacts, through the thin TiC layer, with SiC leading to the formation of both the MAX-phase and $Ti_5Si_3C_x$ grains depending on the Ti amount entered inside the liquid.

The formation of these phases is sustained by the thermodynamic calculation reported in the graph of *Figure 6.73*(b).Indeed, from this graph it is visible that at 1260°C, the Al-25at%Si liquid requires a small amount of Ti to be saturated and reach the MAX-phase + liquid domain.

The MAX-phase constitutes the main interfacial layer (≈ 20 µm thick) generated as a result of the first chemical reaction occurring at the contact zone and its presence is confirmed by the calculations of *Figure 6.73*(a) and *Figure 6.74:*

- the dotted line, connecting the reacting materials in contact at 1260°C, crosses, on both the SiC and $Al_{75}Ti_{25}$ sides, the equilibria involving liquid +MAX-phase;
- the graph showing the phase fraction formation as a function of the C amount reveals that the MAX-phase is the first one formed by the liquid at 1260°C.

It is also possible to calculate that Ti amounts needed to reach the liquid + MAX-phase and liquid + MAX-phase + $Ti_5Si_3C_x$equilibria are about 0.018 and 0.042 mole, respectively.

In both the cases, the Ti amount required to cross both the equilibria is below its solubility limit, demonstrating a good agreement with the calculated solubility range for this element.

After this first interaction, the liquid starts to be enriched in Al and Ti, both coming from the melting

of Al_3Ti, going towards the aluminide direction, as shown by the dotted curve of *Figure 6.73*(b).
At 1500°C, the aluminide becomes totally liquid and it interacts with SiC leading to the formation of the C-based interfacial phases (TiC, MAX-phase) during the isothermal process.
One can then estimate the evolution of the C-saturated liquid, after the interfacial reactions, during the cooling of the system by considering the Al-C-Si-Ti system (with a constant C amount; 1%).
A drastic increase of the Si content inside the liquid is observed depending on the time of contact.

The Ti and Si amounts inside the liquid can be estimated taking into account both the phase percentages(vol%) of the microstructure of the $Al_{75}Si_{25}$/SiC sample (1500°C; 10 min) (*Figure 6.52*) and the density of each phase. The vol% of each phase is converted in the corresponding wt% of it (B).
An example of this procedure is reported here:

- $M_{Al}*\rho_{(Al)}=B_{Al}$
- $M_{Al75Ti25}*\ \rho_{Al75Ti25}=B_{\ Al75Ti25}$

where M and ρ are respectively the atomic mass and the density of each element/phase.
The global weight (S) of the colored area is then calculated as:

- $S= B_y + B_z + B_w$.

where the letters y, z and w represent Ti, Si and Al respectively.
In this example the amount of Ti in the colored area is just related to its presence inside the aluminide:

- $C_y*M_y/ (C_y*M_y+ C_z*M_z+ C_w*M_w)=P_y$

where C represents the number of atoms of the element (y, x, w)inside the phase and M its atomic mass of the considered element. The element weight (P_j) inside the area is then put in relation to the global weight of the area and multiply for its specific weight (B_y):

- $P_y*100/S*B_y$

Following this approximate procedure, the estimated Ti and Si amounts inside the liquid after 10 min of contact are considered to be about 10.22 and 1.00 at%, respectively. Then, considering the amount of C negligible in the liquid because it is trapped inside the interfacial layers, it is possible to simulate the solidification of the liquid (*Figure 6.75*).

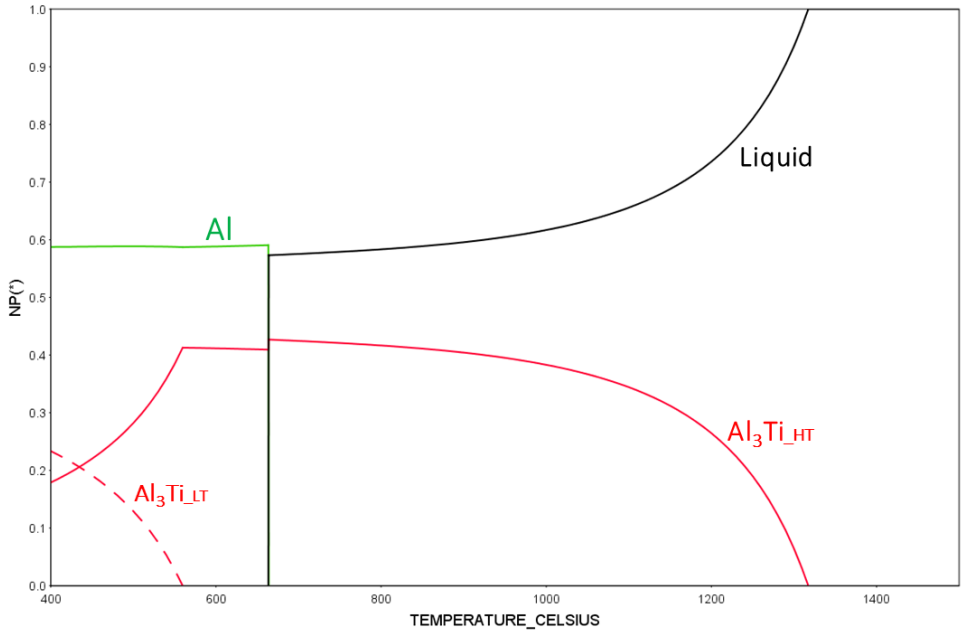

Figure 6.75. Phases composition plotted as function of temperature considering the liquid with the composition defined when $Al_{75}Ti_{25}$/SiC system is maintained at 1500°C for10 min(Ti: 10.22 and Si: 1.00 at%).

The calculated cooling path of the defined liquid composition is performed to control that the resulting products are in a good agreement with the experimental microstructure.

The calculation represented in the graph of *Figure 6.75*, shows the formation of Al_3Ti and Al, as cooling products, according to the experimental results (*Figure 6.52*), revealing the self-consistent character of this approach.

After 10 min of contact the absence of Si-rich phases, as cooling products, in the bulk microstructure is then confirmed.

Following the same approximate procedure and considering the phases percentage of *Figure 6.55*, the Si and Ti amounts in the liquid after 30 min of contact are estimated to be17.34 and8.12 at%, respectively. The experimental microstructure is coherent with the result obtained from the cooling path of*Figure 6.76,* where the Si-based phases (τ-phases) as well as Al and Si appear. A small amount of Al_3Ti is also expected from the thermodynamic prediction and experimentally detected in the bulk. Even if no distinction about the kind of τ-phase obtained is performed here, it is known that two different Al-Si-Ti ternary phases exist called $\tau_1$and τ_2 [160], respectively.

They do not significantly differ in terms of atomic composition while they are characterized by a distinct crystallographic structure [161], [162].

A specific characterization of these phases is not the subject of this study, however, following ref [160], it is possible to suppose that both the phases have been formed during the high temperature

process as well as the subsequent cooling. The Al-rich liquid reaches the equilibrium with τ_1, (Al) and (Si) at the eutectic temperature of 573°C.

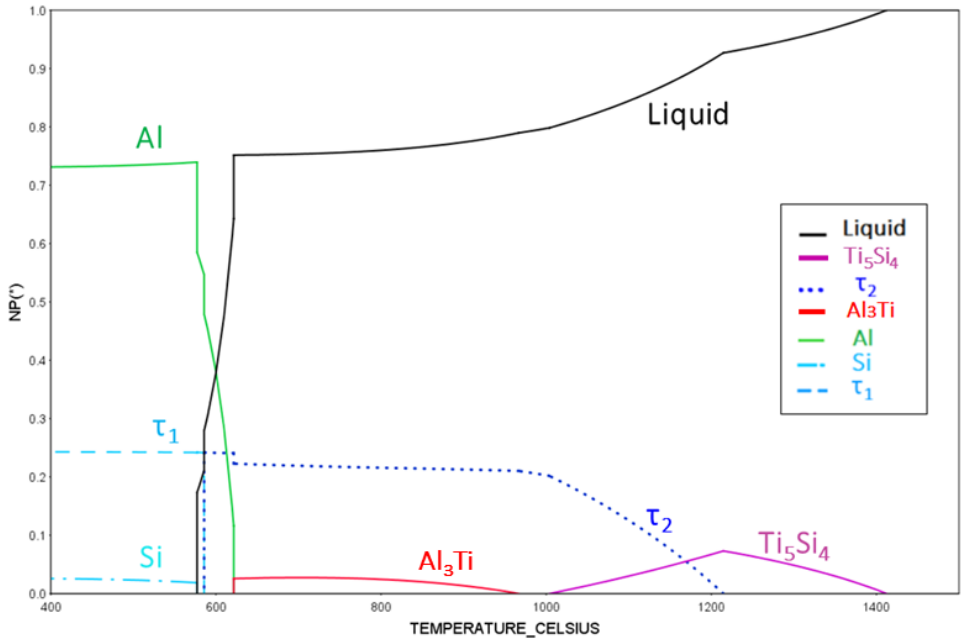

Figure 6.76. Phases composition plotted as function of temperature considering the liquid with the composition defined when $Al_{75}Ti_{25}$/SiC system is maintained at 1500°Cfor 30 min (Ti:8.12, Si 17.30 at%).

After 1h, Si and Ti amounts in the liquid (*Figure 6.58*) reach 51.24 and 4.37 at%, respectively.

The Si-based phases (τ-phases, Si, Al-Si eutectic) formation is confirmed and visualized in the cooling plot of *Figure 6.77.*

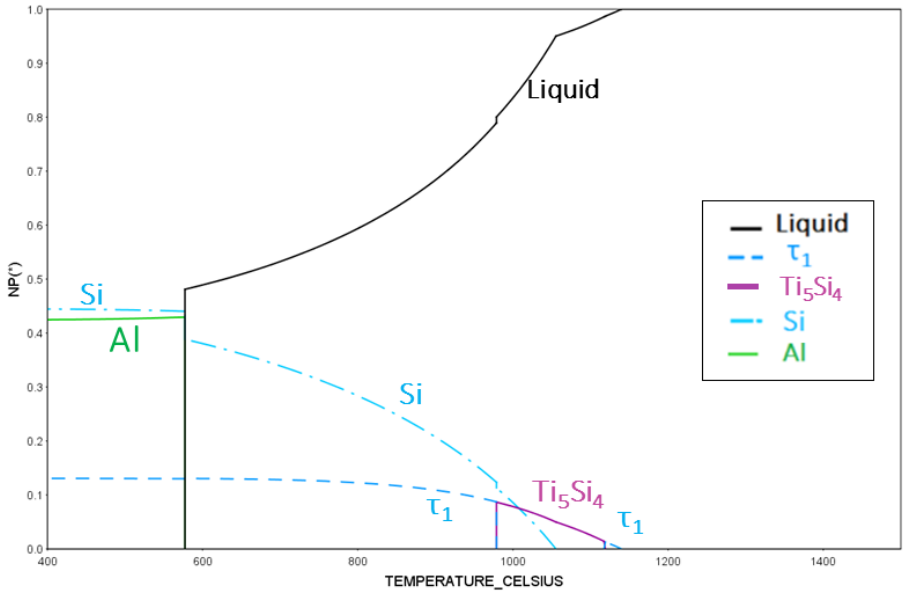

Figure 6.77. Phases composition plotted as function of temperature considering the liquid with the composition defined when $Al_{75}Ti_{25}$/SiC system is maintained at 1500°C for1h (Ti: 4.37, Si: 51.24 at%).

The thermodynamic prediction seems to be in a good agreement with what observed from the microstructure of the sample: Al, Si and τ-phases are, in fact, detected both experimentally and by the thermodynamic prediction.

In order to visualize and follow the evolution of the liquid changing the time of contact, the isothermal section (1500°C) of Al-Si-Ti (constant C amount(1%)) system is calculated and reported in (*Figure 6.78*). One can observe three different points ("b", "c", "d" of *Figure 6.78*) marked on the Al-Si-Ti isothermal section, corresponding to the samples tested at 1500°C changing the contact time, as well as a fourth point ("a") representing the liquid (25 at% of Si) after the first chemical interaction, even if it formed at lower temperature (1260°C).

After the first 10 min of wetting the composition of the first liquid formed (represented by "a" in *Figure 6.78*) moves towards the Al_3Ti side because of the significant Ti and Al amounts dissolved from the melting of the aluminide. It is possible to consider that the release rate of Ti in the liquid phase during heating is related to the dissolution of the aluminide, while the Si release rate during the heating is related to the chemical reaction between the liquid phase and the ceramic substrate.

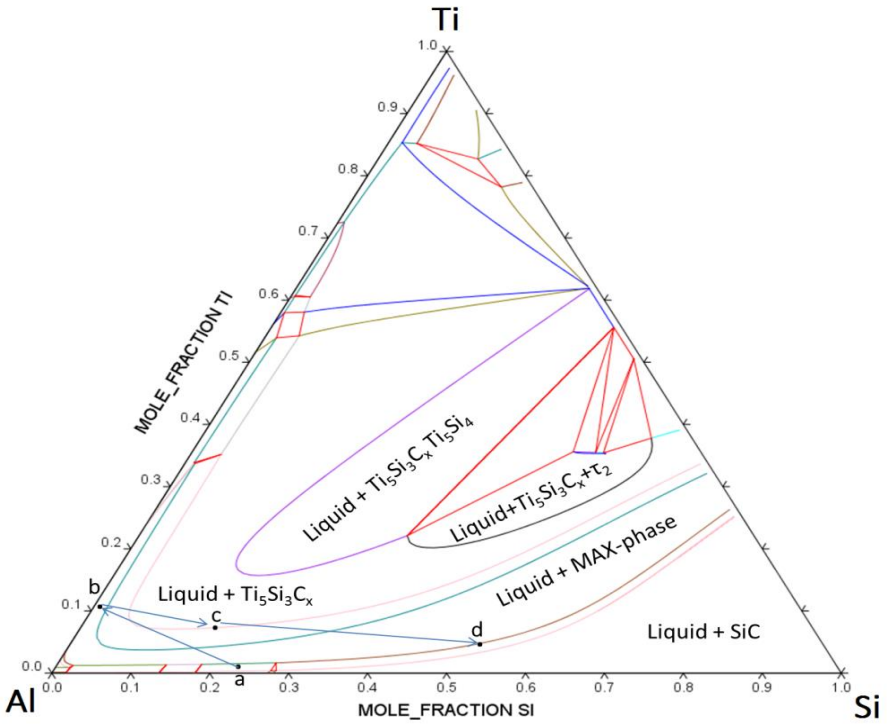

Figure 6.78. Al-Si-Ti isothermal (1500°C) section obtained maintaining the C amount constant (1%).

For this reason, at the beginning, the Ti release rate increases sharply with the temperature and it results too fast to be followed by the Si release rate. However, a depletion of Ti occurred due to the

migration of this active element to the interface forming the interfacial products (TiC and MAX-phase). This fact produced the formation of some (Al) areas at the Al_3Ti grain boundaries.

Then, after 10 min, the amount of Ti inside the liquid is sufficiently high to do not modify the composition of the aluminide after solidification. After the complete melting of the drop, the Al and Ti amounts cannot increase anymore, while the Si content starts to dramatically increase during this reactive and dissolutive wetting process.

This fact is revealed also reading*Table 6.25*:

- after 30 min, in fact, Si-rich phases, as the Al-Si eutectic and the τ-phase formed inside the bulk of the system;
- after 1h, the amount of Si increases again and also pure Si is detected inside the matrix.

It is then clear that the Si amount in the liquid increased drastically with time: from 1.0 at% after 10 min to 17.34 at% after 30 min reaching an amount of 52.40 at% after 1h.

In all the cases, the C-saturated liquid is in equilibrium with the MAX-phase formed during the isothermal wetting.

Table 6.25. Different Si and Ti amount (at%) in the liquid phase of Al_3Ti/SiC system tested at 1500°C changing the time of contact.

Mole of element inside the liquid	Estimated liquid composition at 1500°C		
	10 min	30 min	1 h
Si	0.0100	0.1734	0.0437
Ti	0.1022	0.0812	0.5240

6.2.2.2 $Al_{84}Ti_{16}$/SiC system

In the case of the Al-richer alloy, the first liquid formation is not coming from the metal/ceramic interaction, as before, but from the melting of the Al-Ti drop. The graph reported in *Figure 6.79* shows the Al-Si-Ti section (placed just above the Al-Si-Ti base of the Al-C-Si-Ti tetrahedron) where the C amount is fixed (1%). The liquid, suddenly saturated in C at the first temperature of interaction (1235°C), is located on a biphasic domain and, in particular, very close to the Al-rich corner. Its composition, close to the one of the starting alloy, follows a continuous evolution after the partial melting observed: the liquid continues, in fact, to react, crossing different equilibria (numerated from "1" to "4"; *Figure 6.79*) and remaining close to the Al-Ti axis.

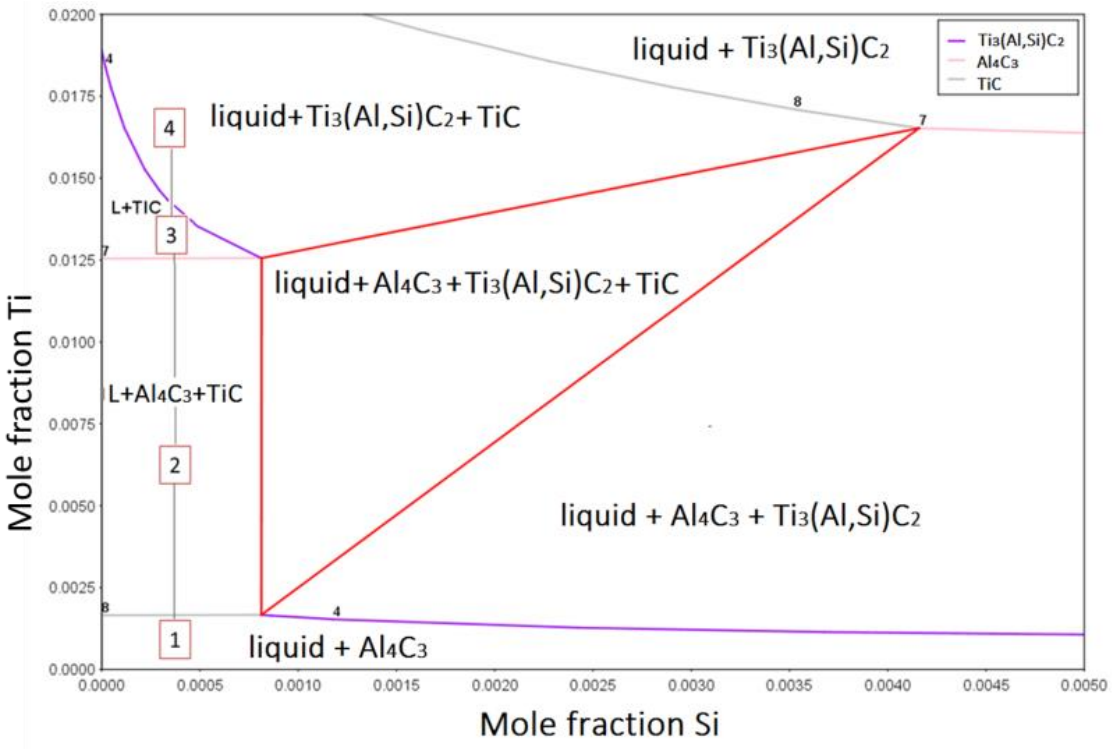

Figure 6.79. Ti-Si corner of Al-Si-Ti isothermal section calculated at 1235°C (where amount the Cwas fixed (1%).

The phases involved in these equilibria are the same ones found during the experimental results: in fact, a very thin Al_4C_3 layer formed in contact to SiC and, above it, TiC grew as a compact and defect-free layer as well as MAX-phase grains are found next to the triple line of the sample (*Figure 6.61*).

At this temperature and alloy stoichiometry, the liquid fraction is not specifically located at the contact zone, as for the previous sample, but it reached about 48 mole%, already at the first interaction temperature 1235°C (*Figure 6.80*). This huge amount of liquid, as one can see from the black curve progress of *Figure 6.80*, increases very sharply during the heating and this is due to the gradual melting of the aluminide.

The increasing of the liquid fraction during the heating is followed by a significant increase of the Ti amount released inside it.

In front of that, the Si amount released inside the liquid cannot follow this rate so that, also after 10 min at 1300°C, the Si amount dissolved by the liquid is still very low.

In fact, just very small traces of the Al-Si eutectic are sporadically detected in the bulk of the spread drop only after an attentive observation of its whole profile. The liquid composition is still located close to the Al axis even if it is more enriched in Ti than at 1235°C.

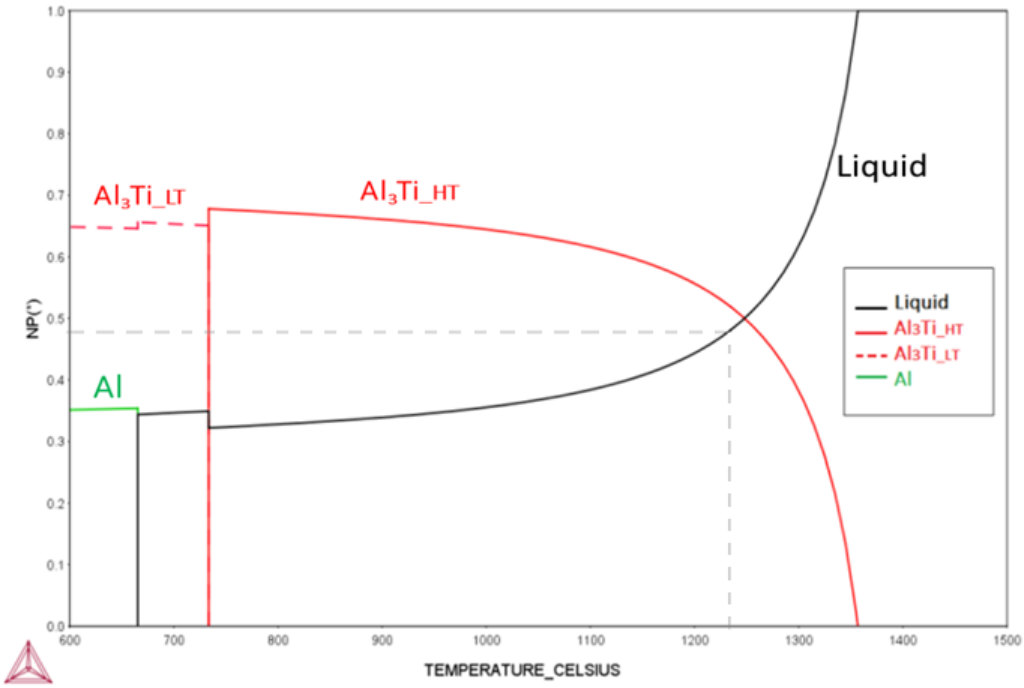

Figure 6.80. Phase fraction plotted as a function of temperature considering the starting alloy composition ($Al_{84}Ti_{16}$).

The Si and Ti amounts dissolved inside the liquid (after 1 h at 1300°C) are estimated taking into account the phases percentage in the bulk (*Figure 6.71*) as well as their density: about 5.60 and 2.00 at%, respectively. In agreement with the detected bulk microstructure, Al_3Ti, Al and Si are the main phases/elements coming from the solidification path (*Figure 6.81*).

Now the Si amount released inside the liquid becomes not negligible because during 1 h of contact the alloy has the time to become totally molten and then the Al and Ti amounts become constant while the Si dissolution can finally take place. It is possible to find a discrepancy between the cooling plot of *Figure 6.81*and the experimental results. In fact, in this case, the τ-phase formation is not observed. However, the τ-phases formation seems to occur at about 600°C. The formation of this ternary phase at such a low temperature is kinetically inhibited. Performing then a second cooling plot "suspending" the τ-phases from the calculation (*Figure 6.82*), one can obtain products that are coherent with the ones coming from the experiments even if the formation of $TiSi_2$is not observed. The Si amount seems to be involved only in the formation of the eutectic structure and it is not found as $TiSi_2$ or τ-phase.

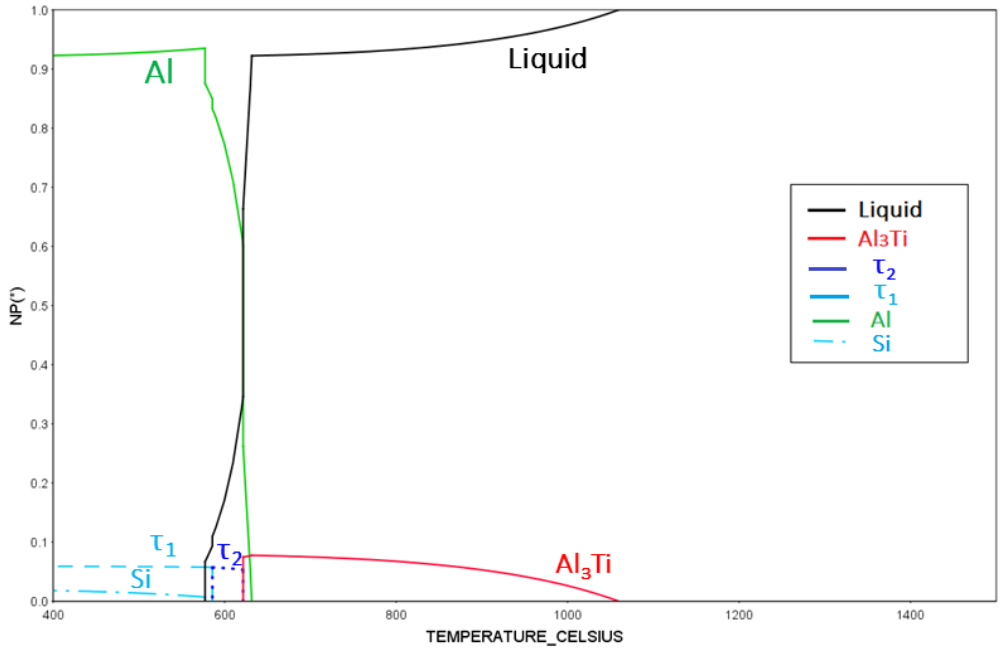

Figure 6.81. Phases composition plotted as function of temperature considering the liquid with the composition defined when $Al_{84}Ti_{16}$/SiC system is maintained at 1300°C for 1h (Ti: 2.00, Si: 5.60 at%).

One can visualize the liquid evolution of this system in terms of composition both increasing the temperature, from 1235°C ("a" in *Figure 6.83*) to 1300°C ("b" in *Figure 6.83*), and the contact time, from 10 min to 1 h.

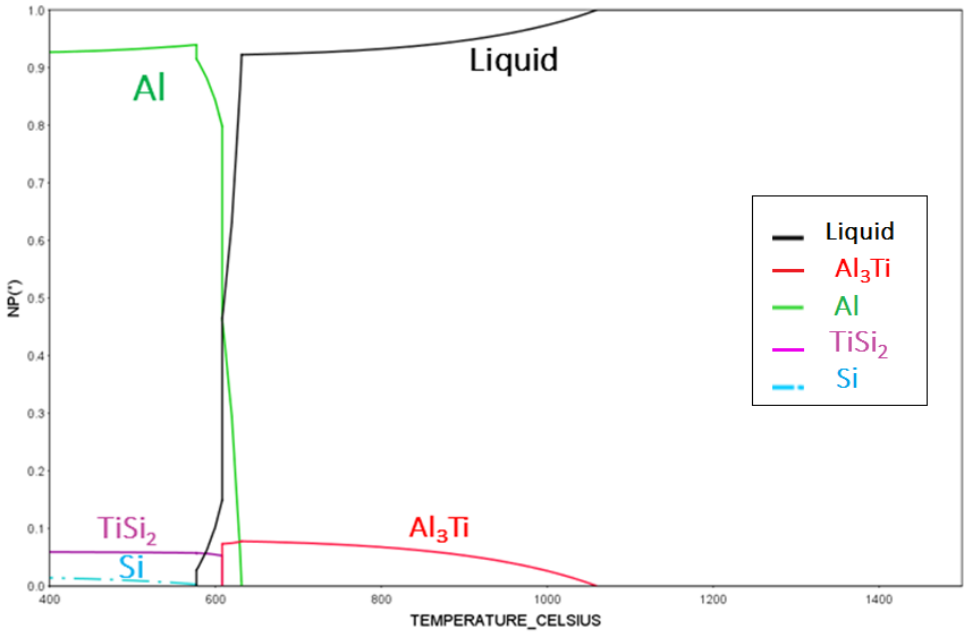

Figure 6.82. Phases composition plotted as function of temperature considering the liquid with the composition determined when $Al_{84}Ti_{16}$/SiC system is maintained at 1300°C for 1h (Ti: 2.00, Si: 5.60 at%) and the τ-phases are suspended from the calculation.

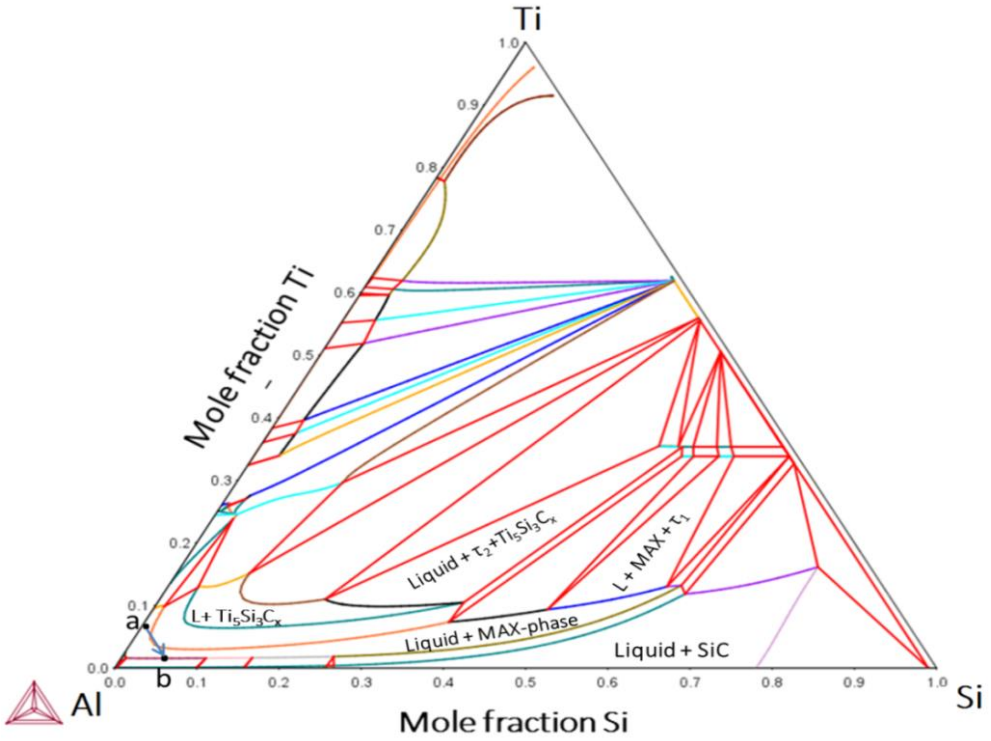

Figure 6.83. Al-Si-Ti isothermal (1300°C) section calculating maintaining constant the C amount (1%).

The liquid composition increases the Si content (from "a" to "b") at the higher testing temperature (1300°C) but it is still not so far from the aluminide side. In both the cases, the C-saturated liquid moves inside equilibria involving the MAX-phase.

6.2.3 Comparison

6.2.3.1 $Al_{75}Ti_{25}$/SiC system

The evolution of this metal-ceramic system in terms of reactivity at 1500°C has been followed analyzing the interfacial microstructures after three different times of contact (10, 30, 60 min) in order to investigate the stability of the phases formed during the isothermal process as well as during the cooling process.

At the selected temperature, 1500°C, the Al_3Ti alloy is totally molten and it spreads covering all the SiC surface.

Taking into account the different times of the test, one can say that:

- after 10 min of contact, interfacial products form as the result of the first metal/ceramic interaction occurring in the system;

- after 30 min, an evolution of both the first interfacial layer and the bulk microstructure of the system occurs;
- after 1 hour, a situation closer to equilibrium can be found; the significant dissolution of the substrate is confirmed by the fact that the bulk of the drop is mainly formed of Si as well as of Si-based phases.

From the comparison of the microstructures reported in *Figure 6.84*(a)-(c), it is clear that the nature of the phases as well as their distribution and morphology after the tests change significantly increasing the contact time from 10 min to 1 h.

Indeed, after maintaining the metal-ceramic couple for 10 min at 1500°C, the starting aluminide (Al_3Ti) remains still the main constituent of the bulk.

From *Figure 6.84*(a) one can also distinguish several (Al) veins at the aluminide grain boundaries coming from the solidification of a liquid that lose some Ti (comparing to the starting aluminide) which has migrated at the interface to form the $Ti_3(Al,Si)C_2$ MAX-phase extended up to about 100 μm far from the substrate. In addition, it is important to underline that after 10 min of contact:

- the MAX-phase, grown at the interface, shows a large amount of Al (X_{Al}>0.05) that substitutes Si in its sub-lattice site;
- the Si amount dissolved by the liquid phase during the process is always below 5.5 at%.

Increasing the testing time from 10 to 30 min, one can notice the partial decomposition of the MAX-phase (that shows the same composition as after 10 min) at the interface: its thickness decreases from 100 μm (the one reached after 10 min) to about 40 μm and an increased amount of TiC (in contact to SiC) growing until about 40 μm far from the substrate (while after 10 min a layer of just 2 μm of TiC was detected). After 30 min one can also find a totally different situation in the bulk microstructure (*Figure 6.84*(b)):

- a matrix composed of Al-Si lamellar eutectic structure with (Al) solid solution islands inside it (light areas);
- several elongated τ-phase and dendritic Al_3Ti grains dispersed inside the matrix.

After 30 min the Al_3Ti phase changed both its morphology and also its relative amount in the bulk (

Table 6.26*).*

The MAX-phase decomposition as well as the increased amount of Si inside the bulk determine a modification of the liquid–phase composition; it means that the mixed TiC/MAX-phase layer formed at the interface do not act as barrier for the diffusion of Si from the SiC surface to the rest of the drop.

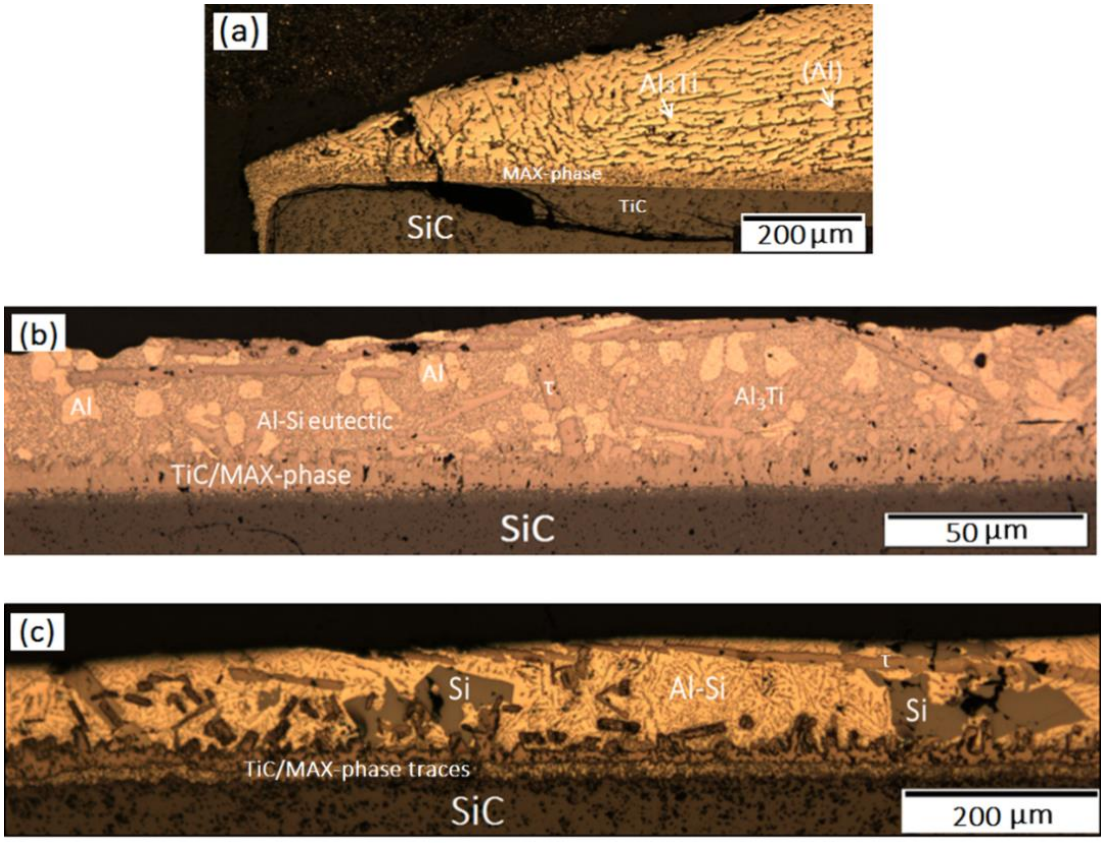

Figure 6.84. Drop profile microstructure of the $Al_{75}Ti_{25}$/SiC sample; after 10 min (a), 30 min (b) and 1 h (c) of contact at 1500°C.

Table 6.26 Approximated percentage of phases formed in the three Al_3Ti/SiC samples.

Phases after the interaction	Al_3Ti on SiC at 1500°C		
	10 min	30 min	1 h
Al_3Ti	73%	20%	-
Al-Si	-	15%	30%
τ-phase	-	40%	30%
Al	27%	25%	-
Si	-	-	40%

Increasing then the testing time from 30 min to 1 h (*Figure 6.84*(c)), one can notice an increased decomposition of the Ti_3SiC_2 (now a pure MAX-phase) that it is found just as traces inside the TiC layer that reaches a thickness of about 50 µm. So after 1h, the MAX-phase is nearly completely decomposed while the TiC is stabilized constituting the main interfacial product.
Moreover, after 1 h,the situation in the bulk microstructure changes again: in this case, no traces of the starting Al_3Ti are detected analyzing the whole section but an amount of Al-Si eutectic structure higher than that after 30 min can be found (Tab.6) with the presence of several polygonal pure Si crystals. The percentage of τ-phase is estimated to be almost the same as after 30 min.

The significant modification of the microstructure as a function of the contact time is due to the fact that the composition of the liquid is drastically shifted from the Al-Ti axis toward the Si corner of the ternary system (*Figure 6.78; Figure 6.85*). In fact, to simplify the thermodynamic calculations, as already explained, the C amount dissolved by the liquid phase was approximated to 1% hypothesizing that it is just contained inside the first layers involved in the formation of the solid and C-based phases (TiC and $Ti_3(Al,Si)C_2$).

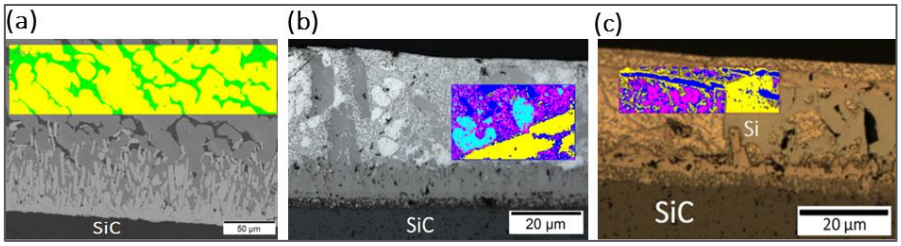

Figure 6.85. Different percentage of the phase formed at the Al_3Ti/SiC interface after the test at 1500°C changing the time of contact.

This is demonstrated by the microstructure of *Figure 6.86* where there is evidence of the Al migration to the SiC surface across the TiC grains that do not act anymore as a diffusion barrier.

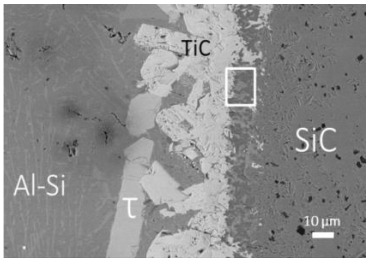

Figure 6.86. Al_3Ti/SiC microstructure after 1h at 1500°C; the white rectangular underlines the presence of the liquid phase in contact to the SiC surface.

6.2.3.2 $Al_{84}Ti_{16}$/SiC system

The reactivity evolution of this metal-ceramic system was followed:

- analyzing the interfacial microstructure changing the testing temperature (1235, 1270, 1300°C; as explained in the procedure of *6.2*) but maintaining the same contact time of 10 min;
- analyzing the interfacial and bulk microstructures after two different times of contact (10 min and 1h) at the same temperature of 1300°C.

The interfacial as well as the bulk microstructures of the samples tested at 1235 and 1270°C for 10 min are not significantly different in terms of both morphology, composition, Ti activity ($3.5 \cdot 10^{-3}$ vs $5.2 \cdot 10^{-3}$) and liquid fraction of the system (48 mole% vs 55 mole%).

In both the cases, the Al-Ti drops did not melt completely, a matrix composed of Al_3Ti and (Al) is found and the Al-Ti alloy did not dissolve a Si amount higher than the value of 0.5 at%, while the (Al) dissolved Si until a maximum of 4.0 at%. At the contact zone of both the samples (1235 and 1270°C) the following phases are present (*Figure 6.87*):

- a TiC layer, characterized by the same thickness of 2 µm, grown on SiC surface;
- some MAX-phase grains grown mainly at the triple line.

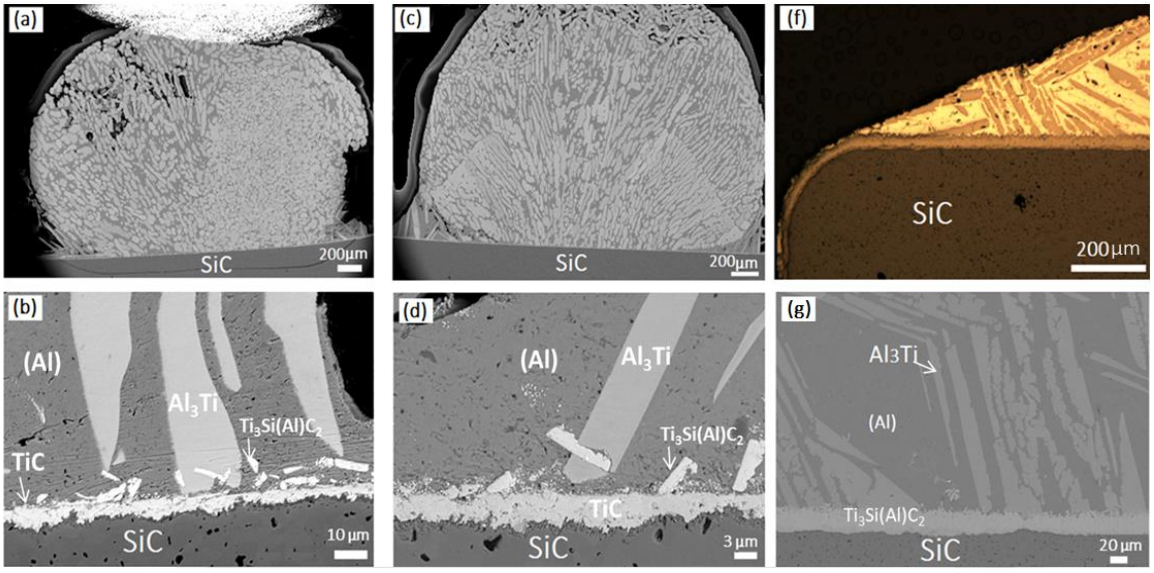

Figure 6.87. $Al_{84}Ti_{16}$/SiC tested for 10 min at 1235°C (a) and the zoomed image of its interfacial zone (b); at 1270°C (c) and the zoomed image of its interfacial zone (d); at 1300°C (f) and its interfacial zone (g).

The MAX-phase composition did not change increasing the temperature from 1235 to 1270°C; it contains about 5.0 at% of Al that substitutes Si in the sub-lattices.

The only difference consists in the MAX-phase distribution at the interfacial zone: at 1270°C, indeed, these grains are detected not only at the triple line but also in some areas close to the central part of the drop (*Figure 6.87*(b) and (d)).

Increasing the temperature from 1270 to 1300°C, one can see that the alloy completely melted and covered all the SiC substrate (*Figure 6.87*(f)).

In this case, the bulk microstructure is still formed of Al_3Ti and (Al) but here the two phases formed during the cooling process. The Al_3Tidissolved an amount of Si 10 times higher than the one dissolved at 1270°C (from about 0.5 at% to about 5.0 at%) while the Si amount contained inside the (Al) is not significantly changed. Comparing this bulk microstructures to the previous ones (1235, 1270°C), one can notice a higher amount of the (Al) matrix as well as several elongated Al_3Ti grains both coming from the solidification of the molten drop.

The MAX-phase formed at 1300°C after 10 min shows the same composition than the ones formed at 1235 and 1270°C.

Maintaining then the same testing temperature of 1300°C but increasing the contact time from 10 min to 1 h, one can notice some discrepancies in terms of nature as well as morphology and distribution of the different phases. The matrix is not formed only of Al_3Ti grains (now grown assuming a dendritic shape, well visible in *Figure 6.88*(b) and of (Al)areas but one can also find some areas composed of Al-Si lamellar structure at the grain boundaries. This means that the Si amount of the liquid is significantly increased and its composition moves from the Al-Ti axis toward the Si corner. In addition, at the contact zone of $Al_{84}Ti_{16}$/SiC sample after 1 h of contact at 1300°C, one can observe that the TiC layer did not change but the MAX-phase shows an increased thickness (about 50 µm) and a different composition then the one found after 10 min. The MAX-phase after 1 h of contact is, in fact, mainly composed of Si (just 1.0 at% of Al was detected).

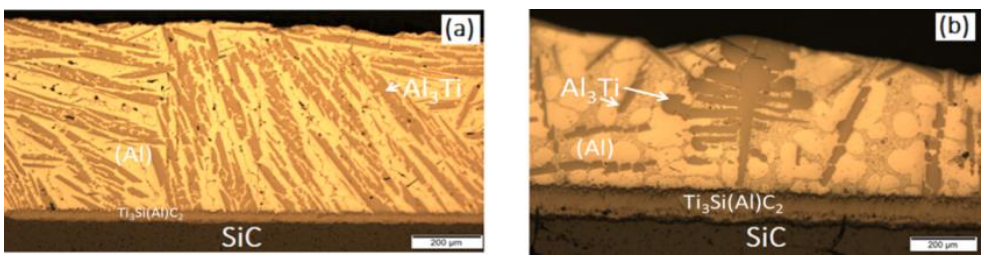

Figure 6.88. $Al_{84}Ti_{16}$/SiC tested at 1300°C for 10 min (a) and for 1 h (b).

6.2.4 Conclusions: SiC/Al-Ti alloys system

Two different Al-Ti alloys were analysed in terms of wettability and reactivity in contact to SiC and the first interaction in terms of temperature and microstructure was defined.
The morphology as well as the composition of the bulk of each system was also investigated, as a function of time of contact and temperature, with the aim to define the liquid composition and the extent of the dissolution of the substrate by the molten alloy.
Both the Al-Ti alloys show an excellent wettability (at 1300 and 1500°C) and reactivity that allows to obtain an adherent and continuous interfacial layer mainly formed by the MAX-phase.
This phase formation is very promising because, as already explained, it has characteristics in between those of the metallic and ceramic materials, representing a very convenient interfacial product if one takes into account the SiC-SiC joining performances.

Even if the two alloy compositions are fairly close to each other, their solidification products when in contact with SiC are significantly different.
Indeed, the EDS analysis conducted on the Al-rich sample (84 at% of Al tested at 1235°C) reveals that the first interaction of this metal-ceramic couple leads to the formation of a continuous TiC layer, adherent to the substrate, characterized by a thickness of about 10 µm, that represents the main interface layer of this system.
In the second case (75 at% of Al tested at 1260°C), a new liquid, containing 25 at% of Si coming from the substrate dissolution, is suddenly released at the interface.It is important to underline that, even if the real melting of this aluminide occurs at 1396°C, a first liquid appears before that temperature due to the chemical reaction occurring at the metal/ceramic interface. This fact is proved both by the experiments (EDS, DSC) and by the thermodynamic approach (CALPHAD): the calculations performed at this temperature confirm that a liquid phase appears when a very small amount of C (X_c=0.05) is dissolved and that the two first phases formed from the liquid are the MAX-phase and $Ti_5Si_3C_x$. This newly formed Si-rich liquid leads, in fact, to the formation of a continuous MAX-phase layer, characterized by a thickness of about 10 µm, that constitutes the main interfacial product

Using $Al_{75}Ti_{25}$ as brazing alloy, one can observe that, at the interface, a more pronounced MAX-phase formation in terms of thickness occurred, in particular when the sample is maintained 10 min

at 1500°C.Indeed, under these experimental conditions, it extends up to 100 µm far from the SiC and its Al amount is the highest compared to the one of the other samples.
This fact allows to obtain the in situ formation of this metal-ceramic phase combining both the elements of the metallic and the ceramic parts.

Thus, the $Al_{75}Ti_{15}$ alloywas considered the more promising to be used for brazing SiC to itself.

In particular, the fast quenching test of the samples, together with the observation of the phase diagram, let us to state that the $Ti_3Si(Al)C_2$ phase is formed in-situ at 1500°C and not during the cooling of the samples (*Figure 6.89*).
The liquid phase, during the isothermal process, assures the contact between the adjoining materials and the (transient) liquid phase evolves by reaction and diffusion, solidifies at the testing temperature and forms the $Ti_3Si(Al)C_2$ MAX phase at the interface.

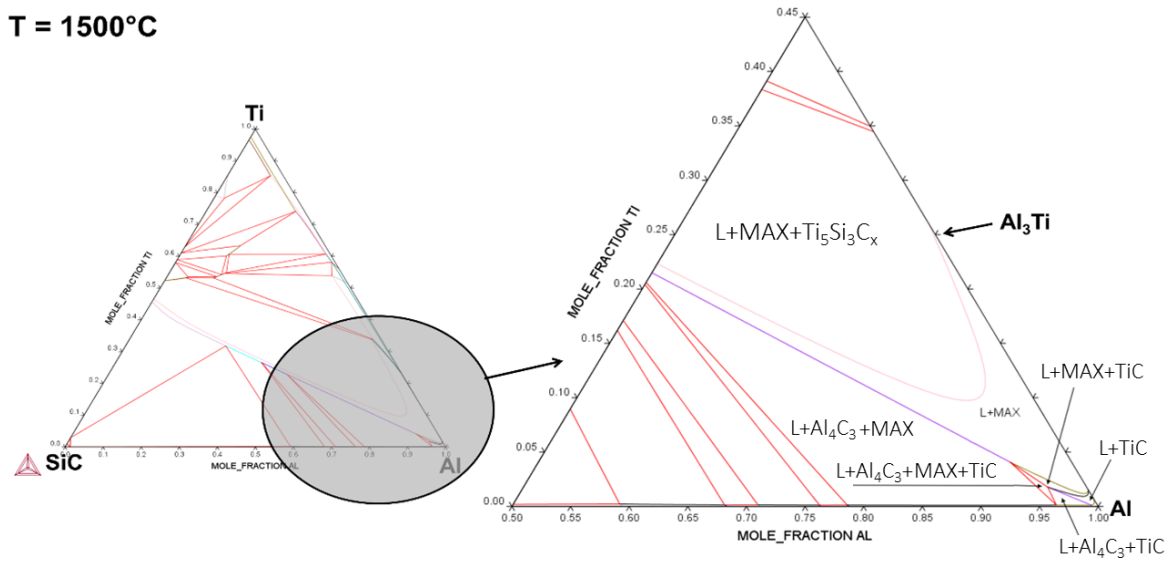

Figure 6.89. SiC-Al-Ti isothermal section calculated at 1500°C.

6.2.5 Joining results

Following the hints deriving from wetting tests, the $Al_{75}Ti_{25}$ alloy was chosen to obtain a set of joined specimens. In particular, two different kinds of processes were pursued, following two pressure-less methods (Table 6.27), to join together sintered SiC pieces (described in *4.1.2*):

- Joining by capillary infiltration of Al_3Ti inside the seam between the adjoining materials;
- Joining by $Al_3Ti/Ti/Al_3Ti$ interlayers.

In the first procedure, that has the advantage to be easy in preparation and suitable for rough and curved surfaces (*Figure 6.90*(a), (b)), the joining process takes place by capillary infiltration: a piece of alloy, previously melted and homogenized by arc melting (described in 4.1.2), was put near the adjoining surfaces and let wet and infiltrate between the two materials.

In the second method, the following assembly geometries were designed:

1. SiC/Al_3Ti paste/SiC schematized in *Figure 6.90*(c);
2. SiC/Al_3Ti paste/Ti foil/Al_3Ti paste/SiC schematized in *Figure 6.90*(d).

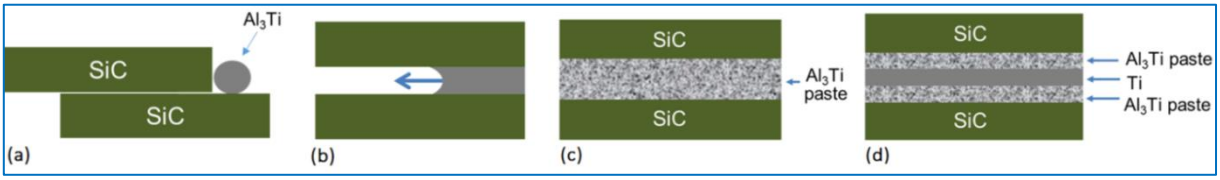

Figure 6.90. Schematic representation of the capillary infiltration assembly (a); scheme of the infiltration method mechanism (b); scheme of the Al_3Ti paste (c) and Al_3Ti-Ti-Al_3Ti paste assembly (d) conducted before the joining test.

A paste was prepared from a mixture of Al_3Ti powder (Goodfellow, Cambridge, UK; described in*4.1.2*) and α-Terpineol, and then applied on the SiC surfaces by slurry coating.

The α-Terpineol was allowed to evaporate during a period of 72 h in an oven at 70°C.

Table 6.27. Different SiC/SiC joining samples tested at 1500°C.

Filler	Process	Temperature [°C]	Time [min]
Al_3Ti	infiltration	1500	10
Al_3Ti	assembly	1500	10
$Al_3Ti/Ti/Al_3Ti$	assembly	1500	10

The slurry coating process was designed to assure a thickness of about 100 µm, in the first case, and between 40 and 60 µm in the second one.

Afterwards, the coated SiC pieces were sandwiched together with 50 µm thick Ti foils (Goodfellow, Cambridge, UK, purity > 99.99 %).

For both the procedures, the assemblies were introduced into the furnace (*4.2*) at 1500°C under a static Ar/H_2 atmosphere; after a holding period of 10 min, the samples were cooled down at 5°C/min.

The main goal of this joining procedure is to obtain SiC-SiC joints through the in-situ formation of a $Ti_3Si(Al)C_2$ phase starting from simple Al-Ti alloys.

Similarly to a transient liquid phase bonding process, the in-situ formation of the desired phase at the process temperature would allow to overcome the thermal stresses associated with the solidification by cooling of the interfacial phases over a broad temperature range.

SiC/Al_3Ti/SiC joint obtained by infiltration and assembly

The following picture (*Figure 6.91*) shows the cross-section of the SiC-SiC joint obtained by capillary infiltration of Al_3Ti at 1500°C for 10 min.

The joining region, which was formed after the infiltration of the brazing alloy, has a thickness of about 30 µm and contains several big $Ti_3Si(Al)C_2$ grains (with an Al amount always below 5.0 at%), small TiC grains and the Al_3Ti phase. In addition, a few Al spots were detected that can be detrimental from the point of view of high-temperature applications.

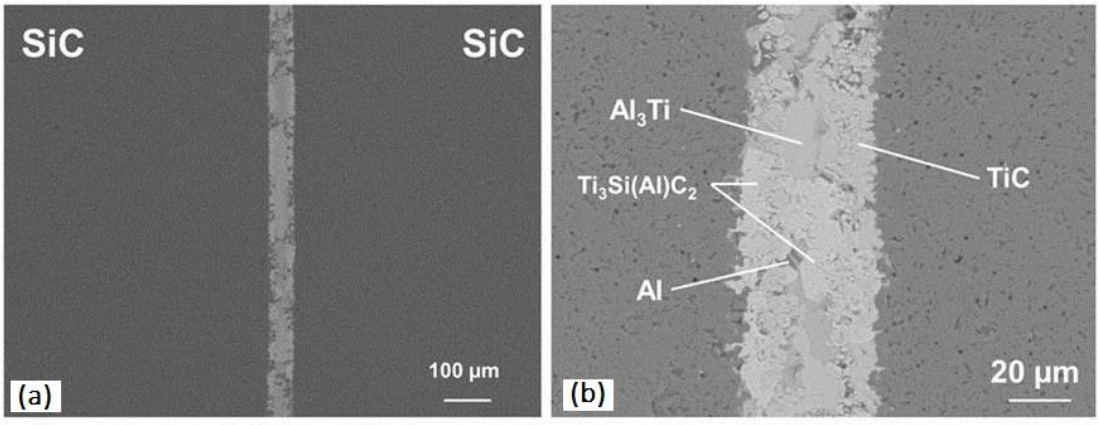

Figure 6.91. SiC/Al_3Ti/SiC sample section (1500°C; 10 min) obtained after the infiltration process (a) and the zoomed image of the contact zone (b).

However, a perfect infiltration was obtained and the adhesion between the different phases seems to be successful: no macro-cracks or gaps were observed along the joined region of the samples (*Figure 6.92*).

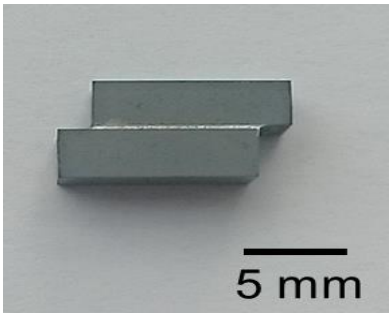

Figure 6.92. SiC/Al_3Ti/SiC sample after the infiltration joining test (1500°C; 10 min).

SiC/Al_3Ti paste/SiC joint obtained by assembly

The following picture (*Figure 6.93*) shows the cross-section of the SiC-SiC joint obtained by deposition of an Al_3Ti layer (100 µm of thickness) on the ceramic surface after having been maintained at 1500°C for 10 min.

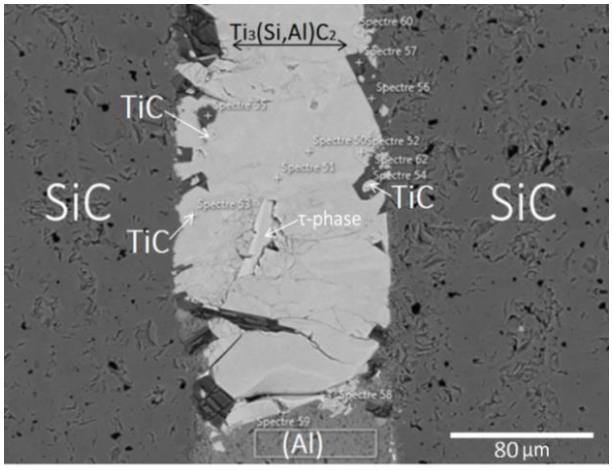

Figure 6.93. SiC/Al_3Ti paste/SiC sample section obtained after the joining process at 1500°C (10 min).

The joint region, which was formed after the melting of the brazing alloy, has a thickness of about 100µm and contains:

- sporadic and small TiC grains close to SiC;
- some Al_4C_3 grains extending also close to SiC (with an Al amount always below 5.0 at%);

- big grains of MAX-phase also close to SiC covering all the interface also containing the ternary τ-phase;
- Al_3Ti (with a composition of 60 at% of Al, 25 at% of Ti, 15 at% of Si);
- some (Al) areas.

SiC/Al_3Ti paste/Ti/ Al_3Ti paste SiC joint obtained by assembly

In order to increase the expected service temperature by eliminating the residual Al and increasing the amount of interfacial MAX-phase, in the second method Ti was added in the form of foils sandwiched between Al_3Ti coated SiC pieces. The sample was tested at the same temperature of 1500°C and for the same time of 10 min. In this case the use of the capillary infiltration was unfeasible and the Al_3Ti was brushed on both the SiC surfaces in form of paste. The microstructure reported in *Figure 6.94* shows an example of the obtained interfacial zone.

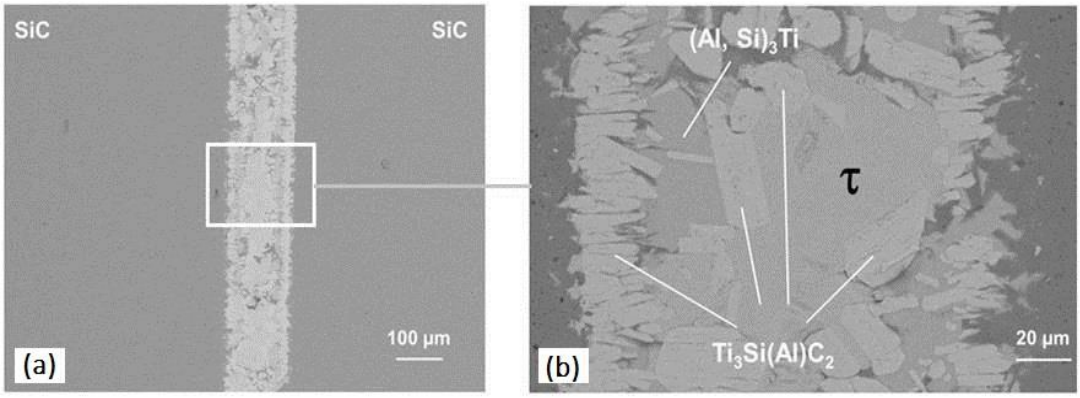

Figure 6.94. SiC/Al_3Ti paste/Ti/Al_3Ti paste/SiC sample section obtained after the assembly joining process at 1500°C (a) and the zoomed image of the contact zone (b).

The thickness of the obtained brazing seam is about 150 µm indicating that there is not significant loss of material, e.g. squeezed out the SiC surfaces, during the process.

Microstructural examination showed the presence of the $Ti_3Si(Al)C_2$ phase (with an Al amount always below 5.0 at%)both adhered at the interface with SiC and interspersed in the brazing seam; other phases were the Al_3Ti phase with Si substituting Al up to 10 at% and the ternary phase identified as the τ-phase that already formed in the wetting test at 1500°C (after 30 min and 1 h).

6.2.6 Joining conclusions

On the basis of the previous wetting tests, the $Al_{75}Ti_{25}$ alloy was considered the most promising in view of joining processes of SiC-based materials destined to applications in harsh environments.
In order to maximize the amount of MAX-phase formed at the interface, the temperature of 1500°C and the time of contact of 10 min were chosen after the specific reactivity evaluation (*6.2.1*).
When just $Al_{75}Ti_{25}$was used as filler, in both the processes (infiltration and assembly methods), the $Ti_3Si(Al)C_2$ mixed MAX-phase constitutes the main interfacial product (*Table 6.28*). Some TiC grains are detected close to the SiC sides and few Al-rich areas were detected in the bulk. These areas could be detrimental for high temperature applications.

Table 6.28 . Resulting phases coming from the different joining samples tested.

Joining method	Resulting phases		Thickness [µm]
	Contact zone	Bulk	
$Al_{75}Ti_{25}$ infiltration	$Ti_3Si(Al)C_2$,	$Al_{75}Ti_{25}$, (Al)	50
$Al_{75}Ti_{25}$ assembly	$Ti_3Si(Al)C_2$, τ-phase traces	$Al_{75}Ti_{25}$, (Al)	100
$Al_{75}Ti_{25}$/Ti/$Al_{75}Ti_{25}$ assembly	$Ti_3Si(Al)C_2$, τ-phase	$Al_{75}Ti_{25}$, τ-phase	150

With the aim to avoid their formation, the Ti amount in the system has been increased by the insertion of a Ti foil between the two layers of metallic paste. It was proven that no more (Al) areas have been formed at the metal/ceramic interface but only $Al(Si)_{75}Ti_{25}$ areas have been detected in the central part of the joint.
In particular, this phase is characterized by a significantly higher melting temperature (1396°C) if it is not in direct contact to SiC. The increased Ti amount produced also a more pronounced formation of the τ-phase that should not constitute a weak point of the interface. However a deep mechanical evaluation is needed and in progress to test and determine the interface resistance.

6.2.7 Future work: CALPHAD approach on SiC/SiC joining samples

By the use of Thermo-Calc software, the kinetics of this metal-ceramic system is approximately estimated following a particular approach that can predict what happens when a system is at equilibrium.

Taking into account the $Al_{75}Ti_{25}$/SiC system at 1500°C, the first reaction occurring at the interface has been defined: both in the wetting and joining tests, TiC is found as a kinetic product generated in contact to SiC. The first reaction between the liquid alloy and the SiC substrate forms TiC and a second Si-richliquid:Al_3Ti_{liq} + (1-x)SiC -> xTiC + $Al_3(Ti_{1-x}Si_x)$.

The definition of the "x" value is the crucial point. It reflects the kinetic competition between several processes such as:

(a) the initial reaction between Al_3Ti and SiC;

(b) the heating rate of the experimental process;

(c) the formation-disappearance of other solid phases.

The competition between all these phenomena induce an evolution in the liquid composition.

The experimental results obtained are related to the different pathways that are connected to the evolution composition of the liquid.

The following approach has the aim to approximately estimate the kinetics of the system.

The reagents that will take part of the equilibrium, are chosen and set step by step considering the first reaction as well as following the system evolution in terms of driving force.

It is possible to summarize the approach as follows:

- definition of system;
- definition of the first reaction occurring at the interface:

$$Al_3Ti_{liq} + (1-x)SiC \rightarrow xTiC + Al_3(Ti_{1-x}Si_x)$$

- definition of the first reagents and calculation of the equilibrium;
- insertion of new phases as "entered" and calculation of the new equilibrium;
-

After the different evolution steps are considered, it is possible to follow the cooling processes and to compare the experimental results (EDS analysis) to the theoretical data obtained.

The first equilibrium calculation is then between L_1 and SiC; all the other phases of the Al-C-Si-Ti data-base are set as "dormant" phases. In this way they will not be considered in the equilibrium calculation.

After the first equilibrium calculation, it is possible to discover that TiC is the "dormant" phase that shows the higher driving force value (after the two selected reagents: SiC and L_1).

For this reason, TiC is add as "entered" phase and a second equilibrium between SiC, $L_1$and TiC is evaluated**.** From this calculationit is possible to discover:

- TiC formation (about 2 moles);
- a new liquid (L_2) formation (75Al, 23Si, $5x10^{-3}$Ti, $2.5x10^{-3}$C moles),
- a decreased amount of SiC (from 2 moles it arrives to 0.15 moles). It is possible to observe that the L_2 composition depends on the initial L1 composition and also on its quantity.

The L_2 results more enriched in Si compared to L_1, that is more Ti-rich.

It is now possible to make the hypothesis that the TiC formation creates a barrier between the liquid and SiC blocking the diffusion. For this reason SiC is set as "dormant" phase and the equilibrium between the "entered" phases TiC and the new liquid is calculated.

Among the "dormant" phases, the MAX phase has the highest driving force.

The MAX phase is then selected as "entered" phase and the equilibrium is evaluated again.

Now it is possible to take into account two different evolutions of the system under investigation:

1) TiC forms an uniform layer that totally blocks any further SiC-liquid interactions;
2) TiC does not form an uniform layer allowing SiC-liquid interactions to take place.

In the first case, during the isothermal process the formation of MAX-phase is considered but the equilibrium is not reached. SiC is put as "dormant" phase and is not considered anymore.

This option involves then liquid, TiC and MAX-phase as "entered" phases.

The cooling of the liquid after MAX formation is calculated (*Figure 6.95*).

This result, coming from the thermodynamic approach, confirm the experimental observation already discussed: the liquid still reacts with the substrate even if the TiC layer extended at the interface.

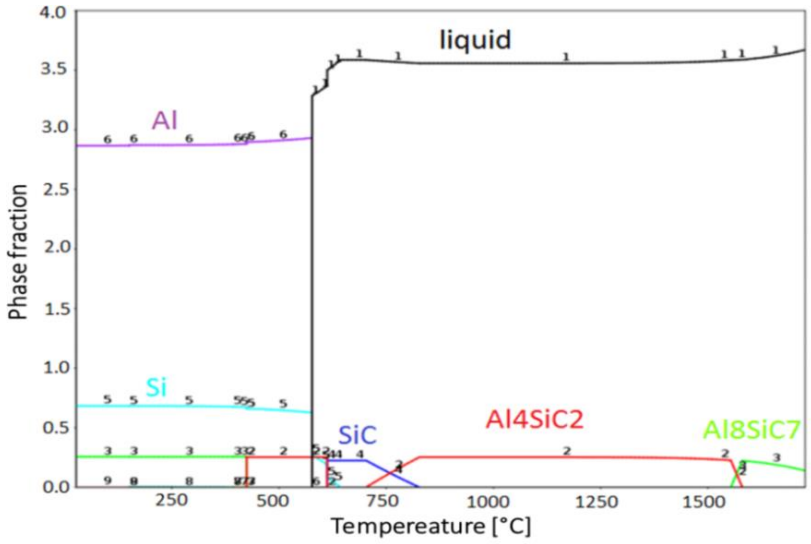

Figure 6.95. Cooling plot obtained when liquid, TiC and MAX-phase are set as "entered" phases.

In the second and more realistic case, the liquid can still react with SiC and during the isothermal process the equilibrium is reached. This option involves then liquid, TiC, SiC and MAX-phase as "entered" phases. The cooling plot of the liquid, reported in *Figure 6.96,* seems to be in a good agreement with the experimental results showing that ternary (τ-phase) and quaternary ($Ti_3Si(Al)C_2$) phases should form from this solidification process.

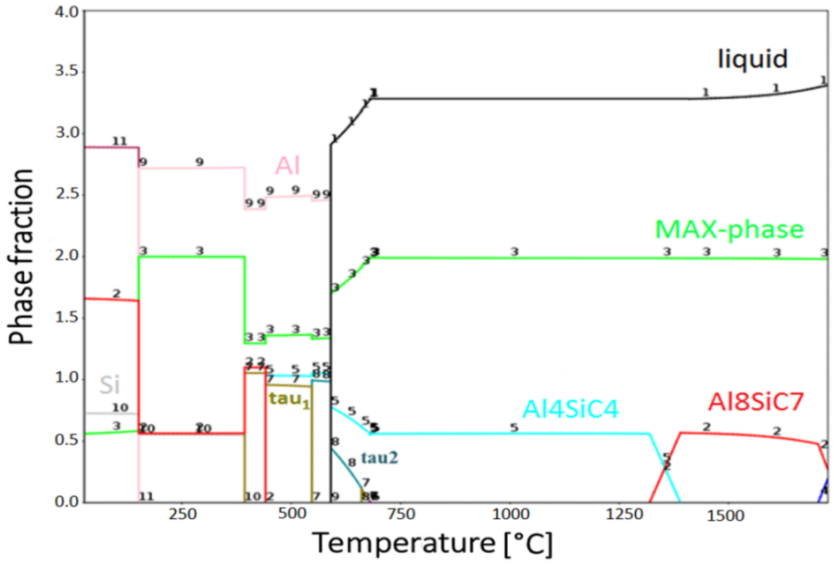

Figure 6.96.Cooling plot obtained when liquid, SiC, TiC and MAX-phase are set as "entered" phases.

6.3 Evaluation of joint performances- Critical aspects

YAG-Ti6Al4V samples

The study of the mechanical behaviour of the brazed samples was not the focus of this Thesis, that was mainly aimed at understanding the complex solid-liquid interaction phenomena at the basis of metal-ceramic brazing processes. In the particular case of the application as ceramic windows (joints YAG/AgCuTi/Ti6Al4V) these products are not meant to undergo severe mechanical loads and, for this reason, mechanical tests were not planned. Rather, a performance characterization should involve the determination of the corrosion and galvanic behavior in the presence of seawater [163] and the determination of the vacuum tightness. However, in order to plan the study of the mechanical response of these joints, it is fundamental to take into account the structure transitions occurring in the metallic substrate (Ti6Al4V) as a function of temperature.

The Ti6Al4V alloy is an α+β alloy, with 6 wt% Al stabilizing the α phase and 4 wt% V stabilizing the β phase. At room temperature the equilibrium microstructure consists mainly of the α phase (hcp) with some retained β phase (bcc). Depending on cooling rate and prior heat treatment the micro constituents and microstructures are divided into several types, namely: grain boundary allotriomorph α, globular or primary α (called bi-modal microstructure when the globular α is surrounded by Widmanstätten platelets), Widmanstätten, basketweave, and martensitic. A recently described microstructure is the bi-lamellar, in which the retained β phase, lying between the α platelets in a Widmanstätten structure, contains thinner secondary α platelets. For very slow cooling rates from the high temperature α+β region or above the β-transus temperature (995°C ± 20°C) the β phase mainly transforms into a globular type of α. Increasing the cooling rate enhances the α nucleation rate in the β grain boundaries thereby enhancing the formation and growth of α platelets into the prior β grains. The length and width of these α platelets are determined by the cooling rate, an increased cooling rate enhancing the nucleation rate and slowing the diffusion process (growth rate). At a certain point the cooling rate is fast enough for nucleation of α to occur inside the prior β grains as well, leading to the formation of the basketweave structure. Finally, if quenched, the β phase will fully or partly transform into a martensitic type of α. Vanadium enrichment of the β phase occurs in proportion to the reduction of the volume fraction of β phase. At V contents ≥15 wt%, the β phase is stabilized and retains its bcc crystal structure upon quenching. When β phase with 10 ± 2 wt% vanadium is quenched (from a temperature range of approximately 750-900°C), it partly retains the bcc structure and partly transforms into soft

orthorhombic α'' martensite. The higher the solution heat treatment temperature, the smaller is the V enrichment in the β phase, leading to transformation into hexagonal α' upon quenching (from temperatures above 900°C) [164]. Figure 6.97 is a schematic illustration of the microstructures resulting from quenching from various temperatures. The figure attempts only to illustrate the principle transformations upon quenching; in reality mixtures of both α', α'' and metastable/stable β can occur, depending on chemical compositional variations. The grain boundary allotriomorph α phase starts to form as soon as the temperature drops below the β transus temperature. To what extent it then continues to grow along β grain boundaries depends on the cooling rate [165].

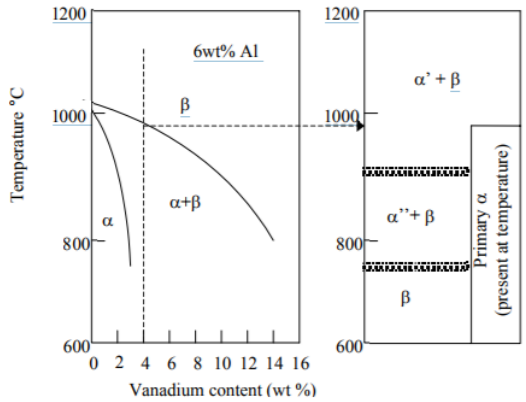

Figure 6.97. A schematic illustration of microstructures occurring in Ti-6Al-4V after quenching from different temperatures [165].

SiC-SiC samples

The mechanical strength evaluation of the SiC-SiC joined samples is necessary and planned in order to validate the use of these materials in extreme condition applications as the aerospace ones. However, this characterization is not part of the Thesis work. The shear strength tests are performed at Politecnico of Turin Laboratories.

In particular, the shear strength tests are conducted using a tensile testing machine (Sintech 10/D) at a speed of 0.5 mm/min at room temperature. The details of the are described in [166].

Additional mechanical tests are performed using the torsion test on hourglass shaped adherents described in [167].

7. Conclusions

General conclusions

This work has been foreseen as an important step to acquire a good and updated knowledge of the interfacial phenomena occurring, at high temperatures, when liquid metals come into contact with solid phases, in particular ceramic materials. These phenomena are extremely important in many industrial applications. Among them, the metal-ceramic brazing process has been examined, and all experimental and theoretical activities have been designed to comply with this final aim.

Taking advantage of advanced, and sometimes unique, experimental facilities to measure the wettability and reactivity of solid-liquid systems at high temperatures, the interactions between the different phases have been measured in real time as well as ex-post by optical and electron microscopy, EDS analyses, DSC, surface profilometry.

The experimental work has been supported, both for designing experiments and interpreting the resulting microstructures, by thermodynamic calculations made by the CALPHAD methods, by using both standard databases and by setting up also their extension to multicomponent systems, as required by the materials under study.

More in detail, this work provides a wetting and reactivity investigation of an oxidic substrate ($Y_3Al_5O_{12}$) in contact to Ag-based alloys (no data exist in the literature), and of a non-oxidic substrate (SiC) in contact to Al-Ti alloys.

Specific conclusions concerning the wettability (*6.1.3; 6.2.4*) and the joining (*6.1.5; 6.2.6*) results are given and explained in detail.

As already said, the interpretation of the experimental results by the thermodynamic approach has a central role in the discussion, having also oriented the experimental work towards the verification of specific conditions of temperature and phase composition, otherwise nearly impossible to single out in a reasonably limited time.

Specifically, the capability has been acquired to follow and investigate the metal-ceramic interactions occurring at high temperatures by the selection of the more appropriate way to perform calculations representing the system from the thermodynamic point of view.

Through the prevision of the equilibria reached at different temperatures, of the elements activity, of the liquid composition under the selected conditions, as well as, for example, of the cooling products, several process parameters such as the brazing alloy composition, time and temperature have been defined.

For each system a specific thermodynamic approach was selected to define and explain the interfacial interactions as well as the evolution of the whole bulk, namely:

- the oxidic system behaves as reactive system where no significant substrate dissolution occurs. For this reason, the thermodynamic approach takes into account just the alloys evolution under the selected conditions. An existing Ag-Cu-Ti thermodynamic database was used to recalculate the isothermal sections or, for example, the Ti activity at the temperatures under investigation;
- the non-oxidic-system behaves as a reactive and dissolutive one; in this case, the Al-rich liquids wet and dissolve a consistent amount of C and Si from the substrate. For this reason, the thermodynamic approach has to take into account all the elements of the system. A home-made quaternary database (Al-C-Si-Ti) was built merging the literature parameters and adapting them to obtain a self-consistent set of phase-models and interaction parameters.

In both the cases, the alloy/substrate interaction leads to the formation of interfacial products involving elements coming from the metallic and the ceramic parts.

The formation of these intermediate compounds improves the wettability of the systems and ensure a good adhesion between the two different materials. Ti, in both the systems, has the role of the active element migrating at the interface and promoting the formation of these intermediate compounds.

A new metal-ceramic layer involving both Cu and Ti and all the elements of the ceramic is detected on the YAG surface in the case of the AgCuTi/YAG sample tested at 950°C; a second intermediate compound, known as "M_4X";was also found at the interface of this sample and associated to the significant improvement in the wettability because of its more pronounced metallic behaviour allowing to reach a contact angle values of about 10°.

However, a good wettability (θ=73°) was also obtained testing the same sample at a lower temperature (850°C) where just the first metal-ceramic compound is detected.

Thermodynamic calculations allowed us to highlight the relevant role of the Ti activity in the liquid alloy to determine the final contact angles, as well as to clarify the interplay of the L_1 and L_2 liquids, coexisting in the miscibility gap between 910 and 950°C, with respect to the wetting process.

Moreover, from the analyses of the binary alloys/YAG interfaces, it is possible to evaluate the different role the elements have in the wetting phenomena.

The YAG/Ag-based alloys/Ti6Al4V system, never studied before, appears very promising to be considered to design transparent optical window; indeed, the ceramic maintains its transparency also after each high temperature test and the alloy/substrate interaction guarantees a good adhesion.

The future work foresees a sea-water resistance and corrosion tests where the samples will be exposed in the water at different natural conditions depending on the selected period of the year (season).

The reactivity between two different Al-Ti alloys and SiC, was, for the first time, evaluated both from the experimental and thermodynamic sides, and this interpretation is related to the results obtained after several wetting and joining tests.

The DSC and EDS analyses are conducted to determine the first interaction in terms of temperature and phase compositions.

A compact and defect-free TiC and a continuous $Ti_3Si(Al)C_2$layers constitute the main interfacial phases formed on the SiC surface in the cases of $Al_{84}Ti_{16}$/SiC and $Al_{75}Ti_{25}$/SiC, respectively.

Even if temperature and alloy composition are not so far, the interfacial reactivity as well as the subsequent liquid evolution above the interface are found to be significantly different as a function of temperature and time. The Si dissolution from the substrate is pronounced in the case of the $Al_{75}Ti_{25}$/SiC sample; in particular, after 1 h of contact the amount of Si inside the liquid is drastically increased leading to the formation of several pure Si crystals and proving that the interfacial layers (TiC and Ti_3SiC_2) do not play the role of diffusion barrier in this kind of reactive and dissolutive wetting.

The reactivity of both the systems was followed by the use of the thermodynamic prediction by calculating isothermal sections at the testing temperatures fixing as constant the C amount inside the liquid because of its low calculated solubility.

By the knowledge of the first interaction occurring at the interface as well as of the evolution of this system with time and temperature, the best process parameters to obtain the more promising interface are defined and the Al_3Ti is used in a preliminary SiC-SiC joining investigation that will include a deep mechanical evaluation to determine the joint performances.

References

[1] E. Wucina, E. Opila, M. Opeka, W. Fahrenholtz, and I. Talmy, 'UHTCs : Ultra-High Temperature Ceramic Materials for Extreme Environment Applications', *Electrochem. Soc. Interface*, pp. 30–36, 2007.

[2] S. M. Hong, T. B. Reynolds, C. C. Bartlow, and A. M. Glaeser, 'Rapid transient-liquid-phase bonding of Al_2O_3 with microdesigned Ni / Nb / Ni interlayers', *Int. J. Mater. Res.*, vol. 101, pp. 133–142, 2010.

[3] N. Eustathopoulos, M. G. Nicholas, and B. B. Drevet, *Wettability at high temperatures*, vol. 3. 1999.

[4] A. S. Skapski, 'A theory of surface tension of solids—I application to metals', *Acta Metall.*, vol. 4, no. 6, pp. 576–582, 1956.

[5] H. Ghasemi and C. A. Ward, 'Sessile-Water-Droplet Contact Angle Dependence on Adsorption at the Solid-Liquid Interface', pp. 5088–5100, 2010.

[6] D. Chatain, 'Anisotropy of Wetting', *Annu. Rev. Mater. Res.*, vol. 38, no. 1, pp. 45–70, 2008.

[7] T. Young, 'An Essay on the Cohesion of Fluids', *Philos. Trans. R. Soc. London*, vol. 95, no. 1805, pp. 65–87, 1805.

[8] A. Dupré, 'Théorie Méchanique de la chaleur'. p. 207, 1869.

[9] A. Passerone, M. L. Muolo, and F. Valenza, 'Wetting at high temperature - Drops and bubbles', pp. 300–334, 2013.

[10] R. Shuttleworth and G. L. J. Bailey, 'The spreading of a liquid over a rough solid', *Discuss. Faraday Soc.*, vol. 3, no. 16, p. 16, 1948.

[11] R. E. Johnson, 'Conflicts between Gibbsian Thermodynamics and Recent Treatments of Interfacial Energies in Solid-Liquid-Vapor', *J. Phys. Chem.*, vol. 63, no. 4, pp. 1655–1658, 1959.

[12] D. Chatain and W. C. Carter, 'Wetting dynamics - Spreading of metallic drops', *Nat. Mater.*, vol. 3, no. 12, pp. 843–845, 2004.

[13] E. Saiz, A. P. Tomsia, and R. M. Cannon, 'Triple line ridging and attachment in high-temperature wetting', vol. 44, pp. 159–164, 2001.

[14] G. Levi and W. D. Kaplan, 'Aluminium-alumina interface morphology and thermodynamics from dewetting experiments', *Acta Mater.*, vol. 51, no. 10, pp. 2793–2802, Jun. 2003.

[15] E. Saiz, R. M. Cannon, and A. P. Tomsia, 'Reactive spresading: adsorption, ridging and compound formation', vol. 48, pp. 4449–4462, 2000.

[16] E. Saiz, A. P. Tomsia, and R. M. Cannon, 'Ridging effects on wetting and spreading liquids on solids', vol. 46, no. 7, pp. 2349–2361, 1998.

[17] P. Protsenko, O. Kozlova, R. Voytovych, and N. Eustathopoulos, 'Dissolutive wetting of Si by molten Cu', *J. Mater. Sci.*, vol. 43, no. 16, pp. 5669–5671, 2008.

[18] C. Rado, S. Kalogeropoulou, and N. Eustathopoulos, 'Bonding and wetting in non-reactive metal/SiC systems: weak or strong interfaces?', *Mater. Sci. Eng. A*, vol. 276, no. 1, pp. 195–202, 2000.

[19] G. W. Liu, F. Valenza, M. L. Muolo, G. J. Qiao, and a. Passerone, 'Wetting and interfacial behavior of Ni–Si alloy on different substrates', *J. Mater. Sci.*, vol. 44, no. 22, pp. 5990–5997, 2009.

[20] A. H. Carim, 'Convergent-beam electron diffraction "fingerprinting" of M6X phases at brazed ceramic joints', *Scr. Metall. Mater.*, vol. 25, pp. 51–54, 1991.

[21] A. H. Carim and C. H. Mohr, 'Brazing of alumina with Ti4CU2O and Ti3CU3O interlayers', *Mater. Lett.*, vol. 33, no. 3–4, pp. 195–199, 1997.

[22] M. Aizenshtein, N. Froumin, and N. Frage, 'Experimental Study and Thermodynamic Analysis of High Temperature Interactions between Boron Carbide and Liquid Metals', no. 6, pp. 849–868, 2014.

[23] O. Smorygo, J. S. Kim, M. D. Kim, and T. G. Eom, 'Evolution of the interlayer microstructure and the fracture modes of the zirconia/Cu-Ag-Ti filler/Ti active brazing joints', *Mater. Lett.*, vol. 61, no. 2, pp. 613–616, 2007.

[24] W. B. Hanson, K. I. Ironside, and J. A. Fernie, 'Active metal brazing of zirconia', *Acta Mater.*, vol. 48, no. 18–19, pp. 4673–4676, 2000.

[25] C. Rado, S. Kalogeropoulou, and N. Eustathopoulos, 'Wetting and bonding of Ni–Si alloys on silicon carbide', *Acta Mater.*, vol. 47, no. 2, pp. 461–473, 1999.

[26] A. Passerone, M. L. Muolo, F. Valenza, F. Monteverde, and N. Sobczak, 'Wetting and interfacial phenomena in Ni–HfB_2 systems', *Acta Mater.*, vol. 57, no. 2, pp. 356–364, 2009.

[27] R. Voytovych, A. Koltsov, F. Hodaj, and N. Eustathopoulos, 'Reactive vs non-reactive wetting of ZrB_2 by azeotropic Au–Ni', *Acta Mater.*, vol. 55, no. 18, pp. 6316–6321, 2007.

[28] S. Gambaro, F. Valenza, M. L. Muolo, A. Passerone, and G. Cacciamani, 'Wettability of SiC and graphite by Co–Ta alloys: evaluation of the reactivity supported by thermodynamic calculations', *J. Mater. Sci.*, pp. 1–13, 2017.

[29] J. A. Warren, W. J. Boettinger, and A. R. Roosen, 'Modeling reactive wetting', *Acta Mater.*, vol. 46, no. 9, pp. 3247–3264, 1998.

[30] L. Yin, A. Chauhan, and T. J. Singler, 'Reactive wetting in metal/metal systems: Dissolutive versus compound-forming systems', *Mater. Sci. Eng. A*, vol. 495, no. 1–2, pp. 80–89, 2008.

[31] P. Protsenko, J. Garandet, R. Voytovych, and N. Eustathopoulos, 'Thermodynamics and kinetics of dissolutive wetting of Si by liquid Cu', *Acta Mater.*, vol. 58, no. 20, pp. 6565–6574, 2010.

[32] O. Kozlova, R. Voytovych, P. Protsenko, and N. Eustathopoulos, 'Non-reactive versus dissolutive wetting of Ag–Cu alloys on Cu substrates', *J. Mater. Sci.*, vol. 45, no. 8, pp. 2099–2105, 2010.

[33] W. Villanueva, W. J. Boettinger, G. B. McFadden, and J. A. Warren, 'A diffuse-interface model of reactive wetting with intermetallic formation', *Acta Mater.*, vol. 60, no. 9, pp. 3799–3814, 2012.

[34] L. Yin, B. T. Murray, and T. J. Singler, 'Dissolutive wetting in the Bi-Sn system', *Acta Mater.*, vol. 54, no. 13, pp. 3561–3574, 2006.

[35] N. Ni, Y. Kaufmann, W. D. Kaplan, and E. Saiz, 'Interfacial energies and mass transport in the Ni(Al)–Al_2O_3 system: The implication of very low oxygen activities', *Acta Mater.*, vol. 64, pp. 282–296, 2014.

[36] O. Dezellus and N. Eustathopoulos, 'Fundamental issues of reactive wetting by liquid metals', *J. Mater. Sci.*, vol. 45, no. 16, pp. 4256–4264, 2010.

[37] K. Landry, S. Kalogeropoulou, and N. Eustathopoulos, 'Wettability of carbon by aluminum and aluminum alloys', *Mater. Sci. Eng. A*, vol. 254, no. 1–2, pp. 99–111, 1998.

[38] K. Landry, C. Rado, R. Voitovich, and N. Eustathopoulos, 'Mechanisms of reactive wetting: The question of triple line configuration', *Acta Mater.*, vol. 45, no. 7, pp. 3079–3085, 1997.

[39] R. Asthana and N. Sobczak, 'Wettability in Joining of Advanced Ceramics and Composites: Issues and Challenges', *High Temp. Ceram. Matrix Compos. 8*, no. June, pp. 589–600, 2014.

[40] M. Herrmann, W. Lippmann, and A. Hurtado, 'Y_2O_3-Al_2O_3-SiO_2-based glass-ceramic fillers for the laser-supported joining of SiC', *J. Eur. Ceram. Soc.*, vol. 34, no. 8, pp. 1935–1948, 2014.

[41] N. Sobczak, M. Singh, and R. Asthana, 'High-temperature wettability measurements in metal/ceramic systems – Some methodological issues', *Curr. Opin. Solid State Mater. Sci.*, vol. 9, no. 4–5, pp. 241–253, 2005.

[42] I. Gurrappa, 'Characterization of titanium alloy Ti-6Al-4V for chemical, marine and industrial applications', *Mater. Charact.*, vol. 51, no. 2–3, pp. 131–139, 2003.

[43] A. Neville and B. A. B. McDougall, 'Erosion– and cavitation–corrosion of titanium and its alloys', *Wear*, vol. 250, no. 1–12, pp. 726–735, 2001.

[44] R. A. Zavanelli, G. E. P. Henriques, I. Ferreira, and J. M. D. De Almeida Rollo, 'Corrosion-fatigue life of commercially pure titanium and Ti-6Al-4V alloys in different storage environments', *J. Prosthet. Dent.*, vol. 84, no. 3, pp. 274–279, 2000.

[45] R. J. Morrissey and T. Nicholas, 'Fatigue strength of Ti-6Al-4V at very long lives', *Int. J. Fatigue*, vol. 27, no. 10–12, pp. 1608–1612, 2005.

[46] A. L. Hutson, M. Niinomi, T. Nicholas, and D. Eylon, 'Effect of various surface conditions on fretting fatigue behavior of Ti-6Al-4V', *Int. J. Fatigue*, vol. 24, no. 12, pp. 1223–1234, 2002.

[47] A. G. R. Ebra, Y. Yamada, 'Corrosion-Fatigue Behavior of Ti-6Al-4V in a Sodium Chloride Aqueous Solution', in *Corrosion Fatigue: Mechanism, Metallurgy, Electrochemistry and Engineering, STM STP 801, American Society for Testing*, 2016.

[48] S. Crane and C. R. Ekstrom, 'Nonmagnetic UHV optical viewports', *Proc. IEEE Int. Freq. Control Symp. Expo.*, vol. 2005, pp. 297–300, 2005.

[49] M. Jacobs, G. Van Oost, J. Degrieck, I. De Baere, A. Gusarov, and V. Massaut, 'Modeling and microstructural analysis of temperature effects in fused silica viewport', *Fusion Eng. Des.*, vol. 86, no. 12, pp. 2831–2838, 2011.

[50] A. Gusarov, 'Irradiation effects on the optical and mechanical performance of ITER prototype window assemblies', *Fusion Eng. Des.*, vol. 88, no. 6–8, pp. 1192–1195, 2013.

[51] T. Welker, T. Geiling, H. Bartsch, and J. Müller, 'Design and Fabrication of Transparent and Gas-Tight Optical Windows in Low-Temperature Co-Fired Ceramics', *Int. J. Appl. Ceram. Technol.*, vol. 10, no. 3, pp. 405–412, 2013.

[52] W. Watanabe, Y. Li, and K. Itoh, 'Ultrafast laser micro-processing of transparent material', *Opt. Laser Technol.*, vol. 78, pp. 52–61, 2016.

[53] D. Sciti, A. Bellosi, and L. Esposito, 'Bonding of zirconia to supper alloy with the active brazing technique', *J. Eur. Ceram. Soc.*, vol. 21, no. 1, pp. 45–52, 2001.

[54] M. Singh, T. P. Shpargel, and R. Asthana, 'Brazing of yttria-stabilized zirconia (YSZ) to stainless steel using Cu, Ag, and Ti-based brazes', *J. Mater. Sci.*, vol. 43, no. 1, pp. 23–32, 2008.

[55] W. Fu, X.G. Song, Y.X. Zhao, J. Cao, J. Feng, C. Jin, G.D. Wang,'Effect of Ti content on the wetting behavior of Sn0.3Ag0.7Cu/AlN system', *Mater. Des.*, vol. 115, pp. 1–7, 2017.

[56] T. H. Chuang, M. S. Yeh, and Y. H. Chai, 'Brazing of zirconia with AgCuTi and SnAgTi active filler metals', *Metall. Mater. Trans. A*, vol. 31A, pp. 1591–1597, 2000.

[57] H. Q. Hao, Y. L. Wang, Z. H. Jin, and X. T. Wang, 'Joining of zirconia to zirconia using AgCuTi filler metal', *J. Mater. Process. Tech.*, vol. 52, no. 2–4, pp. 238–247, 1995.

[58] P. Martineau, M. Lahaye, R. Pailler, R. Naslain, M. Couzi, and F. Cruege, 'SiC filament/titanium matrix composites regarded as model composites-Part 1 Filament microanalysis and strength characterization', *J. Mater. Sci.*, vol. 19, no. 8, pp. 2731–2748, 1984.

[59] F. Valenza, S. Gambaro, M.L. Muolo, A. Passerone, M. Salvo, M. Ferraris 'Surface engineering of SiC_f/SiC composites by selective thermal removal', *Int. J. Appl. Ceram. Technol.*, vol. 14, no. 3, pp. 287–294, 2017.

[60] A. E. Martinelli and A. J. A. Buschinelli, 'Review Article: Recent advances in metal-ceramic brazing', vol. 49, pp. 178–198, 2003.

[61] R. K. Shiue, S. K. Wu, J. M. O, and J. Y. Wang, 'Microstructural evolution at the bonding interface during the early-stage infrared active brazing of alumina', *Metall. Mater. Trans. A*, vol. 31, no. 10, pp. 2527–2536, 2000.

[62] K. M. Jasim, F. A. Hashim, R. H. Yousif, R. D. Rawlings, and A. R. Boccaccini, 'Actively brazed alumina to alumina joints using CuTi, CuZr and eutectic AgCuTi filler alloys', *Ceram. Int.*, vol. 36, no. 8, pp. 2287–2295, 2010.

[63] R. Voytovych, F. Robaut, and N. Eustathopoulos, 'The relation between wetting and interfacial chemistry in the CuAgTi/alumina system', *Acta Mater.*, vol. 54, no. 8, pp. 2205–2214, May 2006.

[64] R. Voytovych, L. . Ljungberg, and N. Eustathopoulos, 'The role of adsorption and reaction in wetting in the CuAg–Ti/alumina system', *Scr. Mater.*, vol. 51, no. 5, pp. 431–435, Sep. 2004.

[65] S. Gambaro, M. L. Muolo, F. Valenza, G. Cacciamani, L. Esposito, and A. Passerone, 'Wettability of transparent YAG by molten Ag-Cu-Ti alloys', *J. Eur. Ceram. Soc.*, vol. 35, no. 10, pp. 2895–2906, 2015.

[66] S. Gambaro, F. Valenza, A. Passerone, G. Cacciamani, and M. L. Muolo, 'Brazing transparent YAG to Ti6Al4V: reactivity and characterization', *J. Eur. Ceram. Soc.*, vol. 36, no. 16, pp. 4185–4196, 2016.

[67] M. Naka, 'Controlling of ceramic–metal interfacial structure using moltenmetals. Trans JWRI 1992;21:1–7.', vol. I, no. 1, pp. 1–7, 2001.

[68] F. Valenza, C. Artini, A. Passerone, and M. L. Muolo, 'Zr_2-SiC/Ti6Al4V joints: Wettability studies using Ag- and Cu-based braze alloys', *J. Mater. Sci.*, vol. 47, no. 24, pp. 8439–8449, 2012.

[69] A. Passerone, M. L. Muolo, R. Novakovic, and D. Passerone, 'Liquid metal/ceramic interactions in the (Cu, Ag, Au)/ZrB_2 systems', *J. Eur. Ceram. Soc.*, vol. 27, no. 10, pp. 3277–3285, 2007.

[70] A. Passerone, M. L. Muolo, and D. Passerone, 'Wetting of Group IV diborides by liquid metals', *J. Mater. Sci.*, vol. 41, no. 16, pp. 5088–5098, 2006.

[71] M. L. Muolo, E. Ferrera, and A. Passerone, 'Wetting and spreading of liquid metals on ZrB_2 -based ceramics', vol. 40, pp. 2295–2300, 2005.

[72] F. Valenza, C. Artini, A. Passerone, and M. L. Muolo, 'ZrB_2–SiC/Ti6Al4V joints: wettability studies using Ag- and Cu-based braze alloys', *J. Mater. Sci.*, vol. 47, no. 24, pp. 8439–8449, 2012.

[73] A. Passerone, M. L. Muolo, R. Novakovic, and D. Passerone, 'Liquid metal/ceramic interactions in the (Cu, Ag, Au)/ZrB_2 systems', *J. Eur. Ceram. Soc.*, vol. 27, no. 10, pp. 3277–3285, 2007.

[74] M.L. Muolo, E. Ferrera, L. Morbelli, and A. Passerone, 'Wetting, spreading and joining in the alumina–zirconia–Inconel 738 system', *Scr. Mater.*, vol. 50, no. 3, pp. 325–330, 2004.

[75] M. Paulasto, F. J. J. van Loo, and J. K. Kivilahti, 'Thermodynamic and experimental study of TiAgCu alloys', *J. Alloys Compd.*, vol. 220, no. 1–2, pp. 136–141, 1995.

[76] M.G. Nicholas, T. M. Valentine, and M. J. Waite, 'The wetting of alumina by copper alloyed with titanium and other elements', *J. Mater. Sci.*, vol. 15, no. 9, pp. 2197–2206, 1980.

[77] J.J. Pak, M. L. Santella, and R. J. Fruehan, 'Thermodynamics of Ti in Ag-Cu alloys', *Metall. Trans. B*, vol. 21, no. 2, pp. 349–355, 1990.

[78] L. Rongti, P. Wei, C. Jian, and L. Jie, 'Thermodynamic properties of Ti in Ag – Cu – Ti alloys', vol. 335, pp. 21–25, 2002.

[79] R. Novakovic, E. Ricci, D. Giuranno, and a. Passerone, 'Surface and transport properties of Ag–Cu liquid alloys', *Surf. Sci.*, vol. 576, no. 1–3, pp. 175–187, 2005.

[80] M. Ferraris and V. Casalegno, 'Integration and Joining of Ceramic Matrix Composites', *Ceram. Matrix Compos. Mater. Model. Technol.*, pp. 549–567, 2014.

[81] W.J. Kim, D. Kim, and J. Y. Park, 'Fabrication and material issues for the application of SiC composites to LWR fuel cladding', *Nucl. Eng. Technol.*, vol. 45, no. 4, pp. 565–572, 2013.

[82] L.L. Snead, T. Nozawa, M. Ferraris, Y. Katoh, R. Shinavski, and M. Sawan, 'Silicon carbide composites as fusion power reactor structural materials', in *Journal of Nuclear Materials*, 2011, vol. 417, no. 1–3, pp. 330–339.

[83] B.W. Krenkel, B. Heidenreich, and R. Renz, 'C / C-SiC Composites for Advanced Friction Systems', *Adv. Eng. Mater.*, no. 7, pp. 427–436, 2002.

[84] R. Naslain, 'Materials design and processing of high temperature ceramic matrix composites: state of the art and future trends.', *Adv. Compos. Mater.*, vol. 8, no. 1, p. 3, 1999.

[85] C. Jiménez *et al.*, 'Joining of ceramic matrix composites to high temperature ceramics for thermal protection systems', vol. 36, pp. 443–449, 2016.

[86] S.M. Hong, C. C. Bartlow, T. B. Reynolds, J. T. McKeown, and A. M. Glaeser, 'Ultrarapid transient-liquid-phase bonding of Al_2O_3 ceramics', *Adv. Mater.*, vol. 20, no. 24, pp. 4799–4803, 2008.

[87] X.H. Yin, M. S. Li, and Y. C. Zhou, 'Microstructure and mechanical strength of transient liquid phase bonded Ti_3SiC_2 joints using Al interlayer', *J. Eur. Ceram. Soc.*, vol. 27, no. 12, pp. 3539–3544, 2007.

[88] G.W. Liu, M.L. Muolo, F. Valenza, and A. Passerone, 'Survey on wetting of SiC by molten metals', *Ceram. Int.*, vol. 36, no. 4, pp. 1177–1188, 2010.

[89] B. K. Nogi and K. Ogino, 'Wettability of SiC by Liquid Pure Metals', *Trans. Japan Inst. Met.*, vol. 29, no. 9, pp. 742–747, 1988.

[90] P. Nikolopoulos, S. Agathopoulos, G. N. Angelopoulos, A. Naoumidis, and H. Gr??bmeier, 'Wettability and interfacial energies in SiC-liquid metal systems', *J. Mater. Sci.*, vol. 27, no. 1, pp. 139–145, 1992.

[91] F. Valenza, S. Gambaro, M.L. Muolo, G. Cacciamani, P. Tatarko, T. Saunders, M. Reece, A. Schmiidt, T. Schubert, T.Weißgärber, A. Passerone, 'Wetting and interfacial phenomena of Ni-Ta alloys on CVD-SiC', *Int. J. Appl. Ceram. Technol.*, vol. 14, no. 3, pp. 295–304, 2017.

[92] N. P. Tsoga A, Ladas S, 'Correlation between the oxidation state of SiC and its wettability with non reactive (Sn) or reactive (Ni) metallic components sand their binary Si-alloys', *Acta Mater.*, vol. 45, no. 9, pp. 3515–3525, 1997.

[93] O. Mailliart, F. Hodaj, V. Chaumat, and N. Eustathopoulos, 'Influence of oxygen partial pressure on the wetting of SiC by a Co-Si alloy', *Mater. Sci. Eng. A*, vol. 495, no. 1–2, pp. 174–180, 2008.

[94] S. Kalogeropoulou, L. Baud, and N. Eustathopoulos, 'Relationship between wettability and reactivity in Fe/SiC system', *Acta Metall. Mater.*, vol. 43, no. 3, pp. 907–912, 1995.

[95] B. Drevet, S. Kalogeropoulou, and N. Eustathopoulos, 'Wettability and interfacial bonding in Au-Si/SiC system', *Acta Met. mater.*, vol. 41, no. 11, pp. 3119–3126, 1993.

[96] L. Jian-Guo, 'Wettability of silicon carbide by liquid silver and binary silver-silicon alloy', *Mater. Lett.*, vol. 18, no. 5–6, pp. 291–298, 1994.

[97] A. Gasse, C. Rado, and N. Eustathopoulos, 'Influence of atmosphere on the wettability of SiC by non-reactive Cu-Si alloys', *High Temp.*, vol. 15, pp. 1630–1632, 1996.

[98] K. Landry, C. Rado, and N. Eustathopoulos, 'Influence of Interfacial Reaction Rates on the Wetting Driving Force in Metal/Ceramic Systems', vol. 27, pp. 3181–3186, 1995.

[99] C. Rado and N. Eustathopoulos, 'The Role of Surface Chemistry on Spreading Kinetics of Molten Silicides on Silicon Carbide', *Interface Sci.*, vol. 12, no. 1, pp. 85–92, 2004.

[100] X. S. Cong, P. Shen, Y. Wang, and Q. Jiang, 'Wetting of polycrystalline SiC by molten Al and Al-Si alloys', *Appl. Surf. Sci.*, vol. 317, pp. 140–146, 2014.

[101] X. Fang, T. Fan, and D. Zhang, 'Work of adhesion in Al/SiC composites with alloying element addition', *Metall. Mater. Trans. A Phys. Metall. Mater. Sci.*, vol. 44, no. 11, pp. 5192–5201, 2013.

[102] P. Shen, Y. Wang, L. Ren, S. Li, Y. Liu, and Q. Jiang, 'Influence of SiC surface polarity on the wettability and reactivity in an Al/SiC system', *Appl. Surf. Sci.*, vol. 355, pp. 930–938, 2015.

[103] V. Laurent, C. Rado, and N. Eustathopoulos, 'Wetting kinetics and bonding of Al and Al alloys on α-SiC', *Mater. Sci. Eng. A*, vol. 205, no. 1–2, pp. 1–8, 1996.

[104] N. Sobczak, 'High Temperature Interfaces', *Charact. Control Interfaces High Qual. Adv. Mater.*, pp. 83–91, 2005.

[105] C. Dai, R. Ma, W. Wang, X. Cao, and Y. Yu, 'Microstructure and properties of an Al–Ti–Cu–Si brazing alloy for SiC–metal joining', *Int. J. Miner. Metall. Mater.*, vol. 24, no. 5, pp. 557–565, 2017.

[106] C. Xue, J.K. Yu, and Z.Q. Zhang, 'In situ joining of titanium to SiC/Al composites by low pressure infiltration', *Mater. Des.*, vol. 47, pp. 267–273, 2013.

[107] R.Y. Huang, J.C. Huang, and S.C. Chen, 'Electron and laser beam welding of high strain rate superplastic Al-6061/SiC composites', *Metall. Mater. Trans. A*, vol. 32, no. 10, pp. 2575–2584, 2001.

[108] J. Maity, T.K. Pal, and R. Maiti, 'Transient liquid phase diffusion bonding of 6061-13 vol.% SiCp composite using Cu powder interlayer: mechanism and interface characterization', *J. Mater. Sci.*, vol. 45, no. 13, pp. 3575–3587, 2010.

[109] G.O. Cook and C.D. Sorensen, 'Overview of transient liquid phase and partial transient liquid phase bonding', *J. Mater. Sci.*, vol. 46, no. 16, pp. 5305–5323, 2011.

[110] L. Esposito, L. Silvestroni, C. Melandri, S. Guicciardi, 'Transient liquid phase bonding of HfC-based ceramics', *J. Mater. Sci.*, vol. 49, no. 2, pp. 654–664, 2013.

[111] W. Jeitschko and H. Nowotny, 'Die Kristallstruktur von Ti3SiC2 - ein neuer Komplexearbid-Typ', *Monatsh. Chem.*, vol. 98, no. 2, pp. 329–337, 1967.

[112] M. W. Barsoum, 'The MAX Phases: A New Class of Solids', *Prog. Solid State Chem.*, vol. 28, pp. 201–281, 2000.

[113] M. W. Barsoum and M. Radovic, 'Elastic and Mechanical Properties of the MAX Phases', *Annu. Rev. Mater. Res.*, vol. 41, no. 1, pp. 195–227, 2011.

[114] P. Tatarko, S. Grasso, T.G. Saunders, V. Casalegno, M. Ferraris, and M.J. Reece, 'Flash joining of CVD-SiC coated C_f/ SiC composites with a Ti interlayer', *J. Eur. Ceram. Soc.*, vol. 37, no. 13, pp. 3841–3848,

2017.

[115] P. Tatarko, A. Mahajan, V. Casalegno, M.J. Reece, T. G. Saunders, and I. Dlouh, 'Journal of the European Ceramic Society, "High temperature properties of the monolithic CVD -SiC materials joined with a pre-sintered MAX phase Ti_3SiC_2 interlayer via solid-state diffusion bonding', vol. 37, pp. 1205–1216, 2017.

[116] P. Tatarko, V. Casalegno, C. Hu, M. Salvo, M. Ferraris, and M.J. Reece, 'Joining of CVD-SiC coated and uncoated fibre reinforced ceramic matrix composites with pre-sintered Ti_3SiC_2 MAX phase using Spark Plasma Sintering', *J. Eur. Ceram. Soc.*, vol. 36, no. 16, pp. 3957–3967, 2016.

[117] S. Grasso, S. Rizzo, H.Porwal, H. Chunfeng, Y. Katoh, M. Salvo, M.J. Reece, M. Ferraris, 'Joining of β-SiC by spark plasma sintering', *J. Eur. Ceram. Soc.*, vol. 34, no. 7, pp. 1681–1686, 2014.

[118] S. Grasso, T. Saunders, H. Porwal, and M.J. Reece, 'Ultra-high temperature spark plasma sintering of SiC', *Ceram. Int.*, vol. 41, no. 1, pp. 225–230, 2014.

[119] S. Rizzo, S. Grasso, M. Salvo, V. Casalegno, M.J. Reece, and M. Ferraris, 'Joining of C/SiC composites by spark plasma sintering technique', *J. Eur. Ceram. Soc.*, vol. 34, no. 4, pp. 903–913, Apr. 2014.

[120] X. Yin, M. Li, J. Xu, J. Zhang, and Y. Zhou, 'Direct diffusion bonding of Ti_3SiC_2 and Ti_3AlC_2', *Mater. Res. Bull.*, vol. 44, no. 6, pp. 1379–1384, 2009.

[121] X.H. Yin, M.S. Li, T.P. Li, and Y.C. Zhou, 'Diffusion bonding of Ti_3AlC_2 ceramic via a Si interlayer', *J. Mater. Sci.*, vol. 42, no. 17, pp. 7081–7085, 2007.

[122] L. Esposito, A. Piancastelli, A.L. Costa, M. Serantoni, G. Toci, and M. Vannini, 'Experimental features affecting the transparency of YAG ceramics', *Opt. Mater. (Amst).*, vol. 33, no. 5, pp. 713–721, 2011.

[123] J. Hostaša, L. Esposito, D. Alderighi, and A. Pirri, 'Preparation and characterization of Yb-doped YAG ceramics', *Opt. Mater. (Amst).*, vol. 35, no. 4, pp. 798–803, 2013.

[124] S. Hirnyj and J. E. Indacochea, 'Phase transformations in Ag70.5Cu26.5Ti3 filler alloy during brazing processes', vol. 1, no. 2008, pp. 323–332, 2009.

[125] A. Murari, H. Albrecht, A. Barzon, S. Curiotto, and L. Lotto, 'An upgraded brazing technique to manufacture ceramic-metal joints for UHV applications', *Vacuum*, vol. 68, no. 4, pp. 321–328, 2002.

[126] V.T. Witusiewicz, A.A. Bondar, U. Hecht, S. Rex, and T.Y. Velikanova, 'The Al–B–Nb–Ti system III. Thermodynamic re-evaluation of the constituent binary system Al–Ti', *J. Alloys Compd.*, vol. 465, no. 1–2, pp. 64–77, 2008.

[127] N. Eustathopoulos, N. Sobczak, A. Passerone, K. Nogi, 'Measurement of contact angle and work of adhesion at high temperature', vol. 40, 9-10, pp. 2271–2280, 2005.

[128] L. Liggieri and A. Passerone, 'An automatic technique for measuring the surface tension of liquid metals', *High Temp. Technol.*, vol. 7, pp. 82–86, 1989.

[129] A. Passerone and E. Ricci, 'High temperature tensiometry', Studies in Interface Science, vol.6, C, pp. 475–524, 1998.

[130] F. Valenza, M. L. Muolo, and A. Passerone, 'Wetting and interactions of Ni- and Co-based superalloys with different ceramic materials', *J. Mater. Sci.*, vol. 45, no. 8, pp. 2071–2079,2009.

[131] G. Cacciamani, 'An Introduction To the Calphad Method and the Compound Energy Formalism (CEF)', *Tecnol. em Metal. Mater. e Mineração*, vol. 13, no. 1, pp. 16–24, 2016.

[132] B.S. Hans Lukas, S. G. Fries, B. Sundman,'Computational Thermodynamics The Calphad Method', 2007.

[133] P. J. Spencer, 'A brief history of CALPHAD', *Calphad Comput. Coupling Phase Diagrams Thermochem.*, vol. 32, no. 1, pp. 1–8, 2008.

[134] M. Hillert, 'The compound energy formalism', *J. Alloys Compd.*, vol. 320, no. 2, pp. 161–176, 2001.

[135] A. T. Dinsdale, 'Sgte Data for Pure Elements', *Calphad*, vol. 15, no. 4, pp. 317–425, 1991.

[136] U. R. Kattner, 'Phase diagrams for lead-free solder alloys', *Jom*, vol. 54, no. 12, pp. 45–51, 2002.

[137] O. Dezellus, R. Arroyave, and S.G. Fries, 'Thermodynamic modelling of the Ag–Cu–Ti ternary system', *Int. J. Mat. Res.*, vol. 102, pp. 286–297, 2011.

[138] J. Grobner, H. L. Lukas, and F. Aldinger, 'Thermodynamic of the Ternary System Al-Si-C', *Calphad Comput. Coupling Phase Diagrams Thermochem.*, vol. 20, no. 2, pp. 247–254, 1996.

[139] J. Gröbner, H. L. Lukas, and F. Aldinger, 'Thermodynamic calculations in the Y-Al-C system', *J. Alloys Compd.*, vol. 220, no. 1–2, pp. 8–14, 1995.

[140] V.T. Witusiewicz, B. Hallstedt, A.A. Bondar, U. Hecht, S.V. Sleptsov, and T.Y. Velikanova, 'Thermodynamic description of the Al-C-Ti system', *J. Alloys Compd.*, vol. 623, pp. 480–496, 2015.

[141] H. Seifert, 'Thermodynamic Optimization of the Ti-Si System', *Z. Met.*, vol. 87, pp. 2–13, 1996.

[142] Y. Du, J.C. Schuster, H.J. Seifert, and F. Aldinger, 'Experimental Investigation and Thermodynamic Calculation of the Titanium-Silicon-Carbon System', *J. Am. Ceram. Soc.*, vol. 83, no. 1, pp. 197–203, 2000.

[143] V. N. Eremenko, Y. I. Buyanov, and N. M. Panchenko, 'The liquidus surface of the system titanium–copper–silver', *Porosh- kovaya Metall.*, vol. 4, no. 88, pp. 44–48, 1970.

[144] M. Kolbe, J. Brillo, I. Egry, D.M. Herlach, L. Ratke, N. Tinet, C. Antion, L. Battezzati, S. Curiotto, E. Johnson, N. Pryds, 'Undercooling and Demixing of Copper-Based Alloys', vol. 4, pp. 174–177, 2006.

[145] S. Amore, S. Delsante, H. Kobatake, and J. Brillo, 'Excess volume and heat of mixing in Cu-Ti liquid mixture.', *J. Chem. Phys.*, vol. 139, no. 6, pp. 1-6,2013.

[146] R. Novakovic, E. Ricci, M.L. Muolo, D. Giuranno, and A. Passerone, 'On the application of modelling to study the surface and interfacial phenomena in liquid alloy–ceramic substrate systems', *Intermetallics*, vol. 11, no. 11–12, pp. 1301–1311, 2003.

[147] M.C. Brandes, L. Kovarik, M.K. Miller, and M.J. Mills, 'Morphology, structure, and chemistry of

nanoclusters in a mechanically alloyed nanostructured ferritic steel', *J. Mater. Sci.*, vol. 47, no. 8, pp. 3913–3923, 2012.

[148] H. Makram, L. Touron, and J. Loriers, 'Phase Relations in the System Y_2O_3-TiO_2', *J. Eur. Ceram. Soc.*, vol. 14, no. 3, pp. 585–587, 1972.

[149] A.H. Carim, 'Convergent-beam electron diffraction "fingerprinting" of M_6X phases at brazed ceramic joints', *Scr. Metall. Mater.*, vol. 25, no. 1, pp. 51–54, 1991.

[150] A.H. Carim, 'Brazing of alumina with Ti_4Cu_2O and Ti_3Cu_3O interlayers', vol. 33, pp. 195–199, 1997.

[151] T.D. Uzunov, S.P. Stojanov, and S.I. Lambov, 'Thin films of intermetallic Cu/Ti compounds and their possible uses', *Vacuum*, vol. 52, pp. 321–325, 1999.

[152] R. Xu and J.E. Indacochea, 'Reaction layer characterization of the braze joint of silicon nitride to stainless steel', *J. Mater. Eng. Perform.*, vol. 3, no. 5, pp. 596–605, 1994.

[153] J. Andrieux, O. Dezellus, F. Bosselet, and J.C. Viala, 'Low-temperature interface reaction between Titanium and the Eutectic silver-copper brazing alloy', *J. Phase Equilibria Diffus.*, vol. 30, no. 1, pp. 40–45, 2009.

[154] A. Guedes, A. Pinto, and M. Vieira, 'Multilayered interface in Ti / Macor ® machinable glass-ceramic joints', *Mater. Sci.*, vol. 301, pp. 118–124, 2001.

[155] L. De Adição, J. S. Pimenta, A.J.A. Buschinelli, R.M. do Nascimento, A. E. Martinelli, and J. Remmel, 'Brazing of Zirconia to Titanium using Ag-Cu and Au-Ni Filler Alloys', *Soldag. Insp. Sao Paulo*, vol. 18, no. 4, pp. 349–357, 2013.

[156] J. Andrieux *et al.*, 'Details on the Formation of Ti_2Cu_3 in the Ag-Cu-Ti System in the Temperature Range 790 to 860 C', *J. Phase Equilibria Diffus.*, vol. 29, no. 2, pp. 156–162, 2008.

[157] Z.W. Yang, L.X. Zhang, W.Ren, M. Lei, and J.C. Feng, 'Interfacial microstructure and strengthening mechanism of BN-doped metal brazed Ti/SiO_2-BN joints', *J. Eur. Ceram. Soc.*, vol. 33, no. 4, pp. 759–768, 2013.

[158] O. Dezellus, J. Andrieux, F. Bossolet, M. Sacerdote-Perronet, T. Baffie, F. Hodaj, N. Eustathopoulos, J.C. Viala, 'Transient liquid phase bonding of titanium to aluminium nitride', *Mater. Sci. Eng. A*, vol. 495, no. 1–2, pp. 254–258, 2008.

[159] M.I. Barrena, L. Matesanz, and J. M. G. de Salazar, 'Al_2O_3/Ti6Al4V diffusion bonding joints using Ag–Cu interlayer', *Mater. Charact.*, vol. 60, no. 11, pp. 1263–1267, 2009.

[160] S. Liu, F. Weitzer, J.C. Schuster, N. Krendelsberger, and Y. Du, 'On the reaction scheme and liquidus surface in the ternary system Al-Si-Ti', *International Journal of Materials Research*, vol. 99, no. 7. pp. 705–711, 2008.

[161] H. Nowotny and C.B.F. Benesovsky, 'Untersuchungen in den Systemen Ta-Al-Si and W-Al-Si', vol. 313, 1960.

[162] K. Schubert and K. Frank, 'Einige Strukturdaten metallischer Phase', vol. 50, no. 41, 1963.

[163] A. Benedetti, S. Gambaro, F. Valenza, M. Faimali, M. Colli, J.H. Hostasa, M. Delucchi; "Ag and AgCu as brazing materials for Ti6Al4V-YAG joints:does ennoblement affect galvanic behavior in seawater?"; SUBMITTED TO Electrochimica Acta

[164] Materials Properties Handbook: Titanium Alloys, ASM International; pp. 483-636, 1994.

[165] R. Pederson; "Microstructure and Phase Transformation of Ti6Al4V"; Thesis; Department of Applied Physics and Mechanical Engineering Division of Engineering Materials (2002).

[166] A. Ventrella, M. Salvo, M. Avalle, M. Ferraris, Comparison of shear strength tests on AV119 epoxy-joined ceramics, J. Mater. Sci. 45 (2010).

[167] F. Valenza, S. Gambaro, M.L. Muolo, A. Passerone, M. Salvo, V. Casalegno, Wetting of SiC by Al-Ti alloys and joining by in-situ formation of interfacial $Ti_3Si(Al)C_2$, SUBMITTED to Journal of European Ceramic Society 2018.

Scientific Publications

"Wettability of transparent YAG ($Y_3Al_5O_{12}$) by molten Ag–Cu–Ti alloys"
S. Gambaro, M.L. Muolo, F. Valenza, G. Cacciamani, L. Esposito, A. Passerone.
J.Eur.Ceram.Soc., 2015, v.35 (10), pp. 2895-2906.

"Wetting study of the metal-ceramic system AgCuTi/YAG ($Y_3Al_5O_{12}$) for the production of YAG/AgCuTi/Ti6Al4V brazed joints"
S. Gambaro, F. Valenza, M. L. Muolo, A. Passerone, L. Esposito, J. Hostasa.
La Metallurgia Italiana, 2015, v. 10, pp. 25-32.

"Brazing transparent YAG to Ti6Al4V: reactivity and characterization"
S. Gambaro, F. Valenza, A. Passerone, G. Cacciamani, M. L. Muolo.
J.Eur.Ceram.Soc., 2016, v. 36, 16, pp. 4185-4196.

"Wettability of SiC and graphite by Co-Ta alloys: evaluation of the reactivity supported by thermodynamic calculations"
S. Gambaro, F. Valenza, M.L. Muolo, A. Passerone, G. Cacciamani
Journal of Materials Science, 2017,v. 52, 23, pp.13414–13426.

"Metal-ceramic interactions in brazing UHT diboride ceramics"
Fabrizio Valenza, Cristina Artini, Sofia Gambaro, Maria Luigia Muolo, Alberto Passerone.
C. Artini ed. Alloys and Intermetallic Compounds: From Modeling to Engineering. Science publishers (an Imprint of CRC Press, Taylor and Francis Group).

"Surface engineering for joining SiC composites: effectiveness evaluated by surface analysis and wetting test"
Valenza F., Gambaro S., Muolo M.L., Passerone A., Salvo M., Casalegno V., Ferraris M.
International Journal of Applied Ceramic Technology, 2017, v.14,3, 287-294.

"Wetting and interfacial phenomena of Ni-Ta alloys on CVD-SiC"
Valenza F., Gambaro S, Muolo M.L., Cacciamani G., Tatarko P., Saunders T., Reece M.J., Schmidt A, Schubert T, Weißgärber T, Passerone A.
International Journal of Applied Ceramic Technology, 2017, v.14,3, 295-304.

"Reactivity evaluation of Al-Ti alloys in contact to SiC"
S. Gambaro, F. Valenza, M.L. Muolo, A. Passerone, G. Cacciamani, R. Chiriac, F. Touche, O. Dezellus
TO BE SUBMITTED at ACTA MATERIALIA

"Wetting of SiC by Al-Ti alloys and joining by in-situ formation of interfacial $Ti_3Si(Al)C_2$"
F. Valenza, S. Gambaro, M.L. Muolo, A. Passerone, M. Salvo, V. Casalegno
SUBMITTED to Journal of European Ceramic Society

A. Benedetti, S. Gambaro, F. Valenza, M. Faimali, M. Colli, J.H. Hostasa, M. Delucchi; "Ag and AgCu as brazing materials for Ti6Al4V-YAG joints:does ennoblement affect galvanic behavior in seawater?"; SUBMITTED TO Electrochimica Acta